Ghent University

Faculty of Sciences

Department of Plant Biotechnology and Bioinformatics

VIB department of Plant Systems Biology

Endomembrane trafficking and brassinosteroid signaling from a small molecule perspective.

Wim Dejonghe

Promoter: Prof. Dr. Jenny Russinova

This thesis was submitted as fulfillment of the requirements to obtain the degree of Doctor (PhD) in sciences: Biochemistry and Biotechnology

Academic year 2014-2015

This thesis was carried out at the University of Ghent and Flemish Institute for Biotechnology (VIB) department of Plant Systems Biology (PSB). The research was funded by the Flemish institute for Innovation through Science and Technology (IWT) and VIB.

Plant Systems Biology
A VIB-UGENT DEPARTMENT

agency for Innovation
by Science and Technology

Examination committee

Chair:

Prof. Dr. Geert De Jaeger

Department of Plant Systems Biology. VIB, Ghent University

Promoter:

Prof. Dr. Jenny Russinova

Department of Plant Systems Biology. VIB, Ghent University

Reading committee:

Prof. Dr. Savvas Savvides

Unit for Structural Biology, L-ProBE, Ghent University. Inflammation Research Center, VIB, Ghent University

Prof. Dr. Patrik Verstreken

VIB Center for the Biology of Disease. KU Leuven, Center for Human Genetics, Laboratory of Neuronal Communication

Dr Steffen Vanneste

Department of Plant Systems Biology. VIB, Ghent University

Dr. Erich Kombrink

Max Planck Institute for Plant Breeding Research. Chemical Biology Laboratory

Other committee members:

Prof. Dr. Kris Gevaert

Department of Biochemistry, Ghent University. VIB Department of Medical Protein Research.

Prof. Dr. Johan Winne

Department of Organic and Macromolecular Chemistry. Ghent University

Dr. Daniel Van Damme

Department of Plant Systems Biology. VIB, Ghent University

Contents

List of abbreviations 9

Scope 13

Summary 15

Samenvatting 17

Chapter I: Introduction 19

Abstract 21

1.1. Brassinosteroids and their chemical toolbox* 22

1.1.2 Small molecules affecting BR biosynthesis 24

1.1.3. Small molecules affecting BR signaling 26

1.2. Small molecules for dissecting endomembrane trafficking: a cross‐systems view** 30

1.2.1. Endomembrane trafficking routes in yeasts, plants and mammals: a comparative view .30

1.2.2. In search for small-molecule modifiers of endomembrane trafficking 31

1.2.3. Chemical effectors of exocytosis/secretion/anterograde trafficking 35

1.2.4. Chemical effectors of endocytosis/retrograde trafficking 37

1.2.5. Chemical effectors of vacuolar trafficking and autophagy 38

1.2.6. Special considerations when analyzing drug-induced endomembrane trafficking phenotypes 39

1.3. Target Identification Strategies in Plant Chemical Biology*** 46

1.3.1. Commonly used target identification strategies in plant chemical biology 47

1.3.1.1. Forward genetic screen for compound resistance 48

1.3.1.2. Phenotyping approach 49

1.3.1.3. *In silico*-based target identification strategies 51

1.3.2. Emerging target identification strategies in plant chemical biology 51

1.3.2.1. Activity-based protein profiling (ABPP) 51

1.3.2.2. Yeast 3-hybrid 52

1.3.2.3. Affinity-based technologies 54

1.3.2.4. Phage display....57
1.3.3. Label-free compound based technologies....58
1.3.3.1. Chemical denaturation shift....59
1.3.3.2. Target identification by chromatographic co-elution (TICC)....59
1.3.3.3. Drug affinity-responsive target stability (DARTS)....59
1.4. Future perspectives....61
1.5. Acknowledgments....64
1.6. References....65
Chapter II: Small molecule screen for effectors of clathrin-mediated endocytosis and brassinosteroid signaling....81
Abstract....83
Introduction....84
Results and Discussion....85
Compound Screen for CME inhibitors....85
BR signaling in response to small molecules....88
Small molecule screen on light-grown and dark-grown seedlings....88
Comparative summary of screening results and selection of hit molecules....90
Materials and methods....101
References....102
Chapter III: Protonophore uncouplers are potent inhibitors of clathrin-mediated endocytosis in plants....105
Abstract....107
Introduction....108
Results....109
ES9 blocks clathrin-mediated endocytosis in different systems....109
ES9 affects energy metabolism through uncoupling of oxidative phosphorylation in mitochondria....110
Cytosolic acidification but not ATP depletion rapidly inhibits CME in *Arabidopsis*....112
E S9 activity causes an arrest in dynamic behavior of CME machinery at the plasma membrane....115

Protonophores affect multiple aspects of endomembrane trafficking 116
Discussion....120
ES9 and TyrA23 are mitochondrial uncouplers....120
ATP depletion alone does not efficiently block CME in Arabidopsis root cells and *Drosophila* neuromuscular junctions 121
ES9 and TyrA23 inhibit CME through cytosol acidification and possibly dissipation of proton gradients at the plasma membrane 121
The use of TyrA23 in plants 123
Acknowledgements 125
Material and methods 125
Supplemental information 129
References 135
Chapter IV: Disruption of clathrin-mediated endocytosis in Arabidopsis through small molecule inhibition of clathrin heavy chain function 145
Abstract....147
Introduction 148
Results 149
Identification of ES9-17....149
ES9-17 inhibited CME in *Arabidopsis* 151
Brassinosteroid signaling is enhanced in the presence of ES9-17 154
CHC is a likely target of ES9-17 156
ES9-17 binds to CHC....158
chc1 and *chc2* mutants are more sensitive to ES9-17....161
ES9-17 possibly binds the N-terminal domain of CHC....162
Discussion....165
Acknowledgements 169
Material and methods 169
Supplemental information. 184
References 213

Chapter V: Identification of a trans-membrane protein family through computational target prediction 219
Abstract.....221
Introduction 222
Results 224
Structure-activity relation analysis reveals the core structure of small molecule 39.....224
Small molecule 39 potentially binds a family of 4 membrane proteins in *Arabidopsis* 225
Higher order mutants of the *PTE* gene family were sensitive to 39 227
Sensitivity of mutant lines appeared to be 39 specific. 232
PTE proteins localize mainly to the plasma membrane. 234
PTE1 interacts with MSBP2 236
Discussion.....239
Material and methods 242
Supplemental information 247
References 250
Chapter VI: Discussion 255
Conclusions and future challenges 256
Small molecules and cytotoxicity 256
Small molecules and target deconvolution. 258
Target identification and validation: the importance of biochemical approaches 260
Small molecules and CME.....261
References 263
Acknowledgements 267
Curriculum Vitae.....270

List of abbreviations

ABA	Abscisic acid
ABC	ATP binding cassette
ABPP	Activity-based protein profiling
AFCS	Alexa Fluor 647-Castasterone
AP2	ADAPTOR PROTEIN COMPLEX-2
ARF	ADP-ribosylation factor
BAK1	BRI1-ASSOCIATED KINASE1
BES1	BZR2/BRI1-EMS-SUPPRESSOR1
BFA	Brefeldin A
BG	O^6-benzylguanine
BiFC	Bimolecular fluorescence complementation
BIN2	BRASSINOSTEROID INSENSITIVE2
BKI1	BRI1 KINASE INHIBITOR 1
BL	Brassinolide
BPCS	Biotin-labeled photoaffinity castasterone
BRI1	BRASSINOSTEROID INSENSITIVE 1
BRs	Brassinosteroids
BRZ	Brassinazole
BSK1	BRASSINOSTEROID SIGNALING KINASE1
BSU1	BRI1-SUPPRESSOR1
BZR1	BRASSINAZOLE RESISTANT1
CA	Cucurbic acid
CCCP	Carbonyl cyanide m-chlorophenyl hydrazone
CDG1	CONSTITUTIVE DIFFERENTIAL GROWTH1
CETSA	Cellular thermal shift assay
CHC	Clathrin heavy chain
ChIP	Chromatin immunoprecipitation
CLC	Clathrin light chain
CME	Clathrin-mediated endocytosis
Cpd8	Compound 8
CPK	Ca^{2+}-dependent protein kinase
CPY	Carboxypeptidase Y

CS	Castasterone
DAG	Diacylglycerol
DARTS	Drug affinity-responsive target stability
DHFR	Dihydrofolate reductase
DWF4	DWARF4
EEs	Early endosomes
EGF	Epidermal growth factor
EIN3	ETHYLENE INSENSITIVE 3
EMS	Ethylmethane sulfonate
ER	Endoplasmatic reticulum
ES1	Endosidin 1
FITGE	Fluorescence difference in two-dimensional gel electrophoresis
FKBP12	12-kDa FK506-binding protein
Flg22	Flagellin 22
GAPC	Glyceraldehyde-3-phosphate dehydrogenase
GCA	Golgicide A
GEF	Guanine exchange factor
GFP	Green fluorescent protein
GPRAT2	GLUTAMINE PHOSPHORIBOSYLAMIDOTRANSFERASE 2
HNA	2-hydroxy-1-naphtaldehyde
IAA	Indole-3-acetic acid
IBA	Indole-3-butyric acid
IBR3	INDOLE-3-BUTYRIC ACID RESPONSE 3
IGPD	Imidazole glycerol phosphate dehydratase
ITC	Isothermal titration calorimetry
JA	Jasmonic acid
JAMe	Jasmonic acid methyl ester
JAR1	JASMONATE RESISTANT 1
LBD	Ligand binding domain
LEs	Late endosomes
LOX2	LIPOXYGENASE 2
LRR	Leucine-rich repeat
Kyn	L-Kynurenine
MAP4	MICROTUBULE ASSOCIATED PROTEIN 4

MAPR2	MEMBRANE-ASSOCIATED PROGESTERON BINDING PROTEIN2
MGDG	Monogalactosyldiacylglycerol
MIND	Membrane-based interactome network database
Moco	Molybdenum cofactor
MSBP1/2	MEMBRANE STEROL BINDING PROTEIN 1/2
Mtx	Methotrexate
MVBs	Multivesicular bodies
nar1	*naxillin resistant 1*
NMJ	Neuromuscular junction
PDB	Protein Data Bank
PEG	Polyethylene glycol
PGP19	P-GLYCOPROTEIN 19
Phyre 2	Protein homology/analogy recognition engine 2
PIN	PIN-FORMED
PM	Plasma membrane
PP2A	PROTEIN PHOSPHATASE 2A
PPARγ	Peroxisome proliferator-activated receptor gamma
PSVs	Protein storage vacuoles
PTE	PUTATIVE INTERACTOR OF ENDOSIDIN
PVC	Prevacuolar compartment
PYR/PYL	Pyrabactin resistance/PYR-like
QCM	Quartz-crystal microbalance
RCAR	Regulatory component of ABA receptor
RELIC	Receptor-ligand contacts
SA	Salicylic acid
SAG	SA-2-O-β-D-Glucoside
SAR	Structure activity relation
SERK1	SOMATIC EMBRYOGENSIS RECEPTOR KINASE1
SH	Serine hydrolase
SILAC	Stable isotope labeling with amino acids in cell culture
SIR1	Sirtinol resistant 1
SMIR/SMER	Small-molecule inhibitors/enhancers of rapamycin
SMO	Sterol methyl oxidase
SPR	Surface plasmon resonance

TAA1	TRYPTOPHANE AMINOTRANSFERASE OF ARABIDOPSIS1
Tf	Transferrin
Tfr	Transferrin receptor
TGN	*trans*-Golgi network
TICC	Target identification by chromatographic co-elution
TOR	Target of rapamycin
TriNP	Trifunctional nitrophenol phosphonate
TyrA23	Tyrphostin A23
TyrA51	Tyrphostin A51
TZD	Thiazolidinedione
Y2H	Yeast-2-hybrid
Y3H	Yeast-3-hybrid

Scope

Over the past decades our understanding of plant biology has been ever increasing thanks to elaborate development of genetics approaches. Classical genetics approaches have been, and still are very powerful tools to attribute a phenotype to a gene or group of genes. Different strategies allow us to further inquire gene function once it has been linked to a certain phenotype, such as over expression analysis and fluorescent labeling. Directed mutagenesis (i.e. amino acid substitutions) enables an even higher degree of characterization, as it allows to dissect protein function at the level of its primary sequence. Yet one of genetics inherit characteristics, alteration of the genome, can be a disadvantage in certain occasions. Essential genes can pose a problem as mutations are often lethal, while redundancy might imply that higher order mutants have to be generated, which are difficult to obtain and work with. In addition, highly dynamic processes, such as hormonal signaling and endomembrane traffic are difficult to approach dynamically at the protein level, as alterations in the genome imply a steady state. A possible solution might be provided by application of small molecules which alter protein function. Called chemical biology, application of small molecules to induce a particular phenotype can have important advantages over classical genetics approaches. In particular it's conditional nature, certainly when small molecule binding is reversible, allow to probe essential gene function directly at the protein level. In addition, conditionality of small molecule application can serve as an on-off switch for processes such as hormone signaling and endomembrane traffic. Chemical biology is not restricted to altered protein function in presence of the small molecule of interest, but can also include the study on other mode of actions, such as binding to lipids. Chemical genetics therefore refers to the study of linking the phenotype induced by a small molecule to a protein or protein family, and thus gene function.

This PhD thesis is geared towards an exploration of chemical genetics approaches in plant biology, with a special focus on small molecules which perturb endomembrane traffic and brassinosteroid signaling. Our starting point is a collection of small molecules which have been selected for their potential to affect endomembrane traffic. Screening of these small molecules for a variety of readouts is set to identify a select group which will be subject to further in depth characterization and target identification. We primarily aim to select those small molecules which affect clathrin-mediated endocytosis and brassinosteroid signaling, and to emphasize on biochemical target identification and validation of one hit molecule, as such approaches are best suited to identify the interactome of the small molecule. The interactome is the defined set of proteins which interacts with the small molecule of interest, and which are responsible for the overall phenotype induced by the small molecule. We will emphasize on interactors which are linked to endomembrane trafficking, and more specifically

clathrin-mediated endocytosis, and attempt to characterize their contribution to the trafficking phenotype induced by the small molecule.

In addition, we will attempt to predict target proteins of a small molecule hit by computational means, as this method of target identification is hardly explored in plant chemical genetics.although more of a side project, it concerns a proof of concept study where proteins identified as possible hits are set to be characterized in terms of biological function and as target proteins of the small molecule of interest.

Furthermore, we discuss the advantages and disadvantages of chemical biology and biochemical target identification, and reflect on the future direction of plant chemical biology.

Summary

This work explores chemical biology approaches in plant biology, with an emphasis on small molecules which affect clathrin-mediated endocytosis (CME) and brassinosteroid signaling. It first provides an introduction on small molecules which have contributed to a better understanding of brassinosteroid signaling and endomembrane traffic. The latter set of small molecules is restricted to small molecules identified through screening. Different target identification strategies are introduced, encompassing classical approaches such as resistance screens, and approaches which are less common in plant chemical biology, such as affinity purification. In the next chapter we introduce a screen for small molecule effectors of CME and brassinosteroid signaling which led to the selection of two promising hit molecules. The first hit, namely Endosidin 9 (ES9), was further characterized and different analogs were selected and characterized for structure activity relation analysis in order to identify chemical groups of ES9 which might tolerate modification for affinity purification. Characterization revealed ES9 mainly acts as an chemical uncoupler of proton gradients, with important implications on energy metabolism, pH homeostasis and dynamic processes in the cell, including CME. This mode of action also appeared to be conserved in other systems and is reminiscent of a known chemical uncoupler, but mimics also the known CME inhibitor Tyrphostin A23. The latter observation is new for the plant field, and implications are discussed. An analogue of ES9 was identified which retained the ability to inhibit CME, yet lacked characteristics of an uncoupler. These findings were the result of a further characterization of ES9 in different systems, revealing an additional mode of action aside the uncoupler effect. The analog ES9-17 proved to be more specific compared to ES9, and was found to bind to clathrin heavy chain as a result of affinity purification. We therefore present, what is to our knowledge the only specific small molecule inhibitor of clathrin-mediated trafficking, including CME, in *Arabidopsis*.

A second small molecule hit from the screen was used in a target identification approach which was based on computational prediction of target proteins in plants with a human protein as a template. The human protein binds a drug, Rosiglitazone, which harbors the same chemical groups as our small molecule hit. We identified a plant specific trans-membrane protein family, for which we attempt to prove their binding to the small molecule hit through mutant analysis. In addition, we began to characterize the protein family, as it is a protein family of unknown function. Finally we discuss our findings in a more general perspective, highlighting important findings for the plant chemical biology field, and suggest a preferred target identification approach for small molecule modulators of endomembrane traffic.

Samenvatting

Deze studie omvat een exploratie van chemische biologie in planten, met een speciale focus op kleine moleculen die een invloed hebben op de brassinosteroïde signalisatie en clathrine gemedieerde endocytose. Dergelijke kleine moleculen creëren de mogelijkheid om de onderlinge relatie te onderzoeken tussen brassinosteroïde signalisatie en endomembraan trafiek in *Arabidopsis.*

De introductie schets een overzicht van de huidige stand van zaken in onderzoek naar brassinosteroïden en endomembraan trafiek, waarbij kleine moleculen als werktuig dienen om relevante moleculaire processen op een specifieke en dynamische manier te verstoren. In het kader van endomembraan trafiek vergelijken we dierlijke systemen met planten systemen, maar beperken we ons wel tot enkel kleine moleculen die geïdentificeerd werden door middel van screenings. Vervolgens geven we een plant gericht overzicht van klassieke en relatief nieuwe methoden om de eiwitten te identificeren die de relevante kleine moleculen binden, en bespreken we strategieën die al gebruikt worden in dierlijke systemen, maar die veelbelovend kunnen zijn voor planten.

In het volgende hoofdstuk beschrijven we een screen van kleine moleculen met het doel om zogenaamde ‘hit’ moleculen te identificeren die zowel clathrine gemedieerde endocytose inhiberen als brassinosteroïde signalisatie activeren in *Arabidopsis*. Als gevolg identificeren we twee ‘hit’ moleculen die in de volgende hoofdstukken verder gekarakteriseerd worden, en waarvoor we de eiwitten trachten te achterhalen waarop de kleine moleculen binden.

In hoofdstuk 3 tonen we aan dat een van de ‘hit’ moleculen, Endosisdin 9 (ES9), protonophore karakteristieken vertoont, wat wil zeggen dat ES9 protonen over een membraan kan transporteren door middel van zijn chemische eigenschappen. Dit heeft gevolgen voor verschillende processen in de cel, waaronder ATP productie, pH homeostase, endomembraan dynamiek en clathrine gemedieerde endocytose. Hetzelfde principe is van toepassing voor Tyrphostin A23 (TyrA23), een molecule die specifiek clathrine gemedieerde endocytose inhibeert, en daarvoor veelvuldig gebruikt wordt in de planten biologie. De bevinding dat TyrA23 zich gedraagt zoals een protonophoor, en daardoor endocytose blokkeert, plaats vraagtekens bij het gebruik van TyrA23 om endocytose op een specifieke manier te inhiberen.

Hoofdstuk 4 is een verder gevolg van de karakterisatie van ES9, gezien bepaalde bevindingen aantoonden dat ES9 nog andere effecten kan induceren, naast die van een protonophoor. We gaan specifiek op zoek naar analoge moleculen aan ES9 die nog altijd in staat zijn om clathrine gemedieerde endocytose te inhiberen, maar geen, of sterk verminderde eigenschappen vertonen van een protonophoor. We isoleren ES9-17 als een veelbelovend analoog, en tonen aan dat ES9-17 nog altijd clathrine gemedieerde endocytose blokkeert, maar geen ATP depletie meer induceert, of

dynamische endomembraan processen affecteert. Affiniteit purificatie, en daaropvolgende biochemische validatie identificeert ES9-17 als een inhibitor van clathrine gemedieerde endocytose door het binden op clathrin heavy chain (CHC). Het is daardoor, voor zover wij weten, de meest specifieke inhibitor van clathrine gemedieerde endocytose in *Arabidopsis*, op dit moment.

In hoofdstuk 5 proberen we te achterhalen op welke eiwitten de tweede 'hit' molecule, 39, bindt. We doen dit via een computationele predictie die gebaseerd is op gegevens uit dierlijke systemen voor een molecule met een zelfde chemische groep als 39. We identificeren 4 potentiële bindingspartners die allemaal tot dezelfde plant specifieke familie behoren. Hun functie is echter niet gekend, behalve dat ze trans-membraan eiwitten zijn. Naast de validatie als mogelijke bindingspartners van 39, initiëren we daarom de characterisatie van die eiwit familie.

Tot slot nemen we een stap terug en bespreken we een aantal algemene inzichten die van toepassing zijn wanneer met kleine moleculen gewerkt wordt, en die in het verloop van deze thesis aan bod komen.

Chapter I: Introduction

Abstract

The current striving to understand gene function in plant biology increasingly requires more dynamic and conditional approaches opposed to classic genetic strategies. In addition, gene redundancy and lethality can substantially complicate research. These issues might be solved by applying small molecules to a biological system to induce a phenotype of interest. Application of small molecules often implies a conditional interference with protein function as small molecule treatment can be reversible, and is time and dose dependent. Therefore small molecules offer considerable opportunities to perturb systems in a dynamic and conditional manner, opposed to classical genetics. Now understood as the study of small molecules and their effect on biological systems with subsequent target identification, chemical genetics is a fast developing field with a strong history in pharmaceutical research and drug discovery. In plant biology however, chemical genetics is still largely in the starter blocks, with most studies relying on forward genetics and phenotypic analysis for target identification, while studies including direct target identification are limited.

In this chapter we first provide an overview on small molecules used in brassinosteroid research and the insights they provided, followed by small molecule effectors of endomembrane traffic identified through screening of small molecule libraries in different systems. Finally we provide an overview of recent chemical genetics advances in plant biology with a focus on target identification, as identification of small molecule targets becomes increasingly important. Furthermore, we discuss different strategies for direct target identification and the possibilities and challenges for plant biology.

1.1. Brassinosteroids and their chemical toolbox*

1.1.1 A short introduction to brassinosteroid biosynthesis and signaling

Brassinosteroids (BRs) are plant steroid hormones that play an essential role in plant growth and development and their biosynthesis, signaling, and transcriptional responses are well studied and understood processes in plant biology[1-3]. BRs are the result of several enzymatic conversions of campesterol, a precursor derived from isoprenoid-based sterol biosynthesis[1].Several biosynthetic routes have been described, including the early and late C-22 oxidation to form campestanol. The early C-22 branch appears to be the most prominent of the two in *Arabidopsis*[1]. Similarly, campestanol is further derivatized through two biosynthetic routes, the late and early C-6 oxidation, to form brassinolide (BL) or castasterone (CS). In *Arabidopsis*, as for many other plant species, the late C-6 oxidation route is the most important[1]. Biosynthesis of BRs occurs in the smooth endoplasmatic reticulum (ER), from which it is transported to the plasma membrane. Little is known yet about trafficking of BRs throughout the endomembrane system, but possibly involves MEMBRANE STEROL BINDING PROTEIN1 (MSBP1), as it has been described to bind BL with high affinity[1,4].

The signaling cascade initiates once BRs are perceived by the plasma membrane-localized leucine-rich repeat (LRR) receptor kinase BRASSINOSTEROID INSENSITIVE1 (BRI1). Perception of BRs trigger the binding of BRI1 to BRI1-ASSOCIATED KINASE1 (BAK1), which in turn is required to activate the kinase domain of BRI1 through trans-phosphorylation events. Dissociation of BRI1 KINASE INHIBITOR1 (BKI1) from BRI1, an inhibitor of BRI1 kinase activity in absence of BRs, is triggered by the trans-phosphorylation events upon BRI1-BAK1 binding, and renders the kinase domain fully active. Subsequently, active BRI1 phosphorylates BRASSINOSTEROID SIGNALING KINASE1 (BSK1) and CONSTITUTIVE DIFFERENTIAL GROWTH1 (CDG1), which in turn bind and phosphorylate BRI1-SUPPRESSOR1 (BSU1). The latter is a phosphatase that will inactivate BRASSINOSTEROID INSENSITIVE2 (BIN2), a kinase which is responsible for negative regulation of two key transcriptional regulators, BRASSINAZOLE RESISTANT1 (BZR1) and BZR2/BRI1-EMS-SUPPRESSOR1 (BES1) (**Figure 1**). In absence of BR signaling, BIN2 phosphorylates BZR1/2, which enables 14-3-3 proteins to retain both transcriptional regulators in the cytosol. When BIN2 is inactivated upon BRs signaling, PROTEIN PHOSPHATASE 2A (PP2A) dephosphorylates BZR1/2, which allows them to migrate in the nucleus and exert their function.

*Adapted from: Dejonghe, W., Mishev, K. & Russinova, E. The brassinosteroid chemical toolbox. *Curr Opin Plant Biol* **22C**, 48–55 (2014). D. W. and R. E. wrote the manuscript. M. K. and D. W. designed and made figures. All authors reviewed the manuscript.

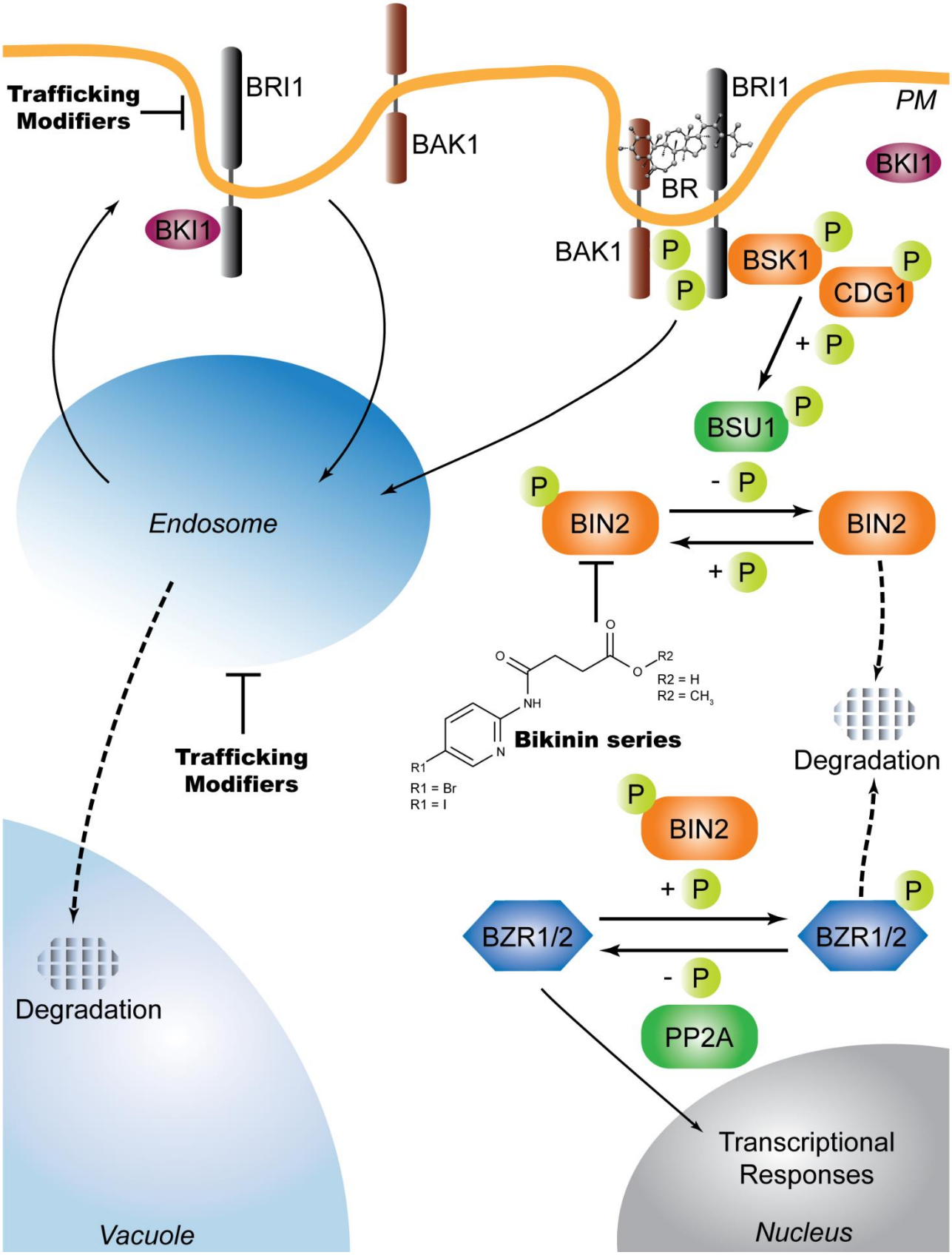

Figure 1. Small-molecule effectors of brassinosteroid signaling.

In the absence of brassinosteroid (BR) hormones, the leucine-rich repeat (LRR) receptor kinase BRASSINOSTEROID INSENSITIVE1 (BRI1) is associated with the BRI1 KINASE INHIBITOR1 (BKI1). Most of the BRI1 molecules undergo continuous cycling between the plasma membrane

(PM) and endosomal compartments, and only a small fraction is sorted for vacuolar degradation to ensure the protein turnover. BR sensing is initiated at the PM. The BR hormone binds to the extracellular domain of BRI1 and induces BKI1 phosphorylation through activation of the intracellular BRI1 kinase domain. The phosphorylated BKI1 dissociates from the PM, allowing the interaction of BRI1 with the BRI1-ASSOCIATED RECEPTOR KINASE1 (BAK1). After a number of autophosphorylations and transphosphorylations, the BRI1-BR-BAK1 complex becomes fully activated and triggers the downstream BR SIGNALING KINASE1 (BSK1) through BRI1 kinase-mediated phosphorylation. In turn, BSK1 activates the BRI1 SUPPRESSOR1 (BSU1). BSU1 dephosphorylates BRASSINOSTEROID INSENSITIVE2 (BIN2), a serine/threonine GSK3/shaggy-like kinase that acts as a negative regulator in the BR signaling pathway through repression of the transcription factors BRASSINAZOLE RESISTANT1 (BZR1) and BZR2/BRI1 EMS SUPPRESSOR1 (BES1). The dephosphorylated form of BIN2 is destined for degradation. Alternatively, effective inhibition of BIN2 can be achieved by exogenous application of bikinin and related derivatives. In the absence of BIN2 activity, the BZR1/2 transcription factors are dephosphorylated by a protein phosphatase 2A (PP2A) and translocate to the nucleus to trigger the expression of BR-responsive genes. Application of chemical modifiers of endomembrane trafficking can efficiently block BRI1 at the level of PM or in the endosomes, thus modulating the receptor availability for its ligand and the BR signaling outputs, respectively.

1.1.2 Small molecules affecting BR biosynthesis

Specific inhibitors of BRs biosynthesis offer a powerful tool to manipulate BR levels in different plant tissues and have been crucial for identifying novel components involved in BR signal transduction pathway[5]. All known inhibitors of BR biosynthesis (**Figure 2**) share an azole moiety that is thought to bind the iron-containing heme prosthetic group of P450 cytochrome enzymes. The best known examples with a specific impact on BR biosynthesis are brassinazole (brz)[6] and brz2001[7]. Both small molecules are similar to uniconazole, a known gibberellin biosynthesis inhibitor that also affects BR biosynthesis[8] and result from uniconazole derivatization to obtain specific BR biosynthesis inhibitors. A similar strategy has been adopted with another BR biosynthesis inhibitor propiconazole[9], which was used to develop a more potent inhibitor, namely brz220[10]. Brz, brz2001, and brz220 target DWARF4 (DWF4), a P450 monooxygenase hydroxylating the C-22 position during BR biosynthesis[11,12] (**Figure 2**). Brz2001, recently used in a quartz-crystal microbalance-based T7 phage display target identification strategy, confirmed DWF4 as its target, mapping the binding site as a potential disordered region of the enzyme[13].

Several other BR biosynthesis inhibitors have been found. Voriconazole inhibits the BR-dependent sterol biosynthesis at the level of the P450 cytochrome CYP51 (**Figure 2**) resulting in accumulation of the sterol biosynthesis intermediate obtusifoliol[14]. In addition, voriconazole appears to be specific to BR biosynthesis, because gibberellin application did not rescue the voriconazole caused growth phenotypes. A group of BR biosynthesis inhibitors, designated the YCZ series, was developed from a ketoconazole scaffold[15] (**Figure 2**). The rationale to use a ketoconazole scaffold is based on (i) its similarity with the most potent BR biosynthesis inhibitor, brz220; (ii) its known ability to inhibit P450 enzymes; and (iii) analogs would retain the phenoxy moiety found in ketoconazole with different substitutions. From this series, the most active inhibitor was used as a scaffold to

generate analogs with different substitutions on either the phenoxy moiety or the aro- matic ring attached at the C2 position from the 1,3- dioxolane moiety[16] (**Figure 2**). An additional structure-activity relation analysis resulted in YCZ-18, a BR biosynthesis inhibitor more potent than brz220[17]. Further developments of the YCZ series include analysis of the absolute stereochemistry of YCZ-2013 on activity[18] and synthesis of a fluorescently labeled YCZ analog[19]. The latter small molecule might play an important role in visualization of BR biosynthetic processes.

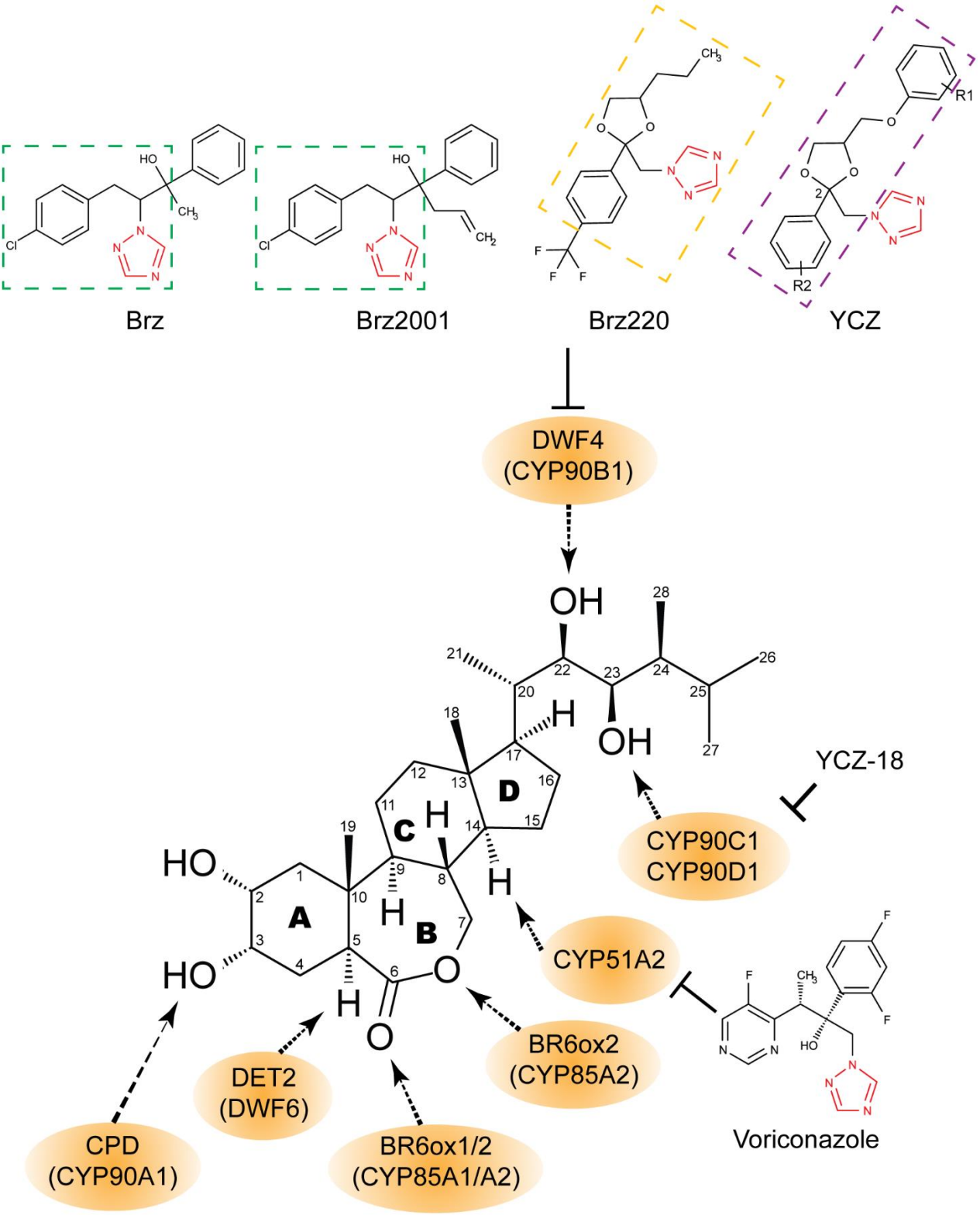

Figure 2. Chemical manipulation of brassinosteroid biosynthesis.

The chemical structure of brassinolide (BL), the most potent natural brassinosteroid is presented. The BL biosynthesis is accomplished by a number of cytochrome P450 enzymes that are involved in highly branched and parallel pathways (enzymes that catalyze key reactions are boxed in orange). Most of the chemical tools that interfere with BL biosynthesis deal with the P450 monooxygenase DWARF4 (DWF4) (implicated in the hydroxylation at the C22 position of the molecule) and share a common triazole moiety (highlighted in red). Brassinazole (Brz) and its derivative Brz2001 have been developed from the uniconazole scaffold (green dashed rectangle). In turn, the propiconazole scaffold (yellow dashed rectangle) has been used to create Brz220. Modifications on the ketoconazole scaffold (purple dashed rectangle) have led to the discovery of the YCZ series of DWF4 inhibitors that differ in substitutions on either the phenoxy moiety (R1 substitutions) or the aromatic ring attached at C2 position from the 1,3-dioxolane moiety (R2 substitutions). The only small molecule that targets an enzyme other than DWF4 is voriconazole. The inhibitor has been shown to be specific for P450 cytochrome CYP51, an enzyme catalyzing a step from the sterol biosynthetic pathway that provides precursors for the BL synthesis.

1.1.3. Small molecules affecting BR signaling

To date, 69 naturally occurring BRs are known, including 5 conjugated forms, with BL and CS being the most abundant and active[20,21]. This natural variation depicts a common 5α-cholestane structure and some essential requirements for highly active BRs, such as an α-hydroxyl group at the C2 position and vicinal hydroxyl groups at positions C22 and C23, both in R orientation[21] (**Figure 2**).

The recent crystallographic structure reports on the extracellular part of BRI1 in the presence of BL allow an improved rationalization of the chemical requirements for proper ligand binding and signaling activation. The extracellular domain forms an atypical superhelical structure comprised of 25 LRRs with an insertion domain in between LRR 21 and 22 that is partially unstructured in the absence of BL. As BL binds BRI1 in between the insertion domain and the LRR domain (**Figure 3**), part of the insertion domain becomes structured, whereas the side chain of BL is accommodated by a hydrophobic pocket[22,23]. The hydroxyl groups at position C2 and C3 and the B-ring are exposed to solvent for a considerable degree and seemingly not implicated in polar interactions. This position of the B-ring might also explain the reported tolerated modification on the 6-oxo position of CS[24,25]. However, structural data of the extracellular domains of BRI1 with either BAK1 or the SOMATIC EMBRYOGENSIS RECEPTOR KINASE1 (SERK1), another BRI1 co-receptor and a close homolog of BAK1, in the presence of BL provided evidence for the requirement of the hydroxyl groups at position C2 and C3 as well as the solvent-exposed A and B rings of the BRI1-bound BL in recognizing and binding the N-terminal part of either BAK1 or SERK1 (**Figure 3**). Besides the BL-mediated interactions, BRI1 makes direct contact with the co-receptors through its last two LRRs and the C-terminal cap domain[26,27].

Development of new BR analogs with different activity can provide further information on the molecular interactions involved in BR recognition and function. Alternatively, bioactive analogs can be used as cheap BR substitutes for massive applications in agriculture. Several structure-activity relation studies have allowed a better understanding of the chemical and structural degrees of freedom in terms of BR signaling activation (**Figure 3**). By means of the bean second internode bioassay, two

BR analogs with a 5α-hydroxy-6-oxo moiety and lacking hydroxylations on the side chain, but with either hydroxylations on both C2 and C3 or only C3 positions were found biologically active[28]. A set of monohydroxylated analogs on C2 and C3 with a carboxyl group as side chain illustrate the importance of the side chain for efficient BR binding[29]. Assessment of the possibility to exchange ring A for an aromatic ring revealed that, compared to 28-homotasterone, one analog bearing an aromatic ring and hydroxy groups on the C3, C22, and C23 positions, but lacking the 6-oxo moiety, was only 30% less active, indicating for the first time that aromatic rings are tolerated for BR activity[30]. To replace hydroxyl groups, fluorination of the A ring has been applied. The electronegativity of fluor is similar to that of oxygen and can replace an -OH group. Although fluor can act as a hydrogen bond acceptor, it cannot act as a donor. Hence, the analog with fluor on both the C2 and C3 positions had a biological activity similar to that of 28-homocastasterone, hinting toward a role for the natural occurring hydroxyl groups at positions C2 and C3 as hydrogen bond acceptors[31]. This hypothesis was supported by the structural data from the BRI1-BL-BAK1 complex at low pH[26].

Thanks to these structural insights, a BR antagonist has been developed for the first time. As the C2 and C3 hydroxyl groups of BL are involved in H-bond formation with BAK1, the search for antagonists was directed to derivatization of the hydroxyl groups at position C2, C3, C22, and C23. Only the BL analogs derivatized on either the C2 and C3 or C22 and C23 positions, creating a 2,3-acetonide and a 22,23-acetonide, showed an antagonistic activity[32]. The antagonistic activity of the analog derivatized on the C2 and C3 positions can be explained easily with the structural data available, but explanation for the C22 and C23-derivatized antagonist might be less straightforward, because both hydroxyl groups are quite distant from BAK1 and buried in the hydrophobic pocket[22,23].

An important tool for BR signaling research is the Alexa Fluor 647-CS (AFCS), an active fluorescent CS analog[25]. Besides being the first reported active fluorescent BR, AFCS also allowed the visualization of the endomembrane trafficking of the green fluorescent protein (GFP)-tagged BRI1 in the presence of its ligand and by means of pharmacological and genetic tools revealed that the major pool of active BRI1 resides in the plasma membrane[25]. Previous reports indicated that BRI1 was endocytosed and present on endosomal structures independent of ligand binding[33,34], yet the implication for signaling were unclear[34,35]. To understand by which endocytic mechanism BRI1-GFP enters the plant cell, AFCS was used to show that BRI1 endocytosis depends on clathrin and ADAPTOR PROTEIN COMPLEX-2 (AP-2)[36]. In addition, AFCS was used as a tool to show that BRI1 is a cargo of the TPLATE adaptor complex, which is required for endocytosis[37]. Thus, thanks to AFCS, light was shed on the BRI1 endomembrane trafficking mechanisms and their implications for signaling, highlighting the importance of functional fluorescent hormone analogs for understanding contextual cellular environments and hormone signaling processes. Other plant

hormones have been labeled for visualization purposes as well, namely gibberellin[38], jasmonic acid[39], and strigolactones[40,41].

Further downstream, the small molecule bikinin has been identified as an inhibitor of a GSK3-like kinase subset, including BIN2[42]. A recent study aimed at increasing affinity for BIN2 and its homologs involved in BR signaling by screening for bikinin analogs with higher activity[42]. An iodo analog of bikinin has been identified with increased potency and its methylated derivatives have been found to be more active than nonmethylated forms. The reason is the rapid hydrolysis upon uptake, making the methyl group a vehicle for enhanced uptake into the cell and, therefore, increased activity. In addition, a novel inactivation mechanism of applied small molecules was detected through conjugation with malate[42]. Bikinin proved to be indispensable for BR research as numerous studies made use of bikinin to reveal BIN2 as a major hub for BR-related crosstalk and to highlight the role of plant GSK3-like kinases in stomatal development[43-45], xylem cell differentiation[46] and lateral root formation[47].

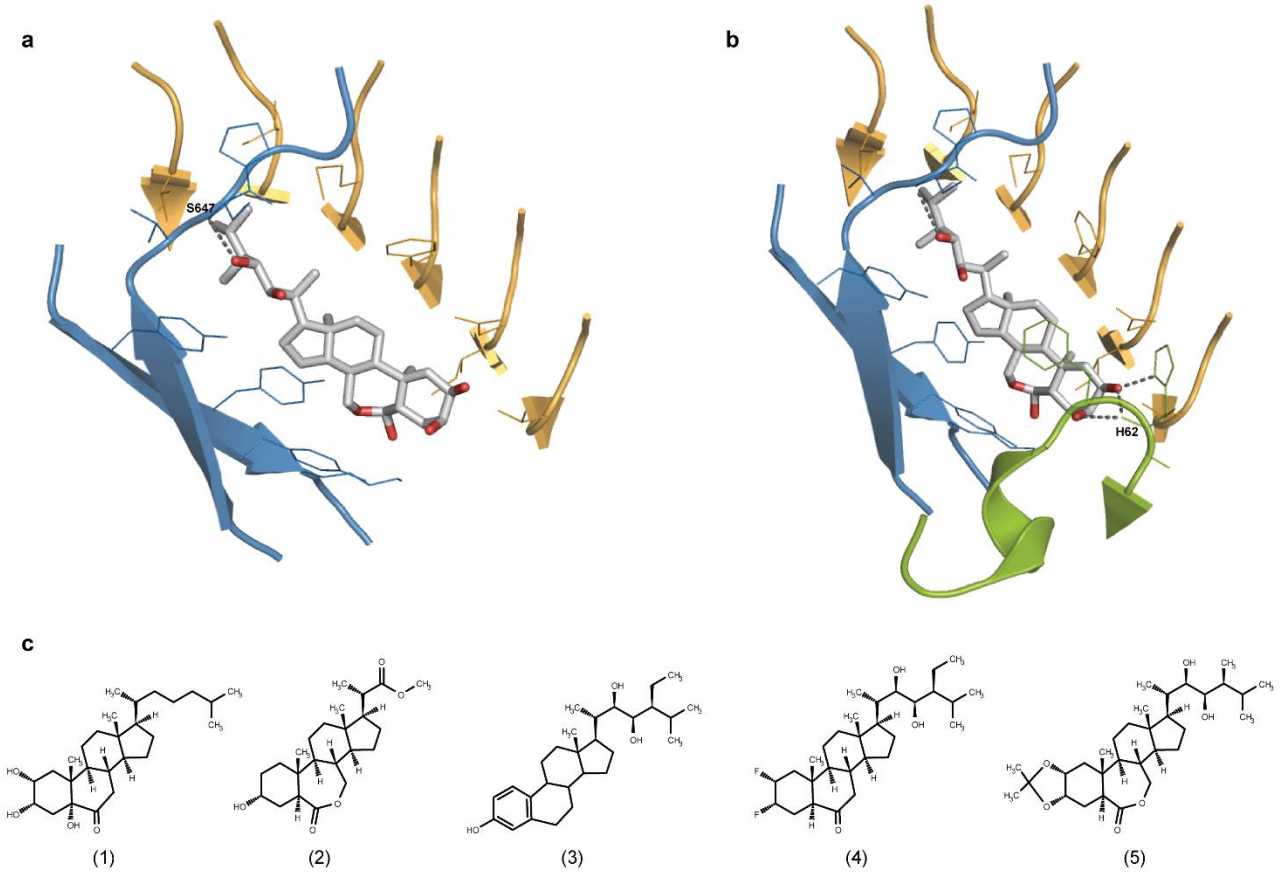

Figure 3. Brassinosteroid analogs as tools to study hormonal recognition.

(a) As revealed by the crystal structure of the BRI1 ectodomain in complex with brassinolide (BL) (PDB code: 3RJ0), the hormonal molecule (stick model; carbons in grey, oxygens in red) binds to a hydrophobic surface formed by amino acid residues (lines representation) from the LRR domain (cartoon model, in yellow) and the island domain (cartoon model, in blue) of BRI1. Besides the hydrophobic interactions with the BL side chain, a direct hydrogen bond (grey dashed line) between the hydroxyl group at C23 position in the steroid and a nitrogen from the main chain of a serine residue (S647) from the island domain is also established (the water-mediated hydrogen bonds are omitted). No polar interactions have been found for the B-ring lactone of BL. In the absence of a co-receptor the hydroxyl groups at C2 and C3 remain solvent exposed. (b) In the BRI1-BL- SOMATIC

EMBRIOGENSIS RECEPTOR KINASE (SERK1) complex (PDB code: 4LSX), the N-terminal cap of SERK1 (cartoon representation, in green) interacts with both the LRR and the island domain of BRI1 as well as with the hormone through hydrogen bond formation between a histidine residue (H62) and the hydroxyl groups at C2 and C3 in the BL molecule (grey dashed lines). (c) Recently created BR analogs, such as sterols with 5α-hydroxy-6-oxo moiety lacking the C22 and C23 OH groups with preserved bioactivity (1) and nonactive derivatives with a carboxyl group (2), have been used to explore the role of the alkyl chain for BR binding to the hydrophobic pocket in BRI1. In turn, active derivatives with an aromatic ring (3), difluorinated analogues with preserved activity (4), and 2,3-acetonides acting as BR antagonists (5) can be used to analyze the involvement of the A ring from the sterol in SERK recruitment and BR receptor complex activation. Crystal structures were visualized using PyMOL molecular viewer (http://www.pymol.org/).

1.2. Small molecules for dissecting endomembrane trafficking: a cross-systems view**

1.2.1. Endomembrane trafficking routes in yeasts, plants and mammals: a comparative view

The eukaryotic endomembrane system is composed of membrane-delimited organelles, small vesicular compartments that shuttle between those organelles and a spectrum of transiently associated, peripheral membrane components from the cytosol that support, regulate and define endomembrane trafficking[48], in a highly dynamic and interconnected manner involving alternating steps of membrane deformation, budding, fission, tethering and fusion. It serves multiple cellular processes essential for survival, including uptake of plasma membrane (PM) cargo and extracellular content, secretion, degradation of cellular content, protein folding and sequestration of ion pools through compartmentalization. Proteins that are co-translationally translocated into the ER are subsequently sorted for trafficking through the Golgi apparatus and the *trans*-Golgi network (TGN). Anterograde transport from the ER is mediated by COPII-coated vesicles which fuse with pre-Golgi intermediates to release their cargo, while Golgi-to-ER protein recycling requires COPI vesicle formation. Unlike mammals, the plant endomembrane system lacks an ER-Golgi intermediate compartment[49]. After reaching the TGN, secretory proteins are packaged into secretory vesicles and targeted to the PM[50]. So far, the secretory route from the TGN to the PM in plants is poorly understood. The TGN compartment also produces clathrin-coated vesicles directed to the lytic compartment (the lysosome in mammalian cells or the vacuole in plants and yeasts). The latter route involves late endosomes (LEs) in mammals, also called prevacuolar compartments/multivesicular bodies (PVCs/MVBs) in plant cells. Unlike mammals, the post-TGN trafficking to the lytic vacuole in plants appears to occur independently of clathrin[51]. Trafficking routes bypassing the LE/PVC/MVB compartment have also been reported in yeasts, mammals and plants[52,53].

The endocytic pathway begins with invagination of the PM and formation of clathrin-coated vesicles through membrane fission. Similar to mammalian and yeast cells, clathrin-mediated endocytosis (CME) appears to be an essential trafficking route in plants, indicating the conservation throughout evolution[54]. Besides CME, growing evidence supports the importance of clathrin-independent endocytosis in mammals, yeasts and plants[55-57]. Most of the cargo internalized by endocytosis undergoes recycling back to the PM. In contrast to mammals, the mechanisms of PM protein recycling in plants are still obscure. A small fraction of the endocytosed cargo is targeted for degradation to the lysosome by passing through early endosomes (EEs), which will gradually maturate into LEs[58].

Adapted from: Mishev, K., Dejonghe, W. & Russinova, E. Small molecules for dissecting endomembrane trafficking: a cross-systems view. *Chem Biol* **20, 475–486 (2013). M. K., D. W. and R. E. wrote the manuscript. D. W. and M. K. designed and made figures. All authors reviewed the manuscript.

Recently, the maturation-based sorting model known from mammalian systems has been considered

in plants in which MVBs/LEs are most likely formed through gradual transformation of parts of the TGN[51].

An additional route to the lysosome and vacuole is provided by autophagy. This process involves the enclosure of cellular contents such as long-lived proteins and organelles by a double membrane structure to form vesicles, called autophagosomes, which will eventually fuse with the lysosome or vacuole in order to degrade their content. Autophagy is an essential process for recycling cellular contents in yeasts, plants and mammals[56,59]. The identification of autophagy-related (*ATG*) genes in *Saccharomyces cerevisiae* and subsequently in other organisms revealed that the molecular machinery responsible for autophagy seems to be well conserved, although plants appear to have a much more diverse array of *ATG* genes to their disposal[56].

Although the fundamental mechanism of intracellular vesicle trafficking appears to be conserved in eukaryotes, there are several notable differences. In contrast to mammalian cells, the TGN in plants is morphologically and functionally distinguished from the *trans* Golgi cisternae[60]. A number of experimental evidences revealed that, the plant TGN possesses features of EEs and is involved in both endocytic and secretory pathways. The TGN in plants can be subdivided into several domains, including domains where secretory vesicles are released to the PM, into domains releasing clathrin-coated vesicles for recycling to the PM and into domains, which mature into MVBs[61]. Another specific feature of the yeast and plant endomembrane systems is the vacuole, which in the plant cell occupies up to 90 % of the total cell volume[61]. Two types of functionally distinct vacuoles coexist in the plant cell, namely protein storage vacuoles (PSVs) and lytic vacuoles which are analogous to lysosomes in mammalian cells[62]. The PSVs can be distinguished by the presence of reserve proteins used mainly during seed germination and by their neutral pH in contrast to lytic vacuoles. However, the two types of plant vacuoles can fuse and give rise to a large central vacuole[63].

1.2.2. In search for small-molecule modifiers of endomembrane trafficking

Small molecules offer major advantages over classical genetics approaches, given the essential and highly dynamic nature of the endomembrane system. Important advantages include the ability to target in a reversible manner essential gene products, but equally important is the scenario where the small molecule targets an entire gene family through perturbation of a common feature of the corresponding proteins, thus addressing redundancy among genes[64,65]. Recent advances in systems biology, bioinformatics and modern cell imaging opened novel opportunities for identifying small molecules that can be used as tools to dissect endomembrane trafficking pathways. Here, we outline the progress in current chemical genetics related to intracellular vesicle trafficking, with an emphasis on the use of small molecules in plants, mammals and yeasts identified through high-throughput screens (**Figure 4**). The central routes and hubs of the endomembrane trafficking network in

eukaryotic cells will be discussed for their sensitivity to the compounds (**Figure 5, Table 1**), which is determined by the extent of conservation of the protein targets. The latter is also reflected in the use of different small molecules across systems (**Figure 6**).

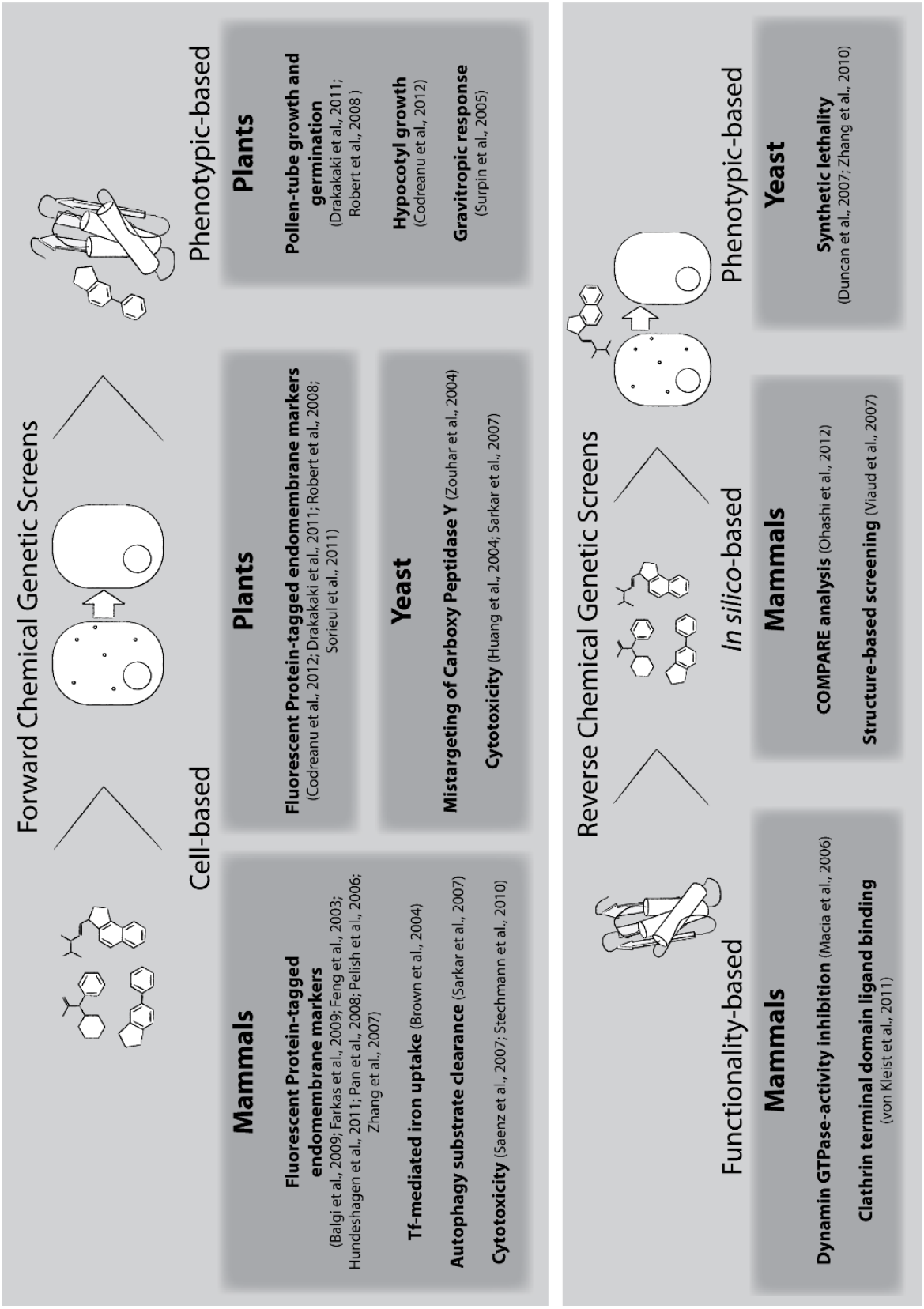

Figure 4 Forward and reverse chemical genetic screens across yeasts, plants and mammals

Forward chemical genetics is represented by cell-based and phenotypic-based screens. Reverse chemical genetics is represented by functionality-based, *in silico*-based and phenotypic-based screens. Only the relevant systems are shown for each screen.

Small bioactive molecules have long been used in medicine and agriculture[66,67]. Recently, large-scale systematic screens have boosted the search for novel chemical regulators for mammalian drug discovery, and this strategy is being rapidly adopted in plants[64,68]. Two types of chemical genetics screens (forward and reverse) have been employed to dissect the endomembrane trafficking in eukaryotes (**Figure 4**).

Forward chemical genetics uses growth phenotype- or cell-based screens for inhibition or activation of a particular cellular process, followed by molecular target identification. Growth phenotype-based forward chemical genetics screens for endomembrane trafficking modulators have been carried out in plants where a high-throughput screen based on the germination and growth of tobacco pollen was used to interrogate more than 46,000 compounds[35,69]. Other growth phenotypes related to endomembrane systems, such as gravitropic responses or cell elongation during hypocotyl growth, were also used in chemical genetics screens[70,71].

The cell-based screens often employ the use of fluorescent marker proteins as readouts for activity or inhibition of trafficking pathways. Examples from the mammalian systems are the high-throughput screen for inhibitors of exocytosis by using BSC1 fibroblast cells infected with GFP-fused vesicular stomatitis virus ($VSVG^{ts}$-GFP)[72], the screen for inhibitors of endocytosis based on transferrin (Tf) receptor-mediated iron uptake in HeLa cells measured by the quenching of calcein fluorescence[73] and the screen for inhibitors of Golgi-mediated trafficking based on the expression of the YFP-tagged Golgi-residing protein p58[74]. Several screens based on autophagosome markers coupled with either GFP or luciferase have assessed the ability of small molecules to affect autophagy[75-78]. Flow-cytometry has also been used to quantify fluorescent protein-based sensors for autophagic and endolysosomal activities in a screen for autophagy modulators[79]. In plants, PM proteins or other endomembrane compartment markers tagged with fluorescent proteins have been used as markers to identify compounds affecting endocytosis, recycling or vacuolar morphogenesis[35,69-71].

Cell-based screens for endomembrane trafficking modulators can also employ other readouts such as cell viability, enzymatic reactions or secretion. For example, cytotoxicity measurements using destabilized firefly luciferase[80] or radioactive-labeled amino acids[81] were used in screens for inhibitors of retrograde trafficking of toxins (shiga, cholera and ricin) in mammalian cells. Small-molecule enhancers and inhibitors of autophagy were identified in a screen for their ability to affect the clearance of the autophagy substrate A53T α-synuclein in mammalian cells[82,83]. In yeasts, high-throughput immunoassays for detection of mis-secreted carboxypeptidase Y (CPY) have been

performed to screen for bioactive compounds which interfere with the sorting of lytic enzymes to the vacuolar lumen[84].

Reverse chemical genetics searches for compounds that inhibit or activate *in vitro* proteins known to be involved in a defined process followed by further characterization of the phenotypic effects at cellular and/or organism level (**Figure 4**). In comparison to forward chemical genetics, this approach has the significant advantage that the targeted protein is known. However, the existence of additional protein targets leading to pleiotropic phenotypes upon chemical treatment *in vivo* cannot be excluded. The reverse chemical genetics strategy has been successful when searching for chemical modulators of protein trafficking components involved in early steps of CME, such as Dynasore and Pitstops[85,86]. Because of the available large collections of deletion mutants, the yeast *S. cerevisiae* has become a powerful tool for small molecule discovery by using synthetic lethality[87]. Synthetic lethality screens were used to identify inhibitors of exocytosis[88] and the trafficking between the TGN and the endosomes[89]. Whole-genome yeast deletion collections have also been screened for responses to chemical libraries in diverse environmental conditions, where genes involved in endomembrane trafficking and vacuolar degradation were found essential for resistance to multiple compounds[90].

Alternative *in silico* screening approaches have enabled the search for novel exocytosis inhibitors in mammals. An example includes an *in silico* screen designed to specifically probe the interaction between the ARF1 GTPase and its guanine exchange factor (GEF) ARNO based on known crystal structures of their complex[91]. Drug sensitivity databases have also been exploited to find novel inhibitors of ARF1 GTPase activation based on functional correlation with compounds with already known properties[92].

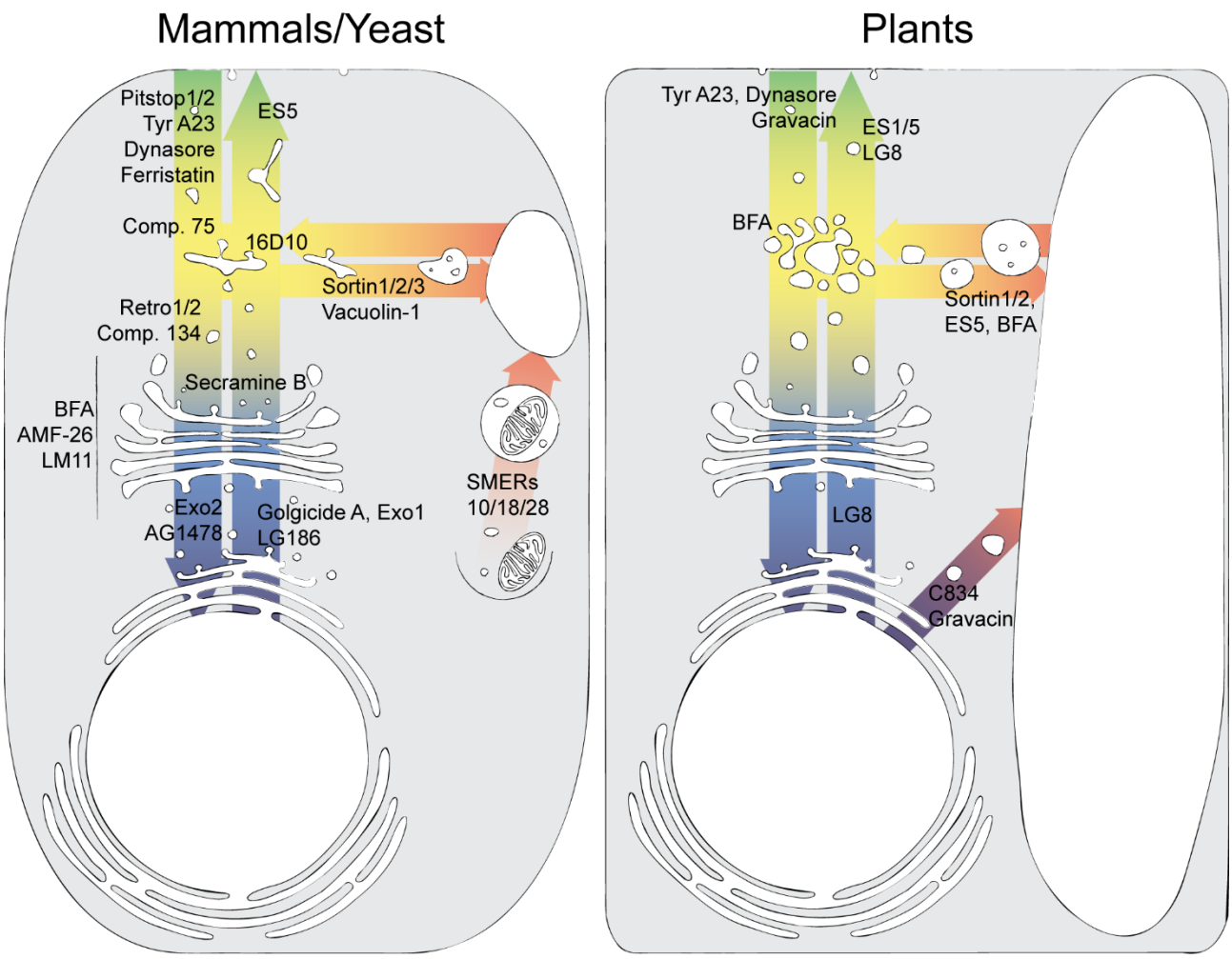

Figure 5 Schematic representation of major trafficking routes and their small molecule effectors in different systems

Shown are a mammalian/yeast cell (left) and plant cell (right). Only endomembrane compartments relevant for this review are shown. Discussed small molecules are indicated close to the compartment or route they affect. Dark blue: nucleus/ER; light blue: Golgi; yellow: EE (mammalian/yeast) or TGN (plants). Yellow to green route: exocytic or recycling pathway with recycling endosomes; green to yellow route: endocytic pathway with endocytic vesicles maturating into EEs. Yellow to red (lysosome/vacuole) route: LE and/or MVB maturation from EE into lysosome/vacuole. Dark blue to red route: Golgi/TGN-independent trafficking from ER to vacuole. Grey (cytosol) to red route: autophagy. Note the absence of an autophagic route in the plant cell since rapamycin has not been shown to affect autophagy in plant cells yet.

1.2.3. Chemical effectors of exocytosis/secretion/anterograde trafficking

In the early 2000s only very few small molecule modulators of the secretory pathways were known. The best example of such an inhibitor of secretion in eukaryotic cells is the fungal macrocyclic lactone Brefeldin A (BFA), which has been instrumental for studying the function of the Golgi[93]. Structural insights into the mechanism of BFA action in mammalian cells have revealed that this compound impedes the interaction between different members of the ARF GTPase family and their associated large GEFs and thus, causes a diversity of effects including tubulation of EEs, redistribution and fusion of the TGN with EEs, and fusion of the ER with the Golgi[94,95]. In contrast to mammalian and

yeast systems, plants, for example *Arabidopsis*, have only large ARF-GEFs, of which some are resistant to BFA[96]. In plants, BFA has been described as an inhibitor of either secretory or endocytic pathways depending on where in the cell, the BFA-sensitive ARF-GEFs are residing[97]. Chemical genetics has been used to search for small molecules with more specific effects on exocytosis than BFA in mammalian systems (**Figure 5, Table 1**). Two compounds structurally different from BFA, Exo1 and Exo2, were found to inhibit the traffic from the ER to the Golgi. Although the direct targets of Exo1 and Exo2 are not known, their mode of action differs from that of BFA[72,98]. Treatment with either Exo1 or Exo2 induces reversible redistribution of Golgi material back to the ER without any concomitant effects on endocytic pathways. In contrast to BFA, Exo1 does not directly inhibit ARF-GEFs and has less effect on the organization of the TGN[72]. The effect of Exo2 on the Golgi and the TGN is similar to that of BFA except that it does not induce tubulation and merging of the TGN and endosomal compartments[98,99]. Therefore, it was proposed that Exo2 is more selective than BFA, possibly inhibiting the function of only the *cis*-Golgi residing ARF-GEF, GBF1. A modified version of Exo2, LG186 was further developed in order to increase selectivity towards GBF1[100]. Another chemical modifier of GBF1 activity, AG1478, was also found to preferentially target the *cis*-Golgi in human cell lines[74].

In contrast to mammalian cells, Exo2 was not active in plant cells[101]. Screening a number of Exo2 derivatives revealed LG8 as an active analog in *Arabidopsis* root cells that causes severe changes in the morphology of the ER and the Golgi, but not the post-Golgi compartments. Unlike BFA, the intracellular targets of LG8 in plants still remain elusive[101].

A high-throughput screen for small molecules that inhibit the toxin retrograde transport has identified a novel inhibitor of protein secretion called Golgicide A (GCA)[80,102]. GCA exhibits BFA-and LG186-like effects by specifically targeting GBF1[100,102]. Other recently identified exocytosis inhibitors, such as AMF-26 and LM11 have been designed to specifically impair the interaction between the ARF1 GTPase and its GEFs in mammals. Although the chemical structure of AMF-26 differs from that of BFA, this compound induces disruption of the *cis*- and *trans*-Golgi, targeting the activation of ARF1 GTPase[92]. To date, BFA is known to inhibit only large, but not small and medium-sized ARF-GEFs[96]. Conversely, LM11 targets the interaction between ARF1 and ARNO, a BFA-insensitive human ARF-GEF. This compound has been shown to induce changes in the Golgi similar to those provoked by BFA, however, it leads to the formation of large endosomal structures differing from the phenotype observed after BFA treatment[91].

The mechanisms of regulation of the anterograde transport from the Golgi to the PM have been approached with the help of Secramine[103]. In mammalian cells, this compound has been shown to perturb the protein export from the Golgi by inhibiting the activation of Cdc42, revealing the essential role of this Rho GTPase for vesicle trafficking. In particular, Secramine targets the association of

Cdc42 with its guanine dissociation inhibitor RhoGDI1 and prevents binding of this Rho GTPase to the Golgi membranes.

1.2.4. Chemical effectors of endocytosis/retrograde trafficking

One way to interfere with endocytosis in mammals and plants is the use of Tyrphostin A23 (TyrA23)[98,104], a low molecular weight compound, which has originally been identified in a chemical screen for inhibitors of protein tyrosine kinases[105]. It has been found that TyrA23, but not its inactive analogue Tyrphostin A51 (TyrA51), perturbs the interaction between the AP-2 adaptor complex and consensus tyrosine-containing motifs in the cytosolic domain of PM cargoes, leading to block of cargo sorting in clathrin-coated vesicles[106]. TyrA23 inhibits both endocytosis and vesiculation at the TGN in plants[97]. Although the function of the plant AP-2 complex is most likely conserved in plants, the target of TyrA23 has not yet been defined. Nevertheless, the use of this compound has been instrumental in studies related to CME in plants[25,36,107-120].

CME in mammals has been successfully approached by means of reverse chemical genetics (**Figure 5, Table 1**), which has been facilitated by the considerable knowledge about the CME machinery in this system. Dynasore has been identified as a non-competitive and reversible inhibitor of the GTPase activity of dynamin, a protein essential for vesicle formation in CME and caveolae-mediated trafficking[85,121]. Dynasore arrests the progression of vesicle coat assembly and the subsequent uncoating. Most of the plant genomes encode dynamin-related proteins, some of which might function in CME[122]. A recent study on the intracellular trafficking of the fungal protein elicitor receptor, LeEix2, demonstrated the use of Dynasore for blocking endocytosis in plant cells[123], yet it remains till date the only study in plants employing Dynasore. In addition, as Dynasore exhibits undesirable side-effects, recent efforts where geared towards improving on the Dynasore scaffold. This led to the generation of the Dyngo series, a group of Dynasore analogues with Dyngo 4a as most potent member in terms of specificity and dynamin inhibition[124]. Supplementing Dynasore and Dyngo series of dynamin inhibitors are the indole-based Dynole series[125,126]. Based on a bisindolylmaleimide scaffold, two generations of focused libraries resulted in Dynole 2-24, the most potent inhibitor of dynamin mediated endocytosis to date[126].

Two structurally different compounds, Pitstop 1 and Pitstop 2, have also been used to elucidate the mechanisms of clathrin-coated pit formation in mammals[86]. Pitstops have been found to compete with clathrin box-containing accessory proteins for a common binding site on the terminal domain of the clathrin heavy chain. Interference with the function of this domain does not affect clathrin recruitment, but Pitstops severely perturb clathrin-coated pit dynamics, due to the inability of clathrin to bind regulatory proteins required for progression in vesicle maturation. Similar to Dynasore, Pitstops induce the accumulation of endocytic intermediates at the PM representing different stages

of this trafficking route. Pitstop 2 was shown to be effective in blocking the internalization of PM cargo markers like the Tf receptor and the epidermal growth factor in mammalian cells through selective impairment of CME[86]. The Pitstop family has been growing over the recent years, including active and inactive analogues of Pitstop 2[127,128], amidst the discussion about specificity of Pitstops towards inhibition of clathrin mediated endocytosis[129-131].

Several compounds identified through forward chemical genetics have been found to target endosomal compartments from the endocytic pathway downstream of the PM. A group of sulfonamides (with a representative member, the compound 16D10) was identified in the Exo screen[72] and shown to affect trafficking from the Golgi to the PM[132]. Although the protein target of this group is unknown, it is likely that sulfonamides exert their action indirectly by suppressing the V-ATPase function, or directly as proton ionophores[132]. Chemical screens for inhibitors of endocytosis of toxins (shiga, cholera and ricin) in mammalian cells facilitated the identification of compounds specifically affecting the retrograde toxin trafficking at the level of recycling endosomes and the Golgi (compound 75 and 134)[80], or the EEs and TGN (Retro-1 and Retro-2) level[81].

Receptor-mediated endocytosis in mammals has been tackled with the use of Ferristatin, which is a selective inhibitor of Tf-mediated iron uptake[73,133]. Interestingly, Ferristatin has led to the discovery of a novel endocytic route for the PM-localized Tf receptor by inducing its enhanced internalization in a clathrin-independent manner[126]. In plants, the limonoid Endosidin 1 (ES1) has been found to induce selective intracellular accumulation of some, but not all, PM cargoes[35]. ES1 specifically affects the trafficking of PM proteins at the level of TGN/EEs through stabilization of actin filaments[134]. Another Endosidin compound , named ES5, has been implicated in the inhibition of PM protein recycling in both plant and mammalian cells[69], whereas the small molecule TENin1[71] was recently reported to inhibit endocytosis and affect trafficking between TGN and PVC/MVB compartments[135].

1.2.5. Chemical effectors of vacuolar trafficking and autophagy

Studies of vacuolar transport and biogenesis have been approached, for the first time, by forward chemical screens in yeast because of the conserved trafficking machinery between yeasts and plants[136] (**Figure 5, Table 1**). Three compounds called Sortin1, Sortin2 and Sortin3 induced secretion of the vacuolar protein carboxypeptidase Y in yeast and affected the morphology of *Arabidopsis* or yeast vacuoles[136]. Although the targets of Sortins are not identified, evidence has been provided that Sortin1 targets the crosstalk between vacuolar biogenesis and transport[137], whereas Sortin2 and Sortin3 affect vacuolar trafficking, possibly by inhibition of the endosomal trafficking[138,139]. Another small molecule linked to vacuolar trafficking is gravacin, which strongly inhibits gravitropism in *Arabidopsis* and blocks the trafficking of tonoplast markers to the vacuolar membrane by a yet unknown mechanism[71].

Larger chemical genetic screens in plants have revealed several more small molecules affecting PM cargo trafficking to the vacuole or vacuolar morphogenesis the targets of which remain to be identified[69]. For example, apart from perturbing the recycling pathway, ES5 has been proven to severely enhance the vacuolar accumulation of PM proteins[69]. Another compound derived from the same screen, namely C834, has been shown to selectively reduce the levels of PM residing proteins paralleled by an increase in their vacuolar targeting[140]. Remarkably, C834 has also been instrumental in revealing the diversity of pathways for trafficking of newly synthesized tonoplast intrinsic proteins to the vacuole[140].

A compound derived from the Exo screen[72], named Vacuolin-1, has been shown to induce the formation of large swollen vacuoles in different mammalian cell types through fusions of endosomes and lysosomes[141,142].

In mammals and yeast, extensive research has gone into identifying small molecule effectors of autophagy. One of the best examples of small molecules affecting autophagy is rapamycin, the well-known inhibitor of the phosphatidylinositol kinase Target Of Rapamycin (TOR)[143,144]. Screens for chemical modifiers of rapamycin identified several small-molecule inhibitors/enhancers of rapamycin (SMIR/SMER) with an effect on autophagy in yeast and mammalian systems[83]. Despite previous reports[145,146], plants are sensitive to rapamycin, which uncovered a role of TOR in glucose metabolism[147].However, in contrast to mammals and yeasts, no direct link between rapamycin and autophagy has yet been shown in plants.

1.2.6. Special considerations when analyzing drug-induced endomembrane trafficking phenotypes

Growing evidence suggests that, when targets of endomembrane effectors are not known, the interpretation of the observed phenotypes should account for possible effects of the compounds on the cytoskeleton dynamics. The endosomal maturation in mammalian cells is dependent on the microtubule network[148] as disruption of microtubules leads to dispersal of LEs and lysosomes throughout the cytoplasm[58]. In turn, formation and motility of EEs and concurrent sorting of internalized proteins for either recycling or lysosomal degradation are largely dependent on the actin dynamics[92,149]. Similarly, stabilizing actin in plant cells by using chemicals interferes with endocytosis and vesicle transport[150]. Examples exist where the observed endomembrane trafficking phenotype in the presence of a bioactive compound is not due to disturbance of the function of an endomembrane protein but rather is a result of a modulation of the cytoskeleton organization. This is illustrated by the endocytic inhibitor ES1, also called prieurianin[35,134]. Recent findings suggest that ES1 acts primarily as an actin stabilizer by an unknown mechanism without affecting the microtubules, thus possibly inhibiting intracellular vesicle movement. The effect of ES1 on actin

dynamics has been observed in both plants and mammals, pointing to conservation of its molecular target in eukaryotes[134]. Another example concerns the use of Secramine which affects the cellular functions of the Rho GTPase Cdc42 and in this way impairs the Golgi-to-PM vesicle trafficking, but also inhibits actin polymerization[103]. Taken together, these examples corroborate the need the chemical screening hits to be routinely tested for their possible impact on the cytoskeleton components. Such studies are already greatly facilitated by the recent advances in light microscopy-based approaches.

Another consideration in studying endomembrane trafficking through chemical biology is the need to discriminate between primary compound-specific effects and general changes in the cellular homeostasis. Essentially all steps from the intracellular vesicle transport are ATP- or GTP-dependent, hence any energy depletion induced by the compound hit would lead to a global disruption of the endomembrane system. Notably, cytotoxicity assays, such as those dealing with ATP content determination, could reveal the borderline dose and time of exposure, beyond which the compound hit induces unspecific responses.

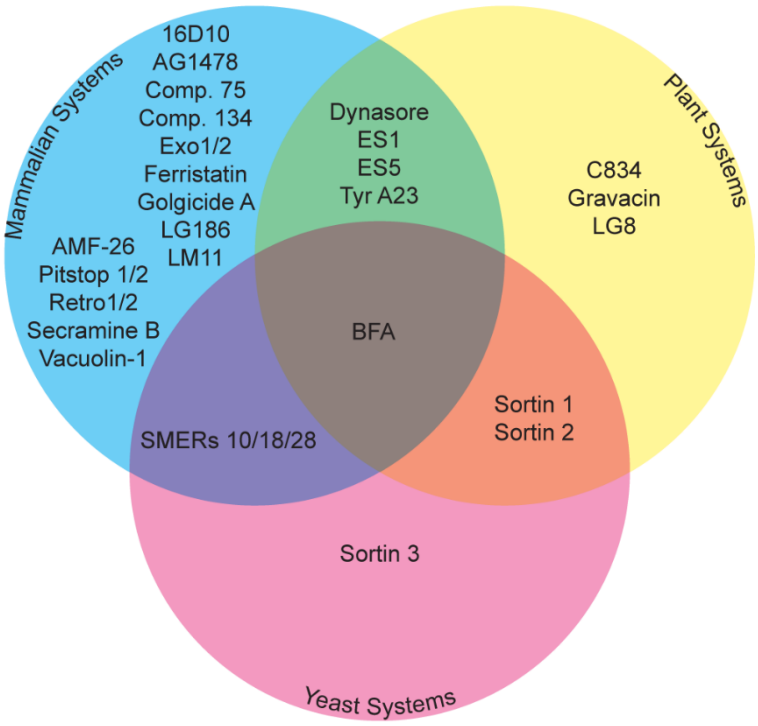

Figure 6 Distribution of discussed small molecules with activity in mammalian, yeast and plant systems.

Small molecules are distributed according to overall activity, thus not specific to endomembrane compartments.

Table 1 Small molecule effectors of endomembrane trafficking identified through large-scale chemical genetic screens

Name	Structure	Affected endomembrane compartment	Known target	Screen	References
Chemical effectors of exocytosis/secretion/anterograde trafficking					
Exo1	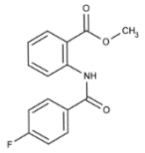	ER to Golgi trafficking		Fluorescence-based imaging screen of VSV-G^{ts} trafficking	Feng et al., 2003
Exo2	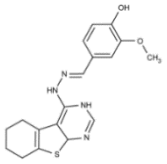	ER to Golgi trafficking, Golgi, TGN	Arf-GEF GBF1	Fluorescence-based imaging screen of VSV-G^{ts} trafficking	Spooner et al., 2008
LG186	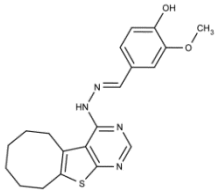	Golgi	Arf-GEF GBF1		Boal et al., 2010
AG1478	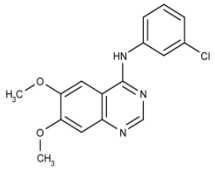	*Cis*-Golgi		P58-YFP based screen in H4 human glioblastoma cells	Pan et al., 2008
LG8	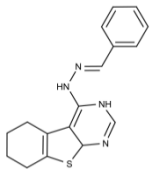	ER, Golgi		Exo2 analog screen for activity in *A. thaliana*	Sorieul et al., 2011
Golgicide A	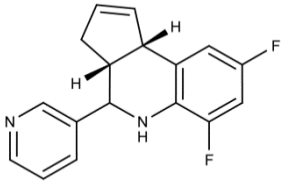	Golgi	Arf-GEF GBF1	Luciferase-based toxin susceptibility screen	Saenz et al., 2009

AMF-26	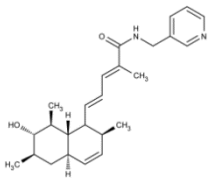	*Cis*- and *trans*-Golgi		COMPARE-guided *in silico* screening	Ohashi et al., 2012
LM11	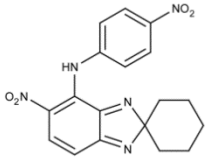	Golgi, endosomal structures	Arf1-GDP/ARNO complex	*In silico* structure-based screen	Viaud et al., 2007
Secramine B	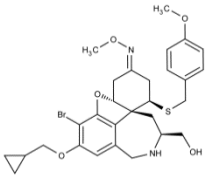	Golgi to PM trafficking	Rho GTPase Cdc42	Fluorescence-based imaging screen of VSV-G^{ts} trafficking	Pelish et al., 2006
Chemical effectors of endocytosis/retrograde trafficking					
Tyrphostin A23	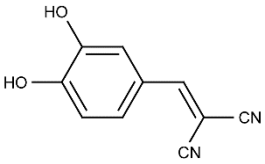	Endocytosis	Interfering between tyrosine motifs and AP2 complex	Screen for tyrosine kinases	Yaish et al., 1988
Dynasore	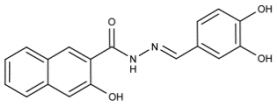	Endocytosis	Dynamin	Dynamin GTPase-activity inhibitor screen	Macia et al., 2006
Pitstop 1	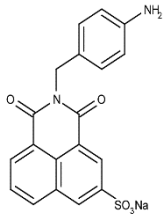	Endocytosis	Clathrin terminal domain (TD)	ELISA-based screen for inhibition of amphiphysin and clathrin TD association	Von Kleist et al., 2011
Pitstop 2	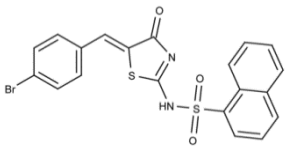	Endocytosis	Clathrin terminal domain (TD)	ELISA-based screen for inhibition of amphiphysin and clathrin TD association	Von Kleist et al., 2011

16D10	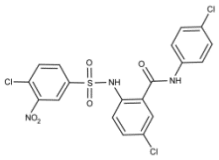	Endosomes, lysosomes	Likely inhibition of V-ATPases or as proton ionophore	Fluorescence-based imaging screen of VSV-G^{ts} trafficking	Nieland et al., 2004
Comp. 75	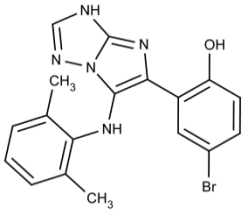	Early retrograde transport		Luciferase-based toxin susceptibility screen	Saenz et al., 2007
Comp. 134	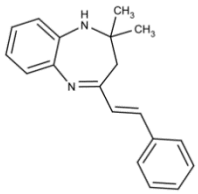	Recycling endosomes to Golgi, retrograde transport		Luciferase-based toxin susceptibility screen	Saenz et al., 2007
Retro-1	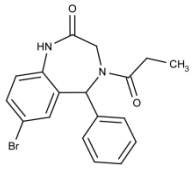	EE to TGN retrograde trafficking		Screen for inhibitors of ricin toxicity	Stechmann et al., 2010
Retro-2	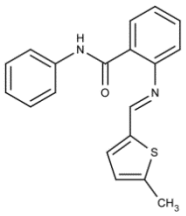	EE to TGN retrograde trafficking		Screen for inhibitors of ricin toxicity	Stechmann et al., 2010
Ferristatin	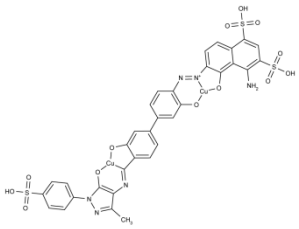	Increased transferrin receptor internalization and degradation		Fluorescence-based screen for calcein quenching	Brown et al., 2004
ES1	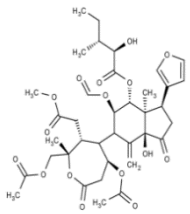	Endosomes		Screen for pollen tube growth and germination inhibitors	Robert et al., 2008

ES5	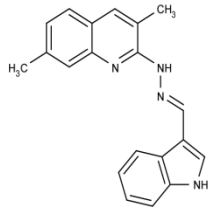	Endosomes, recycling		Screen for pollen tube growth and germination inhibitors	Drakakaki et al., 2011
Chemical effectors of vacuolar trafficking and autophagy					
Sortin 1	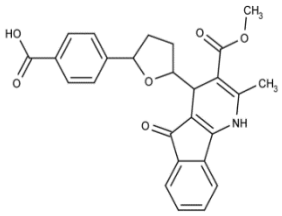	Vacuolar traffic and morphology		Screen for mis-targeting of carboxypeptidase Y	Zouhar et al., 2004
Sortin 2	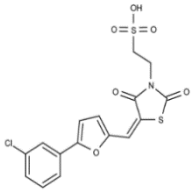	Vacuolar traffic and morphology		Screen for mis-targeting of carboxypeptidase Y	Zouhar et al., 2004
Sortin 3	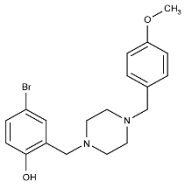	Vacuolar traffic and morphology		Screen for mis-targeting of carboxypeptidase Y	Zouhar et al., 2004
Gravacin	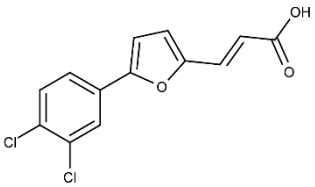	ER to vacuole trafficking	PGP19	Screen for gravitropic response	Surpin et al., 2005
C834	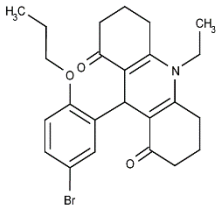	Vacuolar trafficking		Screen for pollen tube growth and germination inhibitors	Rivera-Serrano et al., 2012
Vacuolin-1	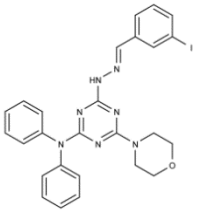	Induction of vacuole formation, inhibition of exocytic PM-lysosome fusion		Fluorescence-based imaging screen of VSV-G^{ts} trafficking	Cerny et al., 2004

SMER 10	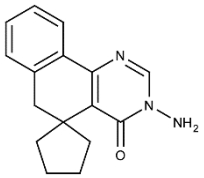	Enhancer of autophagy	Cytotoxicity screen in yeast and autophagy substrate clearance in mammals	Sarkar et al., 2007
SMER 18	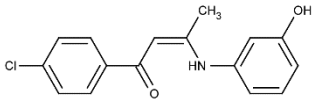	Enhancer of autophagy	Cytotoxicity screen in yeast and autophagy substrate clearance in mammals	Sarkar et al., 2007
SMER 28	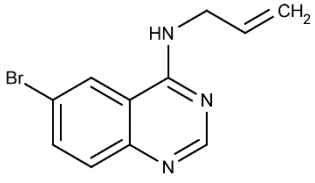	Enhancer of autophagy	Cytotoxicity screen in yeast and autophagy substrate clearance in mammals	Sarkar et al., 2007

1.3. Target Identification Strategies in Plant Chemical Biology***

A proven way to study how something works is to perturb the process of interest in a well-defined and controlled way. In biology, this is often accomplished by introducing alterations in the genome of an organism, such as mutations or ectopic expression. A major disadvantage of working at the gene level, is that the resulting organism will live in a steady state with the induced genetic change. Additionally, perturbation of essential gene functions will lead to lethality, unless conditional, and perturbation of a gene member of a large gene family might have no effect due to redundancy. In order to address gene redundancy and lethality problems, together with the possibility to perturb a system in a more dynamic manner, chemical biology approaches can be adopted. In chemical biology, typically small molecules are applied to a biological system, altering the process of interest by binding target molecules. A key feature of chemical biology is its conditional nature. Small molecules can be applied for any desired time and concentration, and in most cases can be washed out of the system of choice, making them an ideal tool to study dynamic processes for a certain period of time. Crucially, small molecules will not alter an organism over generations and are not restricted to bind only proteins, but can modulate a biological system by binding lipids or nucleic acids[151]. Finally, using different approaches, the target of small molecules needs to be identified in order to get a better understanding of the affected process.

Chemical genetics strategies in plant biology lag behind the animal field, in which drug development provided a plethora of different target identification strategies. In plant biology, most target identification strategies consist of a phenotypical approach or forward genetics strategy based on small molecule resistance screens. A few examples exist of strategies such as affinity purification that were successfully applied[152].

An important aspect of chemical biology is linking the induced phenotype to one or more targets (**Figure 7**). Usually, only the relevant target, or target with the highest affinity for the small molecule is identified and validated, although so-called 'off-targets' might contribute substantially to the overall phenotype. Therefore, it becomes increasingly important to understand and generate the small molecule interactome, in order to explain the observed phenotypes[153]. This becomes especially important for small molecules with a commercial application in healthcare or agriculture.

Several reviews have addressed chemical genetics approaches and aspects in plant biology, and the challenges and opportunities that lay ahead[64,65,154,155]. Other recent reviews include a comprehensive overview of target identification strategies in mostly animal systems[151], and a thorough overview of small molecules with known targets and mode of action in plant biology[152]. Given that plant

***Adapted from: Dejonghe, W. & Russinova, E. Target identification strategies in plant chemical biology. *Front Plant Sci* **5**, 352 (2014). D. W. and R. E. wrote the manuscript. D. W. designed and made the figures. All authors reviewed the manuscript.

biological research is using limited target identification strategies, this review will briefly discuss current target identification approaches, and will mostly focus on emerging new strategies, which have not found a broad application in plant biology yet (**Table 2**). Where applicable, examples from plant biology will be given, and benefits and shortcomings will be discussed.

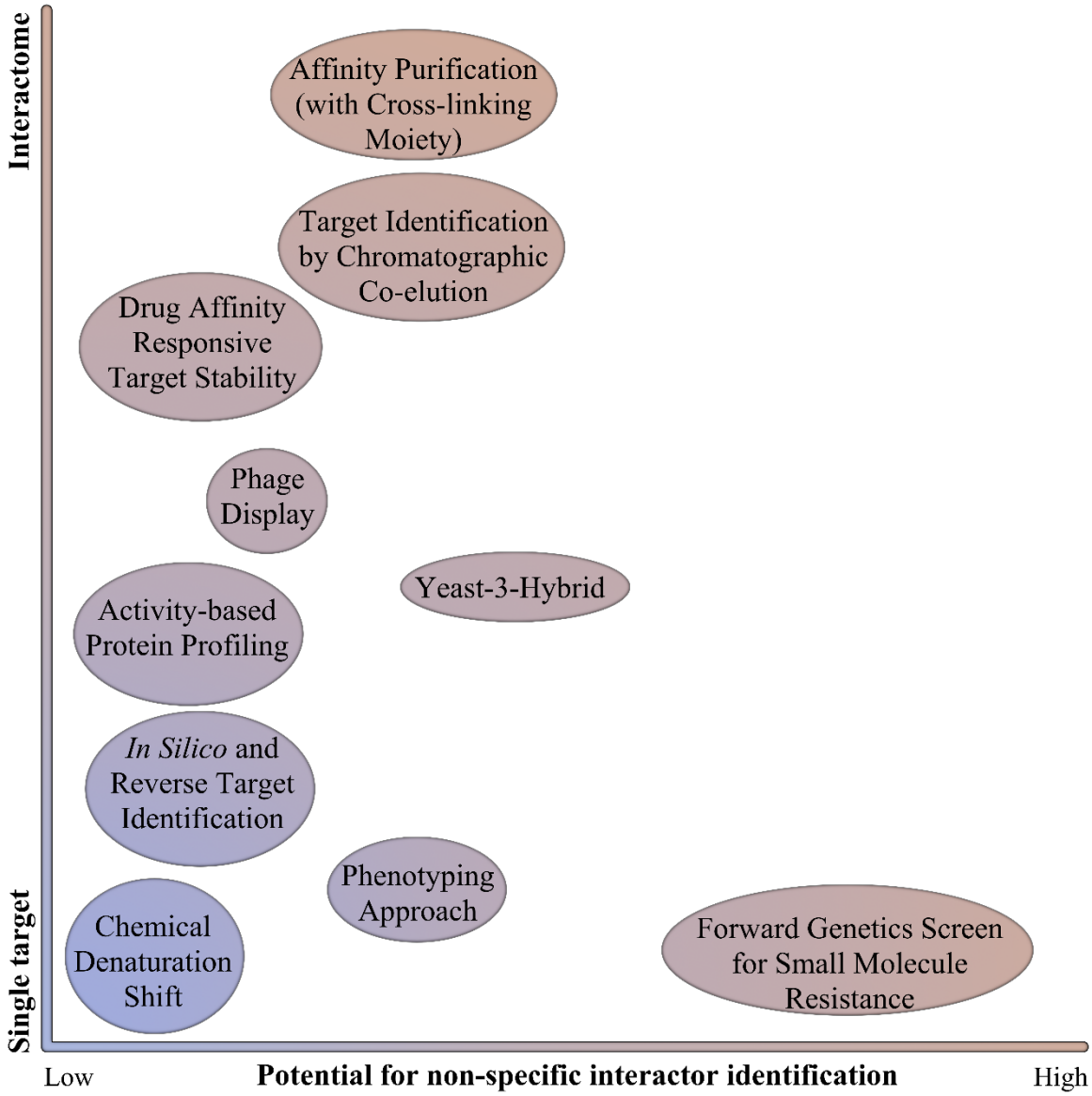

Figure 7. Schematic representation of target identification strategies.

Target identification strategies are represented in function of their ability to identify only one target or several targets (interactome), and the potential to identify non-specific interactors (e.g. proteins which will confer resistance or induce the appropriate readout without actually binding specifically the small molecule).

1.3.1. Commonly used target identification strategies in plant chemical biology

1.3.1.1. Forward genetic screen for compound resistance

Forward genetic screen for compound resistance is a commonly used target identification strategy in plant chemical biology where a mutant population is grown in the presence of small molecules and screened for resistance. Selected resistant individuals are subsequently characterized in terms of their mutations. A major disadvantage is the inherent selection against targets with an essential gene product, provided that the induced mutation induces a knock-out or renders the protein inactive. Essential gene targets might still be selected in case the mutation allows proper protein function, but prevents the small molecule from binding. Additionally, gene redundancy can prevent identification of the target, and certain mutations might render plant resistance to compound treatment, without affecting the true target. A small molecule called 'non-auxin-like lateral root inducer' or naxillin illustrates the latter scenario. Identified from a screen for small molecules able to enhance lateral root development, naxillin was found to affect lateral root development more specifically than auxin. The only identified resistant mutant from an ethylmethane sulfonate (EMS)-mutagenized *Arabidopsis* population, *naxillin resistant 1* (*nar1*), proved to be affected in the *INDOLE-3-BUTYRIC ACID RESPONSE 3* (*IBR3*) gene, which is involved in the conversion of idole-3-butyric acid (IBA) to indole-3-acetic acid (IAA). The identification of *nar1* helped to reveal that naxillin acts upstream of auxin signaling by positively affecting the IBA to IAA conversion at specific sites in the root, thereby inducing lateral root development, but failed to identify the true target of naxillin[156]. Major advantages of the forward genetic screen approach are the straightforward experimental setup and the availability of high-throughput next-generation sequencing techniques, which allow relatively quick target identification once the resistant individuals are identified.

Whether or not mutants are more sensitive to the compound depends on the nature of the mutation. Resistant mutants might occur from mutations affecting small molecule binding, or from the absence of the target protein, although the latter is not applicable to proteins with essential function. Alternatively, less, or no protein might mean a higher sensitivity of the mutant, as less small molecule is required to exert the same phenotypical effect. This dosage response is in line with resistance to the small molecule upon over expression of the target protein.

Examples of such approach are the identification of targets for pyrabactin, gravacin and DAS734. The synthetic seed germination inhibitor pyrabactin was shown to act as a specific agonist of abscisic acid (ABA). Specific because transcriptional responses for seed growth in presence of ABA compared to pyrabactin were highly correlated, while this was not the case in seedlings[157]. Pyrabactin allowed to identify the PYR/PYLs (for "pyrabactin resistance" and "PYR-like"), members of the ligand binding cyclase subfamily of the START protein superfamily, through a forward genetics screen for compound resistance since pyrabactin targets the conserved ABA binding domain [157,158]. This protein family was independently identified as RCAR (for "regulatory component of ABA

receptor")[159]. The PYR/PYL/RCARs were shown to be ABA receptors[157], which after perception bind to type 2C protein phosphatases, thereby inactivating them. The role as ABA receptor for the PYR/PYL/RCAR protein family was later confirmed by crystallographic data[158].

Gravacin was identified as an inhibitor of the gravitropic response in *Arabidopsis* seedlings[71]. A population of 220,000 EMS-mutagenized F2 seeds were screened for a gravitropic response when grown on gravacin, identifying through a map-based cloning approach an E to K substitution in the gene coding for P-GLYCOPROTEIN 19 (PGP19)[160]. Several different mutant alleles for PGP19 showed resistance to gravacin, confirming the identified mutation as the cause of gravacin resistance. Furthermore, the authors could show that gravacin binding to PGP19-containing microsomes in *pgp19* mutants was severely reduced compared to wild type controls[160].

A phenyltriazole acetic acid compound, DAS734, was identified as a potent bleaching agent of developing leaves. Addition of adenine could alleviate the effects, hinting toward a target in the purine biosynthesis pathway[161]. A screen for DAS734 resistance of 480,000 EMS-mutagenized *Arabidopsis* ecotype Col-0 seedlings resulted in several resistant lines, some of which had the same mutation. Map-based cloning identified *glutamine phosphoribosylamidotransferase 2* (*GPRAT2*) as the gene containing all mutations[161]. Expression of *AtGPRAT2* in *E. coli* allowed to purify the protein, and to evaluate its activity in the presence of DAS734. The small molecule was able to potently inhibit GPRAT2 activity in a slow, but reversible manner. In addition, expression of the mutant *GPRAT2* gene in *E. coli*, identified in the forward genetics screen, showed an increase in the inhibitory concentration (IC_{50}) of more than 500 times, indicating a strong resistance to DAS734, and confirming GPRAT2 as its target[161].

1.3.1.2. Phenotyping approach

Opposed to a forward genetics approach, the phenotyping approach usually starts from a screen of small molecules against an appropriate readout for the biological process of interest, followed by further tests which narrow down the possible target proteins. Biochemical validation is used to confirm the hypothesized target protein. The requirement for proper readouts, which is applicable for known signaling pathways and enzymes involved in primary and secondary metabolism, is a potential drawback. Processes of highly organized, rapid and dynamic nature, such as endomembrane trafficking, or unknown processes will be much harder to approach with such strategy. As one searches specifically within a process of interest, this approach usually will yield only one target, or target family, but cannot provide an overall picture of small molecule interactors. The latter implies however that target identification can be fairly straightforward because the search is directed. Some recent examples are the identification of targets for bikinin, kynurenine imprimatins and Jarin-1.

The small molecule bikinin was identified in a screen for molecules able to induce phenotypes similar to those caused by the application of the most active BR, BL, in young *Arabidopsis* seedlings[42]. The target of bikinin was identified through comparative phenotypical analysis of different BR-related mutants grown on bikinin. As bikinin was able to rescue a gain-of-function *bin2-1* mutant to wild type, it was hypothesized that the GSK3-like kinase BIN2 is the direct target. This hypothesis was confirmed by *in vitro* binding studies. In addition, the list of bikinin targets was expanded to other *BIN2* homologs and it was suggested that a competition with ATP is the mode of compound action.

The selective aminotransferase inhibitor affecting local auxin biosynthesis, L-Kynurenine (kyn), was identified in a screen for suppressors of the constitutive ethylene response[162]. Although kyn did not rescue the constitutive ethylene response phenotypes of the *eto1-2* and *ctr1-1* mutants and wild type plants treated with the synthetic ethylene precursor 1-aminocyclopropane-1-carboxylic acid, it did rescue the shortened root phenotype at submicromolar concentrations. Kyn was shown to inhibit ETHYLENE INSENSITIVE 3 (EIN3) accumulation in *Arabidopsis* roots, which led to a reduction of local auxin responses. Since active ethylene signaling increased the reduction of local auxin responses in presence of kyn, it was concluded that kyn represses ethylene-mediated auxin responses[162]. Further unraveling of auxin responses led to the hypothesis that kyn might inhibit TRYPTOPHANE AMINOTRANSFERASE OF ARABIDOPSIS1 (TAA1). Enzymatic activity tests of kyn on purified TAA1 confirmed it as a competitive and potent inhibitor, thereby inhibiting the conversion of tryptophan to indole-3-pyruvic acid. Computational modeling confirmed kyn as a competitive inhibitor of TAA1, outcompeting tryptophan. In addition, when tryptophan was applied in excess, it reversed the inhibitory effects of Kyn[162].

The third example comes from a screen for small molecules affecting disease resistance in plants, which identified five small molecules belonging to two different structural groups, named imprimatins[163]. The authors showed an increase of salicylic acid (SA) in treated plants, but unlike control plants, after pathogen infection imprimatins did not accumulate the inactive form of SA, SA-2-O-β-D-glucoside (SAG), which usually increases in parallel with an increase in SA. An enzymatic test on UGT74F1 and UGT76B1, two enzymes that convert SA to its inactive form SAG, confirmed imprimatins as inhibitors of these enzymes. The authors concluded that the increased *Pst-avrRpm1*-induced cell death after imprimatins treatment is due to an inhibition of SA to SAG conversion.

The last and most recent example concerns Jarin-1, a small molecule inhibitor of jasmonate responses identified through a screen for suppression of LIPOXYGENASE2 (LOX2) expression in presence of jasmonic acid (JA) methyl ester (JAMe)[164]. Its binding to the biosynthetic enzyme JASMONATE RESISTANT1 (JAR1), which conjugates JA to isoleucine to form the active JA-Ile conjugate, was shown through narrowing down on possible candidate target proteins by evaluating different JA induced cellular responses, and eventually enzymatic assays with purified JAR1. Jarin-1 was subsequently shown to inhibit JAR1-mediated synthesis of JA-Ile *in planta*[164].

1.3.1.3. *In silico*-based target identification strategies

Not only forward, but also reverse and *in silico* design strategies have been successfully used. The starting point is a protein of interest, or a small molecule scaffold. Screening of additional small molecules aims at finding a specific interactor for the protein of interest, or at improving binding characteristics for an existing small molecule. A validation step *in vivo* confirms the findings of the reverse or *in silico* strategy.

A first example concerns a study of more than a decade ago in search of novel inhibitors of imidazole glycerol phosphate dehydratase (IGPD), an attractive herbicide target[165]. Based on previously identified IGPD triazole inhibitors[166], a pharmacophore model was developed to search available 3D-databases[165]. A pharmacophore model contains spatial information on functional groups essential for small molecule action. The model was used to search commercial databases of about 370,000 small molecules in total. From the approximately 1,200 hits, small molecules, which were too high in molecular weight or too expensive, were excluded. From the resulting 140 hits, a group of bispyrroles proved to be interesting from a chemistry perspective and was chosen to perform a substructure search on about 600,000 small molecules. Finally a group of monopyrrole aldehydes was selected as a new class of IGPD inhibitors with activity in the low micromolar range. As this group does not fit the original pharmacophore model perfectly, it might be possible this new group acts through a different mechanism as the original triazole inhibitors[165].

A second example illustrates a screen for inhibitors of monogalactosyldiacylglycerol (MGDG) synthesis in *Arabidopsis*, which made use of *E. coli* lipid vesicles containing recombinant MGD1 and a small molecule library of a little less than 24,000 entries. After initial screening, a new set of small molecules was put together based on chemical similarities with the hits from the first screen, which led to a selection of 2 small molecules: galvestine-1 and 2, two competitive inhibitors relative to diacylglycerol (DAG) of MGDG synthases MGD1, 2 and 3[167].

1.3.2. Emerging target identification strategies in plant chemical biology

1.3.2.1. Activity-based protein profiling (ABPP)

The activity-based protein profiling (ABPP) target identification strategy relies on small molecules with a so-called ‘warhead’, which react with residues in the active site of enzymes in an irreversible manner[168]. The small molecules are attached via a linker to a functionality such as biotin for affinity purification, or to a fluorophore for visualization. Since the small molecules react with their respective target proteins to form a covalent bond, no additional cross-linking is required for further affinity

purification. However, not every small molecule is capable of reacting with its target protein, therefore ABPP is only applicable for such small molecules. Equally, not every protein will react with a small molecule to form a covalent bond, and thus ABPP results in a substantially less complex proteome, which facilitates a more straightforward analysis. Importantly, ABPP enables to assign activity to a certain protein, not only within the entire proteome, but also within a certain family of proteins, thereby creating sub-classes based on activity. Recent examples of the use of ABPP are illustrated by studying the mode of action of the bicyclic hydantoin and several serine hydrolases (SHs) inhibitors in *Arabidopsis*.

Different putative SH inhibitors were employed in a competitive ABPP approach to evaluate the effect in *Arabidopsis*[169]. Competitive ABPP assesses the ability of small molecules to compete with ABPP probes. A reduced labeling by the probe in presence of the small molecule indicates binding of the small molecule to the protein(s) under investigation. A rhodamine-tagged fluorophosphonate (FP) and a trifunctional nitrophenol phosphonate (TriNP) tagged with both rhodamine and biotin were used as ABPP probes. The main finding of the study was a differential sensitivity of different *Arabidopsis* SHs to the SH inhibitors tested[169]. An additional study on SHs reports the development of a paraoxon-like para-nitrophenol phosphonate activity-based probe predominantly labeling carboxylesterase12 in *Arabidopsis*[170].

The bicyclic hydantoin sparked the attention when it was found as a side product from synthesis efforts for syringolins[171]. To identify a molecular target from *Arabidopsis* cell cultures, the bicyclic hydantoin was labeled with biotin and rhodamine, and both versions were used to either detect or pull down the protein target. An affinity purification coupled with a mass spectrometry (MS) was used to identify the glyceraldehyde 3-phosphate dehydrogenase GAPC1 and GAPC2 as targets of the bicyclic hydantoin. Both GAPC1 and GAPC2 were heterologously expressed in *E. coli*, and shown to bind the rhodamine-tagged bicyclic hydantoin in an activity dependent manner[171].

1.3.2.2. Yeast 3-hybrid

The yeast 3-hybrid (Y3H) approach relies on the principles of the yeast 2-hybrid (Y2H) technology, but employs a modified small molecule of interest to allow interaction between the DNA-binding domain and the transcriptional activator (**Figure 8**). When initially described[172], Y3H was based on the Y2H system using the LexA DNA-binding domain and the trans-activation domain from the bacterial protein B42[173]. The so called 'hook' consisted of the LexA DNA-binding domain fused to the hormone-binding domain of the rat glucocorticoid receptor. The latter binds to dexamethasone, which is part of the hybrid small molecule comprising dexamethasone and FK506, or the 'bait'. Finally, the 'fish' consisted of human FKBP12 (for 12-kDa FK506-binding protein) fused to the transcriptional activator B42. FK506 is an immunosuppressant drug in the mammalian field, and the

small molecule interactor of FKBP12. For screening purposes, FKBP12 represents any cDNA library of choice, whereas FK506 represents the small molecule of interest.

To date, Y3H in plant chemical biology was used in an attempt to identify targets for small molecules with implications in plant defense responses[174]. The Y3H system used to this end was based on the LexA DNA-binding domain fused to dihydrofolate reductase (DHFR), which binds with high affinity to methotrexate (Mtx), and was used previously with success[175]. The hybrid ligand was composed of Mtx fused via a polyethylene glycol (PEG) linker to several small molecules, namely JA, ABA, compound 8 (cpd 8), cucurbic acid (CA), cucurbic acid methylester (CAMe) and 2,6 dihydroxybenzoic acid (6OH-SA). The 'fish' was a collection of cDNA libraries from wounded or pathogen infected leaves and inflorescence from *Arabidopsis*, fused to the GAL4 transcriptional activator[174]. Although no targets were identified for Mtx-ABA and Mtx-JA, and no interaction could be shown when the known ABA and JA receptors were expressed as 'fish', potential target proteins were identified for the other small molecules. This study validates Y3H as a target identification strategy for plant chemical biology.

The Y3H technique has a few notable advantages as it allows to screen for small molecule-protein interactions *in vivo*; to correct for low abundant proteins, and to easily identify the target protein(s) or even interacting protein domains. In addition, it allows for the identification of essential gene products, and should make it straightforward to identify an entire protein family as the target of a small molecule. However, although Y3H is an *in vivo* method, the ability of the protein to bind the small molecule of interest is assessed out of its biological context and one protein at a time, and therefore is less suited if small molecules require more than one protein to bind or the proper biological context. Moreover, proteins not able to translocate to the yeast nucleus such as trans-membrane or membrane associated proteins cannot be screened, and the fact that the small molecules need to be modified, and the occurrence of multi-drug resistance in yeast can pose a problem. Variants of the Y3H system have been described[151], but have not found an implementation in plant chemical biology yet.

An improved version of Y3H screening is based on covalent labeling of SNAP-tag fusion proteins[176]. The SNAP-tag is based on the human O^6-alkylguanine-DNA alkyltransferase which will covalently attach the alkyl group of its substrate to one of its cysteine residues. As its substrate specificity is not so high, it can also accept O^6-benzylguanine (BG) as a substrate[177]. The Y3H is modified in such a way that the DNA-binding domain LexA is fused to a SNAP-tag, and the small molecule of interest is derivatized with BG[176]. The improved Y3H approach includes first, the use of a triple mutant for broad-spectrum drug-transporters. Second, false-positives are eliminated by a negative selection using 5-fluoroorotic acid in the absence of the modified small molecule, and later colonies are grown both in the presence and absence of the modified compound to score for specific interactions.

Additionally, growth of colonies in the presence of the 'bait' and an excess of free, unmodified small molecule could potentially pinpoint colonies expressing a specific target, as the free small molecule will out-compete the 'bait', thereby preventing further growth or reporter expression[172]. The SNAP-tag can also be combined with a GST-tag and thus, the GST-SNAP-tagged fusion protein can readily be used in affinity purification approaches with the same modified small molecules[176].

Concerning synthesis of the modified small molecule for Y3H, a recent study evaluated the length and nature of the linker[178]. An important conclusion using a triazole-containing linker opposed to a PEG linker was the lower background growth of yeast in the presence of a negative control, and thus a decreased amount of possible false-positives.

1.3.2.3. Affinity-based technologies

A much less explored target identification strategy in plant chemical biology is affinity purification. Typically, a derivatized small molecule is generated consisting of a selectivity function, which is the small molecule of interest, bound via a linker moiety to a tag such as biotin, which allows target isolation from a complex mixture. Incubation of an appropriate lysate with the modified compound, immobilizing it on a solid support, and subsequent washing of unbound proteins enables isolation of target proteins for liquid chromatography and MS analysis (**Figure 8**). As such, the general principle of this approach is shared with ABPP.

Crucial for derivatization is structure activity relation (SAR) analysis. SAR analysis involves testing a collection of analogs of the original small molecule to assess which functional groups and moieties are essential for its activity. SAR analysis is not only important for derivatization, but can also provide crucial information about the mode of action of small molecules. A good illustration of the latter is sirtinol, identified as an inhibitor of sirtuin deacetylases in yeast and human cells[179]. Sirtinol in *Arabidopsis* was characterized as an enhancer of auxin signaling, and was found to bind and inhibit SIRTINOL RESISTANT 1 (SIR1), a negative regulator of auxin signaling upstream of the *Aux/IAA* genes. *SIR1* and other *SIR* genes encode proteins involved in molybdopterin biosynthesis, and the incorporation of molybdenum to form molybdenum cofactor (moco), an essential cofactor in for example aldehyde oxidases. The target was identified through a sirtinol resistance screen on 60,000 EMS-mutagenized *Arabidopsis* seeds[180]. A later study however, showed that sirtinol is enzymatically or non-enzymatically hydrolyzed into 2-hydroxy-1- naphthaldehyde (HNA). HNA is subsequently converted by a moco-containing aldehyde oxidase into 2-hydroxy-1- naphtoic acid (HNC). The latter is an active auxin analog, hence explaining the sirtinol induced phenotypes[181].

An important advantage of affinity purification is the ability to probe for target proteins of any molecular process of interest, hence any small molecule can be potentially used, and does not require activity toward the target in contrast to ABPP. It provides the possibility to uncover the small molecule interactome, thus not only the main target, but also 'off-targets', which might contribute to

the observed phenotype. The latter implies that specific readouts should be available to distinguish the target of interest from off-targets in the validation procedure. Additionally, affinity purification yields data on potential targets as well as biochemical proof of binding, provided proper controls are included.

A variant of affinity purification consists of the incorporation of a cross-linking moiety, which results into the formation of a tri-functional probe. These so called 'capture compounds' consist of a selectivity function which is the small molecule of interest, a reactivity function, which is the cross-linking moiety, and a sorting function (e.g. Biotin)[182-184]. The cross-linking moiety usually is activated by UV-light, thereby forming covalent bonds with proteins in close proximity. As the small molecule-target interaction is secured by a covalent bond, washing can be stringent, removing unspecific binders, and, hence, incorporating a cross-linking moiety might solve problems with weak interactions and low abundant or less accessible protein targets. Crucial for both affinity purification and procedures involving cross-linking moieties are proper controls, to distinguish 'true' targets from non-specific interactors. Preferably an inactive analog of the small molecule modified in the same way is used, but it should be noted that inactivity in vivo does not necessarily mean it will not bind the target protein in a lysate, as inactivity might be due to altered uptake. In addition, the 'interactome' used for the solid phase (e.g. streptavidin coated beads), or the linker with biotin alone might serve as an essential background list. Equally, multiple repeats with different probes can distinguish targets from background signals in a statistical manner. Competition experiments with unmodified compounds may reveal specific binders from non-specific binders, and serve as an essential control. However, in order to detect a competition with the unmodified small molecule, quantification of eluted proteins is required. To this end, stable isotope labeling with amino acids in cell culture (SILAC)[185,186] can be used or other forms of differential labeling of peptides or proteins[187,188]. In short, two samples are prepared and differentially labeled (e.g. heavy and light) according to the SILAC protocol. Both samples are differentially treated: one with the probe only, the other with the probe and free small molecule in competition. If the concentration of the free small molecule is high enough, and it has a higher affinity toward the target than the modified small molecule, specific targets should not be retained after pull-down. Subsequent combination of both samples in a 1:1 ratio and MS analysis results in a distinguishable peptide pair originating from the different samples as they only differ by their isotopic mass-difference. Non-specific binders should be represented by peptides of equal intensity for both samples, opposed to peptides representing specific binders, as those peptides should be much lower in intensity due to the imposed competition with the free small molecule[186]. Additional issues might arise if the target protein is low abundant, or when of hydrophobic nature.

One of the first examples of compound photo-affinity labeling in plant research concerns the modification of atrazine with a photo-reactive azido group. The subsequent azido-atrazine was

radioactively labeled to allow detection of covalently bound polypeptides on a polyacrylamide gel[189]. Although atrazine is a well-characterized inhibitor of photosystem II reactions, and azido-atrazine was shown by the authors to act in a very similar way, target identification stops at the level of radioactively labeled polypeptides of 32-34 kDa on a polyacrylamide gel, be it from purified chloroplast thylakoids.

A second example is given by efforts to identify the molecular target of the small molecule responsible for nyctinastic leaf movement of *Albizzia saman*[190]. The tri-functional probe consisted of the small molecule of interest, a jasmonate glucoside, benzophenone as the reactivity function and biotin as the selectivity function. Additionally, an inactive enantiomeric analog was modified in the same way, serving as a control[190]. Both probes were activated at 365nm, and SDS-PAGE analysis revealed a differential band, which disappeared using the unmodified small molecule as competitor. Until now to our knowledge no examples exist in plant research of an affinity purification approach without covalent binding to the target protein.

A third example concerns the biotin-labelled photoaffinity castasterone (BPCS)[24]. This report shows the ability of castasterone, one of most active BRs aside BL[1], to bind the receptor BRI1. The binding site is mapped to an island domain in between LRR21 and LRR22 of the extracellular domain of BRI1. This observation was later confirmed by structural data of BRI1 in complex with BL[22;23].

In order to circumvent the bio-availability problems that are likely to arise with biotin tags or fluorophores attached to the small molecule, a two-step labeling of small molecules was optimized in *Arabidopsis* using so called mini-tags, based on azide and alkyn functional groups[191]. The well-known cystein-protease inhibitor E64 was used to study and establish the two-step labeling technique. Because E64 is a covalent inhibitor of its targets, the two-step labeling consists of a first modification of E64 with a mini-tag, minimizing interference of the tag on E64 activity and bioavailability. After incubation of the sample with modified E64, a second step attaches biotin modified with the appropriate mini-tag in a click-chemistry reaction, allowing subsequent purification and detection of the target protein[191]. One of the main advantages is the ability to label *in vivo*, which, in the explained setup is not possible for small molecules that do not bind covalently to their target protein. This problem can be solved by introducing a photo-activatable group together with a mini-tag, which allows cross-linking *in vivo*, with subsequent preparation of the lysate and attaching biotin for affinity purification.

Although *in situ* proteome profiling with a small molecule modified for photo-cross-linking has the advantage of identifying target proteins in the proper biological context, care should be taken with possible effects of UV irradiation on the proteome. Certainly if exposure remains for several minutes, damage might be induced, which eventually might compromise the final protein target list.

In order to perform *in situ* proteome profiling, the small molecule of choice should be modified with a photo-cross-linking group, together with a group which allows additional bioorthogonal modification, usually done with a clickable group. In this way, after cross-linking in live cells, a group for affinity purification or visualization can be added afterward. The latter option allows the usage of a technique called fluorescence difference in two-dimensional gel electrophoresis (FITGE). This method uses two samples, one labeled with the active small molecule, the other with an inactive form or other control, and labels both samples with a different fluorophore. This differential labeling allows detecting both samples together on a 2D SDS-PAGE gel. Spots that are labeled by both fluorophores are probably because of unspecific binding events, whereas spots only labeled with the fluorophore attached to the active small molecule are potential hits that can be identified by subsequent MS approaches[192]. Differences between lysates and live cells as starting material were reported, where live cells might likely provide more reliable target identification and can be even a requirement to detect the main target.

1.3.2.4. Phage display

The phage display strategy relies on whole, fragmented cDNA or random peptide sequences being translationally fused to the phage coat protein, so that the peptides are displayed on the outside. An immobilized small molecule can retain those peptides binding to the small molecule. A subsequent bacterial infection allows to identify selected peptides. A recent example in plants used a quartz-crystal microbalance (QCM) biosensor in combination with T7 phage display and the receptor-ligand contacts (RELIC) bioinformatics server to identify binding sites of brassinazole (Brz2001) on the cytochrome P450 DWF4[13]. Brz2001 is an improved version of brassinazole, a BR biosynthesis inhibitor acting at the level of DWF4, which catalyzes the rate limiting hydroxylation of the C22 position in the BR biosynthesis[1,6,7].The QCM measures voltage-induced crystal vibrations on a gold electrode, which will decrease as the overall mass on the gold electrode increases. A modified version of Brz2001 was used, which forms a monolayer on the gold electrode. The QCM-measured vibrations will decrease as peptides bind the immobilized small molecule. A random 15-mer peptide library was incubated with the Brz2001-covered gold electrode, which resulted in the identification of 34 peptides. Subsequent use of the RELIC bioinformatics platform[193] identified within the 34 selected peptides a subset of amino acids potentially involved in small molecule binding which map to a potential disordered loop of DWF4[13].

Given the possibility to modify the small molecule of interest, and the ability to coat the gold electrode, this technique allows for a quick assessment of possible target proteins. It allows for a coverage of the proteome without the possibility of missing out on low abundant proteins due to the easy amplification of the signal by bacterial infection. It is less suited for those interactions requiring

post-translational modifications, very hydrophobic peptides, and protein-small molecule interactions, for which several amino acid residues involved in binding are scattered across the protein primary sequence. When the small molecule only binds if the appropriate amino acid residues are forming a binding pocket after protein folding, phage display with a random small peptide library will likely not work. Phage display with entire proteins might solve the problem, but will select against any hydrophobic protein, besides the possibility that the protein might not fold properly.

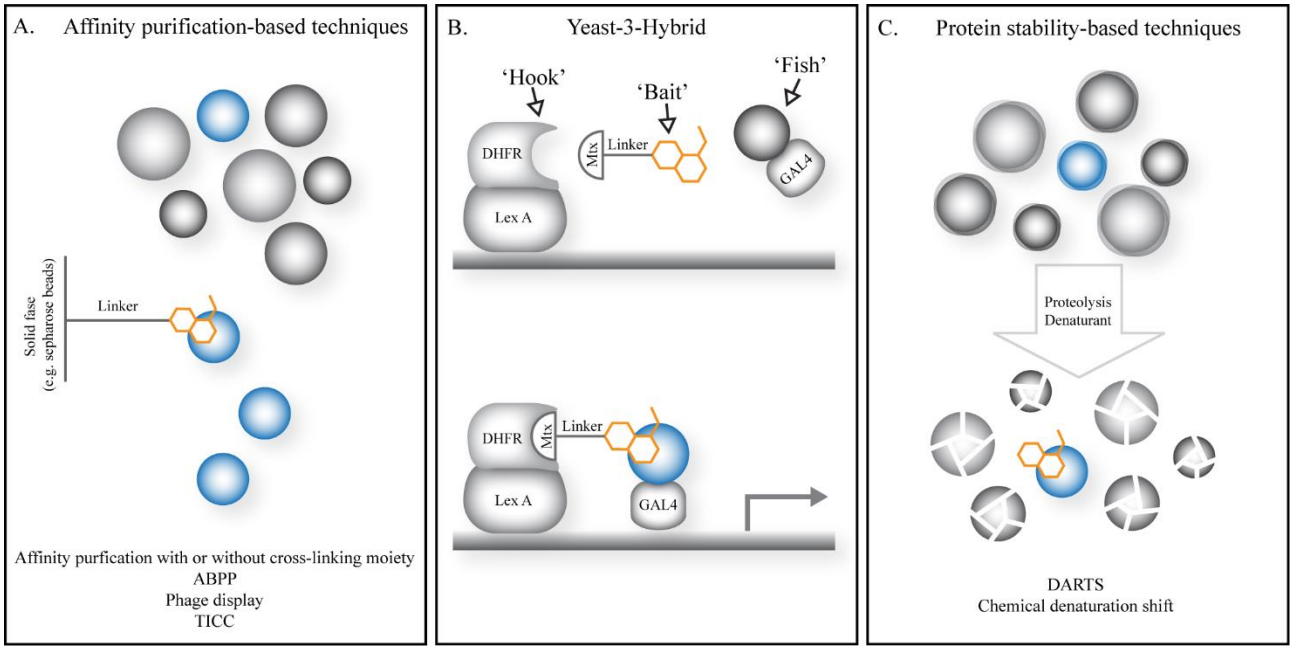

Figure 8. General principle of emerging and novel target identification strategies in plant chemical biology

A. Strategies relying on the affinity of the small molecule to isolate the target protein from a complex mixture such as a lysate or cellular environment. B. The yeast-3-hybrid approach employs the activation of a transcriptional response by bringing together a DNA binding domain and transcriptional activator via a fusion of the small molecule of interest and a known small molecule with high affinity for a known protein target. The latter is fused to the DNA binding domain. The small molecule probes a cDNA library fused to the transcriptional activator. C. Strategies relying on increased protein stability employ small molecules to stabilize the increased dynamics, instability and degradation upon treatments such as denaturants or proteases, preventing or slowing down target protein degradation. Grey spheres: non-target proteins; blue spheres: target protein; orange cartoon: small molecule of interest; Lex A: Lex A DNA binding domain; Mtx: methotrexate; DHFR: dihydrofolate redutase, target protein of Mtx; GAL4: GAL4 transcriptional activator.

1.3.3. Label-free compound based technologies

An obvious drawback of affinity purification is the requirement for 'taggable' positions on the small molecule of interest. In addition, the small molecule should still be active with at least part of the intended modification (e.g. the linker), as the modification might hinder proper binding of the small molecule to its targets. Efficient isolation of the target is also dependent on the affinity of the small molecule, as low affinity interactions might be lost during washing. Therefore, rather gentle washing

conditions should be used, which have the disadvantage of generating extensive lists of possible target proteins. In an effort to solve these problems, approaches which do not require labeled small molecules are being developed.

1.3.3.1. Chemical denaturation shift

One way of testing ligand interactions is by measuring protein stability, which is dependent on a number of factors, including temperature, denaturants and ligand binding. An increase of protein stability, and thus denaturing conditions, to higher temperatures is indicative of ligand binding. Classically, this is measured by fluorescence or differential scanning calorimetry[194,195]. However, as estimations on binding affinities require prior knowledge on enthalpy and heat capacity of protein denaturation and ligand binding, such an approach is not suited for high throughput screening, because binding thermodynamics are yet unknown for small molecules in a library. Additionally, the rank order given to small molecule interactors based on the induced shift in protein denaturation temperature (T_m) is not necessarily the same at the physiological temperature and the measured T_m. An alternative approach was proposed based on a chemical denaturation shift[196], where instead of measuring T_m, the increase in concentration of a denaturant is measured required to denature the protein in the presence of its ligand. Although the study is an optimization and proof of concept of the chemical denaturation shift approach, it illustrates the usability to provide proof of ligand binding, and is additionally suited for high throughput screening setups in a reverse chemical genetics strategy.

1.3.3.2. Target identification by chromatographic co-elution (TICC)

Another example of a label free approach is the TICC technology[197]. The idea is to look for a shift in the retention time of the small molecule of interest in a complex protein mixture compared to the small molecule alone during non-denaturing high performance liquid chromatography. The shift in retention time would be indicative of binding to a particular protein target, which can be identified by further deconvolving the fraction in which the small molecule elutes by additional complementing and orthogonal fractionations. Key to the success of this approach is the ability to separate free from protein-bound ligand[197].

1.3.3.3. Drug affinity-responsive target stability (DARTS)

The DARTS approach takes advantage of the stabilization of a protein target upon small molecule binding, thereby rendering the protein less susceptible to proteolytic digestion[198,199]. This idea also formed the basis for the chemical denaturation shift approach[200]. DARTS can be used to confirm a

certain small molecule-protein interaction by specifically evaluating proteolytic digestion via western blotting, but equally can be used to evaluate possible new small molecule-protein interactions by looking at entire lysates. Although the latter situation might result in visibly stabilized targets when high abundant, low abundant target proteins might not be readily visible on gel[199].

Both DARTS and TICC share some important advantages. First they are label free, require no derivatization and use the original small molecule. This is not only important in terms of small molecule tolerance toward modification, but also saves time, as SAR analysis can be limited. A second important advantage is their independency of any protein nature, mode of action or model system. Both techniques solely rely on affinity of the small molecule for its target protein. The latter also dictates an inherent weakness: interactions of lower affinity might be missed. Both techniques have their specific weaknesses too. While membrane proteins remain challenging for TICC, DARTS is not applicable to any protein, as some proteins are more resistant to digestion and might be missed. In addition, the small molecule might interact in such a way that digestion of the protein is not, or hardly affected.

Table 2. Overview of the target identification strategies

Target identification strategy	**Examples[a]**	**Modified small molecule**	**References**
Established strategies			
Forward genetics screen for small molecule resistance	Pyrabactin, gravacin, DAS734	No	Park et al. (2009), Rojas-Pierce et al. (2007), Walsh et al. (2007)
Phenotyping approach	Bikinin, kynurenine, imprimatins, Jarin-1	No	De Rybel et al. (2009), He et al. (2011), Noutoshi et al. (2012) Meesters et al. (2014)
In silico and reverse target identification	IGPD inhibitors, galvestine 1 and galvestine 2	No	Schweitzer et al. (2002), Botté,et al. (2011).
Emerging strategies			
Activity-based protein profiling	Bicyclic hydantoin, serine hydrolases	Yes	Kaschani et al. (2012a, 2012b)
Yeast-3-Hybrid	Jasmonic acid, abscisic acid, compound 8, cucurbic acid, cucurbic acid methylester, 2,6 dihydroxybenzoic acid	Yes	Cottier et al. (2011).
Affinity purification with cross linking moiety	Atrazine, a jasmonate glucosate	Yes	Pfister et al. (1981), Nakamura et al. (2008), (Kinoshita et al., 2005)
Phage display	Brz2001	Yes	Takakusagi et al. (2013)

Promising strategies			
Affinity purification	None yet	Yes	Ziegler et al. (2013)
Chemical denaturation shift	None yet	No	Schön et al. (2013)
Target identification by chromatographic co-elution	None yet	No	Chan et al. (2012)
Drug affinity responsive target stability	None yet	No	Lomenick et al. (2009)

[a]The examples correspond with those given in the text.

1.4. Future perspectives

To date BR research has benefited from four different classes of small molecules, namely brz-based molecules, the ketoconazole scaffold-containing molecules, BR analogs, and bikinin-based molecules. Brz and bikinin have both been used extensively. Brz resistance screens have recently led to the discovery of several components involved or related to BR signaling[200-203] and bikinin revealed crosstalk between BR signaling and other developmental pathways[43-47]. Although the major components of BR signaling and biosynthesis are known, small molecules can still play an important role. The recent characterization of YCZ-18 as an inhibitor of BR biosynthesis is a good illustration of the potential of new small molecules, as it targets CYP90D1 (**Figure 2**), a different biosynthetic enzyme as DWRF4[204]. It therefore offers the opportunity to inhibit BR biosynthesis in an alternative way, which potentially offers the ability to assess the role of different BR biosynthetic intermediates on cell growth and development. Small molecules can also offer opportunities to dissect different molecular functions within the same protein. For example, the recent insights gained on the kinase domains of BRI1[205] and BAK1[206] could provide a reverse chemical genetics platform for the development of small molecules targeting specific domains of the kinase. This would allow altering interactions and output of the kinase in a dynamic and reversible manner. As illustrated before[207], the development of specific agonists, or antagonists, both chemically and at the target protein level, could constitute a small molecule toolbox which allows specific targeting of BR signaling components. This in turn would allow a better understanding of crosstalk between different BR signaling components and a plethora of other developmental, growth or stress responses. In addition, affinity purification with tagged small molecules could improve our understanding on binding partners of components involved in BR signaling and biosynthesis. Finally, because little is understood about the molecular mechanisms involved in delivering BR upon biosynthesis to the site of BRI1 perception at the PM, small molecules might serve to disrupt or visualize molecular components involved.

BR signaling in relation to endomembrane traffic has benefited from a pharmacological approach as well[25,36,37]. A collection of small molecules that can provide valuable new hit molecules to decipher

the endomembrane regulation of BR signaling, transport or turnover has been obtained from a large-scale screen for inhibitors of pollen germination and growth[69]. A number of chemicals have been identified in a secondary screen for small molecules capable of affecting endomembrane trafficking of BRI1-GFP, which when explored might provide valuable leads for BR research. Taken together, the above examples of chemical biology approaches illustrate the potential of small molecule tools for BR research in the future.

Not only the studies of the relation between BR signaling and endomembrane traffic, but also studies of endomembrane traffic in general will benefit from the small molecule screen for inhibitors of pollen germination and growth[69] This is exemplified by two recent reports on the characterization of ES7[208] and ES8[209]. ES7 was characterized as an inhibitor of callose deposition during cell plate maturation, and has since been used in localization studies of different RAB GTPases involved in cell plate formation[210], while ES8 was shown to affect early secretory pathways mediated by GNOM and GNOM-LIKE1, with effects on polar distribution of the auxin efflux carrier PIN-FORMED1 (PIN1). Although ES8 and the other examples of endomembrane affectors described in this introduction will likely provide important insights on endomembrane traffic in the future, target identification and knowledge on off-target proteins contributing to the overall phenotype are lacking for most of them, yet is an important step in developing the hit molecule as a research tool, and by extension as agrochemical or drug. Depending on which aspect of plant biology the small molecule of choice is affecting, and what the intended use will be, knowledge on the interactome of the small molecule is essential. Since the induced phenotype is only the sum of multiple affected targets, a deconvolution of the phenotype toward the individual contributions of the affected targets is of paramount importance. To this end, current commonly used target identification strategies in plant biology fall short. Therefore, an evolution toward more biochemical and alternative strategies is required. Surprisingly, one of the most successful target identification strategies in animal research is much less used in plant research: affinity purification. Although the technique has important shortcomings such as the need for small molecule modification and the preference for abundant soluble protein targets, it is one of the few strategies capable of revealing the small molecule interactome. Several variants exist of the basic affinity-based pull-down principle to accommodate for shortcomings of the technique, and their implementation in fundamental plant biology research as well as in a more commercial research environment should spur our understanding of dynamic cellular mechanisms. In addition, development of affinity purification based approaches in combination with other well-established techniques might provide additional dimensions to the interactome resulting from classic affinity-based setups. One such example is Chem-seq, in which a combination of affinity purification and chromatin immunoprecipitation (ChIP) technology can provide new insights in the role of small molecules at a genome-wide level[211].

Other approaches more established in other systems than plants, besides the ones mentioned in this introduction, might find their way into plant biology as well. A possible example could be multi-copy suppression profiling, where the central idea relies on increased tolerance toward the small molecule if the target protein is present in higher copy numbers[158]. Similarly to EMS-screens, overexpression line collections such as activation-tag collections could be screened for more tolerance toward small molecules. Problems with gene redundancy and lethality would be overcome, and identification of the potential target should be simple. Equally, one overexpression line could be used to screen an entire collection of small molecules for more tolerance. In addition, adaptation of the Cellular Thermal Shift Assay (CETSA)[212] for target identification purposes might be the onset towards a relatively easy strategy to identify possible target proteins without the need of small molecule modification. The technique relies on increased stability of the target protein in presence of the small molecule at higher temperatures, according to a similar principle as DARTS and the chemical denaturation shift. The major difference with the latter two is that CETSA works at the cell and even tissue level[210]. In addition, a recent report illustrates the compatibility of CETSA with a proteome-wide assessment of small molecule binding to target proteins[213], which opens the possibility to assess small molecule binding to target proteins for the entire proteome, without modification, and at the cell or tissue level. Computational approaches are likely to find their way into plant chemical biology as well, and will mature into essential tools for target and off-target predictions for any new small molecule tool in plant chemical biology, given the surge of new algorithms in mammalian drug discovery[214,215]. A major limitation for plant chemical biology, and holding back the breakthrough of computational approaches, is the availability of large scale data-bases and repositories for small molecule data in plant biology.

Finally, the choice for a particular target identification strategy greatly depends on the aim of the study and available resources, yet considering several complementary approaches to prove protein target binding will only make the study stronger. Although initial efforts to setup an affinity purification target identification approach are greater compared to for example resistance screens, affinity purification has important advances over the well-established target identification strategies in plant biology. Therefore, plant biology can only benefit from adapting affinity-based target identification approaches in future chemical biology projects.

This thesis aims at adopting new and less common target identification strategies as part of the characterization of small molecule affectors of BR signaling and endomembrane traffic. As such we hope to develop new chemical tools for cell biology , which can probe endomembrane traffic in a specific way, and provide new insights into the complex relation between BR signaling and endomembrane traffic. The small molecules will be derived from the previously mentioned screen

for inhibitors of pollen germination and growth[69], and further screened to identify hit molecules targeting BR signaling and specific aspects of endomembrane traffic.

1.5. Acknowledgments

We would like to thank Martine De Cock and Annick Bleys for help in preparing the manuscripts.

1.6. References

1. Vriet, C., Russinova, E. & Reuzeau, C. From squalene to brassinolide: the steroid metabolic and signaling pathways across the plant kingdom. *Mol Plant* **6**, 1738–1757 (2013).
2. Zhu, J.-Y., Sae-Seaw, J. & Wang, Z.-Y. Brassinosteroid signalling. *Development* **140**, 1615–1620 (2013).
3. Wang, W., Bai, M.-Y. & Wang, Z.-Y. The brassinosteroid signaling network-a paradigm of signal integration. *Curr Opin Plant Biol* **21**, 147–153 (2014).
4. Yang, X.-H., Xu, Z.-H. & Xue, H.-W. Arabidopsis membrane steroid binding protein 1 is involved in inhibition of cell elongation. *Plant Cell* **17**, 116–131 (2005).
5. Wang, Z.-Y. et al. Nuclear-localized BZR1 mediates brassinosteroid-induced growth and feedback suppression of brassinosteroid biosynthesis. *Dev Cell* **2**, 505–513 (2002).
6. Asami, T. et al. Characterization of brassinazole, a triazole-type brassinosteroid biosynthesis inhibitor. *Plant Physiol* **123**, 93–100 (2000).
7. Sekimata, K. et al. A specific brassinosteroid biosynthesis inhibitor, Brz2001: evaluation of its effects on Arabidopsis, cress, tobacco, and rice. *Planta* **213**, 716–721 (2001).
8. Rademacher, W. Growth retardants: Effects on Gibberellin Biosynthesis and Other Metabolic Pathways. *Annu. Rev. Plant Physiol. Plant Mol. Biol.* **51**, 501–531 (2000).
9. Hartwig, T. et al. Propiconazole is a specific and accessible brassinosteroid (BR) biosynthesis inhibitor for Arabidopsis and maize. *PLoS ONE* **7**, e36625 (2012).
10. Sekimata, K. et al. A specific and potent inhibitor of brassinosteroid biosynthesis possessing a dioxolane ring. *J. Agric. Food Chem.* **50**, 3486–3490 (2002).
11. Asami, T. et al. Selective interaction of triazole derivatives with DWF4, a cytochrome P450 monooxygenase of the brassinosteroid biosynthetic pathway, correlates with brassinosteroid deficiency in planta. *J Biol Chem* **276**, 25687–25691 (2001).
12. Sekimata, K. et al. Brz220 interacts with DWF4, a cytochrome P450 monooxygenase in brassinosteroid biosynthesis, and exerts biological activity. *Biosci Biotechnol Biochem* **72**, 7–12 (2008).
13. Takakusagi, Y. et al. Mapping a disordered portion of the Brz2001-binding site on a plant monooxygenase, DWARF4, using a quartz-crystal microbalance biosensor-based T7 phage display. *Assay Drug Dev Technol* **11**, 206–215 (2013).
14. Rozhon, W. et al. Genetic variation in plant CYP51s confers resistance against voriconazole, a novel inhibitor of brassinosteroid-dependent sterol biosynthesis. *PLoS ONE* **8**, e53650 (2013).

15. Oh, K., Yamada, K., Asami, T. & Yoshizawa, Y. Synthesis of novel brassinosteroid biosynthesis inhibitors based on the ketoconazole scaffold. *Bioorg. Med. Chem. Lett.* **22**, 1625–1628 (2012).
16. Yamada, K., Yoshizawa, Y. & Oh, K. Synthesis of 2RS,4RS-1-[2-phenyl-4-[2-(2-trifluromethoxy-phenoxy)-ethyl]-1,3-dioxolan-2-yl-methyl]-1H-1,2,4-triazole derivatives as potent inhibitors of brassinosteroid biosynthesis. *Molecules* **17**, 4460–4473 (2012).
17. Yamada, K., Yajima, O., Yoshizawa, Y. & Oh, K. Synthesis and biological evaluation of novel azole derivatives as selective potent inhibitors of brassinosteroid biosynthesis. *Bioorg. Med. Chem.* **21**, 2451–2461 (2013).
18. Oh, K., Yamada, K. & Yoshizawa, Y. Asymmetric synthesis and effect of absolute stereochemistry of YCZ-2013, a brassinosteroid biosynthesis inhibitor. *Bioorg. Med. Chem. Lett.* **23**, 6915–6919 (2013).
19. Hoshi, T., Matsumoto, T., Yamada, K., Yoshizawa, Y. & Oh, K. Synthesis of New Brassinosteroid Biosynthesis Inhibitor with Coumarin Moiety as a Fluorescent Probe. *Int J Chem Eng Appl*. **5**:379-383 (2014).
20. Piotrowska, A. & Bajguz, A. Conjugates of abscisic acid, brassinosteroids, ethylene, gibberellins, and jasmonates. *Phytochemistry* **72**, 2097–2112 (2011).
21. Bajguz, A. Brassinosteroids — occurence and chemical structures in plants. In Brassinosteroids: A Class of Plant Hormone. *Springer* 1–27 (2011).
22. Hothorn, M. et al. Structural basis of steroid hormone perception by the receptor kinase BRI1. *Nature* **474**, 467–471 (2011).
23. She, J. et al. Structural insight into brassinosteroid perception by BRI1. *Nature* **474**, 472–476 (2011).
24. Kinoshita, T. et al. Binding of brassinosteroids to the extracellular domain of plant receptor kinase BRI1. *Nature* **433**, 167–171 (2005).
25. Irani, N. G. et al. Fluorescent castasterone reveals BRI1 signaling from the plasma membrane. *Nat Chem Biol* **8**, 583–589 (2012).
26. Sun, Y. et al. Structure reveals that BAK1 as a co-receptor recognizes the BRI1-bound brassinolide. *Cell Res* **23**, 1326–1329 (2013).
27. Santiago, J., Henzler, C. & Hothorn, M. Molecular mechanism for plant steroid receptor activation by somatic embryogenesis co-receptor kinases. *Science* **341**, 889–892 (2013).
28. Rosado-Abón, A., de Dios-Bravo, G., Rodríguez-Sotres, R. & Iglesias-Arteaga, M. A. Synthesis and plant growth promoting activity of polyhydroxylated ketones bearing the 5α-hydroxy-6-oxo moiety and cholestane side chain. *Steroids* **77**, 461–466 (2012).
29. Kvasnica, M. et al. Biological activities of new monohydroxylated brassinosteroid analogues with a carboxylic group in the side chain. *Steroids* **85**, 58–64 (2014).

30. Acebedo, S. L., Alonso, F., Ramírez, J. A. & Galagovsky, L. R. Synthesis of aromatic stigmastanes: application to the synthesis of aromatic analogs of brassinosteroids. *Tetrahedron* **68**, 3685–3691 (2012).
31. Acebedo, S. L., Alonso, F., Galagovsky, L. R. & Ramírez, J. A. Synthesis and biological activity of ring-A difluorinated brassinosteroids. *Steroids* **76**, 1016–1020 (2011).
32. Muto, T. & Todoroki, Y. Brassinolide-2,3-acetonide: a brassinolide-induced rice lamina joint inclination antagonist. *Bioorg. Med. Chem.* **21**, 4413–4419 (2013).
33. Russinova, E. et al. Heterodimerization and endocytosis of Arabidopsis brassinosteroid receptors BRI1 and AtSERK3 (BAK1). *Plant Cell* **16**, 3216–3229 (2004).
34. Geldner, N., Hyman, D. L., Wang, X., Schumacher, K. & Chory, J. Endosomal signaling of plant steroid receptor kinase BRI1. *Genes Dev* **21**, 1598–1602 (2007).
35. Robert, S. et al. Endosidin1 defines a compartment involved in endocytosis of the brassinosteroid receptor BRI1 and the auxin transporters PIN2 and AUX1. *Proc Natl Acad Sci USA* **105**, 8464–8469 (2008).
36. Di Rubbo, S. et al. The clathrin adaptor complex AP-2 mediates endocytosis of brassinosteroid insensitive1 in Arabidopsis. *Plant Cell* **25**, 2986–2997 (2013).
37. Gadeyne, A. et al. The TPLATE adaptor complex drives clathrin-mediated endocytosis in plants. *Cell* **156**, 691–704 (2014).
38. Shani, E. et al. Gibberellins accumulate in the elongating endodermal cells of Arabidopsis root. *Proc Natl Acad Sci USA* **110**, 4834–4839 (2013).
39. Gao, Y. H., Yu, Y., Hu, X. G., Cao, Y. J. & Wu, J. Z. Imaging of jasmonic acid binding sites in tissue. *Anal. Biochem.* **440**, 205–211 (2013).
40. Rasmussen, A. et al. A fluorescent alternative to the synthetic strigolactone GR24. *Mol Plant* **6**, 100–112 (2013).
41. Prandi, C. et al. Strigolactone analogs as molecular probes in chasing the (SLs) receptor/s: design and synthesis of fluorescent labeled molecules. *Mol Plant* **6**, 113–127 (2013).
42. De Rybel, B. et al. Chemical inhibition of a subset of Arabidopsis thaliana GSK3-like kinases activates brassinosteroid signaling. *Chem Biol* **16**, 594–604 (2009).
42. Rozhon, W. et al. Bikinin-like inhibitors targeting GSK3/Shaggy-like kinases: characterisation of novel compounds and elucidation of their catabolism in planta. *BMC Plant Biol* **14**, 172 (2014).
43. Kim, T.-W., Michniewicz, M., Bergmann, D. C. & Wang, Z.-Y. Brassinosteroid regulates stomatal development by GSK3-mediated inhibition of a MAPK pathway. *Nature* **482**, 419–422 (2012).

44. Gudesblat, G. E. et al. SPEECHLESS integrates brassinosteroid and stomata signalling pathways. *Nat Cell Biol* **14**, 548–554 (2012).
45. Khan, M. et al. Brassinosteroid-regulated GSK3/Shaggy-like Kinases Phosphorylate Mitogen-activated Protein (MAP) Kinase Kinases, Which Control Stomata Development in Arabidopsis thaliana. *J Biol Chem* **288**, 7519-7527. (2013).
46. Kondo, Y. et al. Plant GSK3 proteins regulate xylem cell differentiation downstream of TDIF–TDR signalling. *Nat Commun* **5**, 3504 (2014).
47. Cho, H. et al. A secreted peptide acts on BIN2-mediated phosphorylation of ARFs to potentiate auxin response during lateral root development. *Nat Cell Biol* **16**, 66–76 (2014).
48. Foresti, O. & Denecke, J. Intermediate organelles of the plant secretory pathway: identity and function. *Traffic* **9**, 1599–1612 (2008).
49. Robinson, D. G., Herranz, M.-C., Bubeck, J., Pepperkok, R. & Ritzenthaler, C. Membrane Dynamics in the Early Secretory Pathway. *Critical Reviews in Plant Sciences* **26**, 199–225 (2007).
50. Vázquez-Martínez, R. et al. Revisiting the regulated secretory pathway: from frogs to human. *Gen. Comp. Endocrinol.* **175**, 1–9 (2012).
51. Scheuring, D. et al. Multivesicular bodies mature from the trans-Golgi network/early endosome in Arabidopsis. *Plant Cell* **23**, 3463–3481 (2011).
52. Dell'Angelica, E. C. AP-3-dependent trafficking and disease: the first decade. *Curr Opin Cell Biol* **21**, 552–559 (2009).
53. Feraru, E. et al. The AP-3 β adaptin mediates the biogenesis and function of lytic vacuoles in Arabidopsis. *Plant Cell* **22**, 2812–2824 (2010).
54. Chen, X., Irani, N. G. & Friml, J. Clathrin-mediated endocytosis: the gateway into plant cells. *Curr Opin Plant Biol* **14**, 674–682 (2011).
55. Howes, M. T., Mayor, S. & Parton, R. G. Molecules, mechanisms, and cellular roles of clathrin-independent endocytosis. *Curr Opin Cell Biol* **22**, 519–527 (2010).
56. Li, F. & Vierstra, R. D. Autophagy: a multifaceted intracellular system for bulk and selective recycling. *Trends Plant Sci* **17**, 526–537 (2012).
57. Prosser, D. C., Drivas, T. G., Maldonado-Báez, L. & Wendland, B. Existence of a novel clathrin-independent endocytic pathway in yeast that depends on Rho1 and formin. *J Cell Biol* **195**, 657–671 (2011).
58. Huotari, J. & Helenius, A. Endosome maturation. *EMBO J* **30**, 3481–3500 (2011).
59. Yang, Z. & Klionsky, D. J. Eaten alive: a history of macroautophagy. *Nat Cell Biol* **12**, 814–822 (2010).

60. Viotti, C. et al. Endocytic and secretory traffic in Arabidopsis merge in the trans-Golgi network/early endosome, an independent and highly dynamic organelle. *Plant Cell* **22**, 1344–1357 (2010).
61. Surpin, M. & Raikhel, N. Traffic jams affect plant development and signal transduction. *Nat Rev Mol Cell Biol* **5**, 100–109 (2004).
62. Zouhar, J. & Rojo, E. Plant vacuoles: where did they come from and where are they heading? *Curr Opin Plant Biol* **12**, 677–684 (2009).
63. Frigerio, L., Hinz, G. & Robinson, D. G. Multiple vacuoles in plant cells: rule or exception? *Traffic* **9**, 1564–1570 (2008).
64. Hicks, G. R. & Raikhel, N. V. Small Molecules Present Large Opportunities in Plant Biology. *Annu Rev Plant Biol* **63**, 261-282 (2012).
65. Tóth, R. & van der Hoorn, R. A. L. Emerging principles in plant chemical genetics. *Trends Plant Sci* **15**, 81–88 (2010).
66. Cong, F., Cheung, A. K. & Huang, S.-M. A. Chemical Genetics-Based Target Identification in Drug Discovery. *Annu. Rev. Pharmacol. Toxicol.* **52**, 57-78 (2011).
67. Delaney, J., Clarke, E., Hughes, D. & Rice, M. Modern agrochemical research: a missed opportunity for drug discovery? *Drug Discov Today* **11**, 839–845 (2006).
68. Knight, Z. A. & Shokat, K. M. Chemical genetics: where genetics and pharmacology meet. *Cell* **128**, 425–430 (2007).
69. Drakakaki, G. et al. Clusters of bioactive compounds target dynamic endomembrane networks in vivo. *Proc Natl Acad Sci USA* **108**, 17850–17855 (2011).
70. Codreanu, M.-C., Audenaert, D., Nguyen, L., Beeckman, T. & Russinova, E. Small-molecule dissection of brassinosteroid signaling. *Methods Mol Biol* **876**, 95–106 (2012).
71. Surpin, M. et al. The power of chemical genomics to study the link between endomembrane system components and the gravitropic response. *Proc Natl Acad Sci USA* **102**, 4902–4907 (2005).
72. Feng, Y. et al. Exo1: a new chemical inhibitor of the exocytic pathway. *Proc Natl Acad Sci USA* **100**, 6469–6474 (2003).
73. Brown, J. X., Buckett, P. D. & Wessling-Resnick, M. Identification of small molecule inhibitors that distinguish between non-transferrin bound iron uptake and transferrin-mediated iron transport. *Chem Biol* **11**, 407–416 (2004).
74. Pan, H. et al. A novel small molecule regulator of guanine nucleotide exchange activity of the ADP-ribosylation factor and golgi membrane trafficking. *J Biol Chem* **283**, 31087–31096 (2008).

75. Balgi, A. D. et al. Screen for chemical modulators of autophagy reveals novel therapeutic inhibitors of mTORC1 signaling. *PLoS ONE* **4**, e7124 (2009).
76. Farkas, T., Høyer-Hansen, M. & Jäättelä, M. Identification of novel autophagy regulators by a luciferase-based assay for the kinetics of autophagic flux. *Autophagy* **5**, 1018–1025 (2009).
77. Farkas, T., Daugaard, M. & Jäättelä, M. Identification of small molecule inhibitors of phosphatidylinositol 3-kinase and autophagy. *J Biol Chem* **286**, 38904–38912 (2011).
78. Zhang, L. et al. Small molecule regulators of autophagy identified by an image-based high-throughput screen. *Proc Natl Acad Sci USA* **104**, 19023–19028 (2007).
79. Hundeshagen, P., Hamacher-Brady, A., Eils, R. & Brady, N. R. Concurrent detection of autolysosome formation and lysosomal degradation by flow cytometry in a high-content screen for inducers of autophagy. *BMC Biol.* **9**, 38 (2011).
80. Sáenz, J. B., Doggett, T. A. & Haslam, D. B. Identification and characterization of small molecules that inhibit intracellular toxin transport. *Infect. Immun.* **75**, 4552–4561 (2007).
81. Stechmann, B. et al. Inhibition of retrograde transport protects mice from lethal ricin challenge. *Cell* **141**, 231–242 (2010).
82. Huang, J. et al. Finding new components of the target of rapamycin (TOR) signaling network through chemical genetics and proteome chips. *Proc Natl Acad Sci USA* **101**, 16594–16599 (2004).
83. Sarkar, S. et al. Small molecules enhance autophagy and reduce toxicity in Huntington's disease models. *Nat Chem Biol* **3**, 331–338 (2007).
84. Zouhar, J., Hicks, G. R. & Raikhel, N. V. Sorting inhibitors (Sortins): Chemical compounds to study vacuolar sorting in Arabidopsis. *Proc Natl Acad Sci USA* **101**, 9497–9501 (2004).
85. Macia, E. et al. Dynasore, a cell-permeable inhibitor of dynamin. *Dev Cell* **10**, 839–850 (2006).
86. Kleist, von, L. et al. Role of the clathrin terminal domain in regulating coated pit dynamics revealed by small molecule inhibition. *Cell* **146**, 471–484 (2011).
87. Roemer, T., Davies, J., Giaever, G. & Nislow, C. Bugs, drugs and chemical genomics. *Nat Chem Biol* **8**, 46–56 (2012).
88. Zhang, L. et al. A high-throughput screen for chemical inhibitors of exocytic transport in yeast. *Chembiochem* **11**, 1291–1301 (2010).
89. Duncan, M. C., Ho, D. G., Huang, J., Jung, M. E. & Payne, G. S. Composite synthetic lethal identification of membrane traffic inhibitors. *Proc Natl Acad Sci USA* **104**, 6235–6240 (2007).
90. Hillenmeyer, M. E. et al. The chemical genomic portrait of yeast: uncovering a phenotype for all genes. *Science* **320**, 362–365 (2008).
91. Viaud, J. et al. Structure-based discovery of an inhibitor of Arf activation by Sec7 domains through targeting of protein-protein complexes. *Proc Natl Acad Sci USA* **104**, 10370–10375 (2007).

92. Ohashi, Y. et al. AMF-26, a novel inhibitor of the Golgi system, targeting ADP-ribosylation factor 1 (Arf1) with potential for cancer therapy. *J Biol Chem* **287**, 3885–3897 (2012).
93. Lippincott-Schwartz, J. et al. Brefeldin A's effects on endosomes, lysosomes, and the TGN suggest a general mechanism for regulating organelle structure and membrane traffic. *Cell* **67**, 601–616 (1991).
94. Dinter, A. & Berger, E. G. Golgi-disturbing agents. Histochem. *Cell Biol*. **109**, 571–590 (1998).
95. Renault, L., Guibert, B. & Cherfils, J. Structural snapshots of the mechanism and inhibition of a guanine nucleotide exchange factor. *Nature* **426**, 525–530 (2003).
96. Anders, N. & Jürgens, G. Large ARF guanine nucleotide exchange factors in membrane trafficking. *Cell. Mol. Life Sci.* **65**, 3433–3445 (2008).
97. Robinson, D. G., Jiang, L. & Schumacher, K. The endosomal system of plants: charting new and familiar territories. *Plant Physiol* **147**, 1482–1492 (2008).
98. Feng, Y. et al. Retrograde transport of cholera toxin from the plasma membrane to the endoplasmic reticulum requires the trans-Golgi network but not the Golgi apparatus in Exo2-treated cells. *EMBO Rep* **5**, 596–601 (2004).
99. Spooner, R. A. et al. The secretion inhibitor Exo2 perturbs trafficking of Shiga toxin between endosomes and the trans-Golgi network. *Biochem J* **414**, 471–484 (2008).
100. Boal, F. et al. LG186: An inhibitor of GBF1 function that causes Golgi disassembly in human and canine cells. *Traffic* **11**, 1537–1551 (2010).
101. Sorieul, M. et al. An Exo2 derivative affects ER and Golgi morphology and vacuolar sorting in a tissue-specific manner in arabidopsis. *Traffic* **12**, 1552–1562 (2011).
102. Sáenz, J. B. et al. Golgicide A reveals essential roles for GBF1 in Golgi assembly and function. *Nat Chem Biol* **5**, 157–165 (2009).
103. Pelish, H. E. et al. Secramine inhibits Cdc42-dependent functions in cells and Cdc42 activation in vitro. *Nat Chem Biol* **2**, 39–46 (2006).
104. Irani, N. G. & Russinova, E. Receptor endocytosis and signaling in plants. *Curr Opin Plant Biol* **12**, 653–659 (2009).
105. Yaish, P., Gazit, A., Gilon, C. & Levitzki, A. Blocking of EGF-dependent cell proliferation by EGF receptor kinase inhibitors. *Science* **242**, 933–935 (1988).
106. Banbury, D. N., Oakley, J. D., Sessions, R. B. & Banting, G. Tyrphostin A23 inhibits internalization of the transferrin receptor by perturbing the interaction between tyrosine motifs and the medium chain subunit of the AP-2 adaptor complex. *J Biol Chem* **278**, 12022–12028 (2003).

107. Ortiz-Zapater, E., Soriano-Ortega, E., Marcote, M. J., Ortiz-Masiá, D. & Aniento, F. Trafficking of the human transferrin receptor in plant cells: effects of tyrphostin A23 and brefeldin A. *Plant J* **48**, 757–770 (2006).
108. Dhonukshe, P. et al. Clathrin-Mediated Constitutive Endocytosis of PIN Auxin Efflux Carriers in Arabidopsis. *Curr Biol* **17**, 520–527 (2007).
109. Konopka, C. A., Backues, S. K. & Bednarek, S. Y. Dynamics of Arabidopsis dynamin-related protein 1C and a clathrin light chain at the plasma membrane. *Plant Cell* **20**, 1363–1380 (2008).
110. Lam, S. K. et al. BFA-induced compartments from the Golgi apparatus and trans-Golgi network/early endosome are distinct in plant cells. *Plant J* **60**, 865–881 (2009).
111. Robert, S. et al. ABP1 mediates auxin inhibition of clathrin-dependent endocytosis in Arabidopsis. *Cell* **143**, 111–121 (2010).
112. Boutté, Y. et al. Endocytosis restricts Arabidopsis KNOLLE syntaxin to the cell division plane during late cytokinesis. *EMBO J* **29**, 546–558 (2010).
113. Fujimoto, M. et al. Arabidopsis dynamin-related proteins DRP2B and DRP1A participate together in clathrin-coated vesicle formation during endocytosis. *Proc Natl Acad Sci USA* **107**, 6094–6099 (2010).
114. Santuari, L. et al. Positional information by differential endocytosis splits auxin response to drive Arabidopsis root meristem growth. *Curr Biol* **21**, 1918–1923 (2011).
115. Li, R. et al. A Membrane Microdomain-Associated Protein, Arabidopsis Flot1, Is Involved in a Clathrin-Independent Endocytic Pathway and Is Required for Seedling Development. Plant Cell **24** 2105-2122 (2012).
116. Luu, D.-T., Martinière, A., Sorieul, M., Runions, J. & Maurel, C. Fluorescence recovery after photobleaching reveals high cycling dynamics of plasma membrane aquaporins in Arabidopsis roots under salt stress. *Plant J* **69**, 894–905 (2011).
117. Beck, M., Zhou, J., Faulkner, C., MacLean, D. & Robatzek, S. Spatio-temporal cellular dynamics of the Arabidopsis flagellin receptor reveal activation status-dependent endosomal sorting. *Plant Cell* **24**, 4205–4219 (2012).
118. Kim, S. Y. et al. Adaptor protein complex 2-mediated endocytosis is crucial for male reproductive organ development in Arabidopsis. *Plant Cell* **25**, 2970–2985 (2013).
119. Smith, J. M., Salamango, D. J., Leslie, M. E., Collins, C. A. & Heese, A. Sensitivity to Flg22 is modulated by ligand-induced degradation and de novo synthesis of the endogenous flagellin-receptor FLAGELLIN-SENSING2. *Plant Physiol* **164**, 440–454 (2014).
120. Carluccio, A. V., Zicca, S. & Stavolone, L. Hitching a ride on vesicles: cauliflower mosaic virus movement protein trafficking in the endomembrane system. *Plant Physiol* **164**, 1261–1270 (2014).

121. Kirchhausen, T., Macia, E. & Pelish, H. E. Use of dynasore, the small molecule inhibitor of dynamin, in the regulation of endocytosis. *Meth. Enzymol*. **438**, 77–93 (2008).
122. Fujimoto, M. & Ueda, T. Conserved and plant-unique mechanisms regulating plant post-Golgi traffic. *Front Plant Sci* **3**, 197 (2012).
123. Sharfman, M. et al. Endosomal signaling of the tomato leucine-rich repeat receptor-like protein LeEix2. *Plant J* **68**, 413–423 (2011).
124. McCluskey, A. et al. Building a better dynasore: the dyngo compounds potently inhibit dynamin and endocytosis. *Traffic* **14**, 1272–1289 (2013).
125. Hill, T. A. et al. Inhibition of dynamin mediated endocytosis by the dynoles--synthesis and functional activity of a family of indoles. *J. Med. Chem*. **52**, 3762–3773 (2009).
126. Gordon, C. P. et al. Development of Second-Generation Indole-Based Dynamin GTPase Inhibitors. *J. Med. Chem*. **56**, 46–59 (2013).
127. Stahlschmidt, W., Robertson, M. J., Robinson, P. J., McCluskey, A. & Haucke, V. Clathrin terminal domain-ligand interactions regulate sorting of mannose 6-phosphate receptors mediated by AP-1 and GGA adaptors. *J Biol Chem* **289**, 4906–4918 (2014).
128. Robertson, M. J. et al. Synthesis of the Pitstop family of clathrin inhibitors. *Nature Protoc* **9**, 1592–1606 (2014).
129. Dutta, D., Williamson, C. D., Cole, N. B. & Donaldson, J. G. Pitstop 2 is a potent inhibitor of clathrin-independent endocytosis. *PLoS ONE* **7**, e45799 (2012).
130. Lemmon, S. K. & Traub, L. M. Getting in touch with the clathrin terminal domain. *Traffic* **13**, 511–519 (2012).
131. Willox, A. K., Sahraoui, Y. M. E. & Royle, S. J. Non-specificity of Pitstop 2 in clathrin-mediated endocytosis. *Biol Open* **3**, 326–331 (2014).
132. Nieland, T. J. F. et al. Chemical genetic screening identifies sulfonamides that raise organellar pH and interfere with membrane traffic. *Traffic* **5**, 478–492 (2004).
133. Horonchik, L. & Wessling-Resnick, M. The small-molecule iron transport inhibitor ferristatin/NSC306711 promotes degradation of the transferrin receptor. *Chem Biol* **15**, 647–653 (2008).
134. Tóth, R. et al. Prieurianin/endosidin 1 is an actin-stabilizing small molecule identified from a chemical genetic screen for circadian clock effectors in Arabidopsis thaliana. *Plant J* **71**, 338–352 (2012).
135. Paudyal, R. et al. Trafficking modulator TENin1 inhibits endocytosis, causes endomembrane protein accumulation at the pre-vacuolar compartment and impairs gravitropic response in Arabidopsis thaliana. *Biochem J* **460**, 177–185 (2014).

136. Zouhar, J., Hicks, G. R. & Raikhel, N. V. Sorting inhibitors (Sortins): Chemical compounds to study vacuolar sorting in Arabidopsis. *Proc Natl Acad Sci USA* **101**, 9497–9501 (2004).
137. Rosado, A. et al. Sortin1-hypersensitive mutants link vacuolar-trafficking defects and flavonoid metabolism in Arabidopsis vegetative tissues. *Chem Biol* **18**, 187–197 (2011).
138. Chanda, A. et al. A key role for vesicles in fungal secondary metabolism. *Proc Natl Acad Sci USA* **106**, 19533–19538 (2009).
139. Norambuena, L., Zouhar, J., Hicks, G. R. & Raikhel, N. V. Identification of cellular pathways affected by Sortin2, a synthetic compound that affects protein targeting to the vacuole in Saccharomyces cerevisiae. *BMC Chem Biol* **8**, 1 (2008).
140. Rivera-Serrano, E. E., Rodriguez-Welsh, M. F., Hicks, G. R. & Rojas-Pierce, M. A small molecule inhibitor partitions two distinct pathways for trafficking of tonoplast intrinsic proteins in Arabidopsis. *PLoS ONE* **7**, e44735 (2012).
141. Cerny, J. et al. The small chemical vacuolin-1 inhibits Ca(2+)-dependent lysosomal exocytosis but not cell resealing. *EMBO Rep* **5**, 883–888 (2004).
142. Shaik, G. M., Dráberová, L., Heneberg, P. & Dráber, P. Vacuolin-1-modulated exocytosis and cell resealing in mast cells. *Cell Signal* **21**, 1337–1345 (2009).
143. Blommaart, E. F., Luiken, J. J., Blommaart, P. J., van Woerkom, G. M. & Meijer, A. J. Phosphorylation of ribosomal protein S6 is inhibitory for autophagy in isolated rat hepatocytes. *J Biol Chem* **270**, 2320–2326 (1995).
144. Noda, T. & Ohsumi, Y. Tor, a phosphatidylinositol kinase homologue, controls autophagy in yeast. *J Biol Chem* **273**, 3963–3966 (1998).
145. Mahfouz, M. M., Kim, S., Delauney, A. J. & Verma, D. P. S. Arabidopsis TARGET OF RAPAMYCIN interacts with RAPTOR, which regulates the activity of S6 kinase in response to osmotic stress signals. *Plant Cell* **18**, 477–490 (2006).
146. Menand, B. et al. Expression and disruption of the Arabidopsis TOR (target of rapamycin) gene. *Proc Natl Acad Sci USA* **99**, 6422–6427 (2002).
147. Xiong, Y. & Sheen, J. Rapamycin and glucose-target of rapamycin (TOR) protein signaling in plants. *J Biol Chem* **287**, 2836–2842 (2012).
148. Hehnly, H. & Stamnes, M. Regulating cytoskeleton-based vesicle motility. *FEBS Lett*. **581**, 2112–2118 (2007).
149. Boulant, S., Kural, C., Zeeh, J.-C., Ubelmann, F. & Kirchhausen, T. Actin dynamics counteract membrane tension during clathrin-mediated endocytosis. *Nat Cell Biol* **13**, 1124–1131 (2011).
150. Dhonukshe, P. et al. Auxin transport inhibitors impair vesicle motility and actin cytoskeleton dynamics in diverse eukaryotes. *Proc Natl Acad Sci USA* **105**, 4489–4494 (2008).

151. Ziegler, S., Pries, V., Hedberg, C. & Waldmann, H. Target identification for small bioactive molecules: finding the needle in the haystack. *Angew Chem Int Ed Engl* **52**, 2744–2792 (2013).
152. Tresch, S. Strategies and future trends to identify the mode of action of phytotoxic compounds. *Plant Sci.* **212**, 60–71 (2013).
153. Lounkine, E. et al. Large-scale prediction and testing of drug activity on side-effect targets. *Nature* **486**, 361–367 (2012).
154. Kumari, S. & van der Hoorn, R. A. L. A structural biology perspective on bioactive small molecules and their plant targets. *Curr Opin Plant Biol* **14**, 480–488 (2011).
155. Xuan, W., Murphy, E., Beeckman, T., Audenaert, D. & De Smet, I. Synthetic molecules: helping to unravel plant signal transduction. *J Chem Biol* **6**, 43–50 (2013).
156. de Rybel, B. et al. A role for the root cap in root branching revealed by the non-auxin probe naxillin. *Nat Chem Biol* **8**, 798–805 (2012).
157. Park, S.-Y. et al. Abscisic acid inhibits type 2C protein phosphatases via the PYR/PYL family of START proteins. *Science* **324**, 1068–1071 (2009).
158. Santiago, J. et al. The abscisic acid receptor PYR1 in complex with abscisic acid. *Nature* **462**, 665–668 (2009).
159. Ma, Y. et al. Regulators of PP2C phosphatase activity function as abscisic acid sensors. *Science* **324**, 1064–1068 (2009).
160. Rojas-Pierce, M. et al. Arabidopsis P-glycoprotein19 participates in the inhibition of gravitropism by gravacin. *Chem Biol* **14**, 1366–1376 (2007).
161. Walsh, T. A. et al. Chemical genetic identification of glutamine phosphoribosylpyrophosphate amidotransferase as the target for a novel bleaching herbicide in Arabidopsis. *Plant Physiol* **144**, 1292–1304 (2007).
162. He, W. et al. A small-molecule screen identifies L-kynurenine as a competitive inhibitor of TAA1/TAR activity in ethylene-directed auxin biosynthesis and root growth in Arabidopsis. *Plant Cell* **23**, 3944–3960 (2011).
163. Noutoshi, Y. et al. Novel plant immune-priming compounds identified via high-throughput chemical screening target salicylic acid glucosyltransferases in Arabidopsis. *Plant Cell* **24**, 3795–3804 (2012).
164. Meesters, C. et al. A chemical inhibitor of jasmonate signaling targets JAR1 in Arabidopsis thaliana. *Nat Chem Biol* **10**, 830–836 (2014).
165. Schweitzer, B. A. et al. Discovery of imidazole glycerol phosphate dehydratase inhibitors through 3-D database searching. *Bioorg. Med. Chem. Lett.* **12**, 1743–1746 (2002).

166. Mori, I. et al. A Novel Class of Herbicides (Specific Inhibitors of Imidazoleglycerol Phosphate Dehydratase). *Plant Physiol* **107**, 719–723 (1995).
167. Botté, C. Y. et al. Chemical inhibitors of monogalactosyldiacylglycerol synthases in Arabidopsis thaliana. *Nat Chem Biol* **7**, 834–842 (2011).
168. van der Hoorn, R. A. L. et al. Mining the Active Proteome of Arabidopsis thaliana. *Front Plant Sci* **2**, 89 (2011).
169. Kaschani, F. et al. Selective inhibition of plant serine hydrolases by agrochemicals revealed by competitive ABPP. *Bioorg. Med. Chem.* **20**, 597–600 (2012).
170. Nickel, S., Kaschani, F., Colby, T., van der Hoorn, R. A. L. & Kaiser, M. A para-nitrophenol phosphonate probe labels distinct serine hydrolases of Arabidopsis. *Bioorg. Med. Chem.* **20**, 601–606 (2012).
171. Kaschani, F. et al. Identification of a selective, activity-based probe for glyceraldehyde 3-phosphate dehydrogenases. *Angew Chem Int Ed Engl* **51**, 5230–5233 (2012).
172. Licitra, E. J. & Liu, J. O. A three-hybrid system for detecting small ligand-protein receptor interactions. *Proc Natl Acad Sci USA* **93**, 12817–12821 (1996).
173. Gyuris, J., Golemis, E., Chertkov, H. & Brent, R. Cdi1, a human G1 and S phase protein phosphatase that associates with Cdk2. *Cell* **75**, 791–803 (1993).
174. Cottier, S. et al. The yeast three-hybrid system as an experimental platform to identify proteins interacting with small signaling molecules in plant cells: potential and limitations. *Front Plant Sci* **2**, 101 (2011).
175. Becker, F. et al. A three-hybrid approach to scanning the proteome for targets of small molecule kinase inhibitors. *Chem Biol* **11**, 211–223 (2004).
176. Chidley, C., Haruki, H., Pedersen, M. G., Muller, E. & Johnsson, K. A yeast-based screen reveals that sulfasalazine inhibits tetrahydrobiopterin biosynthesis. *Nat Chem Biol* **7**, 375–383 (2011).
177. Keppler, A. et al. A general method for the covalent labeling of fusion proteins with small molecules in vivo. *Nat Biotechnol* **21**, 86–89 (2003).
178. Tran, F., Odell, A. V., Ward, G. E. & Westwood, N. J. A modular approach to triazole-containing chemical inducers of dimerisation for yeast three-hybrid screening. *Molecules* **18**, 11639–11657 (2013).
179. Grozinger, C. M., Chao, E. D., Blackwell, H. E., Moazed, D. & Schreiber, S. L. Identification of a class of small molecule inhibitors of the sirtuin family of NAD-dependent deacetylases by phenotypic screening. *J Biol Chem* **276**, 38837–38843 (2001).
180. Zhao, Y., Dai, X., Blackwell, H. E., Schreiber, S. L. & Chory, J. SIR1, an upstream component in auxin signaling identified by chemical genetics. *Science* **301**, 1107–1110 (2003).

181. Dai, X., Hayashi, K.-I., Nozaki, H., Cheng, Y. & Zhao, Y. Genetic and chemical analyses of the action mechanisms of sirtinol in Arabidopsis. *Proc Natl Acad Sci USA* **102**, 3129–3134 (2005).
182. Köster, H. et al. Capture compound mass spectrometry: a technology for the investigation of small molecule protein interactions. *Assay Drug Dev Technol* **5**, 381–390 (2007).
183. Fischer, J. J. et al. Capture compound mass spectrometry sheds light on the molecular mechanisms of liver toxicity of two Parkinson drugs. *Toxicol. Sci.* **113**, 243–253 (2010).
184. Fischer, J. J. et al. Improvement of capture compound mass spectrometry technology (CCMS) for the profiling of human kinases by combination with 2D LC-MS/MS. *J. Biomed. Biotechnol*. **2011**, 850589 (2011).
185. Ong, S.-E. et al. Stable isotope labeling by amino acids in cell culture, SILAC, as a simple and accurate approach to expression proteomics. *Mol Cell Proteomics* **1**, 376–386 (2002).
186. Ong, S.-E. et al. Identifying the proteins to which small-molecule probes and drugs bind in cells. *Proc Natl Acad Sci USA* **106**, 4617–4622 (2009).
187. Collier, T. S. & Muddiman, D. C. Analytical strategies for the global quantification of intact proteins. *Amino Acids* **43**, 1109–1117 (2012).
188. Gant-Branum, R. L., Kerr, T. J. & McLean, J. A. Labeling strategies in mass spectrometry-based protein quantitation. *Analyst* **134**, 1525–1530 (2009).
189. Pfister, K., Steinback, K. E., Gardner, G. & Arntzen, C. J. Photoaffinity labeling of an herbicide receptor protein in chloroplast membranes. *Proc Natl Acad Sci USA* **78**, 981–985 (1981).
190. Nakamura, Y., Miyatake, R. & Ueda, M. Enantiodifferential approach for the detection of the target membrane protein of the jasmonate glycoside that controls the leaf movement of Albizzia saman. *Angew Chem Int Ed Engl* **47**, 7289–7292 (2008).
191. Kaschani, F. et al. Minitags for small molecules: detecting targets of reactive small molecules in living plant tissues using 'click chemistry'. *Plant J* **57**, 373–385 (2009).
192. Park, J., Oh, S. & Park, S. B. Discovery and target identification of an antiproliferative agent in live cells using fluorescence difference in two-dimensional gel electrophoresis. *Angew Chem Int Ed Engl* **51**, 5447–5451 (2012).
193. Mandava, S., Makowski, L., Devarapalli, S., Uzubell, J. & Rodi, D. J. RELIC--a bioinformatics server for combinatorial peptide analysis and identification of protein-ligand interaction sites. *Proteomics* **4**, 1439–1460 (2004).
194. Straume, M. & Freire, E. 2-Dimensional Differential Scanning Calorimetry - Simultaneous Resolution of Intrinsic Protein Structural Energetics and Ligand-Binding Interactions by Global Linkage *Analysis. Anal. Biochem*. **203**, 259–268 (1992).

195. Lo, M. C. et al. Evaluation of fluorescence-based thermal shift assays for hit identification in drug discovery. *Anal. Biochem*. **332**, 153–159 (2004).

196. Schön, A., Brown, R. K., Hutchins, B. M. & Freire, E. Ligand binding analysis and screening by chemical denaturation shift. *Anal. Biochem*. **443**, 52–57 (2013).

197. Chan, J. N. Y. et al. Target identification by chromatographic co-elution: monitoring of drug-protein interactions without immobilization or chemical derivatization. *Mol Cell Proteomics* **11**, M111.016642 (2012).

198. Lomenick, B. et al. Target identification using drug affinity responsive target stability (DARTS). *Proc Natl Acad Sci USA* **106**, 21984–21989 (2009).

199. Lomenick, B., Olsen, R. W. & Huang, J. Identification of direct protein targets of small molecules. *ACS Chem. Biol*. **6**, 34–46 (2011).

200. Komatsu, T. et al. The chloroplast protein BPG2 functions in brassinosteroid-mediated post-transcriptional accumulation of chloroplast rRNA. *Plant J* **61**, 409–422 (2010).

201. Yoshizawa, E. et al. BPG3 is a novel chloroplast protein that involves the greening of leaves and related to brassinosteroid signaling. *Biosci Biotechnol Biochem* **78**, 420–429 (2014).

202. Bekh-Ochir, D. et al. A novel mitochondrial DnaJ/Hsp40 family protein BIL2 promotes plant growth and resistance against environmental stress in brassinosteroid signaling. *Planta* **237**, 1509–1525 (2013).

203. Kim, B. et al. The arabidopsis gulliver2/phyB mutant exhibits reduced sensitivity to brassinazole. *J. Plant Biol*. **57**, 20–27 (2014).

204. Oh, K. et al. YCZ-18 Is a New Brassinosteroid Biosynthesis Inhibitor. *PLoS ONE* **10**, e0120812 (2015).

205. Bojar, D. et al. Crystal structures of the phosphorylated BRI1 kinase domain and implications for brassinosteroid signal initiation. *Plant J* **78**, 31–43 (2014).

206. Yan, L. et al. Structural basis for the impact of phosphorylation on the activation of plant receptor-like kinase BAK1. *Cell Res* **22**, 1304–1308 (2012).

207. Mosquna, A. et al. Potent and selective activation of abscisic acid receptors in vivo by mutational stabilization of their agonist-bound conformation. *Proc Natl Acad Sci USA* **108**, 20838–20843 (2011).

208. Park, E. et al. Endosidin 7 Specifically Arrests Late Cytokinesis and Inhibits Callose Biosynthesis, Revealing Distinct Trafficking Events during Cell Plate Maturation. *Plant Physiol* **165**, 1019–1034 (2014).

209. Doyle, S. M. et al. An early secretory pathway mediated by GNOM-LIKE 1 and GNOM is essential for basal polarity establishment in Arabidopsis thaliana. *Proceedings of the National Academy of Sciences* **112**, E806–15 (2015).

210. Davis, D. J. et al. The RAB GTPase RABA1e localizes to the cell plate and shows distinct subcellular behavior from RABA2a under Endosidin 7 treatment. *Plant Signal Behav* **10**, e984520 (2015).
211. Anders, L. et al. Genome-wide localization of small molecules. *Nat Biotechnol* **32**, 92–96 (2014).
212. Martinez Molina, D. et al. Monitoring drug target engagement in cells and tissues using the cellular thermal shift assay. *Science* **341**, 84–87 (2013).
213. Savitski, M. M. et al. Proteomics. Tracking cancer drugs in living cells by thermal profiling of the proteome. *Science* **346**, 1255784 (2014).
214. Lounkine, E. et al. Large-scale prediction and testing of drug activity on side-effect targets. *Nature* **486**, 361–367 (2012).
215. Cereto-Massagué, A. et al. Tools for in silico target fishing. *Methods* **71**, 98–103 (2015).

Chapter II: Small molecule screen for effectors of clathrin-mediated endocytosis and brassinosteroid signaling

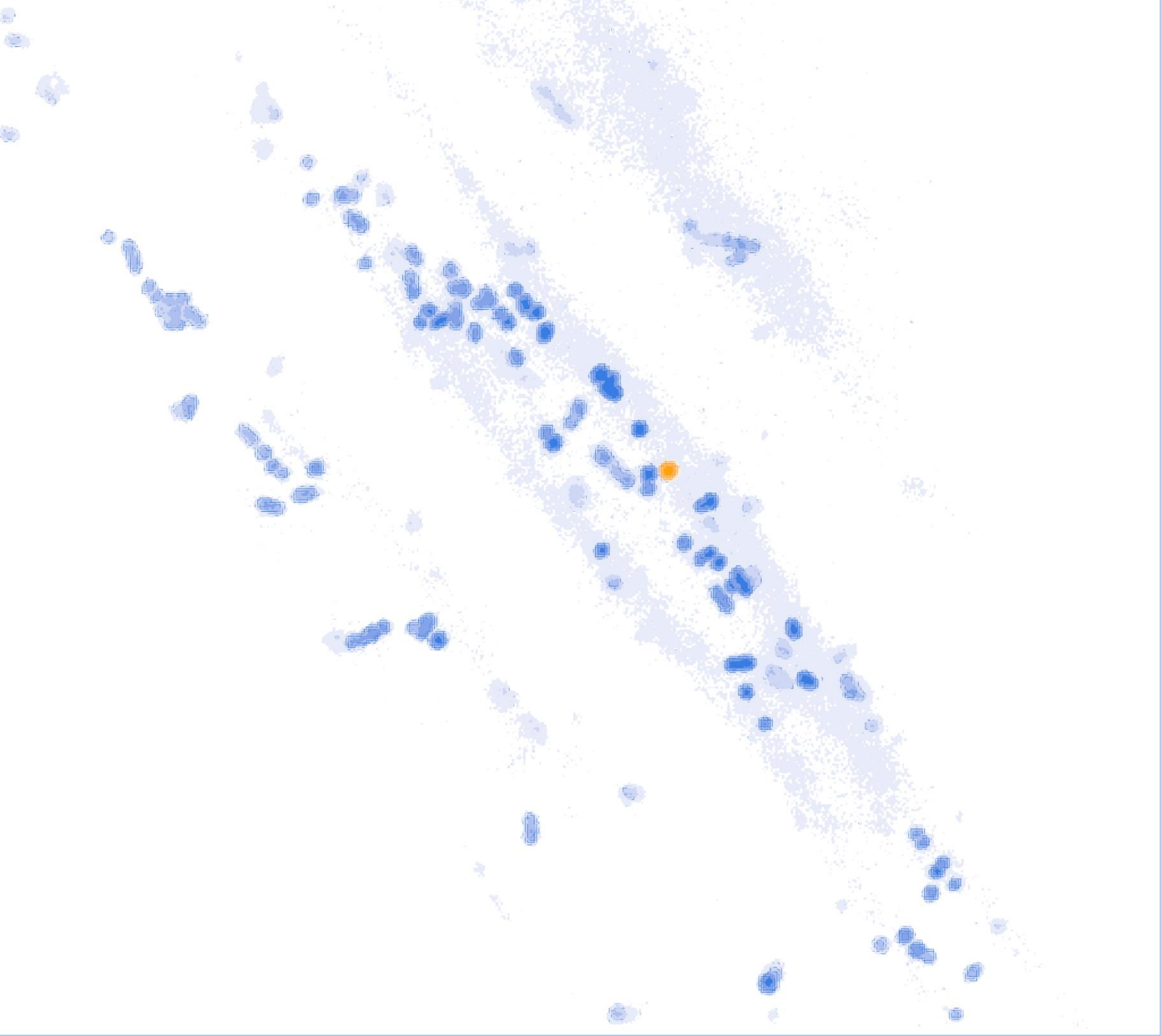

Small molecule screen for effectors of clathrin-mediated endocytosis and brassinosteroid signaling

Wim Dejonghe[1,2], Evelien Mylle[1,2] Simone Di Rubbo[1,2], Anna-Maria Szatmári[1,2] and Eugenia Russinova[1,2]

[1]Department of Plant Systems Biology, VIB, 9052 Ghent, Belgium
[2]Department of Plant Biotechnology and Bioinformatics, Ghent University, 9052 Ghent, Belgium

Author contributions: W.D. did the growth and BES1 de-phosphorylation assays, and was involved in confocal screening of marker lines. W.D. wrote the manuscript and made the figures.

Abstract

The use of small molecules to probe hormone signaling or endomembrane trafficking in plants have proven to be successful. Such small molecules have given us unique insights into brassinosteroid biosynthesis and signaling (brassinazole and bikinin) and clathrin-mediated endocytosis (tyrphostin A23), but also the interplay between both processes. An illustration of the latter concerns the increased signaling output of the brassinosteroid leucine-rich repeat receptor kinase BRASSINOSTEROID INSENSITIVE1 at the plasma membrane upon inhibition of clathrin mediated endocytosis, both by pharmacological and genetic means. Therefore an increase of the available chemical tools which affect brassinosteroid signaling and endomembrane traffic might provide new insights as to how these highly dynamic processes are linked and influence each other. We therefore screened a subset of small molecules originating from a screen for inhibitors of pollen germination and growth in search of small molecules which will potentially inhibit clathrin-mediated endocytosis and enhance brassinosteroid signaling. Identified hits will be considered for further characterization and target identification.

Introduction

Small molecules have been instrumental in providing a better understanding of brassinosteroid (BR) signaling[1]. Examples include bikinin[2] and brassinazole (brz)[3], and both have gained a prominent role in BR research. For example, brz and derivatives are frequently used to inhibit BR biosynthesis, while the original brz has contributed in the discovery of BRASSINAZOLE RESISTANT1 (BZR1)[4], a transcriptional regulator of BR signaling from the same family as BRI1 EMS-SUPPRESSOR1 (BES1)[5]. Especially the latter is used frequently to assess BR signaling, as de-phosphorylation of BES1 can be measured by western blot, and indicates the active state of BES1[5]. Phosphorylation of BES1 or BZR1, which is mediated by the kinase domain of BRASSINOSTEROID INSENSITIVE2[6,7], and retains BZR1/BES1 in the cytosol through binding of 14-3-3 proteins[8], indicates the inactive state of both transcriptional regulators.

BR signaling can also be influenced through endomembrane traffic, similar as seen for receptor kinases in mammalian systems[9]. Two scenarios are commonly recognized, where either signaling is attenuated through receptor uptake in the cell, often through clathrin-mediated endocytosis (CME), or requires uptake, as receptor and other accessory proteins meet in endosomes and initiate signaling. Small molecules are appropriate tools to dissect this relation, and plant endomembrane research can dispose of several small molecule effectors of endomembrane traffic, as identified through screening of small molecule libraries[10]. Yet only one is frequently used as an inhibitor CME in plants: tyrphostin A23 (TyrA23). Identified in mammalian systems as an inhibitor of ADAPTOR PROTEIN-2 (AP-2) mediated cargo recruitment[11], TyrA23 interferes through binding of tyrosine-containing recognition motifs on AP-2, thereby preventing binding of cargo[12]. The mode of action of TyrA23 has been shown to be true in plants as well[13], though biochemical proof of binding is lacking in plants. TyrA23 has since been used in numerous studies to inhibit CME in plants, including the uptake inhibition of the plasma membrane (PM) localized leucine-rich repeat receptor kinase BRASSINOSTEROID INSENSITIVE1 (BRI1)[14]. Previous studies showed that BRI1 is present on the PM and endosomes, and its uptake appears to be independent of ligand binding[15,16], yet the implications for signaling were less clear. The use of TyrA23 to inhibit BRI1 internalization increased the signaling output as more BRI1 is retained on the PM, a finding which was confirmed genetically[14]. The uptake inhibition of BRI1 caused by either TyrA23 or by the expression of a dominant negative clathrin construct supported CME of BRI1, a hypothesis which was later confirmed[17]. Together, the above findings demonstrated that BRI1 mainly signals from the PM, while, supposedly and in analogy with mammalian systems the CME of BRI1 attenuates signaling.

Although in recent years several new insights emerged related to molecular components of CME, including the report on TPLATE complex[18] and characterization of AP-2 subunits[17,19,20], less is known about cargo recruitment and possible implications for downstream signaling. Therefore we set

out to identify and characterize small molecule inhibitors of CME, which at the same time enhance BR signaling as measured through BES1 phosphorylation status. As such we seek small molecules which mimic the phenotype induced by TyrA23, yet aim at identifying other molecular components which are crucial for CME and BR signaling.

Small molecules are ideal tools for this purpose, as they allow for a conditional and reversible perturbation of a system, which in nature is very dynamic and often only occurs through triggers from the environment. Classical genetics strategies to dissect a relation between BR signaling and endomembrane traffic are less suited, as problems might arise with essential or redundant gene products[21]. In addition, they impose a steady state, which even in case of inducibility of transgenes can be a problem, as the intended condition might be established after too long period to dissect rapid changes in signaling and traffic.

Results and Discussion

We have previously shown that CME inhibition by either using drugs or genetic tools enhanced BR signaling[14]. To further dissect the interaction between BR signaling and endocytosis we set to identify small molecules that affect both CME and BR signaling in Arabidopsis. We relied on a previously described large chemical screen for inhibitors of tobacco pollen germination and polar growth[22,23]. Pollen germination and tube growth rely on multiple processes, among which vesicle trafficking and endocytosis, therefore any inhibitor is a potential effector of endomembrane transport[22,23]. The screen identified 360 compounds that affected pollen germination and growth, a success rate of about 0.7%. Out of those 360 small molecules, 123 altered the localization of different plasma membrane proteins including BRI1 and PIN FORMED2 (PIN2)[22]. Based on availability, 51 small molecules of the 123 were considered for the screen, as altered localization of plasma membrane proteins might indicate defects in CME (**Table 1**). Several readouts were used in order to characterize and identify the best candidates and the small molecules were grouped according to different induced phenotypes related to the relevant readouts (**Table 2**).

Compound Screen for CME inhibitors

The amphiphilic styryl dye FM4-64 is commonly used as an endocytic tracer in plant biology[24,25], and inhibition of FM4-64 uptake into the cell is an indication of defective CME. Therefore, 51 small molecules were screened for their ability to inhibit FM4-64 uptake in Arabidopsis root epidermal cells at a concentration of 50 µM. Four different phenotypes of FM4-64 uptake were observed. The first group of small molecules (FM01), allowed uptake of FM4-64, although uptake could be reduced compared to the mock treatment. Important was the visibility of FM4-64 positive endosomal

structures in the cytosol, indication of uptake and functional CME (**Figure 1a**). The second group, FM02 appeared to inhibit FM4-64 uptake to a large extent, as FM4-64 positive endosomal structures were not visible in the cytosol, though often FM4-64 positive structures could be distinguished which localized on the PM, and were never seen separate from the PM (**Figure 1a, inset**). Thus, unlike small molecules belonging to the FM01 group, small molecules from the FM02 group did not show the typical FM4-64 positive foci in the cytosol. The small molecules of the FM03 group allowed PM labeling of FM4-64 but inhibited its uptake completely, and lacked the FM4-64 labeled structures seen in the FM02 group (**Figure 1a**). FM03 therefore encompasses these small molecules which only induce a clean PM labeling by FM4-64. Two small molecules (group FM04) induced cytoplasmic labeling of FM4-64, most likely due to cytotoxicity effects at this concentration (**Figure 1a**). Overall the majority of small molecules severely affected FM4-64 uptake, and belonged either to the FM02 or FM03 groups (**Figure 3a**).

As all 51 small molecules were previously selected and described as effectors of plasma membrane protein localization[22], we validated those observations by evaluating their effect on BRI1-GFP[26] localization in *Arabidopsis* root epidermal cells at a concentration of 50 µM. Again small molecules were divided in several groups, according to the observed phenotypes. The first group (BRI01), encompasses these small molecules that seem to increase the size of BRI1-GFP positive foci in the cytosol (**Figure 1b**) and reduced their number, possibly due to clustering. The second group (BRI02) includes small molecules which seem to reduce the number of BRI1-GFP positive foci, without affecting size of foci in an obvious manner (**Figure 1b**). Compounds in groups BRI03 and BRI04 altered the BRI1-GFP localization in a more profound way. Small molecules from the BRI03 group shifted the GFP signal towards the cytosol, though foci might still be visible (**Figure 1b**). For small molecules PMRA2C05 and PMRA1B07 cytosolic localization corresponds to what appears to be auto-fluorescence, as the cytosolic GFP signal overlaps with signal in the RFP channel, while no RFP or red dye was present. Small molecules from the BRI04 group shifted the GFP signal towards the vacuolar lumen, yet foci are still present. Finally small molecules from the BRI05 group induced a strong reduction in overall GFP signal intensity (**Figure 1c**), without necessarily affecting the BRI1-GFP localization. Globally the overall contribution of the BRI05 group stands out (**Figure 3b**), and might indicate that a considerable amount of small molecules display widespread effects throughout the cell, and possibly toxicity, at a concentration of 50 µM.

Cytoskeletal interactions with different aspects of endomembrane traffic are of paramount importance for proper mechanical and physiological functioning of the endomembrane system[27]. Therefore the MAP4-GFP[28] marker was chosen as a primary readout for screening to assess small molecule effects on the microtubule cytoskeleton. Eventually small molecule hits will also need to be evaluated for their effect on the actin cytoskeleton. Here, we define three different groups. The first group (MAP01), did not affect MAP4-GFP localization (**Figure 1d**). The second group (MAP02), included

small molecules which induced a distinct punctate localization of MAP4-GFP, while the typical bundles were in most cases completely absent (**Figure 1d**). In addition, in almost all cases MAP4-GFP localized to a diffuse cytoplasmic signal as well. Finally MAP03 encompasses small molecules which induced a diffuse cytoplasmic labeling of MAP4-GFP, yet in contrast to the MAP02 group, few or no punctate structures were visible (**Figure 1d**). Both MAP02 and MAP03 groups indicate a heavily affected microtubule cytoskeleton, and together encompass about 75% of screened small molecules (**Figure 3c**), which is a similar distribution seen for inhibition of FM4-64 uptake.

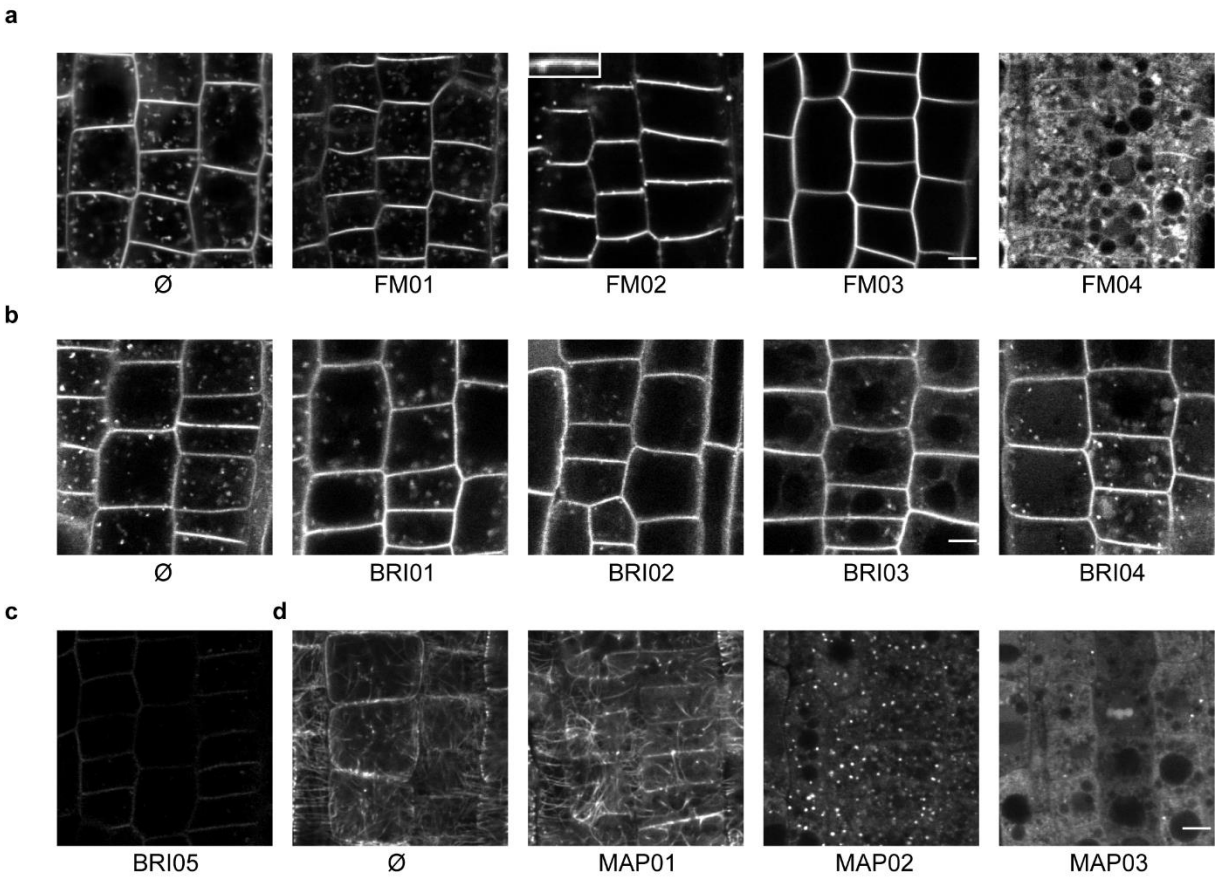

Figure 1. Compound screen for CME inhibitors.

(a) Different patterns of the FM4-64 uptake in presence of small molecules. (**b**) Localization of BRI1-GFP upon small molecule treatment, and (**c**) loss of GFP fluorescence. (**d**) Localization of MAP4-GFP in presence of small molecules. Mock treatment (Ø), no effect of FM4-64 uptake (FM01), complete block of FM4-64 uptake apart from foci at the plasma membrane (FM02), complete uptake inhibition (FM03) and cytosolic signal of FM4-64 (FM04). BRASSINOSTEROID INSENSITIVE1 (BRI1). Slightly bigger BRI1 labelled foci (BRI01), less BRI1 labelled foci (BRI02), apparent cytosolic signal (BRI03) and increased vacuolar signal (BRI04). Loss of overall fluorescence (BRI05). MICROTUBULE ASSOCIATED PROTEIN4 (MAP4). No effect on MAP4 localization (MAP01), appearance of dotted MAP4 localization in presence of small molecule (MAP02) and complete cytosolic signal (MAP03). Arabidopsis root epidermal cells of 5 day old seedlings were used in all experiments. Scale bar: 5 µm.

BR signaling in response to small molecules

To assess the effects of selected 51 small molecules on BR signaling, we evaluated the phosphorylation status of the BR transcriptional regulator BES1[5] after chemical application. In absence of BRs, we expect to see a phosphorylated form on western blot, as this transcription factor is phosphorylated by BIN2 and retained in the cytosol[29]. Upon BR application we expect to detect a de-phosphorylated form of BES1 by using western blot, since inactivation of BIN2 and de-phosphorylation of BES1 causes its migration into the nucleus and is required for activation of transcription[29]. We evaluated the phosphorylation status of BES1 by means of western blot analysis[5], as shown before. Small molecules were applied at a concentration of 50 µM for 1 hour to *Arabidopsis* PSB-D cell suspension cultures transformed with a BES1-TAP construct for easy detection. Three different phenotypes were observed (**Figure 2a**). The first group of compounds (assigned as BES01) had very little or no effect on the phosphorylation status of BES1 compared to the mock treatment. An example of this phenotype is the treatment with 50 µM of compound PMRA1B09 (**Figure 2a**). The second group of small molecules (BES02) induced partial de-phosphorylation of BES1, exemplified by treatment with 50 µM of compound PMRA1B06, while the third group (BES03) caused a complete shift towards the de-phosphorylated form of BES1, exemplified by treatment with 50 µM of compound PMRA1D02 and PMRA1F11 (**Figure 2a**). Both phenotypes indicate a presumably increased activation of BR signaling, with the latter one being the most efficient. In conclusion, small molecules distributed to the three groups in comparable numbers, with the largest group being small molecules which dephosphorylated BES1 completely (**Figure 3d**).

Small molecule screen on light-grown and dark-grown seedlings

In order to assess the effect of the small molecules on overall seedling growth, seedlings were grown on small molecule containing medium for 7 days either in light or in dark. Seedlings grown in the light were categorized in four different groups. The first group, Light Grown01 (LiGr01) includes these small molecules which inhibit germination (**Figure 2b**). Second, LiGr02 encompasses seedlings which compare in growth to the mock treated seedlings (**Figure 2b**). The third group, LiGr03, concerns small molecules which induce a reduction in seedling growth. This can range from severe growth reduction, exemplified by seedlings with very small cotyledons and hardly any root, to seedlings showing only slight reduction in root growth and cotyledon size (**Figure 2b**). Finally, LiGr04 represents small molecules which seem to affect root growth specifically. In this group, seedlings appear to have cotyledons comparable in size to mock treated seedlings, yet root growth is severely affected (**Figure 2b**).

Dark-grown seedlings were divided in 6 different groups. A first group, Dark Grown01 (DaGr01), failed to germinate under test conditions (**Figure 2c**). A second group, DaGr02, induced a phenotype very similar to mock treated dark grown seedlings (**Figure 2c**). Thirdly, DaGr03 represents seedlings

which showed varying degrees of growth inhibition (**Figure 2c**). Phenotypes ranged from little effect on seedling growth to severe growth inhibition, with only few seedlings germinating. Next, DaGr04 represents seedlings which grew agravitropically, while growth was not severely affected (**Figure 2c**). Often root growth is more affected than hypocotyl growth. The latter observation is also true for the group DaGr05. This group seemed to have a normal gravitropic response, while root growth was severely affected. In most cases only a small stub of what is supposedly the root is visible (**Figure 2c**). Finally the group DaGr06 represents seedlings which showed what resembled photomorphogenic responses. The apical hook and closed cotyledons seen for mock treatment was not present and replaced by upwards facing open cotyledons, while seedlings still developed an elongated hypocotyl (**Figure 2c**). As expected, phenotypes induced by small molecule are not always belonging clearly to the groups described above. For example, small molecules PMRA2C05 and PMRA2B11 induced at 25 µM a phenotype which appears to be a mixture between an agravitropic response (DaGr04) and hardly any root growth (DaGr05) (**Figure 2d**). Additionally, small molecule PMRP3B05 induced at 50 µM a phenotype unlike all described groups. Seedlings in most cases developed what appeared to be a normal root, yet the hypocotyl was severely stunted (**Figure 2e**). In summary, light-grown seedlings displayed in more than half of the cases reduced growth (LiGr03) (**Figure 3e**). A similar trend was seen for dark grown seedlings, where growth inhibition (DaGr03) and seedlings without root (DaGr05) were among the most seen phenotypes. In contrast, only 2 small molecules induced a clear agravitropic response without severely affecting either hypocotyl or root growth, or both (**Figure 3f**).

In addition, we compared dark grown seedlings on small molecules to seedlings on brz[3]. In presence of brz in the dark, which is an inhibitor of the BR biosynthetic enzyme DWARF4 (DWF4)[30], seedlings develop a de-etiolated phenotype with short hypocotyl and open cotyledons (**Figure 2c**), which can be rescued by either application of BRs or by overexpressing BR signaling components. Seedlings grown on small molecules, which phenocopy the effect of brz, as an indication of inactive BR signaling or biosynthesis were not favorable in our screen. However, none of the small molecules tested, induced a brz-like phenotype. Later, the brz phenotype was used eventually for a different purpose, where small molecules activating BR signaling could be applied in an attempt to rescue the brz phenotype.

Not all small molecules were screened at the same concentration of 50 µM. The main reason, as sometimes became apparent for short time incubation with the small molecule for cell biological purposes, was acute toxicity. As a substantial amount of small molecules would otherwise inhibit germination, small molecules were often tested at lower concentrations for longer incubations, as indicated (**Table 2**).

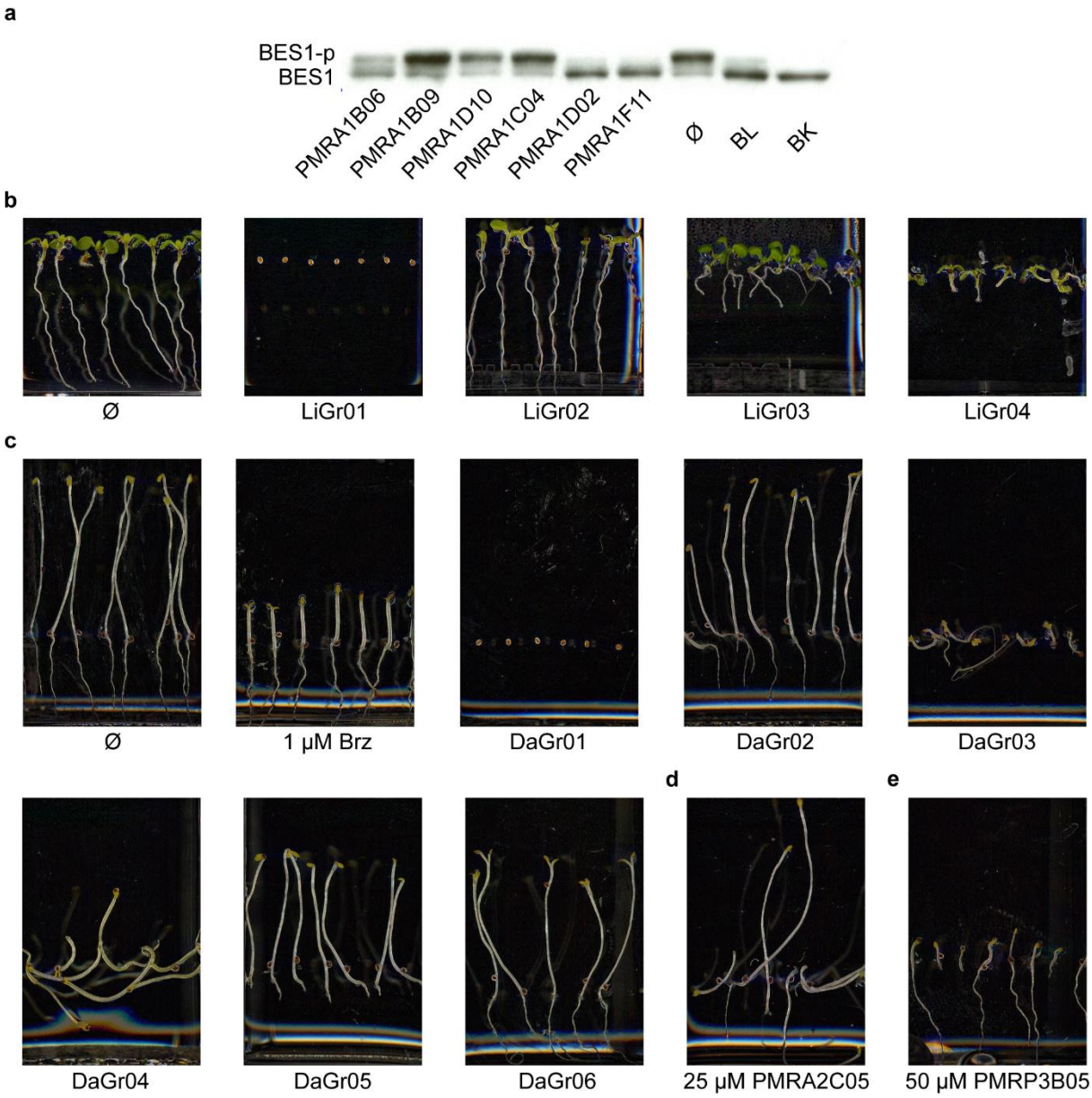

Figure 2. Compound screen for BR signaling activation and overall growth effects.

(a) BES1 phosphorylation as measured in PSB-D cell cultures expressing BES1-TAP, incubated for 1 hour with 50 µM small molecules. **(b)** Different observed phenotypes for 5 day old seedlings grown in the light for 7 days in presence of small molecules and (**c**) in the dark. **(d,e)** examples of specific phenotypes induced by small molecules PMRA2C05 and PMRP3B05. Phosphorylated form of BES1 (BES1-p), dephosphorylated form of BES1 (BES1), Mock treatment (Ø), brassinolide (BL), bikinin (BK), brassinazole (brz). Small molecules inhibiting germination in the light (LiGr01), hardly affecting seedling growth in the light (LiGr02) and affecting overall seedling growth (LiGr03) or root growth specifically in the light (LiGr04). DaGr01 indicates no germination, DaGr02 a mock-like phenotype, DaGr03 various degrees of growth inhibition, DaGr04 an agravitropic response, DaGr05 seedlings which lack a root, and DaGr06 a phenotype which resembles a light response. All small molecule treatments at 50µM, unless indicated differently. BRI1 EMS-SUPPRESSOR1 (BES1)

Comparative summary of screening results and selection of hit molecules

When the different phenotypic groups of compounds were compared amongst screening readouts, a few interesting trends appeared. For example, when BES1 phosphorylation status was evaluated in

function of BRI1-GFP and FM4-64 localizations the predominant distribution of small molecules which retained the phosphorylated state of BES1 (BES01) was in the groups inhibiting FM4-64 uptake (FM02 and FM03), while these small molecules mostly caused an increase in size of BRI1-labelled foci (BRI01) or accumulation of BRI1-GFP in the vacuole (BRI04) (**Figure 4a**). Another possibility for the increased fluorescence in the vacuole is an increase in vacuolar pH[31]. When BES1 was de-phosphorylated, ether partially (BES02) or completely (BES03) a relative high number of small molecules decreased the overall fluorescence of BRI1-GFP (BR05), while inhibited the FM4-64 uptake (FM02 and FM03). We can speculate that these small molecules might impose cytotoxicity at a concentration of 50 µM. Small molecules which hardly affected microtubule organization (MAP01) almost all allowed FM4-64 uptake (FM01) (**Figure 4b**). Similarly, small molecules affecting MAP4-GFP, thus from both MAP02 and MAP03 groups, almost in all cases inhibited FM4-64 uptake (FM02 or FM03) (**Figure 4b**).

Overall, the groups of main interest were the small molecules which inhibited FM4-64 uptake (both the FM02 and FM03 groups) and de-phosphorylate BES1 (BES02 and BES03). However, since this included 33 small molecules, we decided to primarily focus on small molecules belonging to groups FM03 and BES03, thus reducing the number of possible hits to 10 small molecules. The group which completely de-phosphorylated BES1 (BES03) was selected as it presented the strongest phenotype in terms of BES1 de-phosphorylation, while group FM03 contained compounds that clearly inhibited the of FM4-64 uptake without causing an accumulation of FM4-64 in foci as observed for the compounds in group FM02. From this subpopulation of small molecules we explored the possibility if certain small molecules could rescue brz treated seedlings through re-activation of BR signaling. We selected a group of 6 small molecules which completely de-phosphorylated BES1, and grew seedlings in the dark for 7 days in presence of brz and respective small molecules. Only 2 (PMRA2 A05 and PMRA2 B02) were able to partially rescue the dark grown phenotype of wild type seedlings grown on 1 µM brz (**Figure 4c,d**). As BR signaling is largely inactivated upon brz treatment, both small molecules are potentially able to re-activate BR signaling. To test this hypothesis PMRA2 A05 and PMRA2 B02 were tested on a semi-dominant mutant of BIN2, *bin2-1*[6]. However, both PMRA2 A05 and PMRA2 B02 were unable to partially rescue the dark grown *bin2-1* phenotype (**Figure 4c,d**), thus are either increasing hypocotyl length in presence of brz through a mechanism independent from BR signaling, or are rescuing through signaling activation upstream of BIN2.

In conclusion, 51 small molecules were screened for different readouts related to endomembrane traffic and BR signaling, in order to identify small molecule hits which could reveal new mechanisms and proteins involved in cross-talk between BR signaling and endomembrane traffic. We identified a group of small molecules which inhibit endocytosis and activate BR signaling. Of this group, two

small molecules were selected based on their potency for further characterization and target identification, which will be discussed in following chapters.

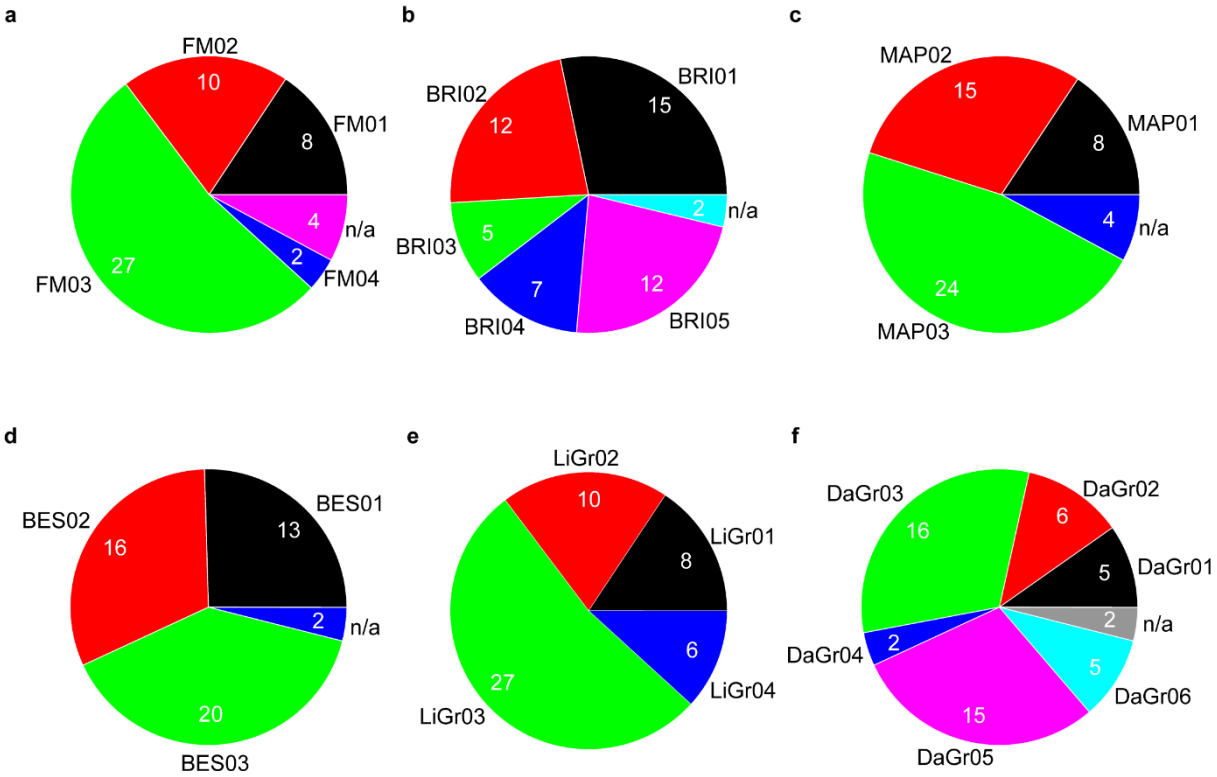

Figure 3. Distribution of the observed phenotypes of different readouts.

(**a**) Phenotypic group distribution for FM4-64 uptake, (**b**) BRI1-GFP localization, (**c**) MAP4-GFP localization (**d**) BES1 phosphorylation , (**e**) light grown seedlings and (**f**) dark grown seedlings. No effect of FM4-64 uptake (FM01), complete block of FM4-64 uptake apart from foci at the plasma membrane (FM02), complete uptake inhibition (FM03) and cytosolic signal of FM4-64 (FM04). Slightly bigger BRI1 labelled foci (BRI01), less BRI1 labelled foci (BRI02), apparent cytosolic signal (BRI03) and increased vacuolar signal (BRI04). Loss of overall fluorescence (BRI05). No effect on MAP4 localization (MAP01), appearance of dotted MAP4 localization in presence of small molecule (MAP02) and complete cytosolic signal (MAP03).Small molecules which are not changing BES1 phosphorylation status are represented by BES01, inducing partial de-phosphorylation BES02, and complete de-phosphorylation BES03. Small molecules inhibiting germination in the light (LiGr01), hardly affecting seedling growth in the light (LiGr02) and affecting overal seedling growth (LiGr03) or root growth specifically in the light (LiGr04). DaGr01 indicates no germination, DaGr02 a mock-like phenotype, DaGr03 various degrees of growth inhibition, DaGr04 an agravitropic response, DaGr05 seedlings which lack a root, and DaGr06 a phenotype which resembles a light response. BRI1 EMS-SUPPRESSOR1 (BES1), number of small molecules not tested (n/a), BRASSINOSTEROID INSENSITIVE1 (BRI1), MICROTUBULE ASSOCIATED PROTEIN 4 (MAP4).

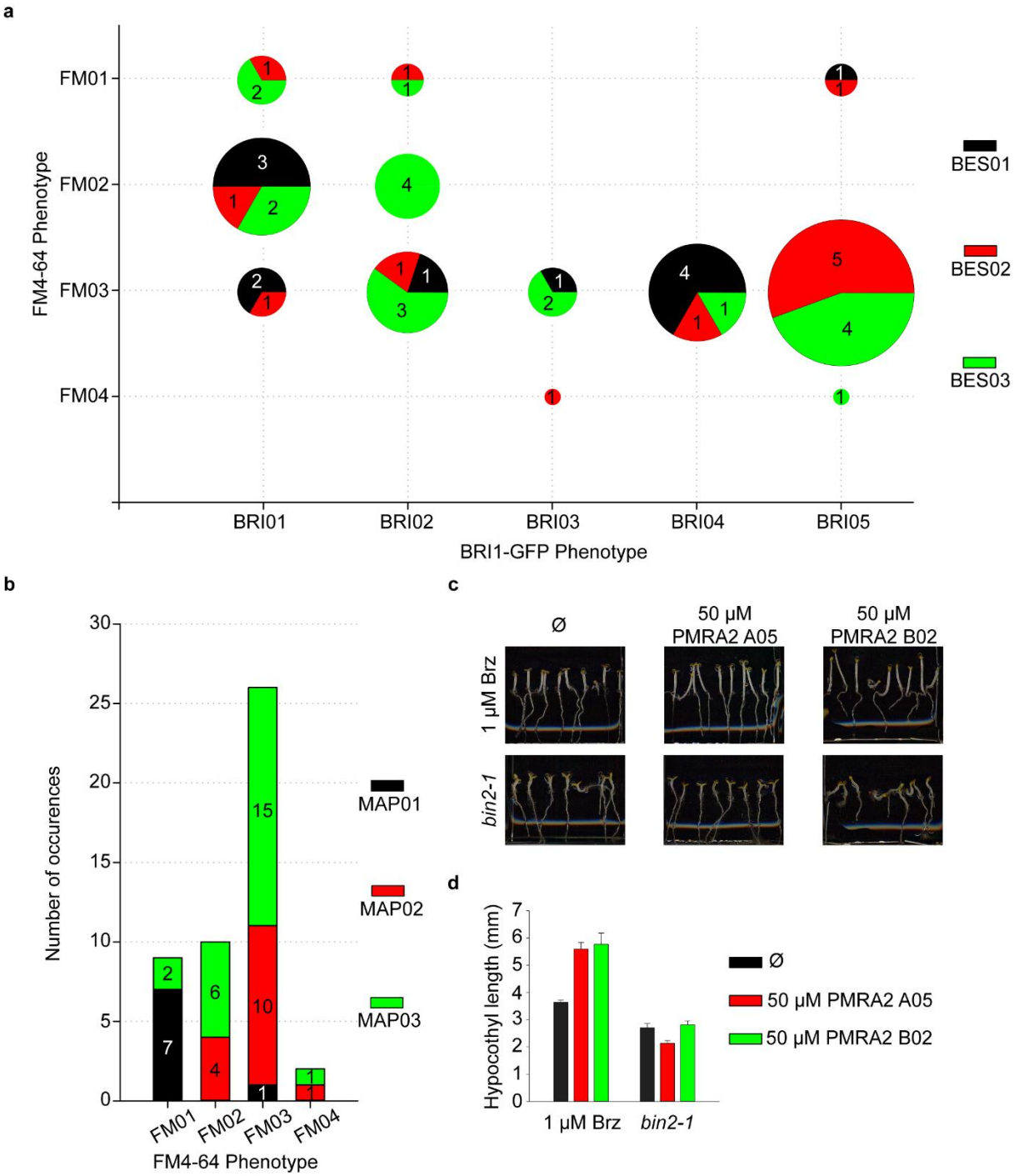

Figure 4. Distribution across different phenotypic groups and initial characterization of small molecules.

(**a**) Distribution of small molecules across different readouts, depicted as BES1 phosphorylation status in function of FM4-64 uptake and BRI1-GFP localization. (**b**) Distribution of small molecules depicted as MAP4-GFP localization in function of FM4-64 uptake phenotypes. (**c**) Two selected small molecules able to de-phosphorylate BES1 partially rescue the brz dark grown phenotype, but not the *bin2-1* dark grown phenotype. (**d**) Quantification of (c). Small molecules which are not changing BES1 phosphorylation status are represented by BES01, inducing partial de-phosphorylation BES02, and complete de-phosphorylation BES03. No effect of FM4-64 uptake (FM01), complete block of FM4-64 uptake apart from foci at the plasma membrane (FM02), complete uptake inhibition (FM03) and cytosolic signal of FM4-64 (FM04). Slightly bigger BRI1 labelled foci (BRI01), less BRI1 labelled foci (BRI02), apparent cytosolic signal (BRI03) and increased vacuolar signal (BRI04). Loss of overall fluorescence (BRI05). No effect on MAP4

localization (MAP01), appearance of dotted MAP4 localization in presence of small molecule (MAP02) and complete cytosolic signal (MAP03). BRI1 EMS-SUPPRESSOR1 (BES1), Brassinazole (Brz), BRASSINOSTEROID INSENSITIVE1 (BRI1), MICROTUBULE ASSOCIATED PROTEIN4 (MAP4), BRASSINOSTEROID INSENSITIVE2 (BIN2).

Table 1. Overview of chemical structures, names and source for small molecules used in this study.

Structure	I.D./ Ordering I.D.	Plate I.D.	Supplier	g/mole	Nr.
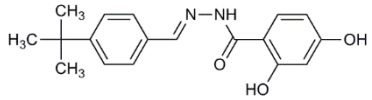	5474792 / 5474792	PMRA1 B09	Chembridge	312.4	1
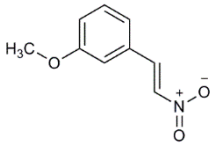	LAT035E07 / S 12156	PMRA2 B04	LATCA-Maybridge	179	2
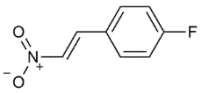	LAT045F06 / S 11468	PMRA2 C06	LATCA-Maybridge	167	3
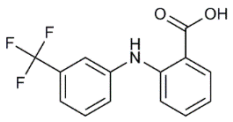	ST026563	PMRA2 C09	Myria-TimTec	281.23	4
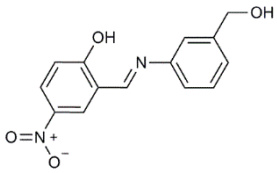	5274192 / 5274192	PMRA1 A04	Chembridge	272.3	5
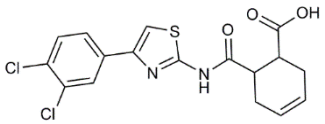	6118237 / 6118237	PMRA1 D10	Chembridge	397.3	6
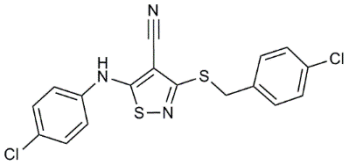	LAT029G06 / DP 00892	PMRA2 A06	LATCA-Maybridge	392	7
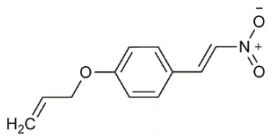	LAT045B08 / S 14817	PMRA2 C04	LATCA-Maybridge	205	8

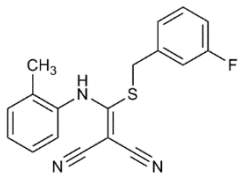	ST014024	PMRA2 C07	Myria-TimTec	323.38	9
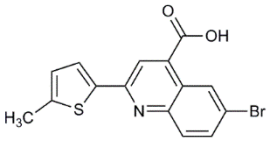	ST026114	PMRA2 C10	Myria-TimTec	347.20	10
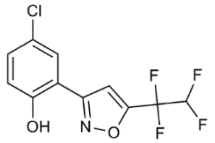	ST034275	PMRA2 D02	Myria-TimTec	295.61	11
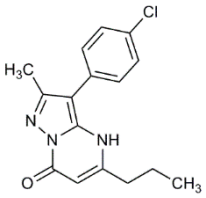	5670720 / 5670720	PMRA1 C04	Chembridge	301.8	12
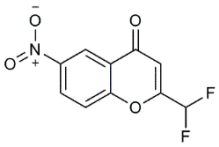	6938485 / 6938485	PMRA1 E11	Chembridge	241.1	13
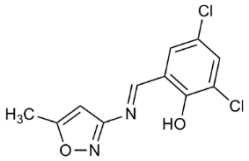	LAT045C05 / S 04777	PMRA2 C05	LATCA-Maybridge	271	14
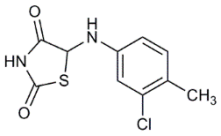	5809280 / 5809280	PMRA1 C10	Chembridge	256.7	15
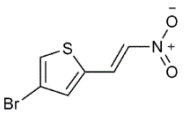	LAT035C06 / S 10775	PMRA2 A11	LATCA-Maybridge	234	16
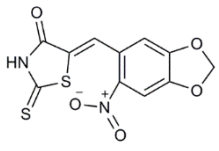	5521757 / 5521757	PMRA1 B06	Chembridge	310.3	17
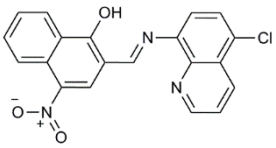	5565929 / 5565929	PMRA1 C02	Chembridge	377.8	18
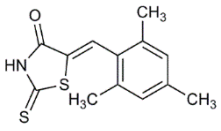	5718008 / 5718008	PMRA1 C09	Chembridge	263.4	19

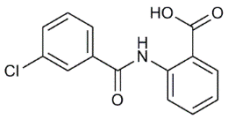	6444878 / 6444878	PMRA1 E05	Chembridge	275.7	20
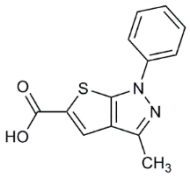	6972268 / 6972268	PMRA1 E09	Chembridge	258.3	21
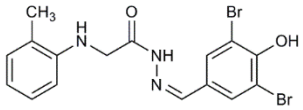	LAT009E04 / 5528794	PMRA1 H06	LATCA-Chembridge	441	22
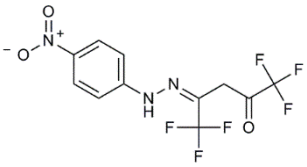	LAT036G07 / SEW 04168	PMRA2 B07	LATCA-Maybridge	343	23
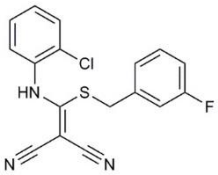	ST014025	PMRA2 C08	Myria-TimTec	343.80	24
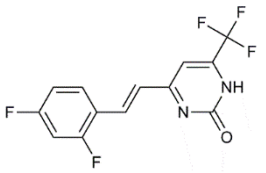	6288782 / 6288782	PMRA1 E02	Chembridge	302.2	25
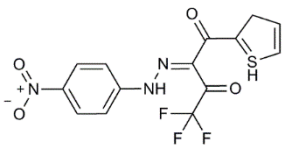	LAT037D08 / SPB 04446	PMRA2 B09	LATCA-Maybridge	371	26
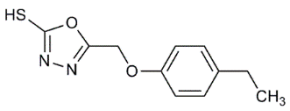	7684211 / 7684211	PMRA1 F10	Chembridge	236.3	27
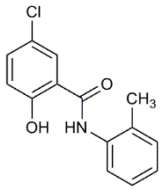	7801871 / 7801871	PMRA1 G05	Chembridge	261.7	28
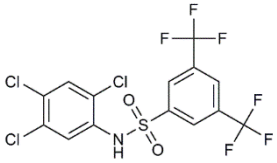	LAT041E04 / HAN 00069	PMRP3 B05	LATCA-Maybridge	473	29
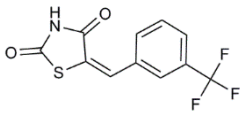	LAT013C05 / 5721666	PMRA1 H10	LATCA-Chembridge	273	30

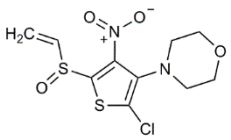	7699278 / 7699278	PMRA1 F11	Chembridge	322.8	31
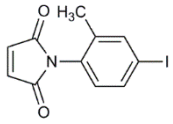	LAT034H07 / S 01528	PMRA2 A07	LATCA-Maybridge	313	32
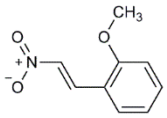	LAT035A07 / S 11753	PMRA2 A09	LATCA-Maybridge	179	33
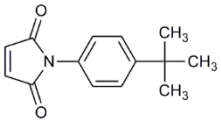	LAT035D03 / S 06736	PMRA2 B02	LATCA-Maybridge	229	34
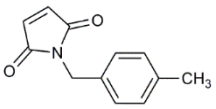	LAT035H11 / S 14672	PMRA2 B06	LATCA-Maybridge	201	35
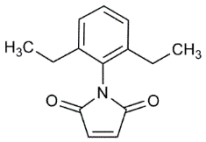	LAT036H11 / S 02113	PMRA2 B08	LATCA-Maybridge	229.27	36
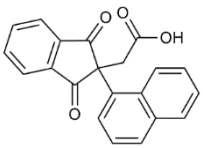	5308158 / 5308158	PMRA1 A07	Chembridge	330.3	37
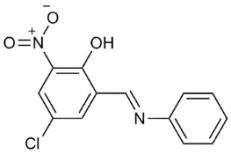	5478801 / 5478801	PMRA1 B07	Chembridge	276.7	38
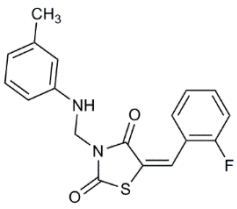	5581956 / 5581956	PMRA1 B11	Chembridge	342.4	39
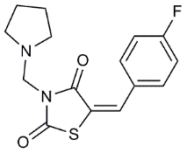	5885031 / 5885031	PMRA1 D02	Chembridge	306.4	40
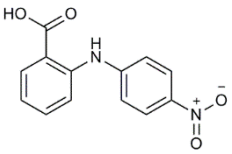	5943276 / 5943276	PMRA1 D11	Chembridge	258.2	41

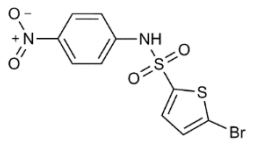	7598798 / 7598798	PMRA1 F07	Chembridge	363.2	42
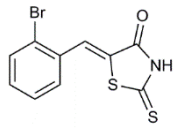	LAT013B05 / 5721479	PMRA1 H08	LATCA-Chembridge	300	43
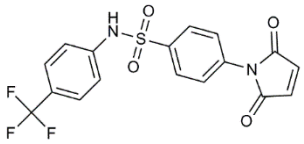	LAT029E10 / GK 01394	PMRA2 A05	LATCA-Maybridge	396	44
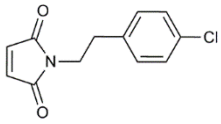	LAT035D05 / S 09759	PMRA2 B03	LATCA-Maybridge	236	45
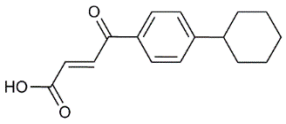	LAT038C03 / XAX 00025	PMRA2 B11	LATCA-Maybridge	258	46
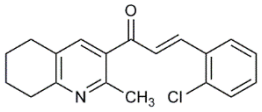	5262578 / 5262578	PMRA1 A06	Chembridge	311.8	47
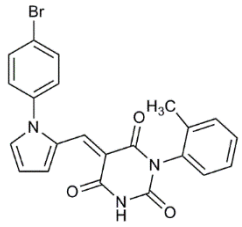	6441066 / 6441066	PMRA1 D06	Chembridge	450.3	48
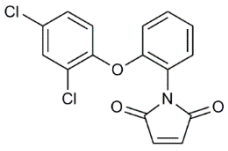	LAT035A05 / S 09528	PMRA2 A08	LATCA-Maybridge	334	49
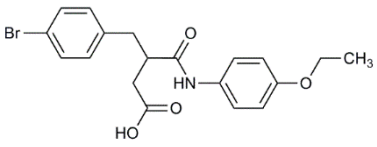	5538434 / 5538434	PMRA1 D09	Chembridge	406.3	50
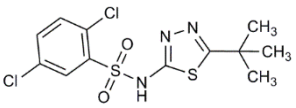	6846814 / 6846814	PMRA1 E08	Chembridge	366.3	51

Table 2. Overview of different phenotypes observed for tested readouts.

Plate ID	BES1-P phosphorylation	Effect on BRI-GFP	Effect on MAP4	FM4-64 uptake	Light-grown phenotype at (µM)	Dark-grown phenotype at (µM)
PMRA1 B09	BES01	BRI05	MAP03	FM01	LiGr02 (50)	DaGr05 (50)
PMRA2 B04	BES01	BRI01	MAP02	FM02	LiGr03 (50)	DaGr03 (50)
PMRA2 C06	BES01	BRI01	MAP02	FM02	LiGr03 (50)	DaGr05 (50)
PMRA2 C09	BES01	BRI01	MAP03	FM02	LiGr02 (25)	DaGr03 (25)
PMRA1 A04	BES01	BRI04	MAP03	FM03	LiGr03 (50)	DaGr05 (50)
PMRA1 D10	BES01	BRI04	MAP02	FM03	LiGr03 (50)	DaGr05 (50)
PMRA2 A06	BES01	BRI04	MAP03	FM03	LiGr04 (50)	DaGr03 (50)
PMRA2 C04	BES01	BRI01	MAP02	FM03	LiGr03 (50)	DaGr06 (50)
PMRA2 C07	BES01	BRI04	MAP03	FM03	LiGr02 (50)	DaGr02 (50)
PMRA2 C10	BES01	BRI03	MAP03	FM03	LiGr01 (50)	DaGr05. (25)
PMRA2 D02	BES01	BRI01	MAP03	FM03	LiGr02 (25)	DaGr02 (50)
PMRA1 C04	BES01	BRI02	MAP03	FM01	LiGr02 (50)	DaGr06 (50)
PMRA1 E11	BES01	BRI03	N/A	N/A	LiGr01 (50)	DaGr01 (50)
PMRA2 C05	BES02	BRI03	MAP03	FM04	LiGr03 (50)	DaGr05 (25)
PMRA1 C10	BES02	BRI01	MAP01	FM01	LiGr03 (50)	DaGr02 (50)
PMRA2 A11	BES02	BRI01	MAP03	FM02	LiGr03 (50)	DaGr03 (50)
PMRA1 B06	BES02	BRI05	MAP03	FM03	LiGr02 (50)	DaGr02 (50)
PMRA1 C02	BES02	BRI05	MAP03	FM03	LiGr01 (50)	DaGr03 (50)
PMRA1 C09	BES02	BRI05	MAP02	FM03	LiGr03 (50)	DaGr03 (50)
PMRA1 E05	BES02	BRI05	MAP02	FM03	LiGr01 (50)	DaGr06 (25)
PMRA1 E09	BES02	BRI01	MAP02	FM03	LiGr04 (50)	DaGr05 (50)
PMRA1 H06	BES02	BRI02	MAP03	FM03	LiGr03 (50)	DaGr05 (50)
PMRA2 B07	BES02	BRI05	MAP03	FM03.	LiGr01 (25)	DaGr01 (12.5)
PMRA2 C08	BES02	BRI04	MAP03	FM03	LiGr02 (50)	DaGr03. (50)
PMRA1 E02	BES02	BRI02	MAP01	FM01	LiGr03 (50)	DaGr05 (50)
PMRA2 B09	BES02	BRI05	MAP01	FM01	LiGr03 (50)	DaGr01 (50)
PMRA1 F10	BES02	BRI02	N/A	N/A	LiGr03 (50)	DaGr03 (50)
PMRA1 G05	BES02	BRI01	N/A	N/A	LiGr02 (50)	DaGr02 (50)
PMRP3 B05	BES02	BRI01	N/A	N/A	LiGr03 (50)	DaGr03 (50)
PMRA1 H10	BES03	BRI05	MAP02	FM04	LiGr02 (12,5)	DaGr06 (50)
PMRA1 F11	BES03	BRI02	MAP02	FM02	LiGr03 (50)	DaGr03 (50)
PMRA2 A07	BES03	BRI02	MAP02	FM02	LiGr04 (50)	DaGr03 (50)
PMRA2 A09	BES03	BRI01	MAP03	FM02	LiGr01 (50)	DaGr01 (50)
PMRA2 B02	BES03	BRI02	MAP03	FM02	LiGr03 (50)	DaGr03 (50)
PMRA2 B06	BES03	BRI01	MAP03	FM02	LiGr03 (50)	DaGr04 (50)
PMRA2 B08	BES03	BRI02	MAP03	FM02	LiGr03 (50)	DaGr06 (25)
PMRA1 A07	BES03	BRI05	MAP02	FM03.	LiGr03 (50)	DaGr05 (50)

PMRA1 B07	BES03	BRI03	MAP03	FM03	LiGr01 (50)	DaGr05 (25)
PMRA1 B11	BES03	BRI05	MAP03	FM03	LiGr03 (50)	DaGr05 (50)
PMRA1 D02	BES03	BRI05	MAP03	FM03	LiGr03 (50)	DaGr01 (50)
PMRA1 D11	BES03	BRI02	MAP03	FM03	LiGr04 (50)	DaGr04 (50)
PMRA1 F07	BES03	BRI04	MAP03	FM03	LiGr03 (12,5)	DaGr05 (12.5)
PMRA1 H08	BES03	BRI03	MAP02	FM03.	LiGr03 (50)	DaGr03 (50)
PMRA2 A05	BES03	BRI02	MAP01	FM03	LiGr02 (50)	DaGr02 (50)
PMRA2 B03	BES03	BRI02	MAP02	FM03	LiGr04 (50)	DaGr03 (25)
PMRA2 B11	BES03	BRI05	MAP02	FM03	LiGr03 (50)	DaGr05 (25)
PMRA1 A06	BES03	BRI02	MAP01	FM01	LiGr03 (50)	DaGr03 (50)
PMRA1 D06	BES03	BRI01	MAP01	FM01	LiGr04 (50)	DaGr05 (50)
PMRA2 A08	BES03	BRI01	MAP01	FM01	LiGr03 (50)	DaGr04 (50)
PMRA1 D09	N/A	N/A	MAP01	FM01	LiGr03 (50)	N/A
PMRA1 E08	N/A	N/A	MAP02	FM03	LiGr01 (50)	N/A

Materials and methods

Plant material and growth conditions

For screening of light and dark grown seedlings, wild type *Arabidopsis thaliana* ecotype Col-0 or *bin2-1*[6] seedlings were stratified for 2 days at 4°C, on half strength Murashige and Skoog (½ MS) plates with 1% (w/v) sucrose supplemented with small molecules or dimethyl sulfoxyde (DMSO) as a mock treatment. Subsequently plates were incubated for 3-4 hours in the light (and remained there in case of light grown seedlings), before transfer to dark for an additional 7 days at 22°C, and grown vertically. For imaging purposes, BRI1-GFP[26] or MAP4-GFP[28] *Arabidopsis thaliana* ecotype Col-0 seedlings were stratified for 2 days at 4°C, and grown on vertical ½ MS plates with 1% (w/v) sucrose for an additional 5 days at 22°C in a light/dark cycle of 16hrs/8hrs respectively, prior to imaging.

Chemical treatments and imaging

Small molecules for screening were acquired through Chembridge (http://www.chembridge.com/), brassinazole through TCI Europe, brassinolide through Fuji Chemical Industries and Bikinin through Sigma-Aldrich. All small molecules were dissolved in DMSO (Sigma-Aldrich). Imaging of seedlings was performed with an Olympus FV10 ASW confocal microscope. For MAP4-GFP and FM4-64 screening, MAP4-GFP seedlings were incubated with the respective small molecules for 30 min in ½ MS, followed by a pulse with 2 µM N-(3-Triethylammoniumpropyl)-4-(6-(4-(Diethylamino) Phenyl) Hexatrienyl) Pyridinium Dibromide (FM4-64, Life technologies) for another 30 min. BRI1-GFP seedlings were incubated with small molecules for 60 min in ½ MS, followed by imaging.

BES1 dephosphorylation assay

PSB-D cell cultures expressing BES1-TAP were generated and maintained as described before[17,32]. Cell cultures were treated with small molecules (50 µM), brassinolide (BL, 1 µM) and Bikinin (BK, 30 µM) for 1 hour while shaking at 130 rpm and harvested and homogenized in liquid nitrogen. Protein extraction was performed with a 20mM Tris-HCl buffer containing 150 mM NaCl, 1% Sodium Dodecyl Sulfate (SDS), 100 mM Dithiothreitol (DTT) and 1 cOmplete ultra tablet per 10 ml of EDTA free protease inhibitor cocktail (Roche). Protein concentration was determined with the Quick start Bradford 1x Dye reagent (Bio-Rad). Samples (30 µg) were run on a 10% SDS-PAGE gel and transferred to polyvinyl difluoride (PVDF) membrane from iBlot Gel Transfer Stack (Novex, Life Technologies) using the iBlot device (Life technologies). Membranes were blocked for 1 hour in Tris buffered Saline with 0.1 % Tween 20 (TBS-T, Sigma-Aldrich) and 3% Difco Skim milk (Becton, Dickinson and Company). Detection of BES1-TAP occurred with a 1/5000 dilution in TBS-

T 3% skim milk of Horseradish peroxidase (HRP) conjugated Peroxidase Anti-Peroxidase (PAP) Soluble Complex antibody produced in rabbit (P1291, Sigma) for 1 hour. Membrane was developed with application of Western Lightning® Plus–ECL, Enhanced Chemiluminescence Substrate (Perkin-Helmer) and Amersham Hyperfilm ECL (GE Healthcare).

References

1. Dejonghe, W., Mishev, K. & Russinova, E. The brassinosteroid chemical toolbox. *Curr Opin Plant Biol* **22C**, 48–55 (2014).
2. de Rybel, B. et al. Chemical inhibition of a subset of Arabidopsis thaliana GSK3-like kinases activates brassinosteroid signaling. *Chem Biol* **16**, 594–604 (2009).
3. Asami, T. et al. Characterization of brassinazole, a triazole-type brassinosteroid biosynthesis inhibitor. *Plant Physiol* **123**, 93–100 (2000).
4. Wang, Z.-Y. et al. Nuclear-localized BZR1 mediates brassinosteroid-induced growth and feedback suppression of brassinosteroid biosynthesis. *Dev Cell* **2**, 505–513 (2002).
5. Yin, Y. et al. BES1 accumulates in the nucleus in response to brassinosteroids to regulate gene expression and promote stem elongation. *Cell* **109**, 181–191 (2002).
6. Li, J. & Nam, K. H. Regulation of brassinosteroid signaling by a GSK3/SHAGGY-like kinase. *Science* **295**, 1299–1301 (2002).
7. He, J.-X., Gendron, J. M., Yang, Y., Li, J. & Wang, Z.-Y. The GSK3-like kinase BIN2 phosphorylates and destabilizes BZR1, a positive regulator of the brassinosteroid signaling pathway in Arabidopsis. *Proc Natl Acad Sci USA* **99**, 10185–10190 (2002).
8. Gampala, S. S. et al. An essential role for 14-3-3 proteins in brassinosteroid signal transduction in Arabidopsis. *Dev Cell* **13**, 177–189 (2007).
9. McMahon, H. T. & Boucrot, E. Molecular mechanism and physiological functions of clathrin-mediated endocytosis. *Nat Rev Mol Cell Biol* **12**, 517–533 (2011).
10. Mishev, K., Dejonghe, W. & Russinova, E. Small molecules for dissecting endomembrane trafficking: a cross-systems view. *Chem Biol* **20**, 475–486 (2013).
11. Crump, C. M., Williams, J. L., Stephens, D. J. & Banting, G. Inhibition of the interaction between tyrosine-based motifs and the medium chain subunit of the AP-2 adaptor complex by specific tyrphostins. *J Biol Chem* **273**, 28073–28077 (1998).
12. Banbury, D. N. et al. Tyrphostin A23 inhibits internalization of the transferrin receptor by perturbing the interaction between tyrosine motifs and the medium chain subunit of the AP-2 adaptor complex. *J Biol Chem* **278**, 12022–12028 (2003).

13. Ortiz-Zapater, E. et al. Trafficking of the human transferrin receptor in plant cells: effects of tyrphostin A23 and brefeldin A. *Plant J* **48**, 757–770 (2006).
14. Irani, N. G. et al. Fluorescent castasterone reveals BRI1 signaling from the plasma membrane. *Nat Chem Biol* **8**, 583–589 (2012).
15. Russinova, E. et al. Heterodimerization and endocytosis of Arabidopsis brassinosteroid receptors BRI1 and AtSERK3 (BAK1). *Plant Cell* **16**, 3216–3229 (2004).
16. Geldner, N., Hyman, D. L., Wang, X., Schumacher, K. & Chory, J. Endosomal signaling of plant steroid receptor kinase BRI1. *Genes Dev* **21**, 1598–1602 (2007).
17. Di Rubbo, S. et al. The clathrin adaptor complex AP-2 mediates endocytosis of brassinosteroid insensitive1 in Arabidopsis. *Plant Cell* **25**, 2986–2997 (2013).
18. Gadeyne, A. et al. The TPLATE adaptor complex drives clathrin-mediated endocytosis in plants. *Cell* **156**, 691–704 (2014).
19. Fan, L. et al. Dynamic analysis of Arabidopsis AP2 σ subunit reveals a key role in clathrin-mediated endocytosis and plant development. *Development* **140**, 3826–3837 (2013).
20. Kim, S. Y. et al. Adaptor protein complex 2-mediated endocytosis is crucial for male reproductive organ development in Arabidopsis. *Plant Cell* **25**, 2970–2985 (2013).
21. Hicks, G. R. & Raikhel, N. V. Small Molecules Present Large Opportunities in Plant Biology. *Annu Rev Plant Biol* **63**, 13.1-13.22 (2012).
22. Drakakaki, G. et al. Clusters of bioactive compounds target dynamic endomembrane networks in vivo. *Proc Natl Acad Sci USA* **108**, 17850–17855 (2011).
23. Robert, S. et al. Endosidin1 defines a compartment involved in endocytosis of the brassinosteroid receptor BRI1 and the auxin transporters PIN2 and AUX1. *Proc Natl Acad Sci USA* **105**, 8464–8469 (2008).
24. van Gisbergen, P. A. C., Esseling-Ozdoba, A. & Vos, J. W. Microinjecting FM4-64 validates it as a marker of the endocytic pathway in plants. *J Microsc* **231**, 284–290 (2008).
25. Rigal, A., Doyle, S. M. & Robert, S. Live cell imaging of FM4-64, a tool for tracing the endocytic pathways in Arabidopsis root cells. *Methods Mol Biol* **1242**, 93–103 (2015).
26. Friedrichsen, D. M., Joazeiro, C. A., Li, J., Hunter, T. & Chory, J. Brassinosteroid-insensitive-1 is a ubiquitously expressed leucine-rich repeat receptor serine/threonine kinase. *Plant Physiol* **123**, 1247–1256 (2000).
27. Kapus, A. & Janmey, P. Plasma membrane--cortical cytoskeleton interactions: a cell biology approach with biophysical considerations. *Compr Physiol* **3**, 1231–1281 (2013).
28. Marc, J. et al. A GFP-MAP4 reporter gene for visualizing cortical microtubule rearrangements in living epidermal cells. *Plant Cell* **10**, 1927–1940 (1998).

29. Zhu, J.-Y., Sae-Seaw, J. & Wang, Z.-Y. Brassinosteroid signalling. *Development* **140**, 1615–1620 (2013).
30. Asami, T. et al. Selective interaction of triazole derivatives with DWF4, a cytochrome P450 monooxygenase of the brassinosteroid biosynthetic pathway, correlates with brassinosteroid deficiency in planta. *J Biol Chem* **276**, 25687–25691 (2001).
31. Tamura, K. et al. Why green fluorescent fusion proteins have not been observed in the vacuoles of higher plants. *Plant J* **35**, 545–555 (2003).
32. Van Leene, J. et al. A tandem affinity purification-based technology platform to study the cell cycle interactome in Arabidopsis thaliana. *Mol Cell Proteomics* **6**, 1226–1238 (2007).

Chapter III: Protonophore uncouplers are potent inhibitors of clathrin-mediated endocytosis in plants

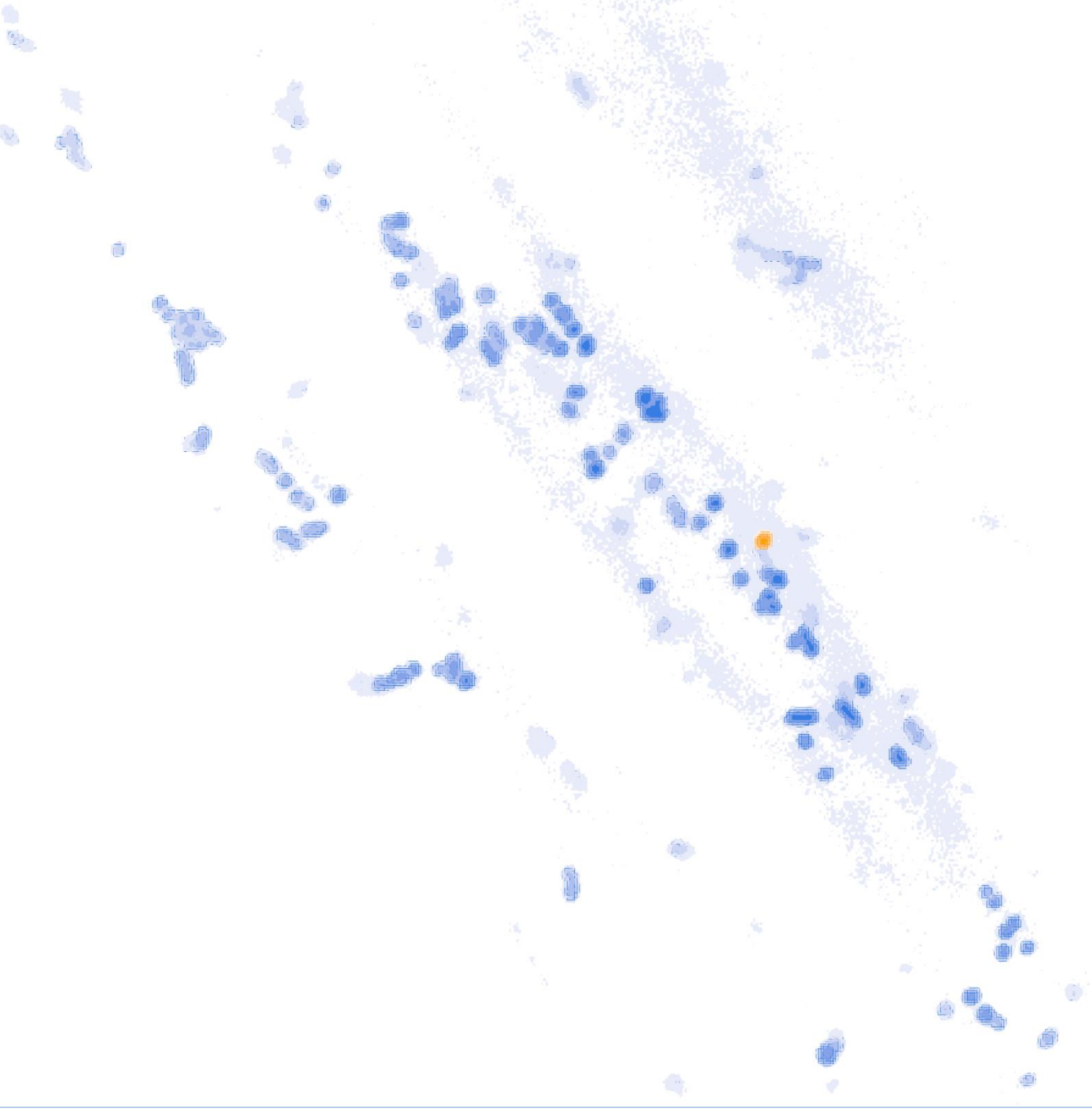

Protonophore uncouplers are potent inhibitors of clathrin-mediated endocytosis in plants

Wim Dejonghe[1], Sabine Kuenen[2], Evelien Mylle[1], Olivier Keech[3], Corrado Viotti[4], Fausto Andres Ortiz-Morea[1], Kiril Mishev[1], Simon Delang[5], Jiorgos Kourelis[6], Jaroslaw Kasprowicz[2], Le Son Long Nguyen[7], Andrzej Drozdzecki[7], Isabelle Van Houtte[1], Matyas Fendrych[8], Mina Vasileva[8], Gary Baisa[9], Sebastian Bednarek[9], Christa Testerink[6], Stephanie Robert[3], Dominique Audenaert[7], Annemieke Madder[11], Daniël Van Damme[1], Karin Schumacher[5], Jiri Friml[8], Johan Winne[11], Patrik Verstreken[3] and Eugenia Russinova[1]

[1]Department of Plant Systems Biology, VIB, Technologiepark 927, 9052 Gent, Belgium; Department of Plant Biotechnology and Bioinformatics, Ghent University, 9052 Gent, Belgium.
[2]VIB Center for the Biology of Disease, Laboratory of Neuronal Communication, Department for Human Genetics, and Leuven Institute for Neurodegenerative Diseases, KU Leuven, 3000 Leuven, Belgium.
[3]Department of Forest Genetics and Plant Physiology, Umeå Plant Science Centre, Swedish University of Agricultural Sciences Umeå, Sweden.
[4]Umeå Plant Science Centre, Department of Plant Physiology, Umeå University Umeå, Sweden
[5]Centre for Organismal Studies, University of Heidelberg, 69120 Heidelberg, Germany
[6]University of Amsterdam, Swammerdam Institute for Life Sciences, Plant Physiology, Postbus 94215, 1090GE Amsterdam, the Netherlands.
[7]Compound Screening Facility, VIB, Technologiepark 927, B-9052 Ghent, Belgium.
[8]Institute of Science and Technology (IST) Austria, 3400 Klosterneuburg, Austria
[9]Department of Biochemistry, University of Wisconsin-Madison, Madison, Wisconsin, USA
[10]Department of Organic Chemistry, Ghent University, 9000 Ghent, Belgium.

Author contributions: W.D. did large parts of the *Arabidopsis*-related cell biology and ATP depletion assays in *Arabidopsis* and *Drosophila*. W.D. wrote the text and made the figures.

Abstract

Because of its highly dynamic nature and importance, classical genetic strategies for studying clathrin-mediated endocytosis (CME) are faced with limitations, especially in plants, where knockouts of CME components are either lethal or absent due to gene redundancy. Hence, specific chemical inhibitors are more suitable for probing CME. Here, we report the identification and characterization of the small molecule Endosidin9 (ES9). ES9 interfered with receptor-mediated endocytosis in *Arabidopsis* and with synaptic vesicle recycling in *Drosophila* similarly to loss-of-function CME mutants. Though ES9 functioned as a mitochondria uncoupler, the ES9-induced inhibition of CME in *Arabidopsis* was primary due to its uncoupling activity at the plasma membrane causing cytoplasmic acidification but not to the reduction in the cellular ATP content. Similar properties were observed for the known tyrosine kinase inhibitor Tyrphostin A23 (TyrA23) routinely used to block CME in plants thus, raising questions about its use as a selective inhibitor in cell biology studies.

Introduction

Clathrin-mediated endocytosis (CME) is a major pathway for the uptake of extracellular and plasma membrane material in all eukaryotic cells[1-3]. CME is of vital importance for the cell to quickly respond to environmental changes and its purposes are manifold including pathogen entry, synaptic vesicle turn-over, uptake of membrane bound receptors either constitutively or following stimuli, which in turn influences signaling outputs[1]. In plants mechanistic understanding of CME is not as advanced as compared to the yeast or mammalian field, even though in recent years important insights have been achieved. For example, part of the core machinery is conserved between plants, yeast and mammals[4], yet differences exist as illustrated by the recent report on the TPLATE adaptor complex[4-6]. Similarly to mammals and yeast, CME in plants has major effects on a plethora of physiological responses[7-10], including hormone signaling, polarity establishment, plant defense responses, transport of nutrients and cell wall materials.

The essential and dynamic nature of CME makes it difficult to dissect with classical genetic tools, as each mutant, if viable, represents a steady state. In order to circumvent those limitations and interfere with CME in a conditional manner, the use of small molecule effectors offers important advantages[11]. A well-known example of an endocytic inhibitor frequently used in the plant field is tyrphostinA23 (TyrA23). TyA23 is a tyrosine-like small molecule originally developed as a substrate-competitive inhibitor of mammalian tyrosine kinases[12]. TyrA23 also interferes with the interaction between the tyrosine-based internalization motifs of different cargos and the medium subunit of the clathrin-associated adaptor complex AP-2, and it inhibited CME *in vitro* and in a yeast two-hybrid growth inhibition assay[13,14]. The inhibitory effect of TyrA23 on CME was later confirmed in plants[15], and has since been used in numerous studies[8-10,16-31], although its mode of action in plants has not been clarified as yet. In contrast to plant systems, where TyrA23 is almost exclusively used to specifically inhibit CME, mammalian and yeast systems can rely on a larger collection of small molecule tools, including dynasore[32] and Pitstops[33], though both display off-target effects and efforts are on-going to further improve on their scaffolds in order to develop novel, specific inhibitors of CME[34-36]. Although dynasore has been used in plants[37], reports for the activity of other compounds in plant cells are still lacking.

Here, we described the identification and characterization of a small molecule inhibitor, Endosidin9 (ES9), of CME in *Arabidopsis* and *Drosophila* and revealed that this molecule is a mitochondrial uncoupler. Furthermore, we showed that the known specific CME inhibitor in plant cells TyrA23 is also a mitochondrial uncoupler, a major activity of this popular small molecule that has been overlooked in previous studies. We demonstrate that the mitochondrial uncouplers such as ES9, TyrA23 and known protonophores inhibited CME in *Arabidopsis* by primary inducing acidification of the cytosol, indicating a possible general inhibitory mechanism through dissipating plasma

membrane potentials rather than through ATP depletion. ATP depletion alone was found not to impair CME to the same extent.

Results

ES9 blocks clathrin-mediated endocytosis in different systems

To identify chemical inhibitors of CME in plants we analyzed a set of 123 small molecules previously identified as inhibitors of both pollen germination and growth[38]. We screened for their ability to inhibit the uptake of the lipophilic styryl dye FM4-64, a well-known and commonly used tracer of CME in plants[39]. We identified ES9, a small molecule which activity allowed binding of FM4-64 to the plasma membrane but effectively inhibited its internalization when co-applied at a concentration of 10 µM for 30 min (**Fig. 1a,b**). To rule out that the effect of ES9 was limited to FM4-64, we tested the uptake of the fluorescent castasterone AFCS, previously shown to be internalized via CME[8,9]. In absence of ES9, AFCS (20 µM, 30 min, 20 min chase) stained the vacuole as previously shown[8]. However, in presence of ES9, AFCS was not internalized, indicating an effective uptake inhibition (**Supplemental Fig. 1a**).

To test whether the inhibitory effect of ES9 was specific to CME in plants, we assessed if ES9 interfered with synaptic vesicle endocytosis in *Drosophila* neurons and with the uptake of transferrin in HeLa cells. When tested on boutons of the neuromuscular junction (NMJ) in third instar larvae of *Drosophila* stimulated with KCl in the presence of FM 1-43, a dye analogous to FM 4-64, treatment with ES9 (10 µM, 30 min) induced the uptake of large FM1-43 positive membrane structures (**Supplemental Fig. 1b,c**). This phenotype is reminiscent of the acute loss of clathrin heavy chain (CHC)[40], clathrin light chain (CLC)[41] or dynamin[42] functions. To strengthen this observation, CHC-HA positive larvae were treated with ES9 either in a non-stimulated (NS) or stimulated situation, where endocytosis and exocytosis are enhanced[40]. Visualization of CHC revealed that ES9 activity (10 µM, 30 min) prevented the recruitment of CHC from the bouton center to the periphery in the induced situation (**Fig. 1c**), a phenotype also observed when dynamin function is impaired[40,42]. Additional graphical explanation on the *Drosophila* NMJ and synaptic boutons, applicable for the CHC and FM1-43 phenotypes, can be found in supplemental figure 1d. Finally we evaluated if ES9 activity was able to inhibit the internalization of transferrin, a hallmark tracer of CME in mammalian systems[1]. In HeLa cells, ES9 inhibited the uptake of transferrin at 50 µM to a comparable extent as 50 µM Dynasore (**Fig. 1d)**. Altogether these data show that ES9 was able to inhibit CME in different model systems, although with different efficiencies.

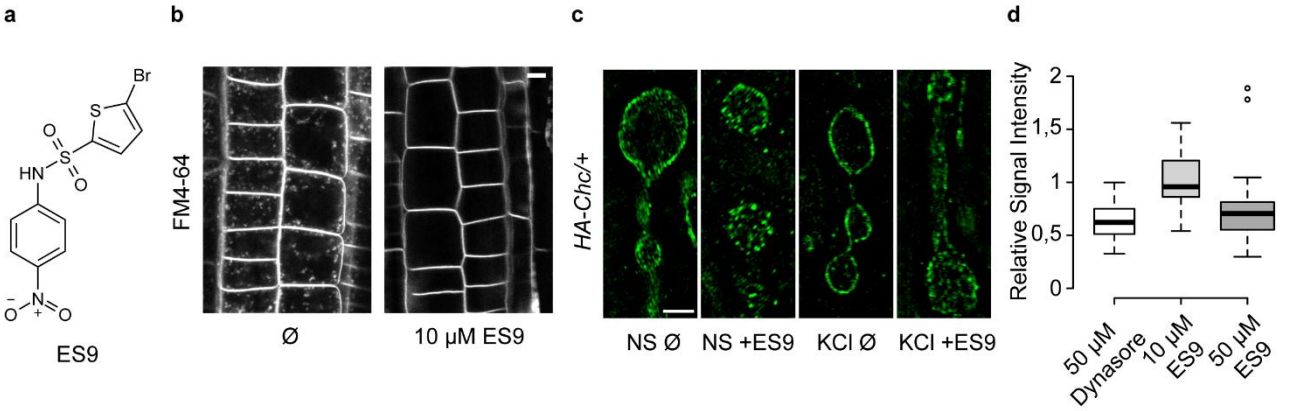

Figure 1. ES9 inhibits CME in different systems

(**a**) Chemical structure of ES9. (**b**) FM4-64 uptake (2 µM, 30 min) in *Arabidopsis* root cells for mock treatment (DMSO, Ø) and in presence of 10 µM ES9. (**c**) Boutons of the neuromuscular junction in third instar larvae of Drosophila positive for HA-tagged clathrin heavy chain (HA-CHC) for mock or 10 µM ES9 30 min pretreatments, in both non-stimulated (NS) or 90 mM KCl stimulated conditions. (**d**) Boxplot representation of transferrin uptake in HeLa cells in presence of 50 µM Dynasore and 10 or 50 µM ES9, relative to mock (DMSO). Center lines show the medians; box limits indicate the 25th and 75th percentiles as determined by R software; whiskers extend 1.5 times the interquartile range from the 25th and 75th percentiles, outliers are represented by dots. Box width relative to sample size. N = 35, 29 and 61 sample points respectively. Scale bars: 5 µm in (**b**), 2 µm in (**c**).

ES9 affects energy metabolism through uncoupling of oxidative phosphorylation in mitochondria

As CME is an energy dependent process[1] and ATP depletion has been shown to either inhibit or severely reduce CME[43,44], we assessed the capacity of ES9 to affect cellular ATP content. Cellular ATP was measured in dark-grown *Arabidopsis* PSB-D wild type cell cultures. Aside ES9 we included the known plant CME inhibitor TyrA23 and its inactive analog TyrA51[15] as negative references, while several known inhibitors of ATP production such as Antimycin A (AA)[45], Oligomycin[46] and carbonyl cyanide m-chlorophenyl hydrazone (CCCP)[47,48] were included as positive controls. ES9 (10 µM) induced a quick initial depletion of ATP to about 50% cellular ATP after 2 min of treatment. The ATP concentration further declined for the following 20 min, after which a base line of about 10% remaining ATP was established compared to mock treatment (**Fig. 2a**). Interestingly, TyrA23, but not TyrA51, induced a reduction in the cellular ATP of about 75% within 2 min, which subsequently stabilized at about 10% residual ATP as compared to the mock control (**Fig. 2a**). The ATP depletion profile of ES9 and TyrA23 were similar to those of AA and CCCP but differed from Oligomycin (**Fig. 2a**), where the reduction in ATP content occurred more gradually. To rule out that ATP depletion was a result of an acute cytotoxic effects of the compounds, all small molecules were tested on PSB-D wild type cell cultures for fluorescein diacetate (FDA) hydrolysis[49], a marker for cell viability. In all cases, FDA profiles increased similar to the control treatment (**Supplemental Fig.**

2a). These results suggest that ES9 and TyrA23 affected ATP production, which was not due to an acute loss in cell viability.

Since PSB-D cell cultures are dark grown, mitochondria represent the main ATP producer for the cell. We therefore hypothesized that ES9 and TyrA23 could alter mitochondrial properties. In order to test this hypothesis, we isolated mitochondria from *Arabidopsis* leaves[50] and performed a series of respiratory measurements *ex cellulo*. Mock treatment did not affect the mitochondrial electron transport chain (mETC) as high respiratory control ratios (RCRs) were maintained (**Supplemental Fig. 2b-c**). Addition of CCCP (1 μM) led to a characteristic rapid and transient increase in the respiratory rate as well as a clear uncoupling between oxidations and phosphorylations within the mETC as shown by the RCR drop even after addition of ADP (**Supplemental Fig. 2b-c**). ES9 (1 μM) and TyrA23 (5 μM) at even lower concentrations, but not TyrA51 (5 μM), had a similar effect as CCCP on respiratory properties (**Supplemental Fig. 2b-c**), suggesting that like CCCP, both TyrA23 and ES9 are mitochondrial uncouplers in *Arabidopsis* cells.

The dissipation of mitochondrial membrane potential in the presence of ES9 and TyrA23 was confirmed *in vivo* using MitoTracker Red CM-H2XRos staining of mitochondria in *Arabidopsis* root cells, which is reduced or prevented when electron transport is uncoupled or inhibited[51]. Therefore, MitoTracker Red CM-H2XRos was subsequently used to visualize disruptions of mitochondrial membrane potential in the early differentiation zone of *Arabidopsis* roots, as individual mitochondria can be easily distinguished in these cells. The mitochondrial labeling was not affected after mock (DMSO) and TyrA51 treatments (50 μM, 30 min) (**Fig. 2b**), whereas in cells treated for the same time with CCCP (1 μM), ES9 (10 μM), AA (20 μM) or TyrA23 (50 μM) no mitochondria were detected, though non-mitochondrial labeling seemed to be increased (**Fig. 2b**).

The ability of ES9 to deplete ATP was also evaluated in *Drosophila*. Comparable to *Arabidopsis*, ES9 depleted ATP in *Drosophila* S2 cell cultures similar to CCCP, TyrA23 and AA (**Supplemental Fig. 2d**). Surprisingly, TyrA51 was also able to deplete ATP in *Drosophila* cells to approximately 50% of control conditions. Active mitochondria in *Drosophila* are labeled with tetramethylrhodamine ethyl ester (TMRE)[52], which was greatly impaired in the presence of ES9 (10 μM, 30 min) and CCCP (10 μM, 30 min), confirming disruption of mitochondrial function (**Fig. 2c, Supplemental Fig. 2e**).

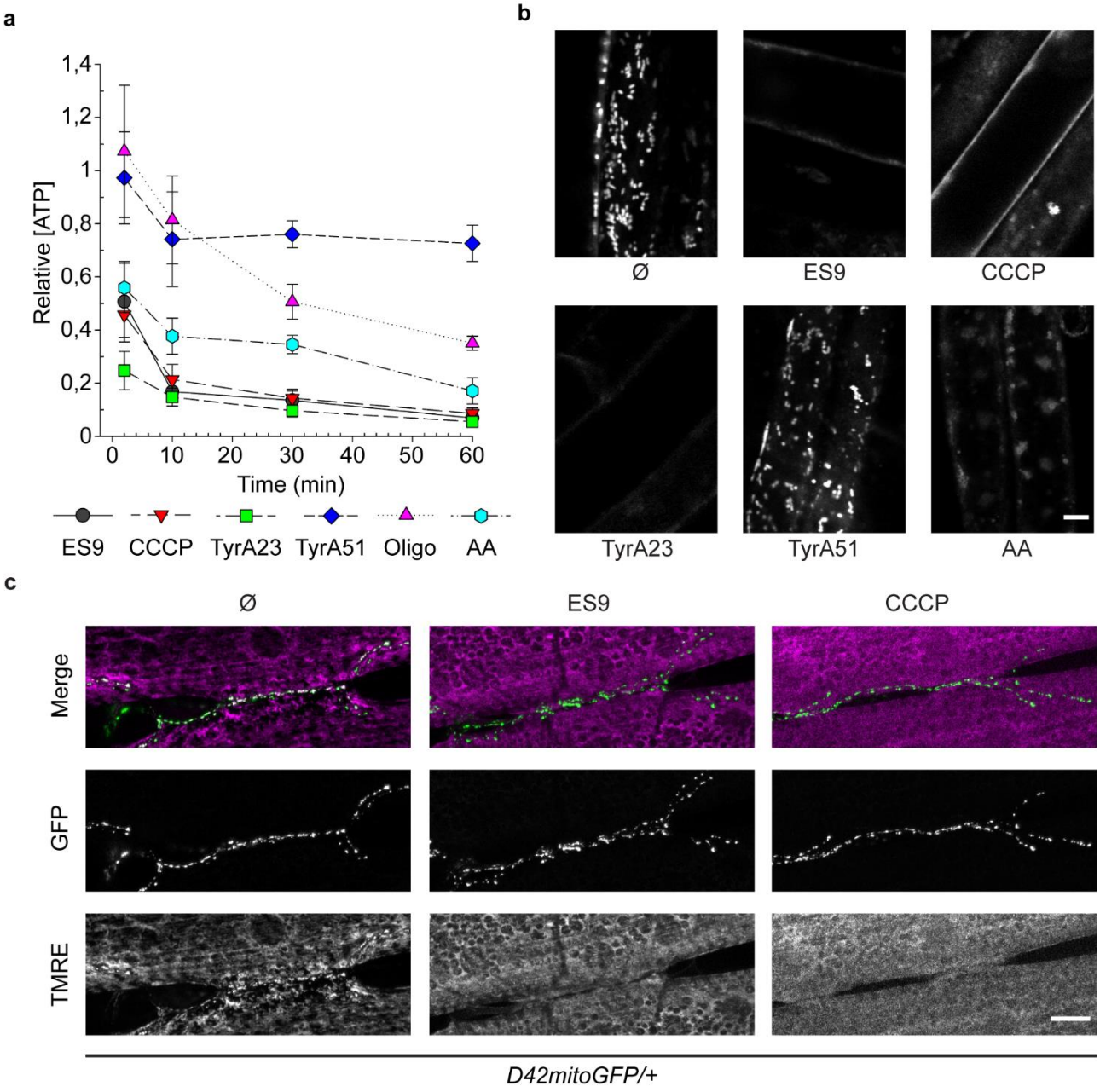

Figure 2. ES9 acts as a protonophore in *Arabidopsis* and *Drosophila*

(**a**) ATP depletion induced by 10 µM ES9 compared to 1 µM carbonyl cyanide m-chlorophenyl hydrazine (CCCP), 50 µM TyrphostinA23 (TyrA23), 50 µM TyrphostinA51 (TyrA51), 50 µM Antimycin A (AA) and 10 µM Oligomycin (Oligo), relative to mock treatment. (**b**) 250 nM MitoTracker Red CM-H2XRos labeling of mitochondria in *Arabidopsis* root cells in presence of 10 µM ES9, 1 µM CCCP, 50 µM TyrA23, 50 µM TyrA51, 20 µM AA and the mock (DMSO, Ø) treatment for 30 min. (**c**) Tetramethylrhodamine ethyl ester (TMRE) labeling of mitochondria in D42mitoGFP positive Drosophila neuromuscular junctions for 10 µM ES9 (30min pretreatment), 10 µM CCCP (and mock (1% DMSO in HL-3 medium) treatment 15 minutes). Scale bar, 5 µm

Cytosolic acidification but not ATP depletion rapidly inhibits CME in *Arabidopsis*

In mammalian systems, AA and CCCP have been linked to inhibition of CME as metabolic inhibitors[43,53,54]. We therefore evaluated the effect of CCCP, AA and Oligomycin on endocytosis in *Arabidopsis*, given that the CME inhibitors ES9 and TyrA23 also depleted cellular ATP. CCCP (1

μM) induced a complete inhibition of FM4-64 uptake when both CCCP and FM4-64 were co-applied for 30 min (**Fig. 3a, Supplemental Fig. 3a**), a pattern very similar to that of ES9 and TyrA23. In contrast, the inhibition of FM4-64 uptake, as measured from the plasma membrane/cytosolic signal intensity ratio, appeared not significant when FM4-64 was co-applied with AA (20 μM, 30 min) or added after pretreatment with Oligomycin (50 μM, 30 min) and imaged after an additional 30 min (**Fig. 3a, Supplemental Fig. 3a**). The pre-incubation with Oligomycin served to reach similar levels of ATP in the cell compared to AA and ES9, based on the ATP depletion results obtained from PSB-D cell cultures (**Fig. 2a**). The results for AA and Oligomycin indicated that depletion of ATP alone is not enough to completely block FM4-64 uptake. Moreover, we also tested whether CCCP caused phenotypes similar to ES9 in *Drosophila* because they both affected TMRE labeling of mitochondria and caused ATP depletion. CCCP treatment (10 μM, 15 min) did significantly reduce the uptake of FM1-43 but failed to form the large FM1-43 labeled inclusions seen when the boutons were incubated in ES9 (**Supplemental Fig. 3b,c**). The latter observation implicates that the CHC- or dynamin-related phenotype of ES9 are not caused by the dissipation of proton gradients and ATP production in mitochondria, further indicating that ES9 also harbors effects on CME beyond ATP depletion.

The differential phenotypes between AA and Oligomycin versus CCCP, TyrA23, and ES9, together with their function as mitochondrial uncouplers led to the hypothesis that, in contrast to AA and Oligomycin, CCCP, TyrA23, and ES9 could uncouple proton gradients throughout the entire cell, and therefore act as general protonophores in *Arabidopsis*. This might result in a substantial flow of protons from either the vacuole or the apoplast to the cytosol. To visualize this, *Arabidopsis* seedlings were treated with the respective small molecules and Lyso Tracker Red DND 99, a dye that labels acidic compartments in the cell[55]. Seedlings were first pre-incubated with Lyso Tracker Red DND 99 for 30 min, in order to label acidic compartments. Subsequent mock treatment of 30 min did not alter staining (**Fig. 3b, Supplemental Fig. 3d**), nor a treatment with 50 μM TyrA51 or 20 μM AA (**Fig. 3b**). However, addition of CCCP (1 μM), ES9 (10 μM) or TyrA23 (50 μM) for 30 min relocated Lyso Tracker Red DND 99 to the cytosol, and increased its signal dramatically, especially for the latter two (**Fig. 3b**). The relocation of Lyso Tracker Red DND 99 suggests a change in proton concentration throughout the cell, possibly as a result of proton gradient dissipation over the tonoplast and plasma membrane. To test this, we measured the pH in the vacuole and the cytosol in root cells in the presence of small molecules. The cytosol acidified significantly in presence of 10 μM ES9, 50 μM TyrA23 and 1 μM CCCP (**Fig. 3c**), with ES9 having the strongest effect. The vacuolar pH was most hardly affected by 50 μM TyrA23 and 1 μM CCCP (**Fig. 3d**), which were comparable to 50 μM TyrA51 (**Supplemental Fig. 3e**) in terms of alkalinisation. Only TyrA23 induced a significant change. ES9 (10 μM) induced a stronger and more significant alkalinisation (**Figure 3d**), comparable to 50 μM AA (**Supplemental Fig. 3e**). Yet ES9 and AA treatment failed to induce an alkalinisation similar to

1 µM Concanamycin A (Conc. A) treatment, or as compared to the vacuolar pH in the *vha-a2 vha-a3* mutant background[56]. Both latter conditions are affected in the vacuolar H^+-proton pumps, and thus have impaired H^+-pumping over the tonoplast. These data suggest that the main uncoupling activity occurred at the plasma membrane, which might indicate that the main influx of protons into the cytosol occurred over the PM.

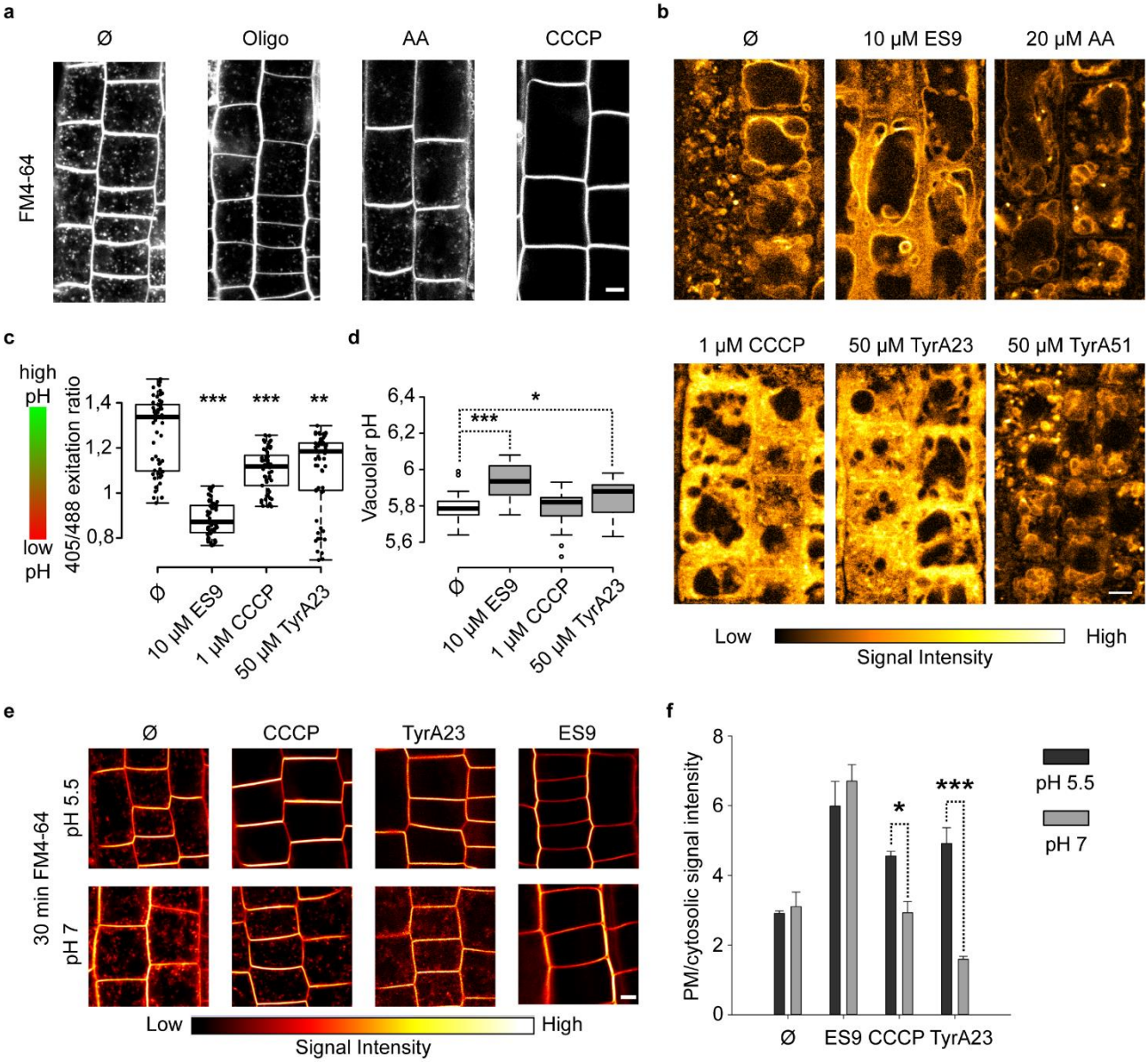

Figure 3. Cytosolic acidification, and subsequent ATP depletion completely inhibit CME

(**a**) FM4-64 uptake (2 µM, 30 min) in Arabidopsis root cells in presence of mock (DMSO, Ø), 50 µM Antimycin A (AA), 1 µM carbonyl cyanide m-chlorophenyl hydrazine CCCP and 50 µM Oligomycin (Oligo). Only in the case of Oligomycin cells were pretreated with the compound for 30 min before FM4-64 application. (**b**) Lyso Tracker Red DND 99 labeling (30 min) followed by an additional 30 min in presence of vehicle, ES9, AA, CCCP, TyrA23 and TyrA51. (**c**) Box plot representation of cytosolic pH measurements for 10 µM ES9, 50 µM TyrA23, and 1 µM CCCP. **P<0.01 and ***P<0.001 with a Kruskal-Wallis ANOVA on Ranks. N = 59, 60, 54 and 61 respectively. Individual data points are represented. (**d**) Vacuolar pH measurement for mock treatment (DMSO, Ø), 10 µM ES9, 50 µM TyrA23, and 1 µM CCCP. *P<0.05 and ***P<0.001 with a Kruskal-Wallis ANOVA on

Ranks. N = 32 for all measurements. (**e**) Comparison of 30 min FM4-64 uptake at pH 5,5 or 7, after 15 min pre-treatment with DMSO (Ø), 1 µM CCCP, 50 µM TyrA23 and 10 µM ES9. (**f**) Quantification of plasma membrane/cytosolic FM4-64 signal intensity for the different conditions in (**e**). Error bars: standard error of the mean. *P< 0,05 and ***P<0.001 with a Student's *t*-test for at least 3 biological repeats. Box plot center lines show the medians; box limits indicate the 25th and 75th percentiles as determined by R software; whiskers extend 1.5 times the interquartile range from the 25th and 75th percentiles, outliers are represented by dots. Scale bar, 5µm.

If a large part of the observed acidification would be caused by influx of apoplastic protons, changing the pH of the apoplast by incubating seedlings in more alkaline conditions would prevent this. Therefore, the FM4-64 uptake was evaluated when seedlings were incubated with small molecules in more alkaline medium (pH 7). An elevated pH of the incubation medium appeared to have little effect on the FM4-64 internalization, as no obvious differences were observed when the FM4-64 uptake (30 and 150 min) was carried out at either pH 5.5 or pH 7 (**Supplemental Fig. 3f**). However, co-application of CCCP (1 µM, 15 min pretreatment) with FM4-64 (30 min) at pH 7 allowed FM4-64 in the cell, indicating CCCP lost the ability to inhibit effectively FM4-64 uptake (**Figure 3e,f**). Similarly, application of TyrA23 (50 µM, 15 min pretreatment) at pH 7 reduced the signal intensity of FM4-64 dramatically, yet FM4-64 appeared not inhibited. ES9 treatment (10 µM, 15 min pretreatment) at pH 7 remained sufficient to inhibit FM4-64 uptake entirely, indicating ES9 might possibly inhibit FM4-64 through an additional mechanism (**Figure 3e,f**). Altogether these data suggest that the primary (very fast) block of CME by ES9, TyrA23 and CCCP is not due to energy depletion, but most likely to cytosolic acidification and possibly dissipation of plasma membrane potential.

E S9 activity causes an arrest in dynamic behavior of CME machinery at the plasma membrane

The apparent inhibition of FM4-64 and AFCS internalization by ES9 activity implies nonfunctional CME machinery. To test this, the behavior of TPLATE Muniscin Like fused to GFP (TML-GFP), a component of the TPLATE adaptor protein complex of CME[5], was evaluated in presence of the different small molecules. The previously reported TML-GFP life time at the plasma membrane of about 20 sec[5] was observed for mock-treated (DMSO) seedlings and seedlings treated with 50µM TyrA51 (**Fig. 4a,b**). However, for seedlings treated with 10 µM ES9, 1 µM CCCP or 50 µM TyrA23, TML-GFP-labeled foci at the plasma membrane lost their dynamic behavior and appeared stationary, often with a life-time of several minutes (**Fig. 4a,b**). The loss of dynamic behavior was established quickly, as images were acquired 3-5 min after start of treatments. AA treatment increased the life-time of the TML-labeled foci, but did not block their dynamics (**Fig. 4a,b**), correlating with the observed uptake of FM4-64 in presence of AA. The ES9 induced phenotype, which appeared to be

representative for CCCP and TyrA23 treatment, was also observed for other components of CME machinery in *Arabidopsis*. The dynamic behavior of TPL-GFP[57] the AP2 complex, represented by AP2A1-GFP[9], AP2M-GFP[29] and AP2S-GFP[31], and the clathrin cage represented by CLC1-GFP, CLC2-GFP, CLC3-GFP and CHC1-GFP appeared to be inhibited similar to TML-GFP (**Supplemental Fig. 4a**). ES9 also affected the phospholipid components involved in CME, such as phosphatidylinositol 4,5-biphosphate ($PI(4,5)P_2$)[58], which was detected with the $2xPH^{PLC}$ (P24Y) marker[59]. Upon ES9 application (10 µM, 30 min), P24Y localized largely to the cytosol, opposed to a predominant plasma membrane localization in control conditions (**Supplemental Fig. 4d**), which possibly reflected the overall decrease of $PI(4,5)P_2$ levels after the compound treatment (**Supplemental Fig. 4e**). In contrast, other phospholipid species were hardly affected in overall concentration (**Supplemental Fig. 4e**), and PI4P maintained its plasma membrane localization, as exemplified by the $2xPH^{FAPP1}$ (P21Y)[59] marker (**Supplemental Fig. 4d**). These results indicate that most of the essential components for CME are affected in their life-time at the plasma membrane, thereby affecting proper unfolding of endocytic events.

Protonophores affect multiple aspects of endomembrane trafficking

In addition to the arrest in dynamic behavior seen at the plasma membrane we also observed impaired dynamics at the level of endomembrane compartments such as the Golgi and the Trans Golgi Network (TGN)/Early Endosome (EE). When seedlings expressing the Golgi (ST-mRFP[60]) or the TGN/EE (Vha-a1-mRFP[61]) markers were treated with AA (20 µM) or TyrA51 (50 µM), a similar dynamic behavior compared to the control was observed for both the Golgi and TGN/EE, although Golgi appeared to move slower compared to mock in presence of AA (**Fig. 4c**). However, application of ES9 (10 µM), CCCP (10 µM) or TyrA23 (50 µM), inhibited movement throughout the cell almost completely (**Fig. 4c**). Again the loss in dynamic behavior was established quickly, as images were acquired 3-5 min after start of treatment, similar as for the measurements of endocytic life-times at the plasma membrane. The arrest in TGN/EE movement might explain a different observation, whereby application of ES9, CCCP or TyrA23 together with Brefeldin A (BFA), a fungal lactone interfering with ARF-GEF mediated vesicle traffic[62,63], prevented the formation of the BFA body (**Supplemental Fig. 4b**), whilst this was not observed for mock (DMSO) treatment or TyrA51 application. The formation of the BFA body might therefore require active vesicle movement in order to facilitate the clustering of TGN/EE.

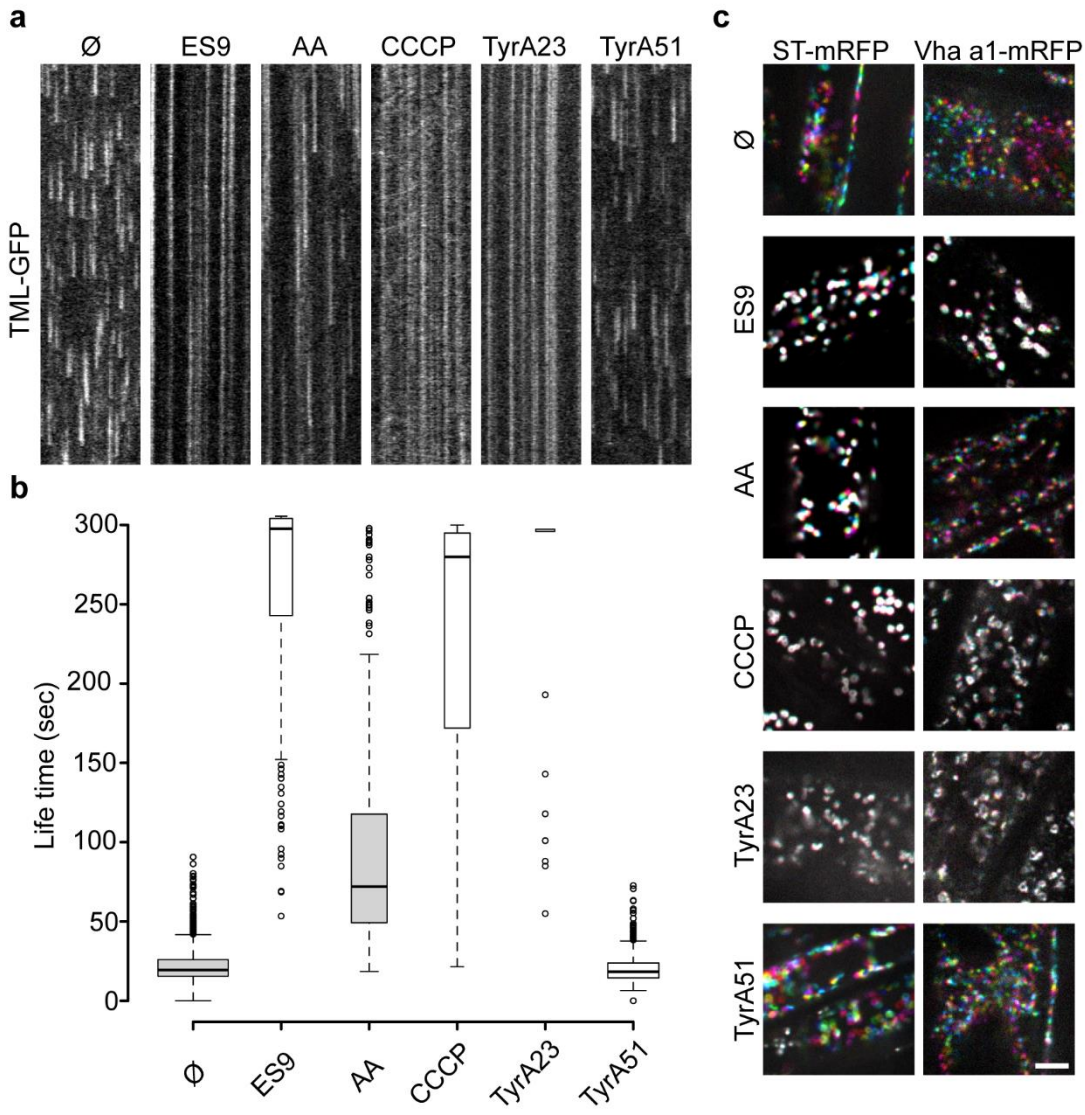

Figure 4. Protonophores inhibit CME dynamics in the plasma membrane and vesicle movement in the cytosol

(**a**) Kymographs representing a set of pixels (horizontal axis) over a period of time (vertical axis, 5 min), illustrating life times of endocytic spots labeled by TML-GFP for the control treatment (DMSO, Ø), 10 µM ES9, 20 µM Antimycin A (AA), 1 µM carbonyl cyanide m-chlorophenyl hydrazine (CCCP), 50 µM TyrphostinA23 (TyrA23) and 50 µM TyrphostinA51 (TyrA51). (**b**) Boxplot representation of measured endocytic spot life times. Center lines show the medians; box limits indicate the 25th and 75th percentiles as determined by R software; whiskers extend 1.5 times the interquartile range from the 25th and 75th percentiles, outliers are represented by dots. N = 1646, 171, 423, 218, 121 and 868 sample points (**c**) Golgi (ST-mRFP) and Trans Golgi Network (TGN, Vha-a1-mRFP) in presence of the control treatment, 10 µM ES9, 20 µM AA, 1 µM CCCP, 50 µM TyrA23 and 50 µM TyrA51 (time of treatment?). Images are composed of 6 differentially colored images with a 10 sec interval. Movement is illustrated by different colors, while static compartments appear white due to overlay of different colored frames. Scale bar, 5 µm.

Interestingly, ES9 also affected the localization of CLC in the TGN/EE. Upon treatment with ES9 (10 µM, 30 min), CLC2, but not CLC1 and CLC3, dislodged from the TGN/EE, a phenotype which

was also observed upon 1 µM CCCP treatment (**Supplemental Fig. 4c**). This suggests a pH sensitivity of CLC2 association with the TGN/EE, which might reflect a different mode of action for CLC2-association with the TGN/EE compared to CLC1 and CLC3.

To better characterize the effects of protonophores on endomembrane trafficking, the impact of ES9 and CCCP was evaluated at the ultrastructural level using transmission electron microscopy of high-pressure frozen and freeze-substituted Arabidopsis root cells. While the plasma membrane and mitochondria were unaffected (**Supplementary Fig. 5**), both ES9 and CCCP induced morphological alterations of both the Golgi apparatus and the TGN/EE, moreover multivesicular bodies (MVBs) were not present anymore (**Fig. 5**). Similar effects were previously reported for CCCP treatment of BHK cells[64]. Treatment with ES9 (5 µM or 10 µM, 30 min) caused the Golgi cisternae to swell, and the TGN/EE sometimes formed circle-like structures. The latter observation well explains the confocal microscopy data, where the TGN/EE marker VHA-a1 labeled circle-like structures in the presence of ES9 (**Supplemental Fig. 6a, arrowheads**). Both compounds also induced the accumulation of large inclusions inside the vacuole, which often contained portions of the cytosol, and are probably of autophagic nature. These inclusions were also observed when the line expressing the tonoplast marker SYP22-YFP[65] was treated with ES9 (**Supplemental Fig. 6b, arrowheads**). Surprisingly, in the meristematic cells of the root tip, but not in the elongation zone, 10 µM ES9 treatment induced the formation of Golgi-ER hybrid compartments (**Fig. 5h**), which were not seen for the CCCP treatment. The presence of Golgi-ER hybrids has been previously reported[66] and is indicative of a non-functional COPI trafficking. The observation that ES9 induced Golgi-ER hybrid compartments, while CCCP did not, might indicate that ES9 targets additional processes, independent from its capability to uncouple proton gradients.

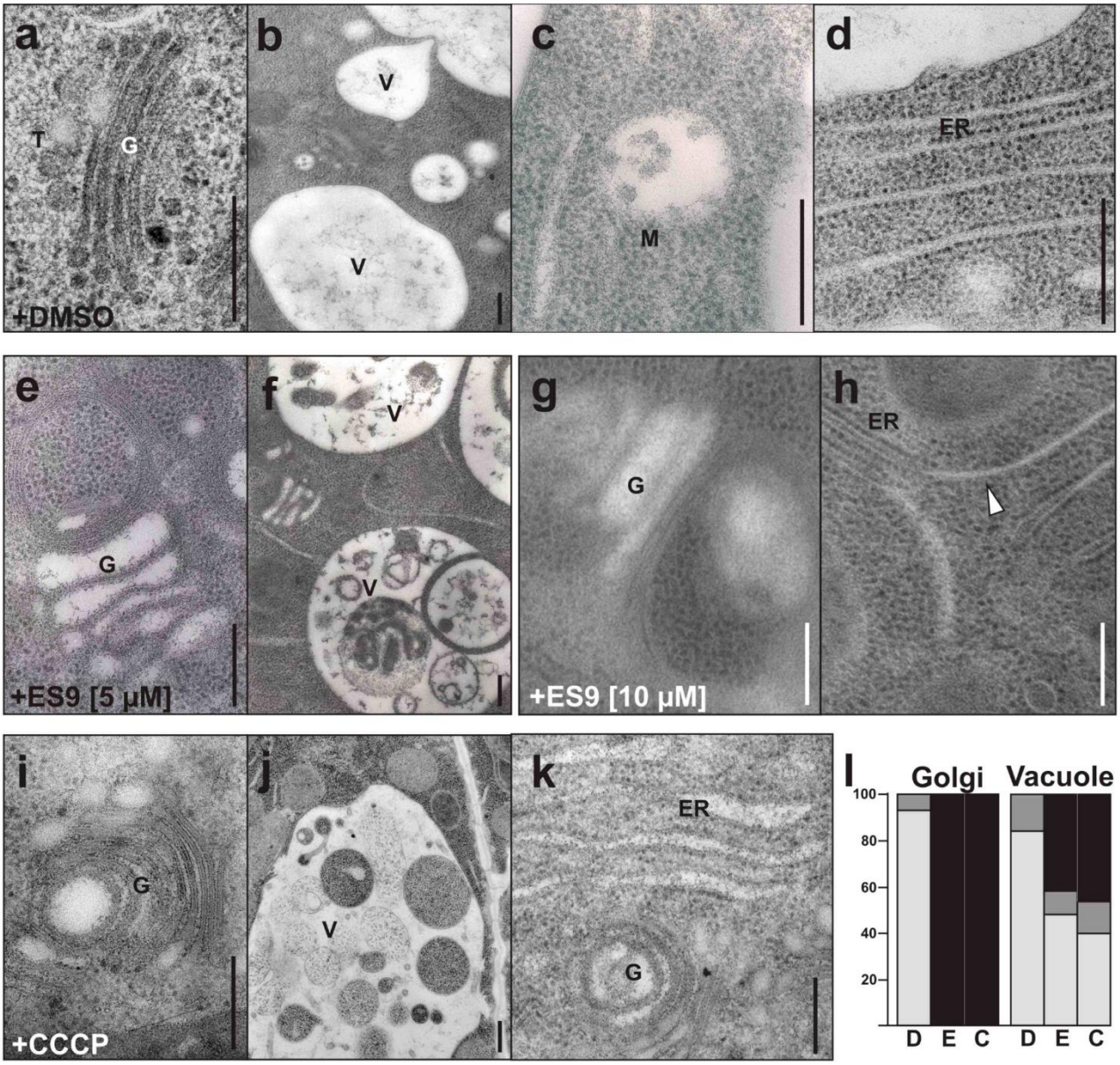

Figure 5. Protonophores causes morphological alterations in the endomembranes

(**a**) The Golgi apparatus (G) and the *trans*-Golgi network (T), (**b**) vacuoles (V), (**c**) multivesicular bodies (M) and (**d**) the endoplasmic reticulum (ER) display a normal morphology upon 30 min exposure to DMSO in meristematic root cells of five-day-old Arabidopsis seedlings. Upon 30 min exposure to 5 µM ES9, (**e**) the Golgi apparatus (G) displays an aberrant morphology with swollen stacks, the *trans*-Golgi network is often not recognizable or displays highly aberrant morphology (black arrowheads), and multivesicular bodies are absent. (**f**) Vacuoles accumulate autophagic bodies due to an impaired post-Golgi trafficking which prevents the delivery of proteolytic enzymes to the vacuolar lumen. Upon 30 min exposure to 10 µM ES9, (**g**) the Golgi apparatus (G) is even more affected, and (**h**) sometimes ER-Golgi hybrid compartments form in meristematic cells (white arrowhead). (i) CCCP causes morphological alteration to the Golgi and the *trans*-Golgi network, often by bending the stacks to form cup-shaped structures (G). (**j**) CCCP also induces the accumulation of autophagic bodies in the vacuole (V), however (**k**) it does not induce the formation of ER-Golgi hybrids, but it locally causes the swelling of the ER cisternae. (**l**) Quantification of the effects of DMSO (D), ES9 (E) and CCCP (C). One-hundred Golgi and one-hundred vacuoles were analyzed for each treatment Black, dark grey and light grey colors refer to altered, partly altered and normal compartments respectively. Scale bars, 200 nm.

Discussion

ES9 and TyrA23 are mitochondrial uncouplers

In this study we have identified and characterized the mode of action of a small molecule ES9, which activity inhibited CME in *Arabidopsis* and synaptic vesicle recycling in *Drosophila*. ES9 affected energy metabolism in both *Arabidopsis* and *Drosophila* cells and reduced the cellular ATP production by acting as a mitochondrial uncoupler, similar to known protonophores such as CCCP. Surprisingly TyrA23, a known and widely used inhibitor of CME in plants[67-69] , similarly showed activity of mitochondrial proton gradient uncoupling. Both ES9 and TyrA23 had a comparable effect as CCCP on the stimulation of mitochondrial respiration and a clear uncoupling activity of oxidations and phosphorylations. Likewise, treatments with ES9 or TyrA23 depolarized the mitochondria membranes *in vivo* in *Arabidopsis* and *Drosophila*. The similarity of phenotypes exhibited by ES9, TyrA23 and CCCP suggest that those compounds share a common mechanism of action as mitochondrial uncouplers, which is different from AA or Oligomycin. Indeed, while AA and Oligomycin are known specific inhibitors of ATP production[45,46], CCCP and Carbonyl cyanide-p-trifluoromethoxyphenylhydrazone (FCCP), a small molecule uncoupler similar to CCCP, are known non-specific inhibitors of ATP production as they depolarize the plasma membrane[47,48,70-74]. Interestingly, an increase in medium pH has been shown to reduce the protonophore action of FCCP over the plasma membrane[74], an observation which could be linked with the inability of CCCP to inhibit FM4-64 uptake in neutral pH, probably as a consequence of the lack in protonophoric activity at neutral pH. In support of the cell-wide complications of CCCP, opposed to a specific mode of action for the mitochondrial electron transport chain complex III inhibitor AA[75,76], is the failure of AA to induce similar cell-wide disruptions as induced by CCCP, ES9 and TyrA23, such as an immediate complete inhibition of FM4-64 uptake, general inhibition of dynamic events and cytosolic acidification. As ES9 and TyrA23 mimicked CCCP action in almost all aspects tested, it is reasonable to assume that ES9 and TyrA23 act through a mechanism similar as CCCP. This is supported by the chemical characteristics of each compound. Like CCCP, both ES9 and TyrA23 are weak acids (sulfonamide and phenol, respectively) that can dissociate into a proton and a stabilised, lipophilic anionic compound at physiological pH, thus fitting the classical biochemical description of uncouplers. Although TyrA23 is quite hydrophilic compared to known potent uncouplers, upon closer inspection, its anionic form can be further stabilised by an intramolecular hydrogen bond, a known chemical feature in uncouplers that further increases anion lipophilicity, and thus, membrane permeability[77]. An overview of the structural and electronic features of CCCP, ES9 and TyrA23 and several related known uncouplers is provided as supplemenatery information (Supplemental Figure 7).

ATP depletion alone does not efficiently block CME in Arabidopsis root cells and *Drosophila* neuromuscular junctions

Because CME is an energy-dependent process and certain levels of ATP are required for the receptor-mediated endocytosis[44], ES9 and TyrA23 might efficiently block CME through ATP depletion. However Oligomycin and AA both reduced cellular ATP in *Arabidopsis* cell culture cells but did not efficiently block endocytosis in root cells, although a longer pretreatment with the compounds reduced the uptake of the endocytic tracer FM4-64. It was previously shown that a reduction in ATP content to a level < 5% with AA is sufficient to prevent endocytosis of epidermal growth factor and the translocation of β-adrenergic receptors[43]. It is possible that the length of treatments with the metabolic inhibitors in root cells used in our study did not efficiently reduce ATP levels to concentrations low enough to block endocytosis. However, in yeast cells CME was not inhibited by depletion of ATP to 1-3 % of the normal level, whereas vacuolar transport was[78], suggesting that different eukaryotic systems might have different ATP requirements for CME. However, the inhibitory effect of ES9 and TyrA23 on CME was instant suggesting that the endocytosis block induced by those compounds is not due to ATP depletion. This conclusion is consistent with the observations in *Drosophila.* Here, the mitochondrial uncoupler, CCCP, did not cause obvious defects in FM1-43 dye uptake. In contrast, ES9 also dissipates the mitochondrial membrane potential and results in lower ATP levels, but in contrast to CCCP, this compound caused mislocalization of CHC-HA and resulted in FM 1-43 dye uptake defects. This supports an additional mode of action for ES9, as defects in mitochondrial functions and reduction in ATP have no clear implications in synaptic vesicle recycling except under intense stimulation of neurons to mobilize reserve pool vesicles[79,80].

ES9 and TyrA23 inhibit CME through cytosol acidification and possibly dissipation of proton gradients at the plasma membrane

In mammalian systems, acidification of the cytosol with weak acids strongly reduced CME of transferrin and epidermal growth factor but had a little effect on the uptake of some toxins and fluid phase endocytosis[81,82]. Mitochondrial uncouplers of oxidative phosphorylation are also weak acids which, due to their ability to cross the membranes in both their protonated and unprotonated form, should be much more effective in perturbing cytosolic pH than those weak acids that cross a membrane mainly in their protonated form. Indeed several reports show that uncouplers like CCCP and others have activity at other membranes that lead to cell acidification and cytotoxicity[74,83]. Related to endomembrane trafficking, protonophore uncouplers were most commonly used to disturb the proton gradients and increase the pH of the endocytic vesicles and lysosomes in mammalian cells[74,84]. The cytoplasmic and vacuolar pH measurements in *Arabidopsis* are in agreement with the mammalian literature, and suggest that the main proton flow into the cytoplasm is established over

the PM. It can be expected that protonophores would induce more drastic effects in *Arabidopsis* compared to mammalian systems, as the pH of the growth medium differs in more than one pH unit.

Furthermore, the large inclusions seen in the vacuole, which are likely of autophagic nature, are in agreement with reports where protonophores are used to induce autophagy and mitophagy[85,86], though recent reports suggest caution when using protonophores to induce autophagy related processes, as the induction is likely not specific, owing to the general effect on cellular proton gradients by protonophores[87]. In contrast, the described effects of the protonophore uncouplers on CME are not consistent for all experimental systems and difficult to interpret. Whereas CCCP blocks the uptake of iron from transferrin, mediated by CME in reticulocytes[82], in yeast cells CCCP did not block the internalization of FITC-dextran into the endosomal compartments[78]. One possible explanation concerning the different effects of protonophore uncouplers on CME might be related to the different cellular environment in differential systems. Our observations that the pH of the incubation media influenced the effect of the uncouplers on CME favor this.

Acidification of the cytosol in mammalian cells interferes with budding of clathrin-coated vesicles from the plasma membrane as well as from the TGN[81,88,89]. Interestingly an altered structure of clathrin lattices on the inside of the plasma membrane was observed, and it was proposed that some acidification is required for the clathrin lattice curvature to occur[88]. Although we were not able to evaluate clathrin lattice structure upon acidification of the cytoplasm in plants, one could expect that acidification would affect a similar deformation of clathrin coated pits and vesicles as in mammalian systems, which in turn could explain the impaired dynamics of CME foci at the plasma membrane, as seen for CCCP, ES9 and TyrA23. More importantly, our results indicate that, similar to mammalian systems, acidification of the cytosol in *Arabidopsis* inhibits CME. Apart from the small molecules described here, other well-known small molecules such as auxin and salicylic acid (SA) can also induce cytosolic acidification[90,91], and inhibit CME[21,92]. It would therefore be of interest to establish if auxin and SA induce a similar effect on CME dynamics compared to ES9, TyrA23 and CCCP, and if the cytoplasmic acidification is the underlying mechanism by which auxin and SA mediate inhibition of CME. Moreover, a possible physiological role for cytosolic acidification and subsequent inhibition of endocytosis in *Arabidopsis* might involve the inhibition of endocytosis in general upon hyperosmotic stress, as shown in *Dictyostelium* cells[93].

The impaired dynamics at the plasma membrane and by extension other endomembrane compartments such as the Golgi and TGN/EE, could be explained by a heavily affected cytoskeleton. Indeed, early reports suggest an effect of protonophores on the microtubule cytoskeleton through a change in pH and the inability of accessory proteins to associate[94]. Similarly, CHC was also mislocalized at synaptic boutons in *Drosophila* when treated with ES9. The ultrastructural analysis

in plant cells did not reveal accumulation of clathrin-coated pits in the plasma membrane or in fact any membrane alterations, consistent with the mislocalization of CHC.

Plant cells treated with either ES9 or CCCP also displayed aberrant Golgi morphology. Similarly, it was previously shown that the protonophore CCCP inhibits secretion in Baby Hamster Kidney fibroblasts (BHK) cells by interfering with Golgi function and causing dilation of the Golgi cisternae and accumulation of large vacuoles in the Golgi region[64,95]. Interestingly, the ATP depletion over time induced by CCCP[95] was similar to what we reported. However, ES9 treatment also led to a Golgi-ER fusion which was not detected in CCCP-treated cells. This presence of Golgi-ER hybrid compartment has been previously reported[66] and is indicative of a non-functional COPI trafficking. The observation that ES9 induces a Golgi-ER hybrid compartment, while CCCP did not, might indicate that ES9 targets additional processes, independent from its capability to uncouple proton gradients. In addition to affecting the Golgi and TGN/EE morphology, treatments with protonophores (ES9, TyrA23 and CCCP) strongly affected the motility of these compartments. This can explain why pretreatment with TyrA23, ES9 and CCCP prevented the formation of BFA bodies, visualized with the TGN/EE markers Vha-a1 (our data) or SCAMP1[96,97]. TyrA23 also affected cytokinesis[98], a process dependent on the Golgi-based secretion, suggesting that TyrA23 similar to ES9 and CCCP might also act at the level of Golgi apparatus.

Finally, the absence of MVBs can be explained by the impairment of TGN/EE function, on which MVB formation depends[99]. This event is probably a consequence of Golgi- and TGN/EE-mediated vacuolar trafficking impairment, since proteolitic enzymes would not be delivered into the vacuolar lumen, leading to an accumulation of undegraded autophagic bodies. This effect, as well as the morphological alteration of both Golgi and TGN/EE, has also been reported by using the well-known V-ATPase inhibitor concanamycin A (ConcA)[61,100].

The use of TyrA23 in plants

As most of the TyrA23 use in plants is related to studies on CME, and given our report on the protonophoric characteristics of TyrA23, data obtained with this inhibitor should be carefully revised. Although our results suggest that TyrA23-mediated inhibition of CME in plants primarily occurs through acidification of the cytosol and possibly dissipation of the proton gradient over the plasma membrane , inhibition of CME through interference with cargo recognition cannot be excluded. Interference of cargo recognition does not affect all cargos to the same extent as shown for epidermal growth factor receptor and transferrin receptor recognition by a dominant negative form of AP-2 medium subunits[101]. While application of TyrA23 strongly reduced, but not abolished transferrin uptake, and no other effect on endomembrane traffic could be concluded[14], one could speculate that

the complete inhibition of FM4-64 by TyrA23 application in *Arabidopsis* is most likely the result of the protonophore nature of TyrA23, similar as what we report for CCCP and ES9, which is much stronger at the plasma membrane compared to other systems given the relative low pH of the surrounding medium.

Small molecule hits which affect mitochondrial functions are of increasing concern in the mammalian drug discovery field, as considerable numbers of small molecule hits appear to affect mitochondrial functions, and thus induce undesirable side effects[102-105]. In this respect TyrA23 does not seem to be an exception, yet questions its further use as a specific inhibitor of CME in plants. In addition, our results illustrate the necessity to fully characterize small molecules which are adopted from the mammalian field. Though TyrA23 still might affect cargo recruitment by AP-2, essential biochemical proof is lacking in plants, as subtle differences in amino acid composition and tertiary or quaternary structure of AP-2 might compromise TyrA23 binding in plants. However, the protonophore activity of TyrA23 overrides any specificity at the level of CME, as cytosolic acidification and possibly the loss of membrane potential will impair CME severely. Unless a TyrA23 analogue is developed, which is unable to dissipate proton gradients, yet maintains the ability to interfere with cargo recruitment, the use of TyrA23 in plant biology to inhibit specifically cargo recruitment to AP-2 should be carefully evaluated.

Acknowledgements

We thank Steffen Vanneste for useful discussion and material. Ikuko Hara-Nishimura for sending AP2M-GFP, and Jinxing Lin for sending AP2S-GFP. Also Yvon Jaillais for sharing the PIP lines, and all colleagues who helped with any practical aspects of this work.

Material and methods

Plant material and growth conditions

Arabidopsis thaliana (accession Columbia-0 [Col-0]) seedlings and other lines were stratified for 2 days at 4°C, and grown vertically on agar plates containing ½ strength Murashige and Skoog (½MS) medium supplemented with 1% (w/v) sucrose for 5 days at 22°C in a light/dark cycle of 16 h/ 8 h respectively, prior to use. *Arabidopsis* seedlings were used as control or for labeling of mitochondria and acidic compartments. Following marker lines were used: TML-GFP[5], TPLATE-GFP (TPL-GFP)[57], CLC1-GFP, CLC2-GFP, CLC3-GFP, CHC1-GFP, AP2A1-GFP[9], AP2M-GFP[29], AP2S-GFP[31], ST-mRFP[60], Vha-a1-mRFP[61], SYP22-YFP[65].

Generation of GFP-tagged CHC1

Entry clone generated before[23] was used together with pDONRRP4-1R_RPS5A, pDONRRP2R-P3_GFPstop and pK7m34GW in multisite Gateway reactions (Life technologies) to yield C-terminal tagged CHC1

Chemical treatments, chemical labeling and imaging in *Arabidopsis*

TyrphostinA23, tyrphostinA51, oligomycin, antimycin A, carbonyl cyanide 3-chlorophenylhydrazone, brefeldin A, and fluorescein diacetate were acquired through Sigma-Aldrich. All were dissolved in DMSO (Sigma-Aldrich) except for Oligomycin (ethanol). ES9 was acquired through Chembridge (http://www.chembridge.com/). Visualization of endocytosis was achieved with 2µM N-(3-Triethylammoniumpropyl)-4-(6-(4-(Diethylamino) Phenyl) Hexatrienyl) Pyridinium Dibromide (FM4-64, Life technologies) application. For staining of mitochondria, seedlings were first treated for 30 min in ¼ MS (a 1:1 dilution of ½ MS with water) with the respective small molecules. Subsequently, seedlings are transferred to liquid ¼ MS with 250 nM MitoTracker Red CM-H2XRos (Molecular Probes®, Life Technologies) and the respective small molecules for an additional 30 min. Similarly, acidic compartments were labeled with Lyso Tracker Red DND 99 (Molecular Probes®, Life Technologies) by treating seedlings with 250 nM Lyso Tracker Red DND 99 in liquid ¼ MS for 30 min. Small molecule treatment was started by adding small molecule at

respective concentrations to seedlings in the Lyso Tracker Red DND 99 containing solution for another 30 min. Imaging of seedlings was performed with an Olympus FV10 ASW confocal laser scanning microscope using a 60x water immersion lens (NA 1.2) and 3x digital zoom. Endocytic foci Life-time measurements were determined using a Perkin Elmer Ultra View Vox Spinning disc confocal imaging system running on the Volocity software package mounted on aNikon Eclipse Ti inverted microscope using a Plan Apo Lambda 100x oil (NA 1.45) corrected lens and third generation perfect focus system (PFSIII) for Z-drift compensation. Time series were acquired at 2 time points per second intervals, for 5 minutes. Excitation was done using a solid state 488nm DPSS laser (50mW) and images were acquired using a Hamamatsu ImagEM C9100-13 512x512 BI (16umx16um pixel size) EmCCD camera. Images were processed using the imageJ (Fiji) software packages. For Kymographs, background was substracted with a rolling ball radius of 50 pixels, and a walking average (2) was performed. Kymographs were generated with a line thickness of 3. For quantification of the plasma membrane/cytosol signal intensity ratio, images were converted in ImageJ to 8-bit, and regions of interest (ROIs) were selected based on the plasma membrane or cytosol localization. Histograms listing all intensity values per ROI were generated, and the averages of the 100 most intense pixels were used for calculations.

ATP measurements

Wild type PSB-D *Arabidopsis* cell cultures were used and maintained as described before[106]. Cell culture of 3 days old was diluted 100 times and mixed thoroughly prior to distribution of 95 µl in 96-well plates. Subsequently, 5 µl of a 1/50 dilution of small molecule stock solution (1000x) in MS medium with Minimal Organics (MSMO) medium was added to cells (final dilution of 1000x) using a Tecan Freedom EVO® robot. ATP levels were detected by addition of 80 µl of ATPlite 1step Luminescence Assay System (Perkin Elmer) after incubation of cells in presence of small molecule for indicated time. Fluorescence was detected using a Perkin Elmer EnVision 2104 multilabel reader with the Wallac Envision manager software package. ATP-lite luminescence was detected with the ultra-sensitive luminescence techonology. Fluorescein diacetate (FDA) stock solution (2% FDA in acetone [w/v]) was diluted 100x in target medium and 5 µl was added to 95 µl cell culture. Fluorescence was detected with an excitation at 485nm (bandwidth 14nm), and emission at 535nm (bandwidth 25nm). Same procedure applies for *Drosophila* Schneider 2 (S2) cell suspension cultures, which were maintained in Sf-900 II SFM (Serum free medium , Gibco) at 25 °C without CO2, and distributed in 96-well plates for analysis (95 µl, 25000 cells).

Isolation of mitochondria and measurement of respiratory control ratios.

Mitochondria from Arabidopsis leaves were isolated as previously described[50] following method A. Respiratory measurements were overall performed according to previous report[50], with a clark-type oxygen electrode (Hansatech) at 25°C and recorded with a sekonic SS-250F recorder. Dioxygen

concentration in air-saturated water was established at 240µM and a final volume of only 0.5mL was used in the cuvett. A mix of Malate/Glutamate (0.1M/1M) was chosen as substrate for the mETC and was injected to a final dilution of 1/100. Mitochondrial respiration was further stimulated by injection of ADP (10mM) to a final dilution of 1/100. TyrA23, TyrA51 and CCCP were solubilized with DMSO. Controls with injection of 5µL DMSO alone at the beginning, the middle and at the end of the measurements were performed. Experiments from independent extractions were performed 4-6 times with identical results. Traces shown are actual traces obtained with the recorder, scanned and digitalized.

pH measurements

For cytosolic pH measurements, 4 days old UB10:pH-GFP plants[107,108] were transferred to 2ml of liquid 1/2MS (pH5.5, 2.15g/l MS salts, 0.5g/l MES) for 30 min with the indicated drugs or mock (DMSO). Imaging was done with a Zeiss 700 confocal, Plan-Apochromat 20x/0.8 M27 objective. pH-GFP was excited by 405 and 488nm diode lasers and the emission was collected separately between 500-555nm. The images were evaluated in Fiji (ImageJ) by measuring intensities of both channels in 6 circulars ROIs per root meristematic zone. Vacuolar pH measurements were performed as described before[56] for a 2hr incubation with the indicated small molecules.

Transmission electron microscopy

Arabidopsis root tips from 5-day-old seedlings were submerged in 200 mM sucrose, 10 mM trehalose, and 10 mM Tris buffer, pH 6.6[109], transferred into planchettes (Leica Microsystems; 3.0x0.5mm, Al, type A and B), and frozen in a high-pressure freezer HPM100 (Leica Microsystems). Freeze substitution was performed in a Leica EM AFS2 unit (Leica Microsystems) in dry acetone supplemented with 0.4% uranyl acetate at −85°C for 16 h, followed by 5 h warm-up to −50°C. After washing with 100% ethanol for 60 min, samples were infiltrated and embedded in Lowicryl HM20 resin at −50°C (intermediate steps of 30%, 50%, 70% HM20 in ethanol, 1 h each). The resin was polymerized with ultraviolet (UV) light for 3 days in the freeze substitution unit. Ultrathin sections were cut on a Leica UC7 (Leica Microsystems) and post-stained with aqueous uranyl acetate/lead citrate. Sections were examined in a JEM 1230 (Jeol) or in a Phillips CM100 transmission electron microscopes, both operating at 80 kV. Micrographs were recorded with a MSC 600CW (Gatan) digital camera or by scanning negatives (MACO EM films TYP S, 6.5x9 cm, ES 206) with an Epson Perfection V750 Pro system.

Drosophila genetics

Fly stocks were maintained on standard maize meal and molasses medium and were obtained from the Bloomington Drosophila Stock Center or from[42].

FM1-43 dye uptake assay and visualization of HA-CHC in Drosophila

FM1-43 labeling was performed as described[110]. Third instar larvae were dissected in HL-3 and prior to a stimulation protocol animals were incubated for 30 minutes in HL-3 supplemented with and without 10µM ES9 or for 10 minutes in HL-3 supplemented with 10µM CCCP or mock (1% DMSO). Next, neurons were stimulated for 5 min in HL-3 with 90 mM KCl and 1.5 mM $CaCl_2$ in the presence of FM 1-43 (4 µM) (Life Technologies) with or without small molecule. After labeling, the preparation was washed several times with HL-3 supplemented with or without small molecule. Images were captured using a confocal microscope (A1R, Nikon) with a 60x NA 1.0 water dipping lens. The boutonic FM1-43 intensity was quantified using ImageJ and was corrected for background labeling in the muscle.

Immunohistochemistry was performed to visualize HA-CHC as described[42]. Larvae were treated in a similar fashion as for the FM1-43 dye uptake assay without the presence of FM1-43. Next, the treated animals were fixed and stained with a mouse anti-HA antibody (Covance) at 1:500. Alexa 555-conjugated secondary antibodies (Life Technologies) were used at 1:1000. Super resolution structural illumination microscopy images were acquired on a microscope (Elyra S.1; Carl Zeiss) using a 63×, NA 1.4 oil lens and three rotations at room temperature. Next, acquired images were processed and stored using the ZEN 2011 software (Carl Zeiss).

TMRE labeling

Tetramethylrhodamine ethyl ester (TMRE) was used to label the mitochondrial membrane potential as described[111]. D42mitoGFP/+ third instar larvae were dissected in HL-3 and incubated for 30 minutes in HL-3 supplemented with and without 10µM ES9. Subsequently, larvae were treated for 15 minutes with HL-3 medium supplemented with 50 mM TMRE (Abcam) and the appropriate small molecule at room temperature. For CCCP treatment, larvae wer incubated for 15 minutes in HL-3 supplemented with 50 mM TMRE and 10 µM CCCP or mock (1% DMSO). Next, fillets were washed with HL-3 with the appropriate small molecule and images were captured using a confocal microscope (A1R, Nikon) with a 60x NA 1.0 water dipping lens. The TMRE labeling intensity was quantified using ImageJ. First, 32-bit image of the mitoGFP channel was thresholded to select the mitochondria of the neuromuscular junction. Subsequently, the TMRE labeling intensity was measured in that region.

Supplemental information

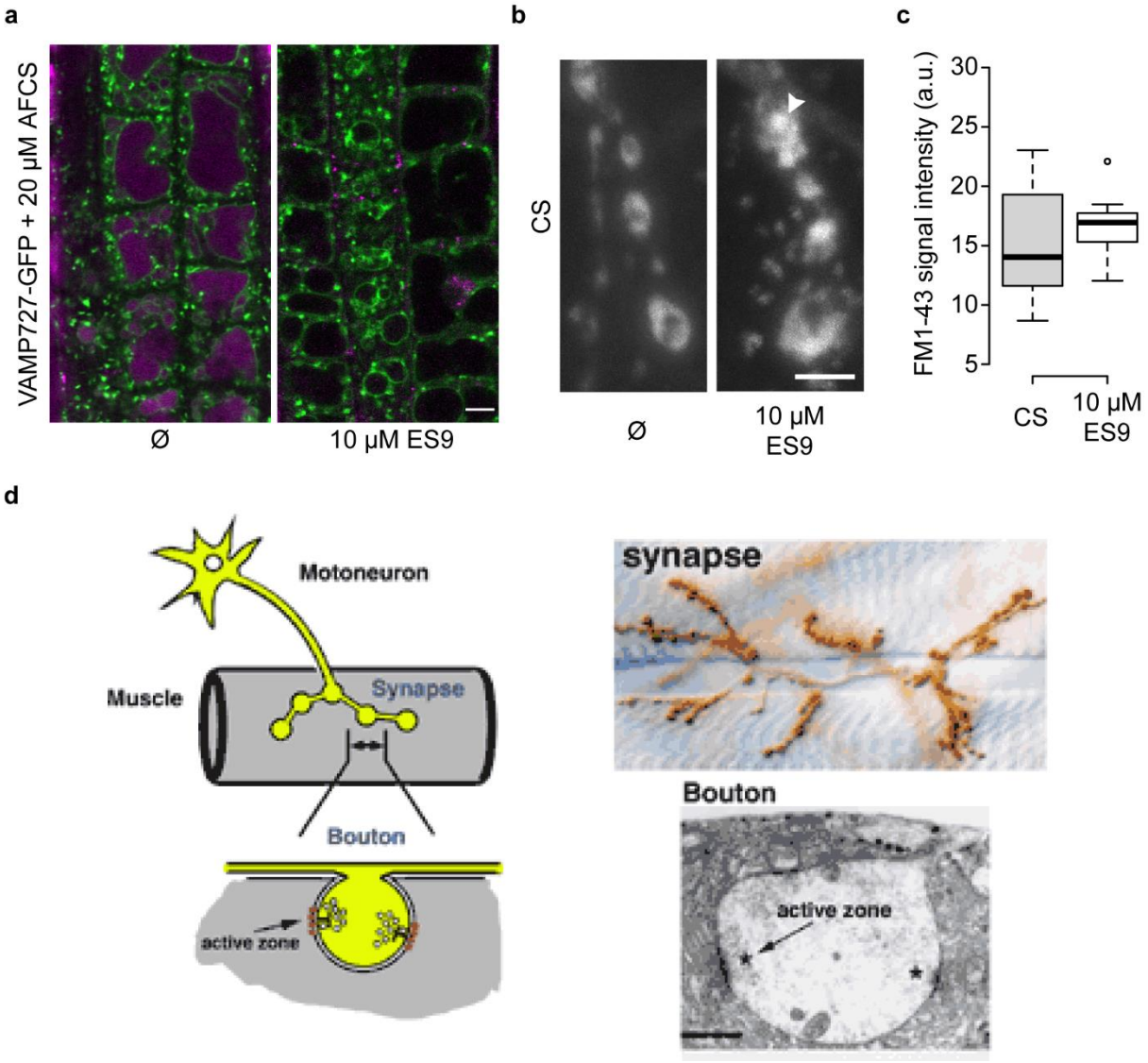

Supplemental Figure 1. ES9 inhibits CME in *Arabidopsis* and *Drosophila*

(**a**) Uptake of AFCS (magenta, 20 µM, 30 min pulse, 20 min chase) for mock (Ø, DMSO) or 10 µM ES9 (30 min) in VAMP727-GFP (green) positive *Arabidopsis* root cells. (**b**) FM1-43 labeling of neuromuscular junction boutons in third instar larvae of Drosophila, in the control situation (CS) and in presence of 10 µM ES9 for 30 min. Note the large FM1-43 labeled structures (arrowhead). (**c**) Signal quantification of (**b**). (**d**) Schematic representation of the neuromuscular junction in *Drosophila*, and the synaptic boutons. Image: http://biochemistry2.ucsf.edu/labs/davis/projects/. Scale bar, 5 µm in (a), 2 µm in (b).

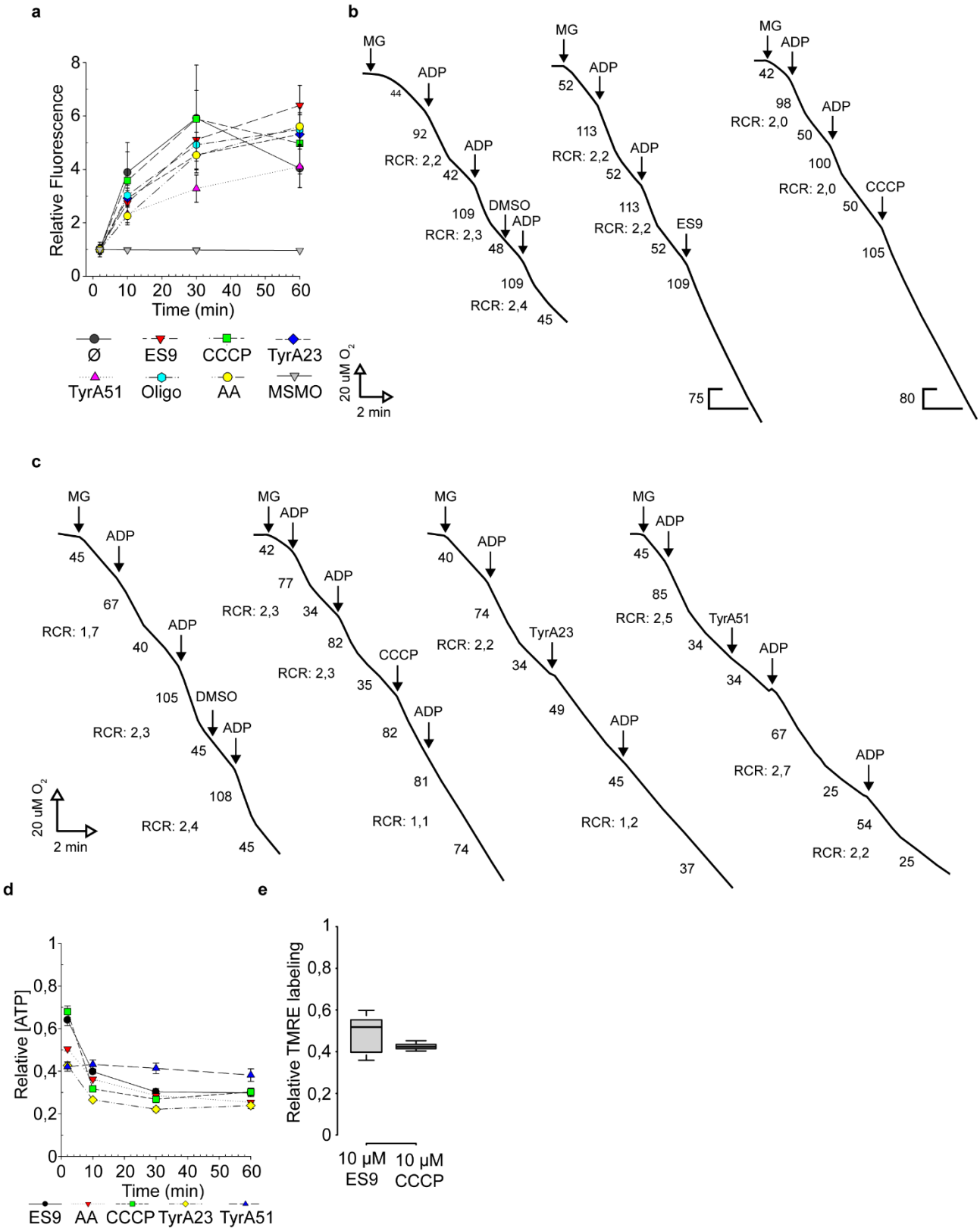

Supplemental Figure 2. ES9 and TyrA23 affect mitochondrial functions, similar to CCCP

(**a**) Fluorescindiacetate (FDA)-based fluorescent measurement PSB-D wild type cell cultures for 1 µM carbonyl cyanide m-chlorophenyl hydrazine (CCCP), 50 µM TyrphostinA23 (TyrA23), 50 µM TyrphostinA51 (TyrA51), 10 µM ES9, 10 µM Oligomycin and 50 µM Antimycin A (AA). Representation of Murashige and Skoog with Minimal Organics (MSMO) medium serves to show the need for active and viable cells to induce fluorescence. (**b-c**) Measurement of mitochondrial electron transport chain (mETC) characteristics, where respiratory control ratios (RCRs) are not affected when treated with mock (DMSO) and 5 µM TyrA51. In presence of 1 µM ES9, 1 µM CCCP

or 5 µM TyrA23, clear uncoupling between oxidations and phosphorylations occurs as shown by a RCR drop, even after addition of ADP. (**d**) Measurement of ATP in Drosophila S2 cell cultures for 10 µM CCCP, 10 µM ES9, 50 µM AA, 50 µM TyrA23 and 50 µM TyrA51. Relative to mock. (**e**) Relative intensity of mitochondrial tetramethylrhodamine ethyl ester (TMRE) labeling in D42mitoGFP positive Drosophila neuronal cells for ES9 and CCCP treatments.

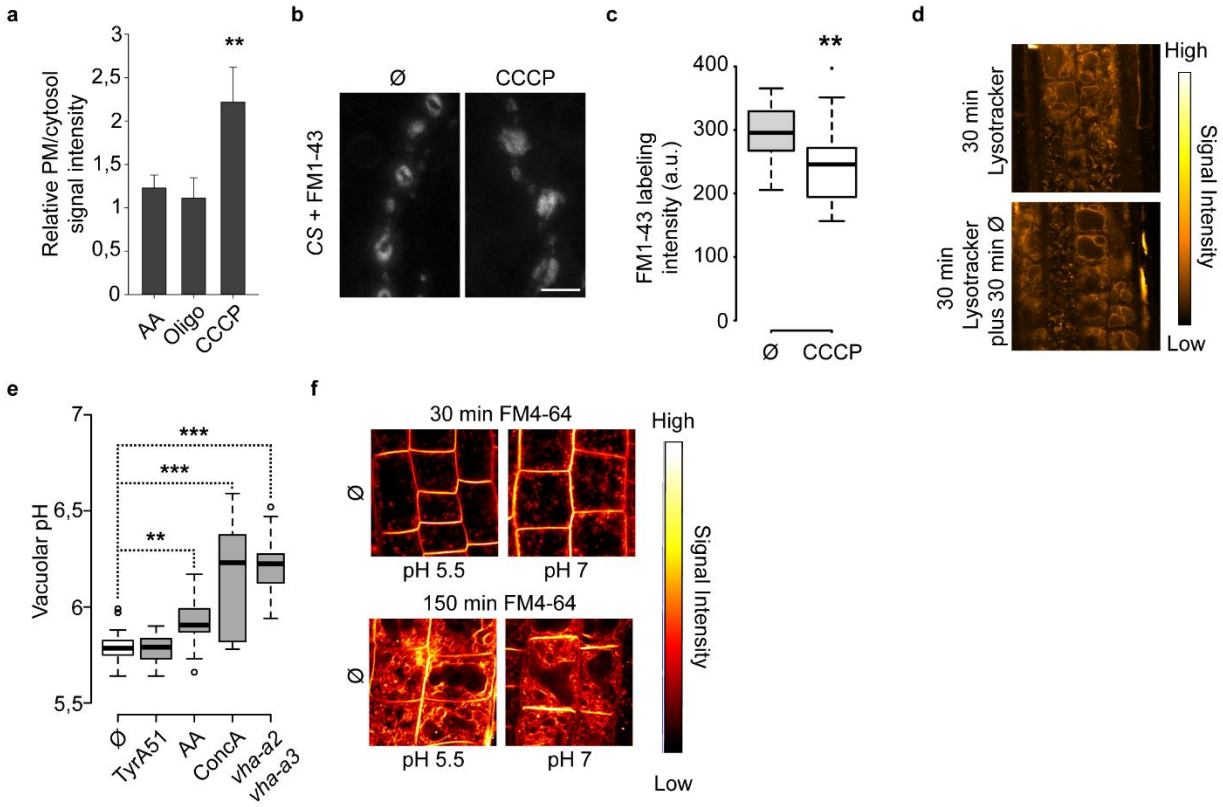

Supplemental Fig. 3. **Inhibition of FM4-64 uptake is dependent on extracellular pH in presence of protonophores in *Arabidopsis***

(**a**) Quantification of plasma membrane derived FM4-64 signal over cytosolic signal, relative to control conditions. 30 min treatment for 20 µM Antimycin A (AA) and 1µM CCCP. Oligomycin (Oligo) treatment (50 µM, 30min) prior to 30 min FM4-64 labeling in continuing presence of Oligomycin. (**b**) FM1-43 labeling of neuromuscular junction boutons in third instar larvae of Drosophila, in the control situation (Ø, 30 min) and in presence of 10 µM CCCP for 30 min. Note the absence of large FM1-43 labeled structures (compare with Supplemental Fig. 1). (**c**) Signal quantification of (**b**). (**d**) Lyso Tracker Red DND 99 labeling (30 min) of *Arabidopsis* seedlings is not altered after the addition of DMSO (Ø) and incubation in presence of Lyso Tracker Red DND 99 for another 30 min. (**e**) Vacuolar pH measurement for mock treatment and 50 µM TyrA51, 50 µM AA 1 µM Concanamycin A (ConcA) and the *vha-a2 vha-a3* double mutant. n = 32, 32, 24, 24 sample points. **P < 0.01 and ***P<0.001 for a Kruskal-Wallis One Way ANOVAon Ranks and pairwise comparison according to Dunn's method. (**f**) Comparison of FM4-64 uptake at pH 5,5 or 7, after 30 min or 150 min mock treatment (Ø, DMSO). Box plot center lines show the medians; box limits indicate the 25th and 75th percentiles as determined by R software; whiskers extend 1.5 times the interquartile range from the 25th and 75th percentiles, outliers are represented by dots. Box width relative to sample size. **P<0.01 with a two-tailed Student's *t*-test for at least 3 biological repeats in (**a**) and (**c**). Scale bar: 5µm

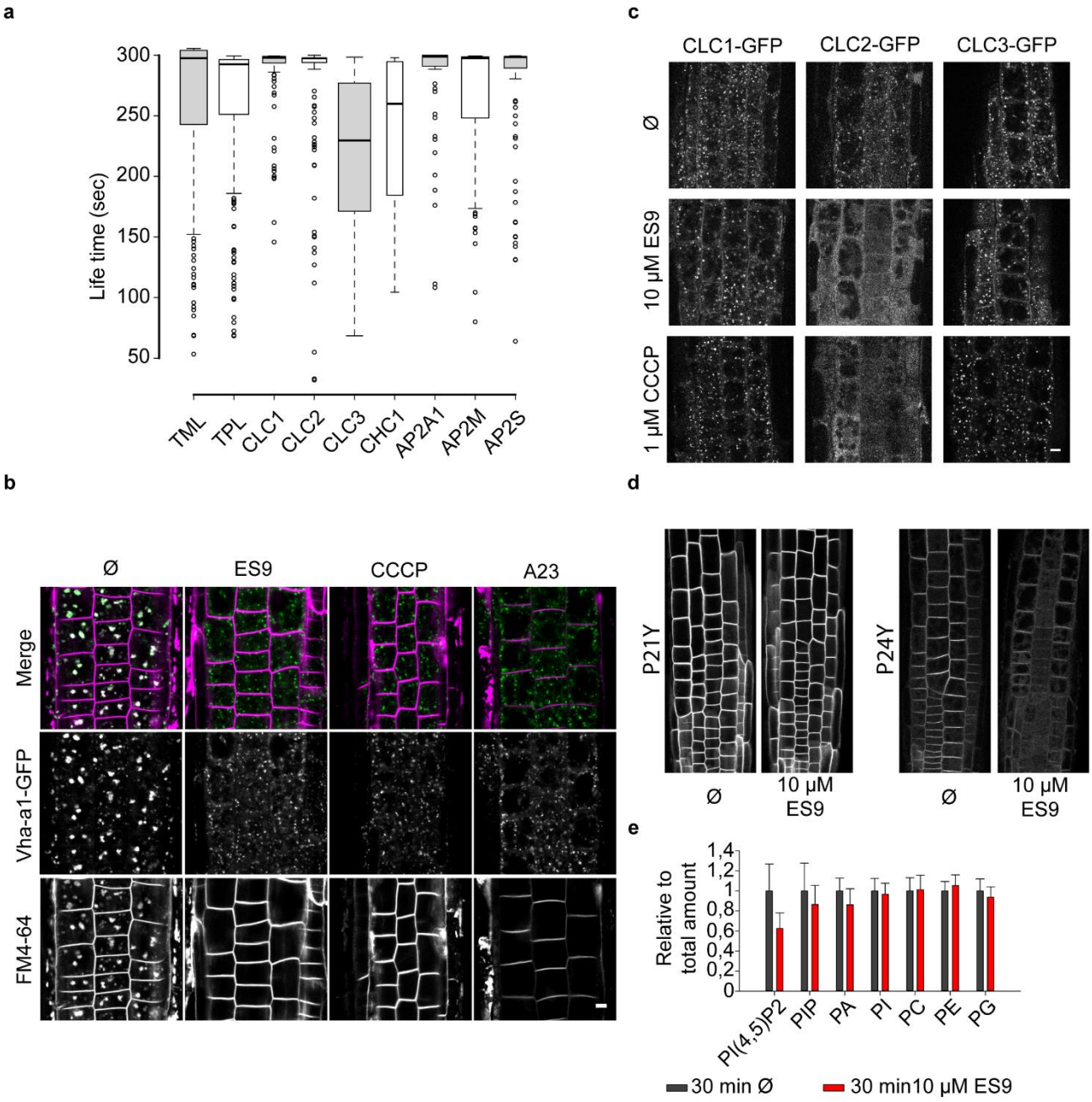

Supplemental Figure 4. Several aspects of endomembrane traffic are affected in presence of protonophores

(**a**) Box plot representation of foci life time at the plasma membrane in presence of 10 µM ES9 for Green fluorescent Protein (GFP) tagged TPLATE Muniscin Like (TML), TPLATE (TPL), Clathrin light chain (CLC), clathrin heavy chain (CHC), and the adaptor complex 2 (AP2), represented by its alpha subunit (AP2A1), mu subunit (AP2M) and sigma subunit (AP2S). Center lines show the medians; box limits indicate the 25th and 75th percentiles as determined by R software; whiskers extend 1.5 times the interquartile range from the 25th and 75th percentiles, outliers are represented by dots. n = 171, 204, 125, 142, 243, 60, 150 and176 sample points (**b**) Brefeldin A (BFA, 50 µM, 30 min) is prevented in presence of 1 µM CCCP, 10 µM ES9 and 50 µM TyrphostinA23 (TyrA23). The Vha-a1-GFP is used to mark the Trans-Golgi network in the BFA body, while FM4-64 (2 µM) indicated the inhibition of CME. (**c**) CLC1/2/3 treated with mock (Ø,?), ES9 and CCCP. Note that CLC2 dislodges from the trans Golgi network and becomes almost entirely cytosolic, which is not the case for CLC1 and CLC3. (**d**) Sensors for phosphatidylinositol 4-phosphate (PI4P, P21Y) and phosphatidylinositol 4,5-biphosphate (PI(4,5)P_2, P24Y) in presence of mock treatment and 10 µM ES9. (**e**) Biochemical quantification of overall phospholipid concentrations for mock treatment and 10 µM ES9 for 30 min. Scale bar, 5µm.

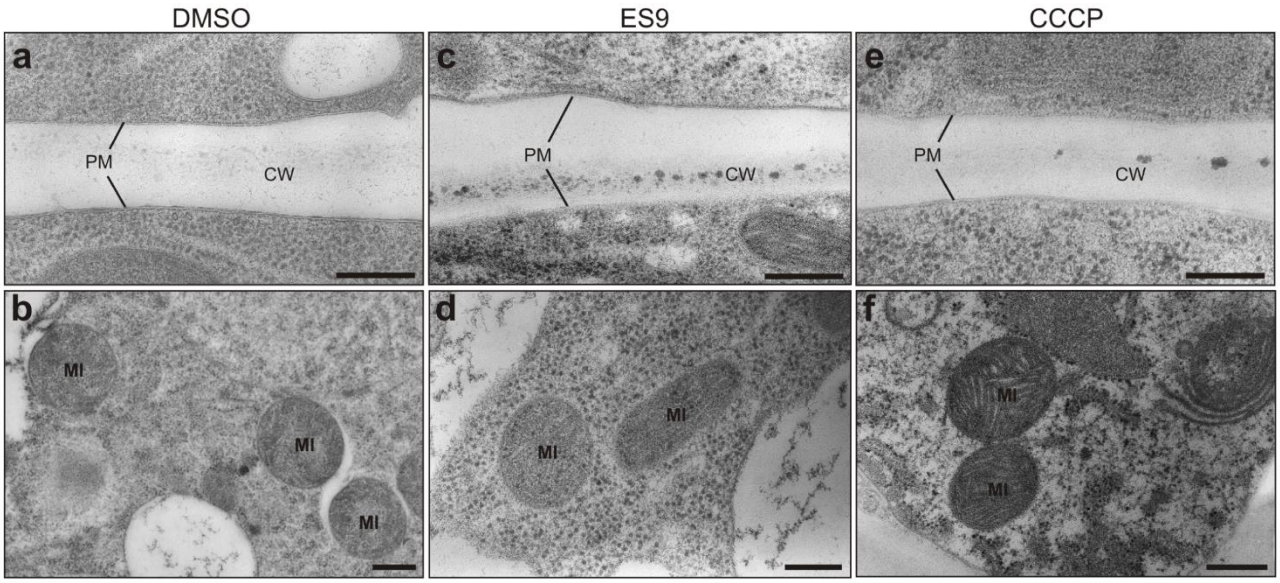

Supplemental Figure 5. The plasma membrane appears not affected by ES9 and CCCP

The plasma membrane (PM) and mitochondria (MI) of DMSO-treated samples (a-b), ES9-treated (10 µM, 30 min) samples (c-d), or CCCP-treated (1 µM, 30 min) samples (e-f) are morphologically normal. CW, cell wall. Scale bars, 200 nm.

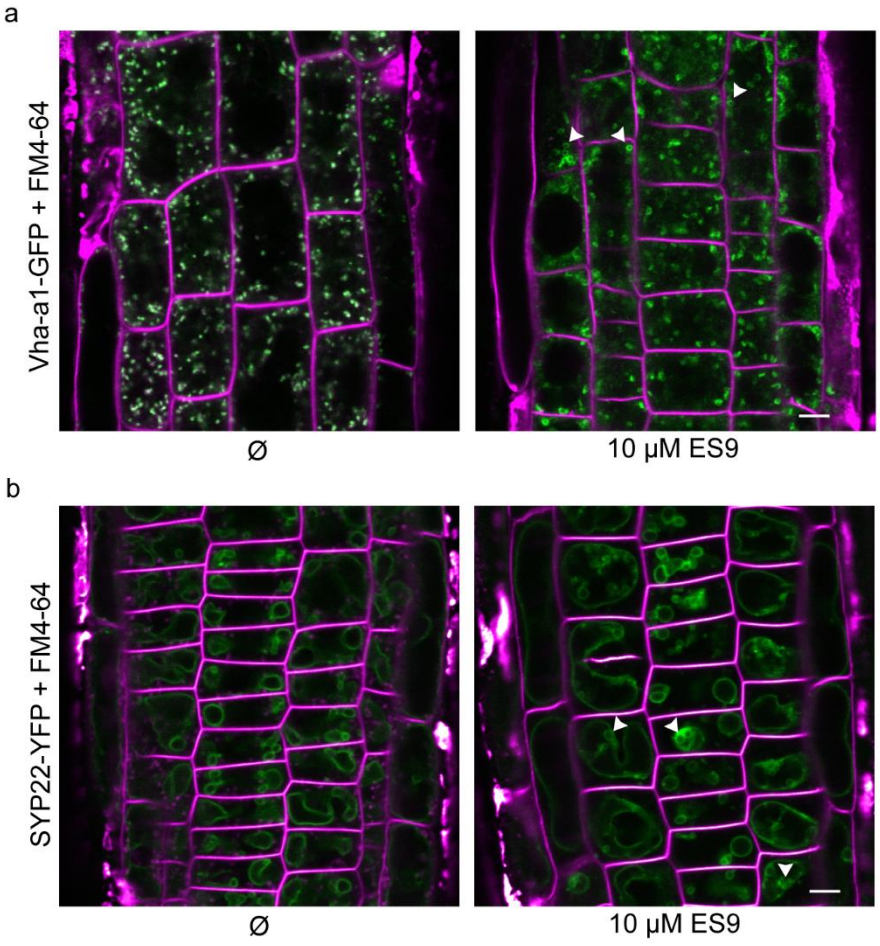

Supplemental Figure 6. ES9 affects vacuolar and TGN morphology

(**a**) Treatment with 10 µM ES9 induced doughnut-like Vha-a1-GFP (green) labeled compartments (arrowheads). (**b**) Treatment with 10 µM ES9 seemed to induce the formation of spherical membrane structures in the vacuole (arrowheads), probably of tonoplastic origin, as they are labeled by SYP22-YFP (green). FM4-64: magenta. Scale bar: 5 µm.

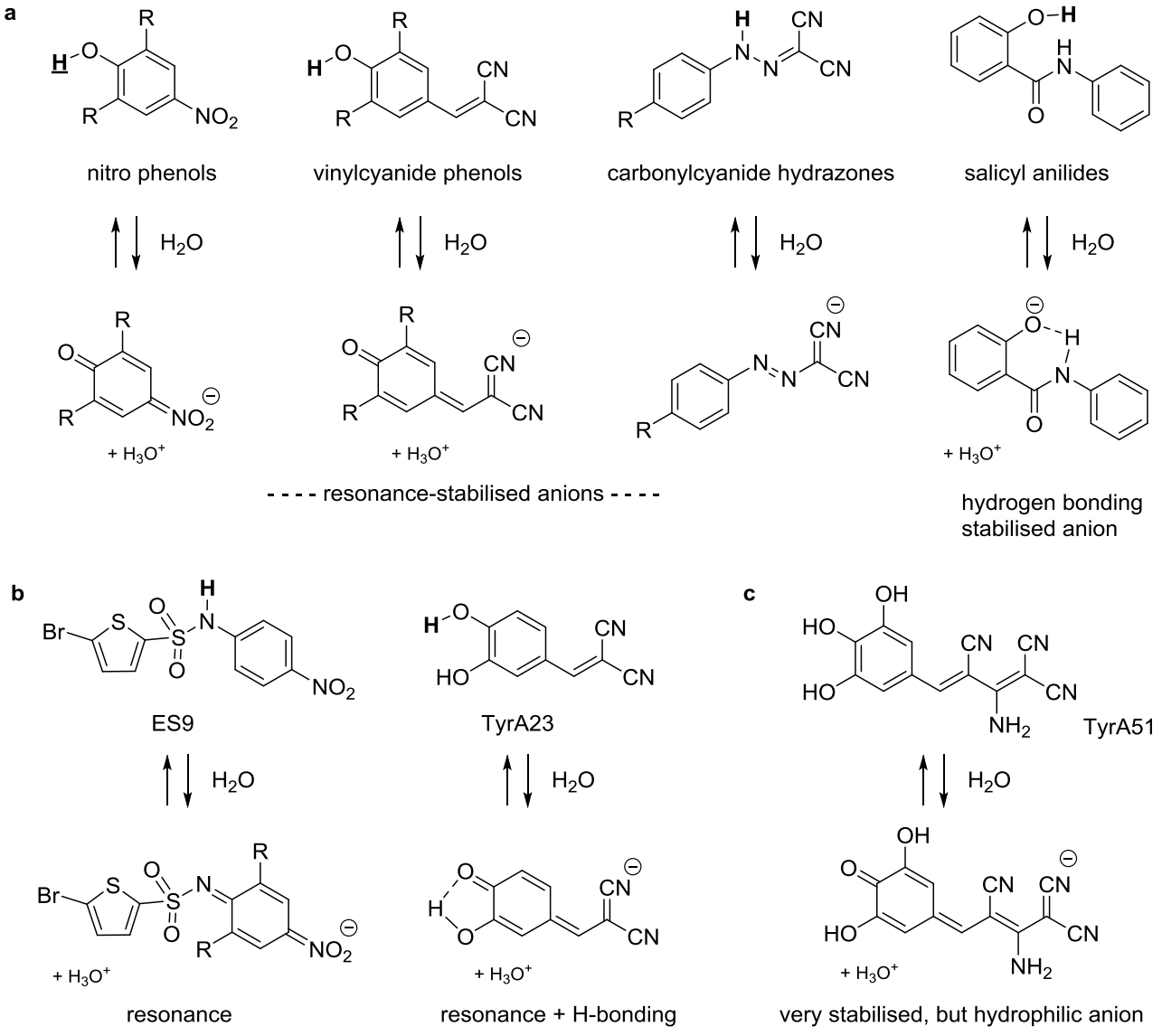

Supplemental Figure 7. Chemical features of protonophores

(**a**). Four known potent chemical classes of protonophore uncouplers of oxidative phosphorylation giving lipohilic anions either through electronic conjugation (charge delocalised resonance stabilisation) or through intramolecular hydrogen bond stabilisation. (**b**). structures of chemicals found to be protonophore uncouplers in this study (ES9 and TyrA23) and the structural features of their anions. (**c**). structure of Tyrphostin A51 which evidently gives a higly stabilised but much less lipophilic anion than the related TyrA23 compound.

References

1. McMahon, H. T. & Boucrot, E. Molecular mechanism and physiological functions of clathrin-mediated endocytosis. Nat Rev Mol Cell Biol 12, 517–533 (2011).

2. Bitsikas, V., Corrêa, I. R. & Nichols, B. J. Clathrin-independent pathways do not contribute significantly to endocytic flux. *eLife Sciences* **3**, e03970 (2014).

3. Baisa, G. A., Mayers, J. R. & Bednarek, S. Y. Budding and braking news about clathrin-mediated endocytosis. *Curr Opin Plant Biol* **16**, 718–725 (2013).

4. Zhang, Y. et al. Change your Tplate, change your fate: plant CME and beyond. *Trends Plant Sci* **20**, 41–48 (2015).

5. Gadeyne, A. et al. The TPLATE adaptor complex drives clathrin-mediated endocytosis in plants. *Cell* **156**, 691–704 (2014).

6. Hirst, J. et al. Characterization of TSET, an ancient and widespread membrane trafficking complex. *eLife Sciences* **3**, e02866 (2014).

7. Luschnig, C. & Vert, G. The dynamics of plant plasma membrane proteins: PINs and beyond. Development 141, 2924–2938 (2014).

8. Irani, N. G. *et al.* Fluorescent castasterone reveals BRI1 signaling from the plasma membrane. *Nat Chem Biol* **8,** 583–589 (2012).

9. Di Rubbo, S. *et al.* The clathrin adaptor complex AP-2 mediates endocytosis of brassinosteroid insensitive1 in Arabidopsis. *The Plant Cell* **25,** 2986–2997 (2013).

10. Smith, J. M., Salamango, D. J., Leslie, M. E., Collins, C. A. & Heese, A. Sensitivity to Flg22 is modulated by ligand-induced degradation and de novo synthesis of the endogenous flagellin-receptor FLAGELLIN-SENSING2. *Plant Physiol* **164**, 440–454 (2014).

11. Hicks, G. R. & Raikhel, N. V. Small Molecules Present Large Opportunities in Plant Biology. *Annu Rev Plant Biol* **63** 13.1-13.22 (2012).

12. Yaish, P., Gazit, A., Gilon, C. & Levitzki, A. Blocking of EGF-dependent cell proliferation by EGF receptor kinase inhibitors. *Science* **242**, 933–935 (1988).

13. Crump, C. M., Williams, J. L., Stephens, D. J. & Banting, G. Inhibition of the interaction between tyrosine-based motifs and the medium chain subunit of the AP-2 adaptor complex by specific tyrphostins. *J Biol Chem* **273**, 28073–28077 (1998).

14. Banbury, D. N., Oakley, J. D., Sessions, R. B. & Banting, G. Tyrphostin A23 inhibits internalization of the transferrin receptor by perturbing the interaction between tyrosine motifs and the medium chain subunit of the AP-2 adaptor complex. *J Biol Chem* **278**, 12022–12028 (2003).

15. Ortiz-Zapater, E., Soriano-Ortega, E., Marcote, M. J., Ortiz-Masiá, D. & Aniento, F. Trafficking of the human transferrin receptor in plant cells: effects of tyrphostin A23 and brefeldin A. *Plant J* **48**, 757–770 (2006).

16. Dhonukshe, P. et al. Clathrin-Mediated Constitutive Endocytosis of PIN Auxin Efflux Carriers in Arabidopsis. *Curr Biol* **17**, 520–527 (2007).

17. Konopka, C. A. et al. Dynamics of Arabidopsis dynamin-related protein 1C and a clathrin light chain at the plasma membrane. *Plant Cell* **20**, 1363–1380 (2008).

18. Lam, S. K. et al. BFA-induced compartments from the Golgi apparatus and trans-Golgi network/early endosome are distinct in plant cells. *Plant J* **60**, 865–881 (2009).

19. Boutté, Y. et al. Endocytosis restricts Arabidopsis KNOLLE syntaxin to the cell division plane during late cytokinesis. *EMBO J* **29**, 546–558 (2010).

20. Fujimoto, M. et al. Arabidopsis dynamin-related proteins DRP2B and DRP1A participate together in clathrin-coated vesicle formation during endocytosis. *Proc Natl Acad Sci USA* **107**, 6094–6099 (2010).

21. Robert, S. et al. ABP1 mediates auxin inhibition of clathrin-dependent endocytosis in Arabidopsis. *Cell* **143**, 111–121 (2010).

22. Kleine-Vehn, J. et al. Gravity-induced PIN transcytosis for polarization of auxin fluxes in gravity-sensing root cells. *Proc Natl Acad Sci USA* **107**, 22344–22349 (2010).

23. Van Damme, D. et al. Adaptin-like protein TPLATE and clathrin recruitment during plant somatic cytokinesis occurs via two distinct pathways. *Proc Natl Acad Sci USA* **108**, 615–620 (2011).

24. Ebine, K. et al. A membrane trafficking pathway regulated by the plant-specific RAB GTPase ARA6. *Nat Cell Biol* **13**, 853–859 (2011).

25. Luu, D.-T., Martinière, A., Sorieul, M., Runions, J. & Maurel, C. Fluorescence recovery after photobleaching reveals high cycling dynamics of plasma membrane aquaporins in Arabidopsis roots under salt stress. *The Plant Journal* **69**, 894–905 (2011).

26. Li, R. et al. A Membrane Microdomain-Associated Protein, Arabidopsis Flot1, Is Involved in a Clathrin-Independent Endocytic Pathway and Is Required for Seedling Development. *Plant Cell* **24**, 2105–2122 (2012).

27. Beck, M., Zhou, J., Faulkner, C., MacLean, D. & Robatzek, S. Spatio-temporal cellular dynamics of the Arabidopsis flagellin receptor reveal activation status-dependent endosomal sorting. *Plant Cell* **24**, 4205–4219 (2012).

28. Wang, C. et al. Clathrin light chains regulate clathrin-mediated trafficking, auxin signaling, and development in Arabidopsis. *Plant Cell* **25**, 499–516 (2013).

29. Yamaoka, S. et al. Identification and dynamics of Arabidopsis adaptor protein-2 complex and its involvement in floral organ development. *Plant Cell* **25**, 2958–2969 (2013).

30. Kim, S. Y. et al. Adaptor protein complex 2-mediated endocytosis is crucial for male reproductive organ development in Arabidopsis. *Plant Cell* **25**, 2970–2985 (2013).

31. Fan, L. et al. Dynamic analysis of Arabidopsis AP2 σ subunit reveals a key role in clathrin-mediated endocytosis and plant development. *Development* **140**, 3826–3837 (2013).

32. Macia, E. et al. Dynasore, a cell-permeable inhibitor of dynamin. *Dev Cell* **10**, 839–850 (2006).

33. Kleist, von, L. et al. Role of the clathrin terminal domain in regulating coated pit dynamics revealed by small molecule inhibition. *Cell* **146**, 471–484 (2011).

34. McCluskey, A. et al. Building a better dynasore: the dyngo compounds potently inhibit dynamin and endocytosis. *Traffic* **14**, 1272–1289 (2013).

35. Dutta, D., Williamson, C. D., Cole, N. B. & Donaldson, J. G. Pitstop 2 is a potent inhibitor of clathrin-independent endocytosis. *PLoS ONE* **7**, e45799 (2012).

36. Willox, A. K., Sahraoui, Y. M. E. & Royle, S. J. Non-specificity of Pitstop 2 in clathrin-mediated endocytosis. *Biol Open* **3**, 326–331 (2014).

37. Sharfman, M. et al. Endosomal signaling of the tomato leucine-rich repeat receptor-like protein LeEix2. *Plant J* **68**, 413–423 (2011).

38. Drakakaki, G. *et al.* Clusters of bioactive compounds target dynamic endomembrane networks in vivo. *Proc Natl Acad Sci USA* **108,** 17850–17855 (2011).

39. Rigal, A., Doyle, S. M. & Robert, S. Live cell imaging of FM4-64, a tool for tracing the endocytic pathways in Arabidopsis root cells. *Methods Mol Biol* **1242**, 93–103 (2015).

40. Kasprowicz, J. *et al.* Inactivation of clathrin heavy chain inhibits synaptic recycling but allows bulk membrane uptake. *J Cell Biol* **182,** 1007–1016 (2008).

41. Heerssen, H., Fetter, R. D. & Davis, G. W. Clathrin dependence of synaptic-vesicle formation at the Drosophila neuromuscular junction. *Curr Biol* **18,** 401–409 (2008).

42. Kasprowicz, J., Kuenen, S., Swerts, J., Miskiewicz, K. & Verstreken, P. Dynamin photoinactivation blocks Clathrin and α-adaptin recruitment and induces bulk membrane retrieval. *J Cell Biol* **204,** 1141–1156 (2014)

43. Liao, J. F. & Perkins, J. P. Differential effects of antimycin A on endocytosis and exocytosis of transferrin also are observed for internalization and externalization of beta-adrenergic receptors. *Mol. Pharmacol*. **44**, 364–370 (1993).

44. Schmid, S. L. & Carter, L. L. ATP is required for receptor-mediated endocytosis in intact cells. *J Cell Biol* **111**, 2307–2318 (1990).

45. Potter, V. R. & Reif, A. E. Inhibition of an electron transport component by antimycin A. *J Biol Chem* **194**, 287–297 (1952).

46. Hong, S. & Pedersen, P. L. ATP synthase and the actions of inhibitors utilized to study its roles in human health, disease, and other scientific areas. *Microbiol Mol Biol Rev* **72**, 590–641 (2008).

47. Heytler, P. G. Uncoupling of oxidative phosphorylation by carbonyl cyanide phenylhydrazones. I. Some characteristics of m-Cl-CCP action on mitochondria and chloroplasts. *Biochemistry* **2**, 357–361 (1963).

48. Kasianowicz, J., Benz, R. & McLaughlin, S. The kinetic mechanism by which CCCP (carbonyl cyanide m-chlorophenylhydrazone) transports protons across membranes. *J. Membr. Biol.* **82**, 179–190 (1984).

49. Clarke, J. M., Gillings, M. R., Altavilla, N. & Beattie, A. J. Potential problems with fluorescein diacetate assays of cell viability when testing natural products for antimicrobial activity. *J. Microbiol. Methods* **46**, 261–267 (2001).

50. Keech, O. & Dizengremel, P. Preparation of leaf mitochondria from Arabidopsis thaliana. *Physiol Plant* **124** 403-409 (2005).

51. Poot, M. et al. Analysis of mitochondrial morphology and function with novel fixable fluorescent stains. *J. Histochem. Cytochem.* **44**, 1363–1372 (1996).

52. Scaduto, R. C. & Grotyohann, L. W. Measurement of mitochondrial membrane potential using fluorescent rhodamine derivatives. *Biophys. J.* **76**, 469–477 (1999).

53. Xie, Y. et al. A novel function for dendritic cell: clearance of VEGF via VEGF receptor-1. *Biochem Biophys Res Commun* **380**, 243–248 (2009).

54. Qian, Z. M. & Morgan, E. H. Effect of metabolic inhibitors on uptake of non-transferrin-bound iron by reticulocytes. *Biochim Biophys Acta* **1073**, 456–462 (1991).

55. Dolman, N. J., Kilgore, J. A. & Davidson, M. W. A review of reagents for fluorescence microscopy of cellular compartments and structures, part I: BacMam labeling and reagents for vesicular structures. *Curr Protoc Cytom* (2013).

56. Krebs, M. et al. Arabidopsis V-ATPase activity at the tonoplast is required for efficient nutrient storage but not for sodium accumulation. *Proceedings of the National Academy of Sciences* **107**, 3251–3256 (2010).

57. Van Damme, D. et al. Somatic cytokinesis and pollen maturation in Arabidopsis depend on TPLATE, which has domains similar to coat proteins. *Plant Cell* **18**, 3502–3518 (2006).

58. McMahon, H. T. & Gallop, J. L. Membrane curvature and mechanisms of dynamic cell membrane remodelling. *Nat Cell Biol* **438**, 590–596 (2005).

59. Simon, M. L. A. et al. A multi-colour/multi-affinity marker set to visualize phosphoinositide dynamics in Arabidopsis. *Plant J* **77**, 322–337 (2014).

60. Teh, O.-K. & Moore, I. An ARF-GEF acting at the Golgi and in selective endocytosis in polarized plant cells. *Nature* **448**, 493–496 (2007).

61. Dettmer, J., Hong-Hermesdorf, A., Stierhof, Y.-D. & Schumacher, K. Vacuolar H+-ATPase activity is required for endocytic and secretory trafficking in Arabidopsis. *Plant Cell* **18**, 715–730 (2006).

62. Donaldson, J. G., Finazzi, D. & Klausner, R. D. Brefeldin A inhibits Golgi membrane-catalysed exchange of guanine nucleotide onto ARF protein. *Nature* **360**, 350–352 (1992).

63. Helms, J. B. & Rothman, J. E. Inhibition by brefeldin A of a Golgi membrane enzyme that catalyses exchange of guanine nucleotide bound to ARF. *Nature* **360**, 352–354 (1992).

64. Burkhardt, J. K., Hester, S. & Argon, Y. The glycoprotein of VSV accumulates in a distal Golgi compartment in the presence of CCCP. *J Cell Sci* **92** (Pt 4)**,** 643–654 (1989).

65. Robert, S. et al. Endosidin1 defines a compartment involved in endocytosis of the brassinosteroid receptor BRI1 and the auxin transporters PIN2 and AUX1. *Proc Natl Acad Sci USA* **105**, 8464–8469 (2008).

66. Richter, S. et al. Functional diversification of closely related ARF-GEFs in protein secretion and recycling. *Nature* **448**, 488–492 (2007).

67. Ortiz-Zapater, E. et al. Trafficking of the human transferrin receptor in plant cells: effects of tyrphostin A23 and brefeldin A. *Plant J* **48**, 757–770 (2006).

68. Dhonukshe, P. et al. Clathrin-Mediated Constitutive Endocytosis of PIN Auxin Efflux Carriers in Arabidopsis. *Curr Biol* **17**, 520–527 (2007).

69. Lam, S. K., Tse, Y. C., Robinson, D. G. & Jiang, L. Tracking down the elusive early endosome. *Trends Plant Sci* **12**, 497–505 (2007).

70. Kenwood, B. M. et al. Identification of a novel mitochondrial uncoupler that does not depolarize the plasma membrane. *Mol Metab* **3**, 114–123 (2014).

71. Park, K.-S. et al. FCCP depolarizes plasma membrane potential by activating proton and Na+ currents in bovine aortic endothelial cells. *Pflugers Arch.* **443**, 344–352 (2002).

72. Brismar, T. & Collins, V. P. Effect of external cation concentration and metabolic inhibitors on membrane potential of human glial cells. *J. Physiol. (Lond.)* **460**, 365–383 (1993).

73. Juthberg, S. K. & Brismar, T. Effect of metabolic inhibitors on membrane potential and ion conductance of rat astrocytes. *Cell. Mol. Neurobiol.* **17**, 367–377 (1997).

74. Buckler, K. J. & Vaughan-Jones, R. D. Effects of mitochondrial uncouplers on intracellular calcium, pH and membrane potential in rat carotid body type I cells. *J. Physiol. (Lond.)* **513** (Pt 3), 819–833 (1998).

75. Alexandre, A. & Lehninger, A. L. Bypasses of the antimycin a block of mitochondrial electron transport in relation to ubisemiquinone function. *Biochim Biophys Acta* **767**, 120–129 (1984).

76. Campo, M. L., Kinnally, K. W. & Tedeschi, H. The effect of antimycin A on mouse liver inner mitochondrial membrane channel activity. *J Biol Chem* **267**, 8123–8127 (1992).

77. Terada, H. Uncouplers of oxidative phosphorylation. *Environ Health Perspect* **87**, 213–218 (1990).

78. Makarow, M. & Nevalainen, L. T. Transport of a fluorescent macromolecule via endosomes to the vacuole in Saccharomyces cerevisiae. *J Cell Biol* **104**, 67–75 (1987).

79. Verstreken, P. et al. Synaptic mitochondria are critical for mobilization of reserve pool vesicles at Drosophila neuromuscular junctions. *Neuron* **47**, 365–378 (2005).

80. Ly, C. V. Mitochondria at the Synapse. *The Neuroscientist* **12**, 291–299 (2006).

81. Sandvig, K. et al. Acidification of the cytosol inhibits endocytosis from coated pits. *J Cell Biol* **105**, 679–689 (1987).

82. Thorstensen, K. & Thorstensen, K. Hepatocytes and reticulocytes have different mechanisms for the uptake of iron from transferrin. *J Biol Chem* **263**, 16837–16841 (1988).

83. Bagar, T., Altenbach, K., Read, N. D. & Bencina, M. Live-Cell imaging and measurement of intracellular pH in filamentous fungi using a genetically encoded ratiometric probe. *Eukaryotic Cell* **8**, 703–712 (2009).

84. Maxfield, F. R. Weak bases and ionophores rapidly and reversibly raise the pH of endocytic vesicles in cultured mouse fibroblasts. *J Cell Biol* **95**, 676–681 (1982).

85. Ding, W.-X. et al. Nix is critical to two distinct phases of mitophagy, reactive oxygen species-mediated autophagy induction and Parkin-ubiquitin-p62-mediated mitochondrial priming. *Journal of Biological Chemistry* **285**, 27879–27890 (2010).

86. Kwon, K.-Y., Viollet, B. & Yoo, O. J. CCCP induces autophagy in an AMPK-independent manner. *Biochem Biophys Res Commun* **416**, 343–348 (2011).

87. Padman, B. S., Bach, M., Lucarelli, G., Prescott, M. & Ramm, G. The protonophore CCCP interferes with lysosomal degradation of autophagic cargo in yeast and mammalian cells. *Autophagy* **9**, 1862–1875 (2013).

88. Heuser, J. Effects of cytoplasmic acidification on clathrin lattice morphology. *J Cell Biol* **108**, 401–411 (1989).

89. Hansen, S. H. et al. Clathrin and HA2 adaptors: effects of potassium depletion, hypertonic medium, and cytosol acidification. *J Cell Biol* 121, **61**–72 (1993).

90. Shishova, M. & Lindberg, S. Auxin-induced cytosol acidification in wheat leaf protoplasts depends on external concentration of Ca 2. *Journal of Plant Physiology* (1999).

91. Lebrun-Garcia, A., Chiltz, A., Gout, E., Bligny, R. & Pugin, A. Questioning the role of salicylic acid and cytosolic acidification in mitogen-activated protein kinase activation induced by cryptogein in tobacco cells. *Planta* **214**, 792–797 (2002).

92. Du, Y. et al. Salicylic acid interferes with clathrin-mediated endocytic protein trafficking. *Proceedings of the National Academy of Sciences* **110**, 7946–7951 (2013).

93. Pintsch, T., Satre, M., Klein, G., Martin, J. B. & Schuster, S. C. Cytosolic acidification as a signal mediating hyperosmotic stress responses in Dictyostelium discoideum. *BMC Cell Biol*. **2**, 9 (2001).

94. Maro, B., Marty, M. C. & Bornens, M. In vivo and in vitro effects of the mitochondrial uncoupler FCCP on microtubules. *EMBO J* **1**, 1347–1352 (1982).

95. Burkhardt, J. K. & Argon, Y. Intracellular transport of the glycoprotein of VSV is inhibited by CCCP at a late stage of post-translational processing. *J Cell Sci* **92** (Pt 4), 633–642 (1989).

96. Robinson, D. G., Jiang, L. & Schumacher, K. The endosomal system of plants: charting new and familiar territories. *Plant Physiol* **147**, 1482–1492 (2008).

97. Lam, S. K., Cai, Y., Tse, Y. C., Wang, J., Law, A. H., Pimpl, P., Chan, H. Y., Xia, J. & Jiang L. BFA-induced compartments from the Golgi apparatus and trans-Golgi network/early endosome are distinct in plant cells. *Plant J* **60**, 865–881 (2009).

98. Reichardt, I. et al. Plant cytokinesis requires de novo secretory trafficking but not endocytosis. *Curr Biol* **17**, 2047–2053 (2007).

99. Scheuring, D., Viotti, C., Krüger, F., Künzl, F., Sturm, S., Bubeck, J., Hillmer, S., Frigerio, L., Robinson, D. G., Pimpl, P. & Schumacher, K. Multivesicular bodies mature from the trans-Golgi network/early endosome in Arabidopsis. *Plant Cell* **23**, 3463–3481 (2011).

100. Yoshimoto, K., Hanaoka, H., Sato, S., Kato, T., Tabata, S., Noda, T., & Ohsumi, Y. Processing of ATG8s, ubiquitin-like proteins, and their deconjugation by ATG4s are essential for plant autophagy. *Plant Cell* **16**, 2967–2983 (2004).

101. Nesterov, A., Carter, R. E., Sorkina, T., Gill, G. N. & Sorkin, A. Inhibition of the receptor-binding function of clathrin adaptor protein AP-2 by dominant-negative mutant mu2 subunit and its effects on endocytosis. *EMBO J* **18**, 2489–2499 (1999).

102. Chan, K., Truong, D., Shangari, N. & O'Brien, P. J. Drug-induced mitochondrial toxicity. *Expert Opin. Drug Metab. Toxicol.* **1**, 655–669 (2005).

103. Swiss, R., Niles, A., Cali, J. J., Nadanaciva, S. & Will, Y. Validation of a HTS-amenable assay to detect drug-induced mitochondrial toxicity in the absence and presence of cell death. *Toxicol In Vitro* **27**, 1789–1797 (2013).

104. Moffat, J. G., Rudolph, J. & Bailey, D. Phenotypic screening in cancer drug discovery - past, present and future. *Nat Rev Drug Discov* **13**, 588–602 (2014).

105. O'Brien, P. J. High-content analysis in toxicology: screening substances for human toxicity potential, elucidating subcellular mechanisms and in vivo use as translational safety biomarkers. *Basic Clin. Pharmacol. Toxicol*. **115**, 4–17 (2014).

106. Van Leene, J. et al. A tandem affinity purification-based technology platform to study the cell cycle interactome in Arabidopsis thaliana. *Mol Cell Proteomics* **6**, 1226–1238 (2007).

107. Fendrych, M. et al. Programmed cell death controlled by ANAC033/SOMBRERO determines root cap organ size in Arabidopsis. *Curr Biol* **24**, 931–940 (2014).

108. Moseyko, N. & Feldman, L. J. Expression of pH-sensitive green fluorescent protein in Arabidopsis thaliana. *Plant Cell Environ*. **24**, 557–563 (2001).

109. Hillmer, S., Viotti, C. & Robinson, D. G. An improved procedure for low-temperature embedding of high-pressure frozen and freeze-substituted plant tissues resulting in excellent structural preservation and contrast. *J Microsc* **247**, 43–47 (2012).

110. Verstreken, P., Ohyama, T. & Bellen, H. J. FM 1-43 labeling of synaptic vesicle pools at the Drosophila neuromuscular junction. *Methods Mol Biol* **440**, 349–369 (2008).

111. Shidara, Y. & Hollenbeck, P. J. Defects in mitochondrial axonal transport and membrane potential without increased reactive oxygen species production in a Drosophila model of Friedreich ataxia. *J. Neurosci*. **30**, 11369–11378 (2010).

Chapter IV: Disruption of clathrin-mediated endocytosis in Arabidopsis through small molecule inhibition of clathrin heavy chain function

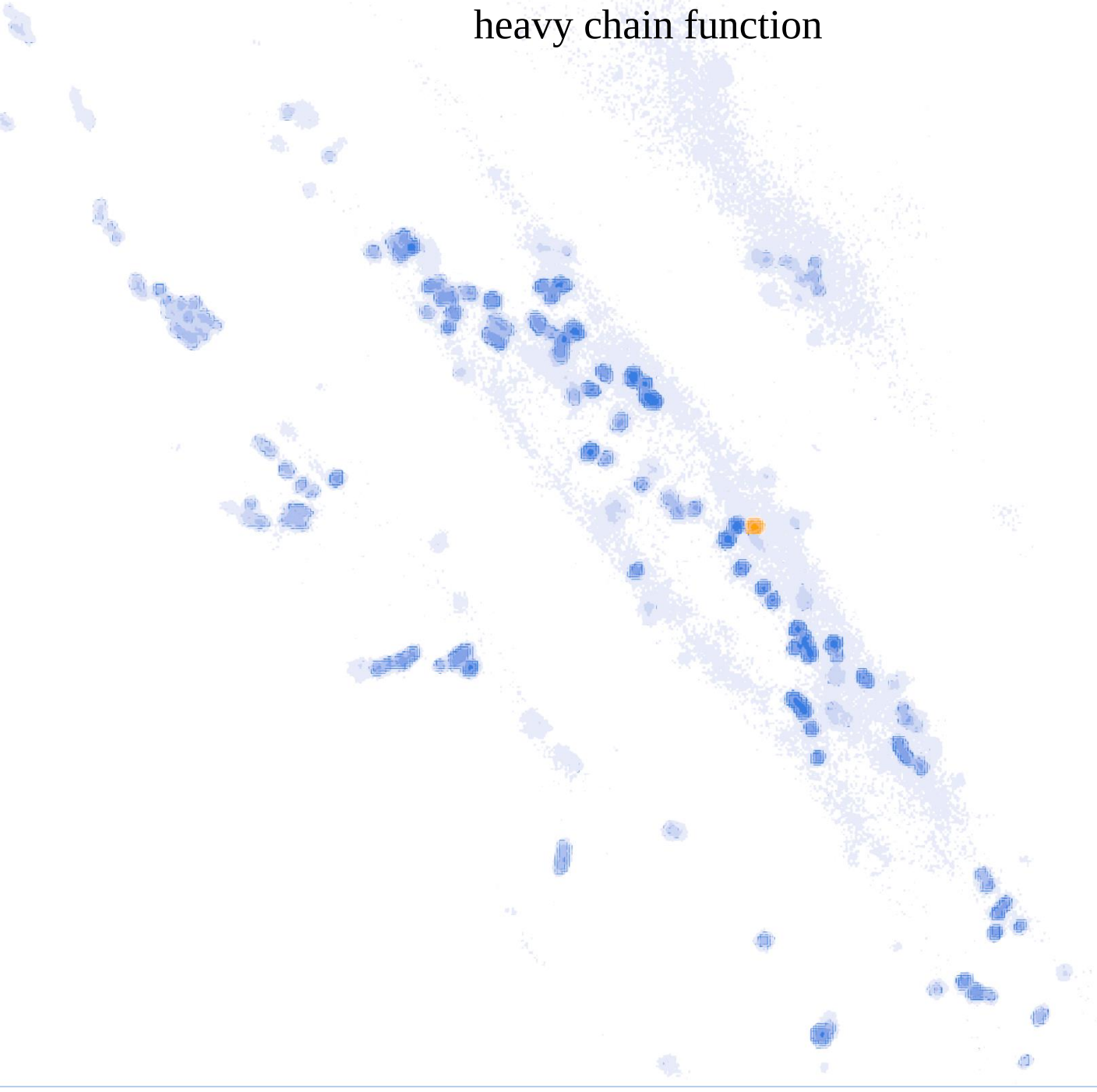

Disruption of clathrin-mediated endocytosis in *Arabidopsis* through small molecule inhibition of clathrin heavy chain function

Wim Dejonghe[1,2], Kiril Mishev[1,2], Bram Denoo[3], Evelien Mylle[1,2], Isabelle Van Houtte[1,2], Sabine Kuenen[4], Corrado Viotti[5], An Staes[6], Long Nguyen[7], Andrzej Drozdzecki, Wim Nerinckx[8], Dominique Audenaert[7], Daniël Van Damme[1,2], Annemieke Madder[3], Patrik Verstreken[4], Kris Gevaert[6], Johan Winne[3] and Eugenia Russinova[1,2].

[1]Department of Plant Systems Biology, VIB, Technologiepark 927, 9052 Ghent, Belgium;

[2]Department of Plant Biotechnology and Bioinformatics, Ghent University, 9052 Ghent, Belgium.

[3]Department of Organic Chemistry, Polymer Chemistry Research Group and Laboratory for Organic Synthesis, Ghent University, Krijgslaan 281 S4-bis, B-9000 Ghent, Belgium.

[4]VIB Center for the Biology of Disease, Laboratory of Neuronal Communication, Department for Human Genetics, and Leuven Institute for Neurodegenerative Diseases, KU Leuven, 3000 Leuven, Belgium.

[5]Umeå Plant Science Centre, Department of Plant Physiology, Umeå University Umeå, Sweden

[6]Department of Medical Protein Research, VIB, 9000 Ghent, Belgium; and Department of Biochemistry, Ghent University, 9000 Gent, Belgium.

[7]Compound Screening Facility, VIB, Technologiepark 927, B-9052 Ghent, Belgium.

[8]Department for Molecular Biomedical Research, VIB, Ghent University, Ghent, Belgium; Department for Molecular Biomedical Research, VIB, Ghent University, Ghent, Belgium.

Author contributions: W.D. did large parts of the *Arabidopsis*-related cell biology and ATP depletion assays. W.D did the affinity purification, biochemical and genetic validation. W.D. wrote the text and made the figures.

Abstract

Clathrin-mediated endocytosis (CME) is an essential and highly dynamic process which ensures proper responses to environmental cues and correct function of the plasma membrane within the eukaryotic cell. Classical genetic strategies have been important tools for our understanding of CME, yet certain aspects such as its dynamic and essential nature are difficult to approach. Small molecules targeting CME can provide a solution, as they impose only temporal changes which can be easily adjusted. Despite their promise, few specific small molecule effectors of CME in plants are known. Mammalian systems can dispose of a larger collection, yet successful translations and implementations to the plant field are scarce. Here, we report on the identification and characterization of a small molecule inhibitor of CME in *Arabidopsis*, ES9-17. Affinity-based target identification revealed clathrin heavy chain as a potential target of ES9-17. Cellular thermal shift and drug affinity responsive target stability assays further validated the ES9-17 mode of action. Hence, this study provides a bioactive molecule that can be used to specifically probe CME in *Arabidopsis*.

Introduction

Chemical inhibitors of endocytosis are an attractive alternative to the current methods for disrupting protein function, but despite extensive structural and biochemical knowledge about clathrin-mediated endocytosis (CME) in eukaryotic cells[1-4], development of chemical tools to interfere with this process is still at an relative early stage. Although small molecule inhibitors of CME such as Dynasore and Pitstop2[5,6] have been described and exploited in mammalian systems, current debates on their off-target effects and lack of specificity[7,8] are spurring on further development of Dynasore or Pitstop2 derivatives with higher specificity[9-11]. Dynasore is described as an inhibitor of dynamin, a molecular component involved in formation and scission of the clathrin-coated vesicle[6]. Since Dynasore appears to have side-effects such as serum protein binding and association with detergents, a new series of Dynasore-based small molecules, named Dyngo[10] were tested. Compared to Dynasore the Dyngo series are more potent and specific, with some analogs able to distinguish different oligomerization states of dynamin[10]. An additional group of dynamin inhibitors have been described, called the Dynoles[11], including different indoles of which one possess higher potency towards dynamin inhibition compared to Dynasore. Similarly, the Pitstop small molecules were reported as specific inhibitors of clathrin heavy chain (CHC)[5]. Both Pitstop1 and Pitstop2 are developed to specifically target the CHC N-terminal domain, yet only Pitstop2 is used in subsequent studies, as Pitstop1 has reduced efficacy compared to Pitstop2[5]. Also in case of Pitstop2, side-effects are reported[7,8], including inhibition of non-clathrin mediated endocytosis. However, a follow-up study on the original report of Pitstops challenges the reports on off-target action by Pitstop2, and reports a further improved version of Pitstop2, Pitstop2-100, together with inactive analogs (Pitnots)[9]. Clearly, the development of specific inhibitors is a very active field of research in mammalian systems, however none of the small molecules mentioned above have found broad application in plant biology yet. One study on the tomato receptor-like protein LeEix2 used Dynasore to successfully reduce uptake of LeEix2-GFP expressed transiently in tobacco[12], yet remains till date the sole plant study using Dynasore.

Typically, plant biology takes advantage of TyrphostinA23 (TyrA23), a small molecule inhibitor of CME. Originally derived from tyrosine kinase inhibitors targeted against the kinase domain of epidermal growth factor (EGF)[13], TyrA23 was found to inhibit endocytosis of the transferrin receptor through interference with cargo recognition by tyrosine containing recognition sequences of the adaptor complex-2 (AP-2) medium subunit[14,15], a finding which was successfully translated to plants[16]. Despite its broad use in the plant field, few studies in mammalian systems use TyrA23 as a specific inhibitor of CME. However, TyrA23 has recently been described as a protonophore in *Arabidopsis*, shuttling protons chemically across membranes and along proton gradients, thereby enabling a complete inhibition of endocytosis (Chapter 3, this thesis). Since the use of TyrA23 as a specific inhibitor of CME in plants is questionable, and as Dynasore and Pitstop2[5,6] have not found

wide application, the plant field would benefit from a novel and specific small molecule inhibitors of CME. As such, the development of novel inhibitors to use in conjunction with existing inhibitors will assist in the molecular and functional dissection of the endocytic pathway, resulting in an increased understanding of many physiological processes that rely on this pathway.

Here, we describe the identification and characterization of a specific inhibitor of CME in *Arabidopsis*, ES9-17. Validation of potential targets, found through affinity purification, with Cellular Thermal Shift Assay (CETSA)[17] and Drug Affinity Responsive Target Stability (DARTS)[18] identified clathrin heavy chain (CHC) as a potential target of ES9-17. In addition, genetic evidence supported this hypothesis. We therefore present a more specific small molecule inhibitor of CME in *Arabidopsis*.

Results

Identification of ES9-17.

We previously described the small molecule ES9 as a nonspecific inhibitor of CME in *Arabidopsis* due to its protonophore activity (Chapter 3, this thesis). Interestingly, ES9 was able to block the synaptic vesicle recycling in *Drosophila*, generating phenotypes reminiscent to a loss-of-function in either CHC, clathrin light chain (CLC) or dynamin[19-21] and this effect was independent of its chemical uncoupling ability (Chapter 3, this thesis). Thus, we hypothesized that ES9 might have protein targets related to CME in plants and in flies, but its strong protonophore activity masked them. In order to identify ES9 analogs that blocked CME but lost their protonophore activity we conducted a structure activity relation (SAR) analysis using the inhibition of the FM4-64 uptake assay (Chapter 3, this thesis) as a readout for compound activity.

Several commercial available and newly synthesized analogs were used for SAR analysis. First, removal of the bromine on the thiophene moiety (ES9-2, **Figure 1a**) enabled complete inhibition of FM4-64, yet at a higher concentration compared to ES9 (**Figure 1b**). The retained activity of ES9-2 in respect to FM4-64 uptake inhibition indicated that the bromine was not essential for ES9 activity. A similar analog, ES9-8, which has the bromothiophene moiety substituted for a bromobenzene moiety (**Figure 1a**), also retained the ability to completely inhibit FM4-64 uptake, though, similarly to ES9-2, at higher concentrations compared to ES9 (**Figure 1b**). Next, analogs representing parts of the original ES9 structure were also tested for activity. Both the 5-bromo-N-methyl thiophene-2-sulfonamide moiety (ES9-3, **Figure 1a**) and the 4-nitroaniline moiety (ES9-7, **Figure 1a**) proved to be inactive in terms of FM4-64 uptake inhibition (**Figure 1b**). We also evaluated the sulfonamide

and nitro moiety for activity. Methylation of the sulfonamide resulted in ES9-6 (**Figure 1a**), and rendered the analog completely inactive in terms of FM4-64 uptake inhibition (**Figure 1b**). Substitution of the nitrobenzene group with a phenol (ES9-15, **Figure 1a**) or pyridine group (ES9-16, **Figure 1a**) resulted in much less potent analogs, as FM4-64 uptake was reduced, but not inhibited (**Figure 1b**). However, ES9-17, which had the nitrobenzene substituted with a benzene moiety (**Figure 1a**) retained the ability to inhibit FM4-64 uptake, even at 10 µM (**Figure 1b**) thus, providing a minimal active structure for ES9.

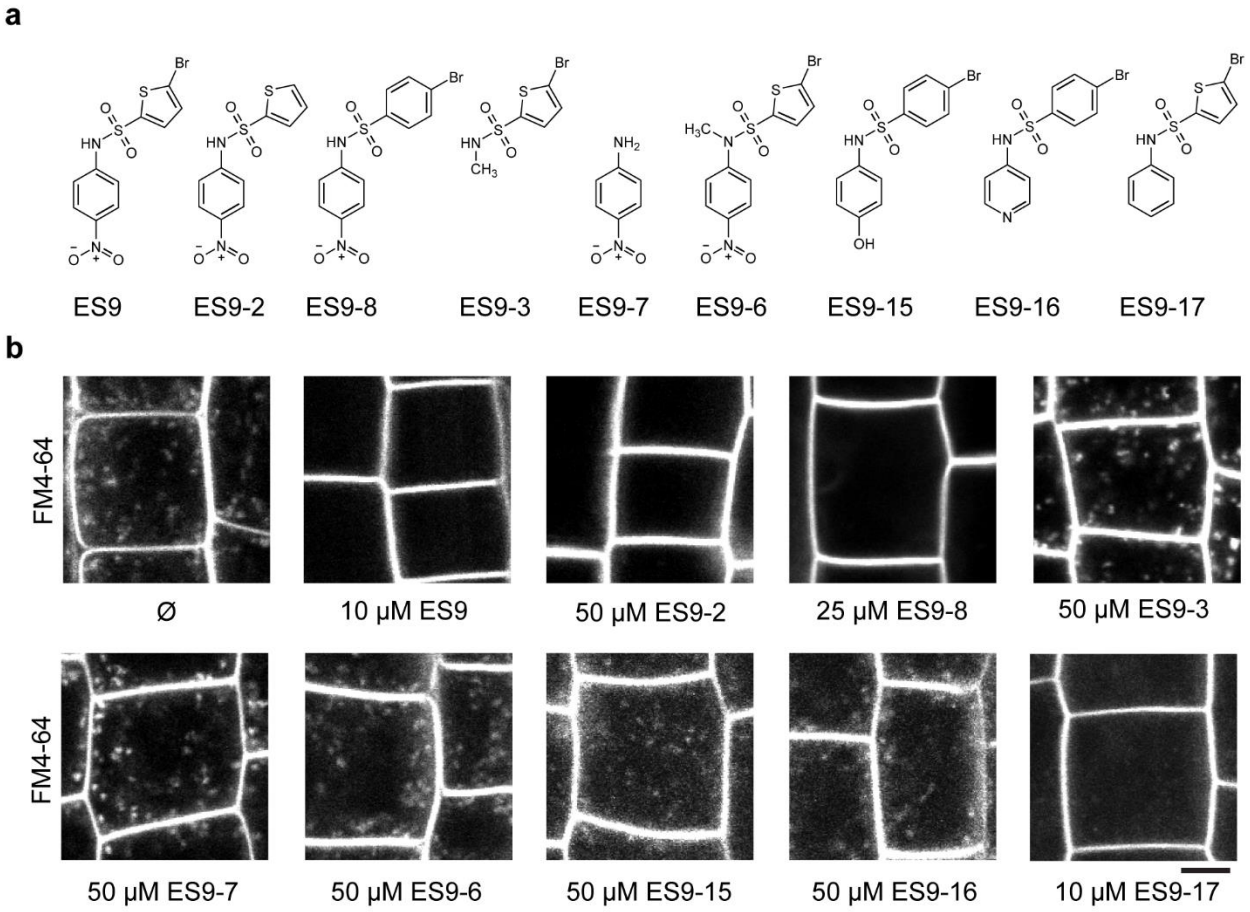

Figure 1. Structure activity relation analysis of ES9.

(**a**) Chemical structures of selected ES9 analogues. (**b**) FM4-64 uptake inhibition assay in *Arabidopsis* seedlings as a readout for activity of ES9 and its analogues (30 min treatment with small molecules and FM4-64). Scale bar, 5µm

Key analogs ES9-6, ES9-8 and ES9-17, which retained the ability to inhibit FM4-64 uptake, were compared to ES9 in terms of ATP depletion in order to assess to what extent the difference in chemical structure would affect the ability to uncouple proton gradients in the mitochondria. As expected, application of 50 µM ES9-6 did not affect ATP levels whereas, 50 µM ES9-8 depleted it to a similar extent as ES9 (**Figure 2a**). Interestingly, 10 µM ES9-17 treatment did not affect the ATP levels. All small molecules increased fluorescein diacetate (FDA) fluorescence over time, indicating metabolically active cells (**Supplemental Figure 1a**). To confirm the inability to uncouple proton

gradients in the mitochondria *in vivo*, mitochondrial function in presence of 10 µM ES9-17 was tested by applying MitoTracker Red CM-H2XRos[22] to wild type *Arabidopsis* root cells. As expected based on the ATP depletion results, ES9-17 was unable to abolish mitochondrial staining (**Figure 2b**), in contrast to ES9, which prevents mitochondrial labeling by MitoTracker Red CM-H2XRos (Chapter 3, this thesis). Altogether our SAR analysis identified the small molecule ES9-17 as a potent inhibitor of FM4-64 uptake in *Arabidopsis* root cells without affecting ATP levels.

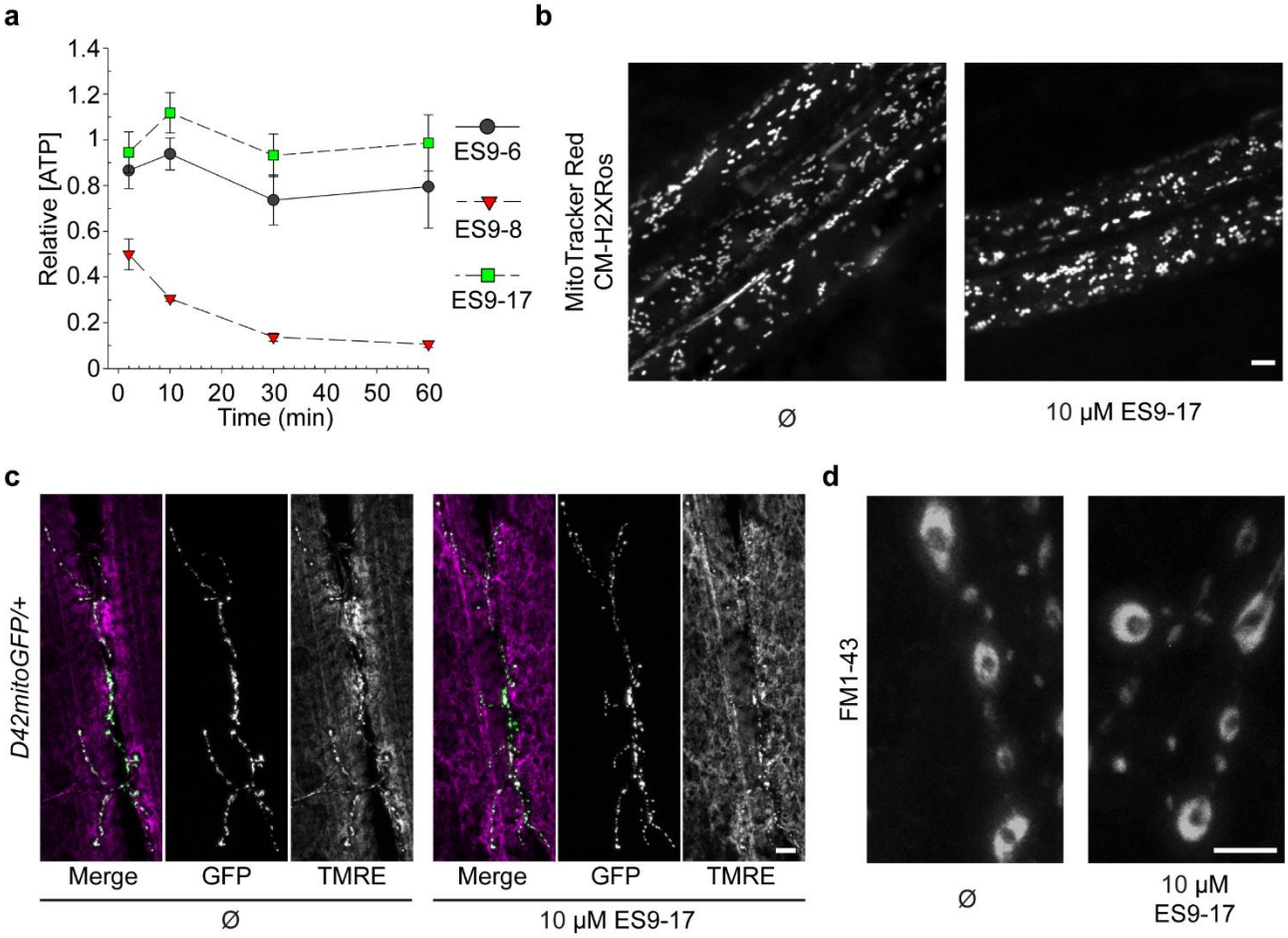

Figure 2. Protonophore characteristics of selected ES9 analogues.

(**a**) ATP depletion analysis in PSB-D wild type cell cultures. (**b**) MitoTracker Red CM-H2xRos labeling of respiring mitochondria in *Arabidopsis* Col-0 roots in presence of mock (Ø, DMSO) or ES9-17 (10 µM). Seedlings were first treated for 30 min with small molecule or mock, followed by 30 min 250 nM MitoTracker Red CM-H2xRos staining in presence appropriate treatments. (**c**) Tetramethylrhodamine ethyl ester (TMRE) labeling of mitochondria in *D42mitoGFP* positive Drosophila neuronal cells for 10 µM ES9-17 and mock treatment. Cells are incubated in the dark for 30 min with ES9-17 or mock, followed by 15 min of TMRE labeling. (**d**) FM1-43 labeling (30 min) of neuromuscular junction boutons in third instar larvae of *Drosophila*, in the control situation (Ø, DMSO) and in presence of 10 µM ES9-17. Scale bars, 5 µM (**b**) and 20 µM (**c,d**).

ES9-17 inhibited CME in *Arabidopsis*

Independent of its chemical uncoupling ability, parent molecule ES9 was able to block the synaptic vesicle recycling in *Drosophila* through possibly affecting either CHC, CLC or dynamin functions

(Chapter 3, this thesis). Therefore, we tested if ES9-17 would have the same effect when applied to *Drosophila* neuronal cells. First, active mitochondria were visualized *in vivo* with tetramethylrhodamine ethyl ester (TMRE)[23] to confirm the preservation of mitochondrial function in presence of ES9-17, as seen in *Arabidopsis.* Indeed, labeling of mitochondria was hardly affected in presence of 10 µM ES9-17, and resembled the control situation (**Figure 2c**). Second, when applied on boutons of the neuromuscular junction in third instar larvae, 10 µM ES9-17 failed to induce the formation of large FM1-43 labeled membrane structures (**Figure 2d**) as seen in presence of ES9 (Chapter 3, this thesis). To strengthen the FM1-43-based observation, HA-CHC positive larvae were treated with 10 µM ES9-17 and stimulated with KCl[19]. As expected, no difference could be seen when compared to the control treatment (**Supplemental Figure 1b**). However, at much higher concentrations (100 µM) ES9-17 partially inhibited FM1-43 uptake, and induced occasional FM1-43 labeled inclusions (**Supplemental Figure 1c-d**). However, at 100 µM ES9-17 affected mitochondrial TMRE labeling substantially (**Supplemental Figure 1e-f**). Together these results indicate that the activity in ES9-17 in *Drosophila* required much higher concentrations of compound than in the plant cells.

We next explored how ES9-17 affected endomembrane trafficking in *Arabidopsis* root epidermal cell. Application of ES9-17 (10µM, 30 min) did not visibly affect the cytoskeleton (**Supplemental Figure 2a-b**) or caused aberrant localization of any of the endomembrane markers tested. The vacuolar compartment appeared the same as compared to the mock treatment (**Supplemental Figure 2c**). Electron microscopy strengthens these observations, as no differences were observed for different endomembrane compartments when compared to mock treatment (**Supplemental Figure 2d**). The vacuole lacked the large inclusions as previously seen for ES9 (Chapter 3, this thesis), while multi vesicular bodies, the trans-Golgi network/early endosome (TGN/EE) and Golgi compartments appeared normal, without swelling.

In contrast to the parent molecule ES9 (Chapter 3, this thesis), ES9-17 did not inhibit or affect the formation of Brefeldin A (BFA) bodies. The TGN/EE marker, VhA-a1-GFP[24] accumulated into the BFA bodies in presence of 10 µM ES9-17 and 50 µM BFA (**Figure 3a**), while FM4-64 uptake was inhibited, and as a consequence unable to label the BFA body. To further strengthen this observation with plasma membrane-localized cargo, we treated PIN2-GFP-expressing seedlings for 60 min with mock or 10 µM ES9-17, both in presence of 50 µM cycloheximide (CHX) to inhibit protein synthesis. The subsequent 30 min pulse of FM4-64 and 50 µM BFA indicated that aside FM4-64, PIN2-GFP failed to label BFA bodies, though smaller PIN2 labeled agglomerations were visible (**Figure 3b**). Therefore, we concluded that ES9-17 inhibited endocytosis of PIN2, and its subsequent delivery to the BFA body. The remaining agglomerations were presumably labeled by PIN2 which was present in the cell prior to the endocytic block.

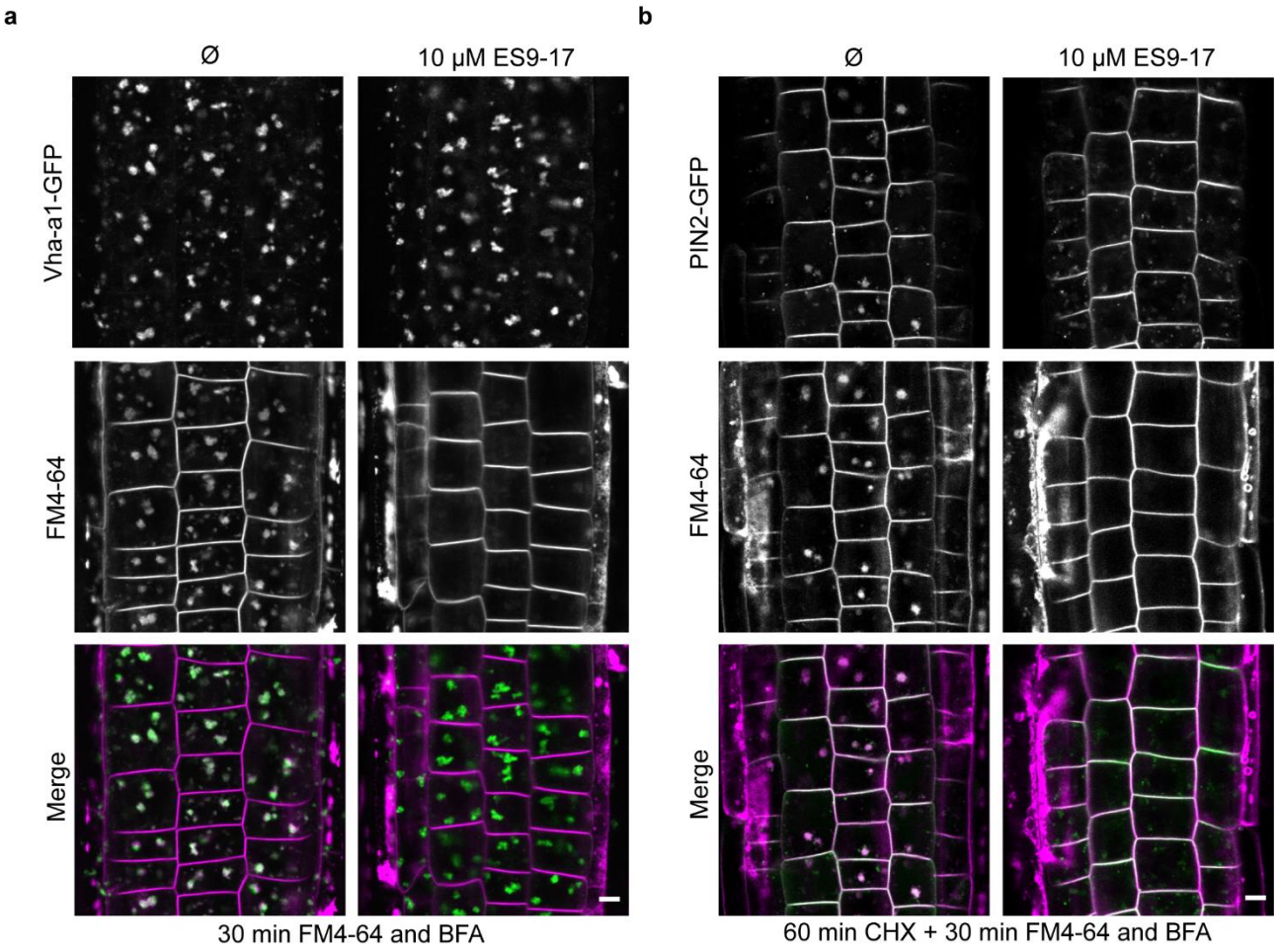

Figure 3. ES9-17 is an inhibitor of CME in *Arabidopsis*.

(**a**) Brefeldin A (BFA) compartments were formed in presence of ES9-17. Seedlings were pre-treated with ES9-17 (10 µM) for 15 min followed by a FM4-64 (2 µM) and 50µM BFA treatment for 30 min. (**b**) ES9-17 inhibited the recruitment of the plasma membrane-localized PIN2 to the BFA body. Samples were pretreated with 50 µM cyclohexemide (CHX) and either mock (Ø, DMSO) or ES9-17 (10 µM), followed by FM4-64 (2µM) and BFA (50 µM) for an additional 30 min. Scale bars, 5 µm.

As the main activity of ES9-17 appeared to be associated with the plasma membrane we sought to characterize the dynamic behavior of known components of CME in *Arabidopsis*. The two adaptor complexes involved in plant CME, TPLATE and AP-2[3] were represented by TML-GFP[25] and AP2S-GFP[26] respectively. In addition, CHC1-GFP and CLC1-GFP were used and represented clathrin (**Figure 4a**). We measured the life-time of foci labeled by the different markers as an indication of correct CME unfolding. In control conditions, all marker lines showed average life-times around 25 seconds, as previously reported for members of the TPLATE complex[25]. We distinguished different populations in presence of 10 µM ES9-17, some with life-times similar to mock (DMSO), others with life-times well over 3 minutes, which resulted in median values between 2-3 times the life-times measured in control conditions (**Figure 4b**). In conclusion, the ES9-17 activity was correlated with

CME inhibition, while the dynamics and the morphology of the endomembrane compartments appeared unaffected by the compound.

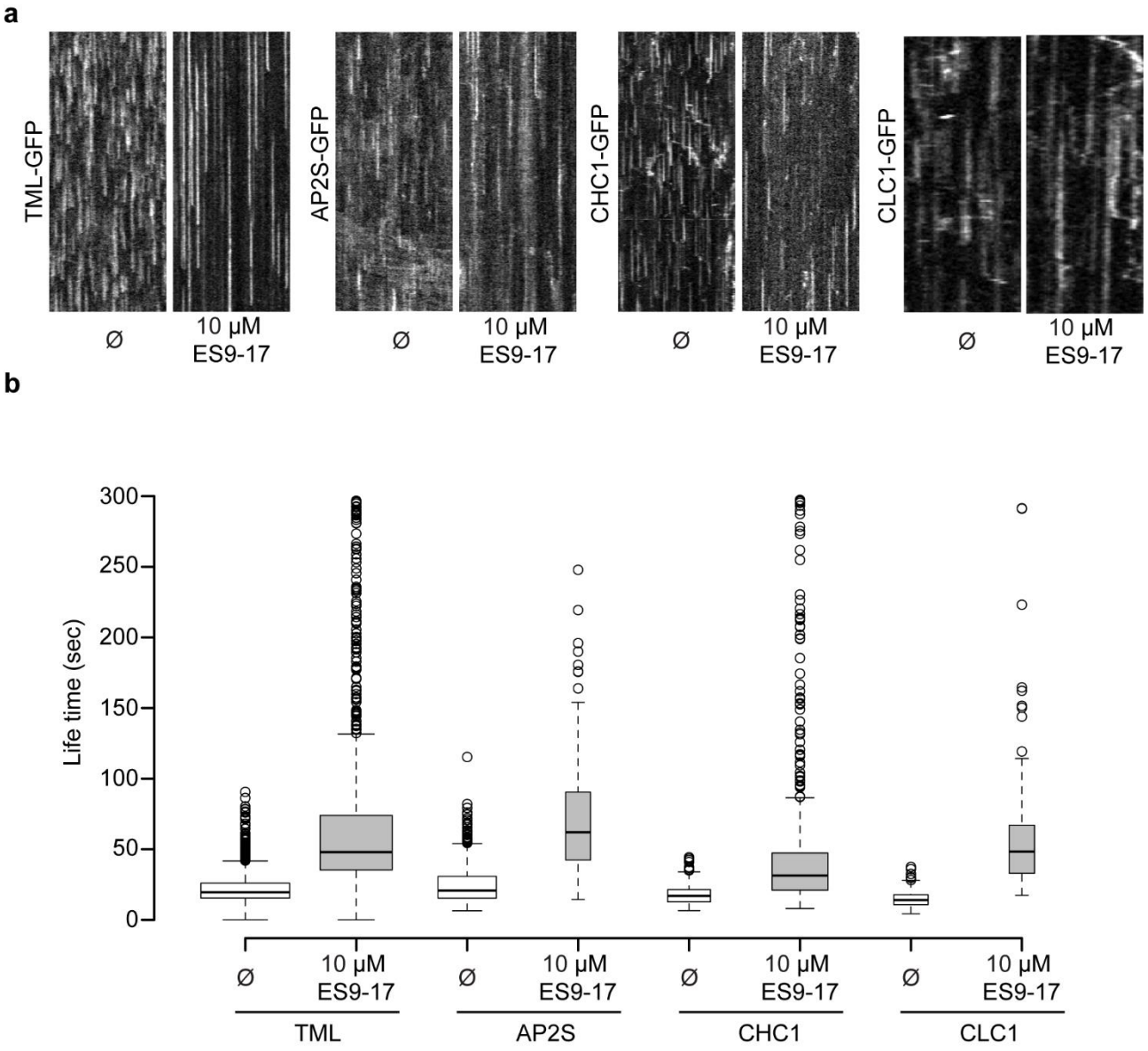

Figure 4. ES9-17 increased the life-time of the endocytic foci in the plasma membrane.

(**a**) Kymographs representing a set of pixels (horizontal axis) over a period of time (vertical axis, 5 min), illustrating life times of endocytic spots labeled by Green fluorescent Protein (GFP) tagged TPLATE Muniscin Like (TML), the Adaptor complex-2 (AP-2), represented by its sigma subunit (AP2S), clathrin heavy chain1 (CHC1) and clathrin light chain1 (CLC1) for the control treatment (Ø, DMSO) and ES9-17 (10 µM) (**b**) Boxplot representation of measured endocytic spot life times. Center lines show the medians; box limits indicate the 25th and 75th percentiles as determined by R software; whiskers extend 1.5 times the interquartile range from the 25th and 75th percentiles, outliers are represented by dots. n = 1646, 1086, 711, 130, 383, 650, 249, 134 sample points.

Brassinosteroid signaling is enhanced in the presence of ES9-17

Inhibition of CME will have a plethora of effects on molecular processes implicated at the plasma membrane, among which receptor-mediated signaling[4]. In previous studies we have shown that the

genetic inhibition of CME enhanced the BRASSINOSTEROID INSENSITIVE1 (BRI1) receptor-mediated signaling from the plasma membrane[27,28]. As a readout for BR signaling activation we used the phosphorylation state of the transcriptional regulator BRI1 EMS-SUPPRESSOR1 (BES1)[29]. In the presence of BRs BES1[30] was dephosphorylated, an indication of active signaling. To evaluate if the pharmacological inhibition of CME by ES9-17 affected BR signaling in a similar way we assessed the phosphorylation status of BES1 in PSB-D wild type cell cultures in the presence of the small molecule (**Figure 5a**). Previously TyrA23 was also used to inhibit CME and to dephosphorylate BES1[27]. However, because our previous findings revealed a protonophore activity for TyrA23 (Chapter 3, this thesis) we also assessed the phosphorylation status of BES1 in the presence of the known protonophore carbonyl cyanide m-chlorophenyl hydrazone (CCCP)[31,32] and the mitochondrial inhibitor Antimycin A (AA)[33]. As expected we observed an almost complete dephosphorylation for the positive control, brassinolide (BL, 0,1µM, 60 min). Treatments with 10 µM ES9, 10 µM CCCP and 50 µM TyrA23 also caused an almost complete dephosphorylation of BES1 (**Figure 5a**). The relative population of dephosphorylated BES1 in mock treatment was about half that of phosphorylated BES1, similar as seen for 50 µM ES9-6 and 50 µM TyrA51, the inactive analog of TyrA23. Both ES9-17 (10 µM) and Antimycin A (AA, 50 µM) induced intermediate levels of BES1 dephosphorylation, approximate 1:1 ratio between the phosphorylated and dephosphorylated forms of BES1. Increasing concentrations of ES9-17 indicated a more pronounced BES1 dephosphorylation (**Figure 5b**). Our results indicated that although the complete shift towards the dephosphorylated form of BES1 might be a consequence of the protonophore characteristics of ES9 and TyrA23, pharmacological inhibition of CME with ES9-17 also enhanced BR signaling, confirming earlier findings[27].

Another straightforward way of assessing active BR signaling is by evaluating BRI1 KINASE INHIBITOR 1 (BKI1) localization at the plasma membrane, as BKI1 dissociates from the plasma membrane into the cytosol upon BR signaling[34,35]. We therefore treated BKI1-mCitrine[35] seedlings with 10µM ES9-17 and compared to mock (DMSO). Treatment of 30 min ES9-17 dissociated BKI1-mCitrine significantly from the plasma membrane (**Figure 5c,d**) compared to mock, strengthening our BES1 observations that inhibition of CME via ES9-17 enhances BR signaling.

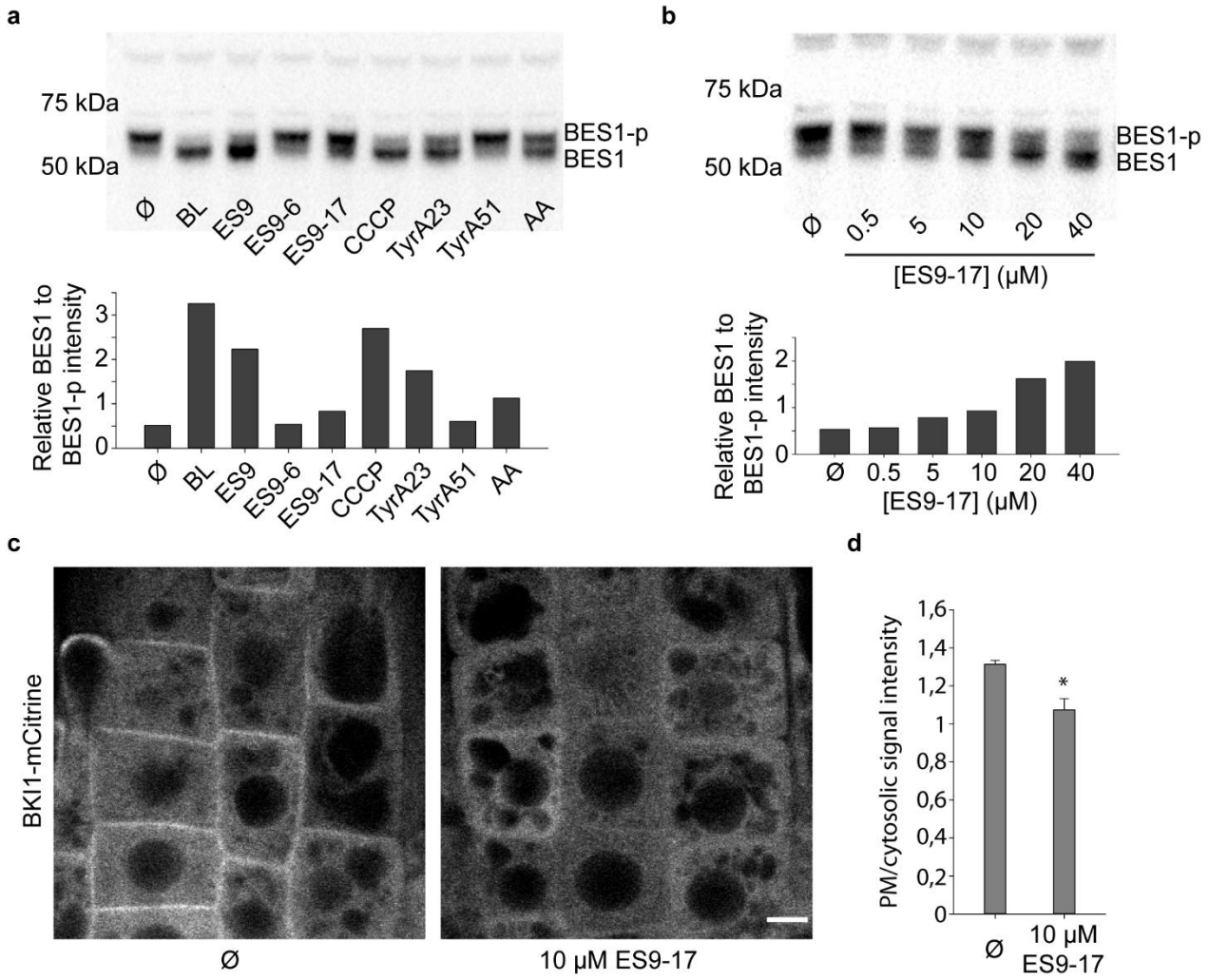

Figure 5. Brassinosteroid signaling was enhanced in the presence of ES9-17.

(a) BES1 phosphorylation was measured in PSB-D cell cultures expressing BES1-TAP, incubated for 1 hour with 0,1 µM brassinolide (BL), 10 µM ES9, 50 µM ES9-6, 10 µM ES9-17, 10 µM CCCP, 50 µM tyrphostinA23 (TyrA23), 50 µM tyrphostinA51 (TyrA51) and 50 µM antimycin A (AA). Quantification of band intensity is shown below. (**b**) BES1 phosphorylation as explained in (a), but with different concentrations of ES9-17. Quantification of band intensity shown below. (**c**) BKI1-mCitrine dissociates from the plasma membrane in presence of 10 µM ES9-17 for 30 minutes compared to the mock (Ø , DMSO) situation. (**d**) Quantitation of plasma membrane localized BKI1-mCitrine as the plasma membrane/cytosol signal intensity ratio. * = p value < 0.01 for a two sided T-Test assuming unequal variances. Scale bar = 5 µm

CHC is a likely target of ES9-17

The SAR analysis of ES9 revealed that the bromine substitution was not essential for its activity, as the ES9-2 analog, which lacked this bromine, was still able to inhibit the uptake of FM4-64. Hence this position could serve as a site for derivatisation of both ES9 and ES9-17 with a linker biotin moiety to facilitate affinity purification of potential target proteins. Substitution of the bromothiophene moiety with a bromobenzene moiety resulted in ES9-8 (**Figure 1a**), which was a better analog to initiate derivatisation compared to ES9-2 due to improved reactivity. We first synthesized the active analog ES9-9, followed by biotin addition, resulting in ES9-10 (**Figure 6a**). Whereas the ES9-9 analog was active in terms of FM4-64 uptake inhibition, ES9-10 was inactive (**Figure 6b**),

presumably because the addition of biotin prevented the uptake of the probe in living cells. A similar strategy was used to generate the ES9-17-linker-biotin construct (ES9-18), including the substitution of the bromothiofene for the bromobenzene moiety. Although ES9-18 was not tested for bioactivity, it was presumed to be impenetrable to cell membranes as it contained a biotin moiety. A linker-biotin probe ES9-13, without small molecule attached, was included as a negative control in the pull-down experiments (**Figure 6a**). Lysate used for affinity purification was prepared from PSB-D wild type cell cultures, and proteins bound to ES9-10, ES9-18 and ES9-13 were analyzed using mass spectrometry. In total three biological repeats were run, each of which was represented by three technical repeats, for the ES9-10 affinity purification and its respective ES9-13 control. Peptides of several hundreds of proteins were identified (**Supplemental Table 1**). Different proteins involved in endomembrane traffic were found, some of which were among the best candidate target proteins (**Table 1**). Several subunits of the coatomer complex were prevalent, while both CHC alleles were present. However, as the coatomer complexes are mostly implicated in ER-Golgi traffic[36], the best candidate target with clear implications in CME was CHC. The ES9-18 affinity purification and ES9-13 control resulted in less purified proteins (**Supplemental Table 2**). Three biological repeats yielded a similar set of proteins implicated in endomembrane traffic, yet the efficiency of purification appeared to be less compared to the ES9-10 purification, as overall quantity seemed reduced, and some proteins were not identified with the ES9-18 analog (**Table 1**).

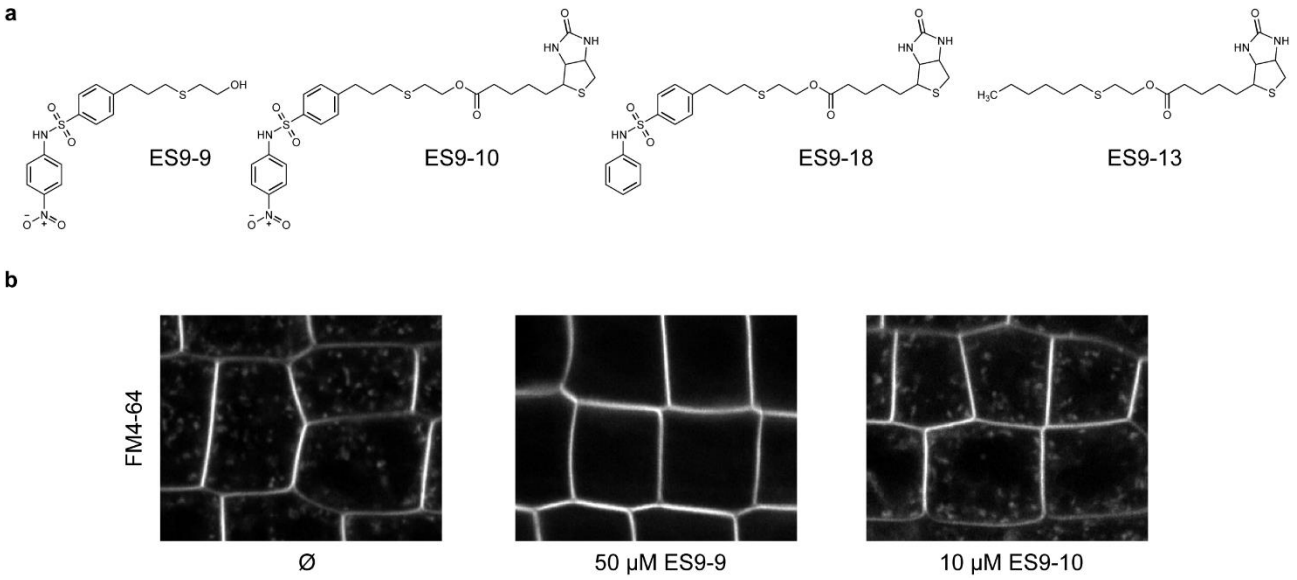

Figure 6. ES9 and ES9-17 linker-biotin derivatisation.

(**a**) Chemical structures for ES9 modified with linker, fictionalized ES9 with linker-biotin, fictionalized ES9-17 with linker-biotin and a linker-biotin control probe. (**b**) FM4-64 uptake for modified ES9 compared to mock (Ø, DMSO) treated seedlings. Co-application of small molecules and FM4-64 (2 µM) for 30 min.

accession	description	ES9-10	ES9-13	ES9-18	ES9-13
AT4G34450	coatomer gamma-2 subunit, putative	5	0	1	0
AT3G11130	Clathrin, heavy chain	4	0	0	1
AT2G21390	Coatomer, alpha subunit	3	0	2	2
AT1G30630	Coatomer epsilon subunit	3	3	3	3
AT1G31730	Adaptin family protein	2	0	0	0
AT1G52360	Coatomer, beta' subunit	2	1	0	2
AT1G62020	Coatomer, alpha subunit	2	1	2	2
AT4G11380	Adaptin family protein	2	2	3	3
AT3G08530	Clathrin, heavy chain	2	3	2	1
AT4G31480	Coatomer, beta subunit	2	0	0	0
AT1G48760	delta-adaptin	1	1	2	2
AT5G22770	alpha-adaptin	1	0	0	0
AT1G23900	gamma-adaptin 1	1	1	0	0

Table 1. Potential target proteins identified through affinity purification with implications in endomembrane traffic

Numbers indicate the times a respective protein was identified out of 9 (ES9-10 and its respective ES9-13 control) or 3 (ES9-18 and its respective ES9-13 control) repeats.

ES9-17 binds to CHC

First, we used Cellular Thermal Shift Assay (CETSA) to validate the binding of ES9 and ES9-17 to the putative target CHC. CETSA is based on the thermal stabilization or destabilization of endogenous target proteins in presence of the small molecule interactor[17], which is quantified after samples are processed by classical western blotting. Alternatively, western blot based quantitation can be circumvented by monitoring thermal denaturation with mass spectrometry[37]. as samples As control proteins we used γCOPI, identified in the affinity purification analysis, the β subunit of ATP synthase (AtpB), and tubulin as negative controls. CHC and γCOPI behaved like potential target proteins in presence of both ES9 and ES9-17, as the thermal denaturation in the presence of the small molecule was shifted to lower temperatures, with the most pronounced effect for CHC (**Supplemental Figure 3a**). Thermal denaturation curves for tubulin and AtpB appeared very similar to the mock treated lysate (**Supplemental Figure 3a**). Isothermal denaturation curves at 40°C

indicated that ES9-17 had the highest affinity to bind CHC with an IC_{50} of approximately 10 µM, whereas ES9 had an IC_{50} of about 100 µM (**Supplemental Figure 3b**). In addition, removal of detergent from the extraction buffer resulted in slightly changed thermal denaturation curves, which is presumably the result of increased overall stability of the protein (**Supplemental Figure 3c**). These results indicate that ES9-17 binds CHC more efficiently compared to ES9. Given the described protonophore characteristics of ES9 (Chapter 3, this thesis) we focused further on ES9-17 in absence of detergent, as the latter appeared to influence the potential binding of ES9-17 to CHC. Interestingly, ES9-17 lost the ability to destabilize γCOPI in absence of detergent, similar to AtpB (**Figure 7a**), while it retained the ability to destabilize CHC (**Figure 7a**).

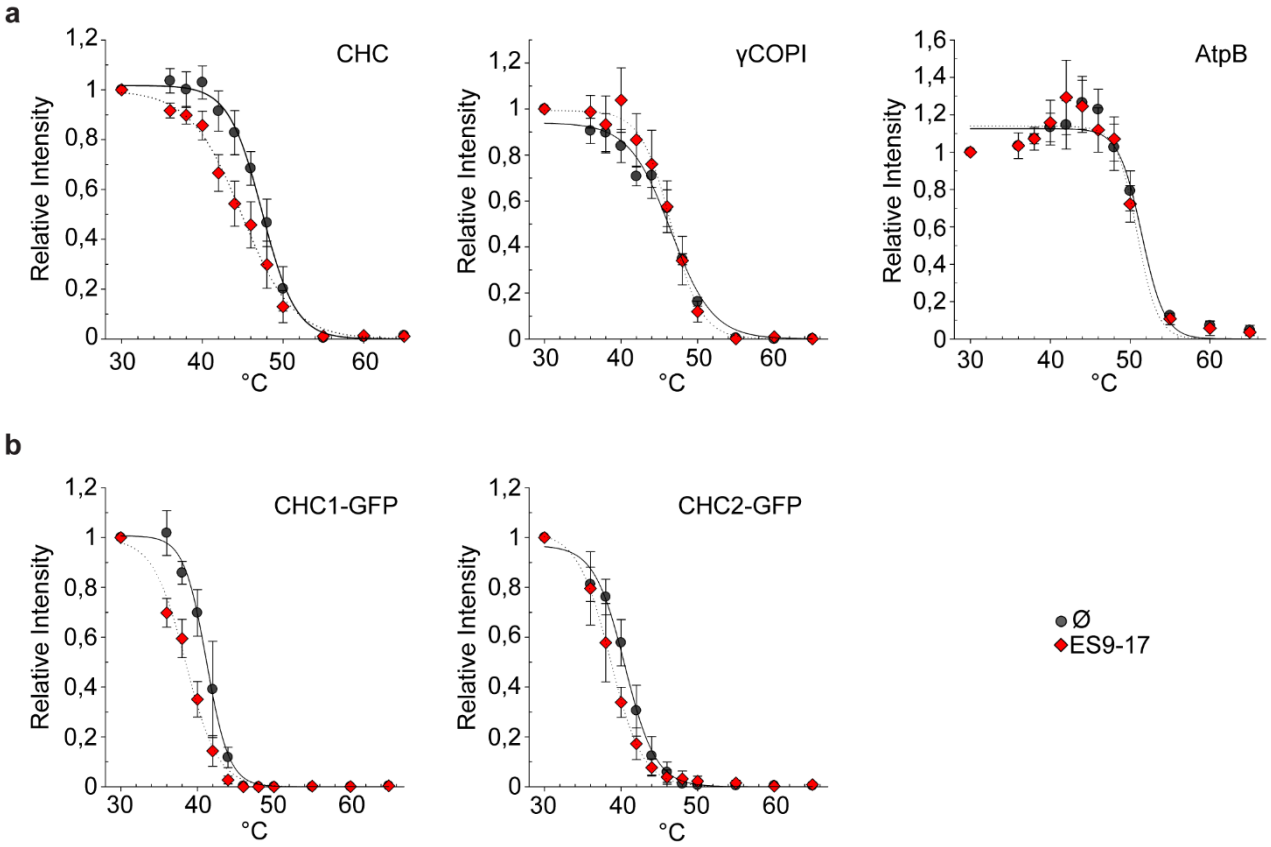

Figure 7. CHC is destabilized by ES9-17 as measured with CETSA.

(**a**) Thermal denaturation for endogenous CHC, AtpB and γCOPI respectively in lysate extracted without detergent and detected with respective antibodies. Average values of CHC from four, AtpB from five, and γCOPI from three biological repeats. (**b**) Thermal denaturation of CHC1-GFP and CHC2-GFP expressed in PSB-D cell cultures, extracted without detergent and detected with anti GFP antibody. Three biological repeats for CHC1-GFP and CHC2-GFP are presented. All compound treatments were done with 100 µM ES9-17. Error bars indicate standard error of the mean.

As the above results did not distinguish the two CHC isoforms in *Arabidopsis*, CHC1 and CHC2 in terms of ES9-17 binding, we re-evaluated the thermal stability for each protein using *Arabidopsis* cell cultures expressing C-terminal GFP-fusions of either CHC1 or CHC2. The difference in thermal

stability in presence of ES9-17 detected with anti-GFP antibody was largely the same for CHC1-GFP compared to detection with endogenous antibody, although thermal denaturation started at slightly lower temperature (compare **Figure 7a** and **Figure 7b**). The shift to lower temperature might be the result from the GFP tag, indicating a decreased overall stability of CHC1. Thermal denaturation of the GFP-tagged CHC2 in presence of ES9-17 was similar to mock-treated lysate (**Figure 7b**). The latter observation could indicate that ES9-17 preferentially binds to CHC1. Interestingly, CHC1-GFP expressed in *Arabidopsis* seedlings was considerable more affected by ES9-17 compared to CHC1-GFP expressed in PSB-D cell cultures (**Supplemental Figure 3d**). Unfortunately, CHC2-GFP expression was too low in *Arabidopsis* seedlings, to quantify in a reliable way.

To strengthen the results obtained with CETSA, DARTS[18] was employed on the same set of proteins. DARTS assesses the potential of a small molecule to protect target proteins from protease digestion, which is subsequently visualized by standard western blot. As such DARTS relies on the same principle as CETSA, yet destabilization is unlikely for DARTS. We expected a stabilization of CHC in presence of ES9-17 upon different dilutions of protease mix (Pronase), as small molecule interactors protect their protein targets from digestion. We observed an overall stabilization of CHC in presence of ES9-17 for different dilutions of Pronase, visible as fewer degradation products compared to the corresponding mock treated sample, a pattern which was even apparent in the undigested control (**Figure 8a**). Stabilization of full-length CHC became visible in the sample with a 1/2500 dilution of Pronase (**Figure 8a, arrowhead**), which represented a more than 2-fold stabilization compared to the corresponding control sample upon quantification of the full-length CHC band (**Figure 8b**). Stabilization and overall degradation of CHC appeared to be unaffected by detergent, as similar results were obtained for samples with and without NP-40 (**Figure 8a**). Quantification of full-length protein bands for other proteins, namely γCOPI and tubulin in samples without detergent, showed no such stabilization (**Figure 8b**). As CETSA revealed a differential effect of ES9-17 on CHC1 and CHC2, both GFP-tagged proteins were evaluated with DARTS in PSB-D cell cultures. A first observation was the overall higher sensitivity to Pronase of CHC1-GFP and CHC2-GFP from Pronase, as higher dilutions had to be used to detect both proteins (**Figure 8c**). A second observation was the consistent overall protection of CHC1-GFP from Pronase in presence of ES9-17, on average a 2-fold stabilization compared to the mock control, while CHC2-GFP displayed very little stabilization except for the 1/10000 Pronase dilution, which, similar to CHC1-GFP had an approximate 2-fold stabilization (**Figure 8d**). Quantification of AtpB in the CHC1-GFP and CHC2-GFP samples indicated that all ES9-17 treated samples contained similar amounts of AtpB compared to mock treatment (**Figure 8d**), suggesting AtpB was unaffected by ES9-17, which is in agreement with the CETSA data.

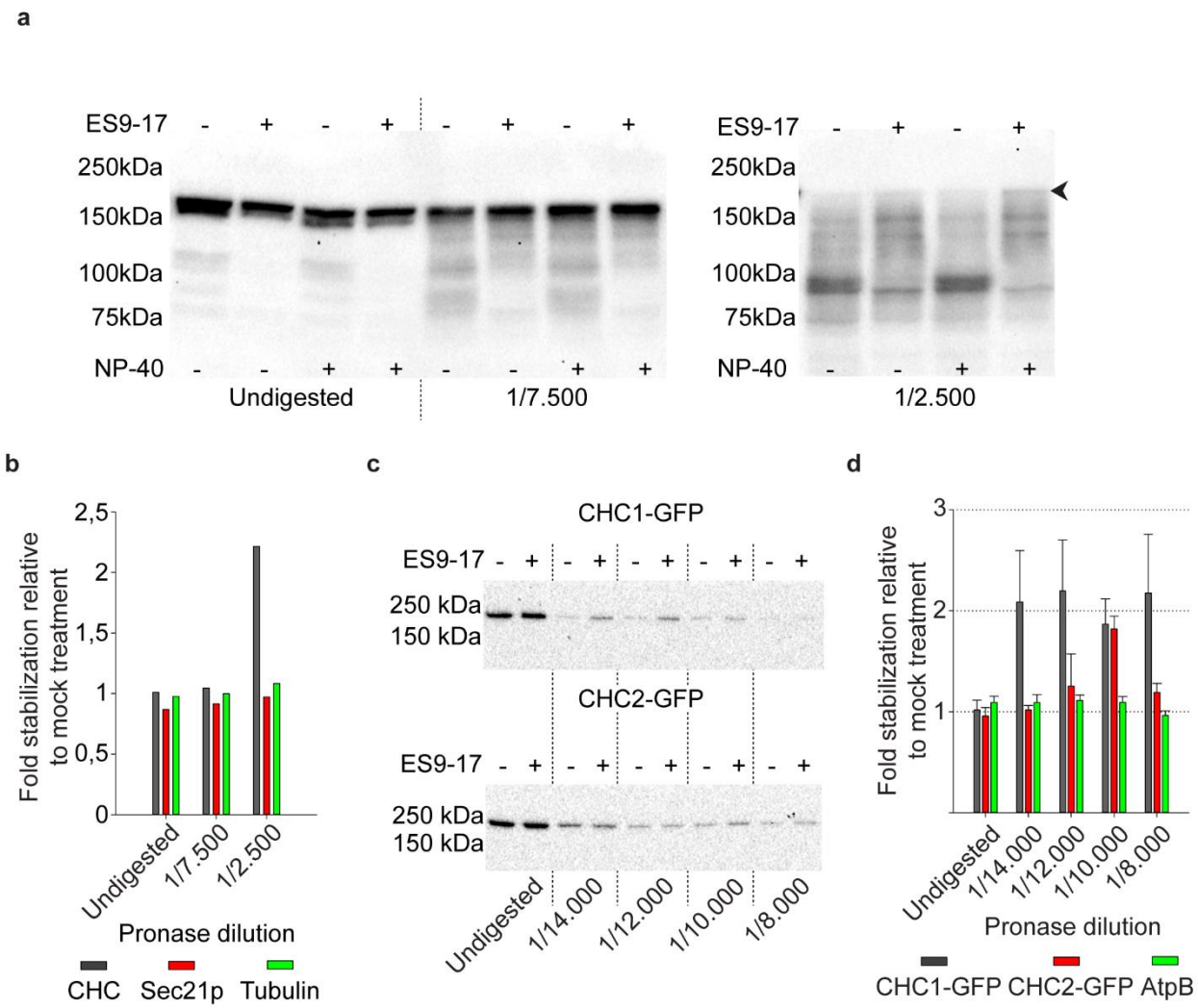

Figure 8. ES9-17 stabilized CHC upon protease digestion.

(**a**) Western blot for CHC detected with endogenous anti CHC antibody in presence or absence of ES9-17 and in presence or absence of detergent (NP-40) Samples were treated with different dilutions of Pronase, with an undigested sample as control. Note the full-length CHC band for the 1/2500 dilution (arrowhead). (**b**) Quantification of signal derived from full-length protein for CHC from the Western blot in (**a**), and γCOPI (anti Sec21p antibody) and tubulin on the same blot. (**c**) Representative blot for CHC1-GFP and CHC2-GFP in presence of mock (Ø) and ES9-17 for undigested samples and samples treated with different dilutions of Pronase. (**d**) Quantification of western blots as shown in (**c**). Four biological repeats are presented for each experiment.. Error bars indicate standard error of the mean

chc1 and *chc2* mutants are more sensitive to ES9-17

To further validate the interaction of ES9-17 with CHC we assessed root growth and FM4-64 uptake for several mutants of CHC1 and CHC2[38] in presence of ES9-17. Primary root growth for *Arabidopsis thaliana* Col-0 seedlings (5 days old) was inhibited at concentrations higher than 10 µM, with an EC_{50} of approximately 6 µM (**Supplemental Figure 4a**). Seedlings of *chc1-1*, and *chc2-2* mutant lines displayed a significant increased sensitivity at the EC_{50} compared to Col-0 seedlings (**Figure. 9a**), while *chc2-1* was more resistant. The increased sensitivity is ES9-17 specific, as all three mutants

were slightly, but significantly more resistant compared to Col-0 when grown on 0.5 µM cyanide m-chlorophenyl hydrazone (CCCP) (**Figure 9b**). To assess if the sensitivity on ES9-17 was translated to CME inhibition, we measured FM4-64 uptake in *chc1-1*, *chc2-1* and *chc2-2* seedlings at 6 µM ES9-17, and compared to wild type seedlings (**Supplemental Figure 4b,c**). FM4-64 uptake as represented by the ratio of the PM/cytosol FM4-64 signal intensity was less in the *chc1-1* background compared to Col-0 in presence of ES9-17, while in *chc2-2* there was a greater reduction in uptake (**Supplemental Figure 9b,c**). Little difference could be detected in the *chc2-1* background compared to the wild type. In addition, treatment with ES9-17 induced an agravitropic response in all backgrounds, though was more pronounced in the *chc1-1*, *chc2-1* and *chc2-2* mutants (**Figure 9c**). This observation is consistent with the agravitropic response of *chc* linked to defective auxin redistribution and transport[38]. Together with the CETSA and DARTS findings we concluded that ES9-17 binds both CHCs in *Arabidopsis*, however binding to CHC1 was more efficient.

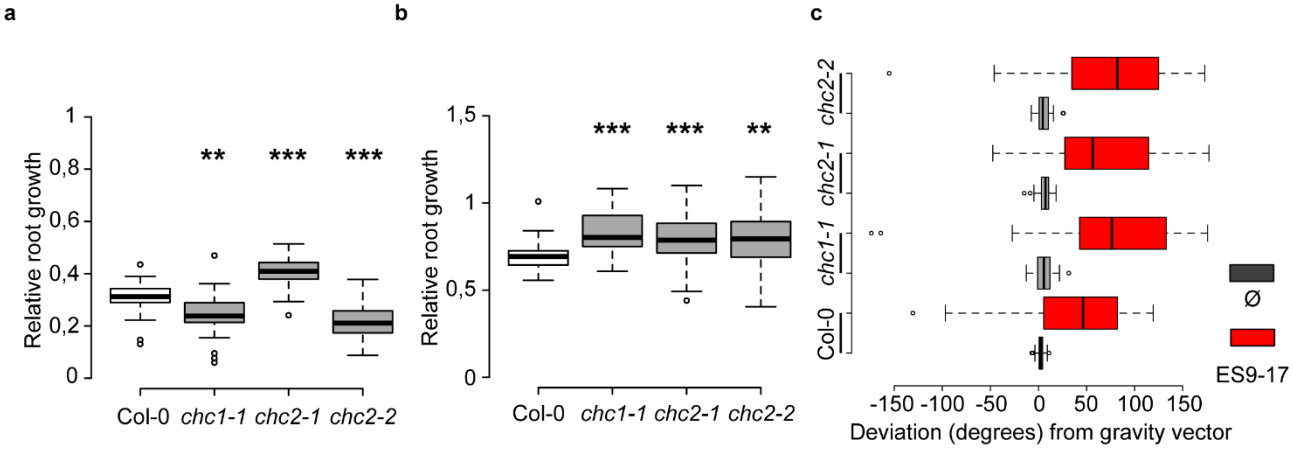

Figure 9 *Arabidopsis chc* mutants were more sensitive to ES9-17.

(**a**) Boxplot representation of relative root growth over 48 hours on 6 µM ES9-17. (**b**) Boxplot representation of relative root growth over 48 hours on 0.5 µM carbonyl cyanide m-chlorophenyl hydrazone (CCCP). (**c**) Box plot representation of agravitropic response as seen for seedling grown on 6 µM ES9-17 and mock. Box plots: Center lines show the medians; box limits indicate the 25th and 75th percentiles as determined by R software; whiskers extend 1.5 times the interquartile range from the 25th and 75th percentiles, outliers are represented by dots. n = 40 sample points. **P<0.01 ***P<0.001 for a Kruskal-Wallis One Way ANOVA on Ranks

ES9-17 possibly binds the N-terminal domain of CHC

The observation that ES9-17 might preferentially bind CHC1, as indicated by our CETSA and DARTS results, provided the opportunity to map the possible binding site of ES9-17 in CHC1 protein. Alignment of the *Arabidopsis* CHC1 and CHC2 amino acid sequences showed little difference in amino acid contents, with only a few amino acid substitutions resulting in a change of amino acid properties (**Supplemental Figure 5**). This, in principle, would allow to swap certain domains of the CHC1 sequence containing possible binding sites and enough differential amino acid contents with the same domains of CHC2. Assessment of ES9-17 binding through CETSA and DARTS of these CHC1 chimeras would allow to assess which domain swap is responsible for the loss of CHC1

sensitivity towards ES9-17, and therefore the identification of the binding site of ES9-17 through docking on that particular CHC1 domain.

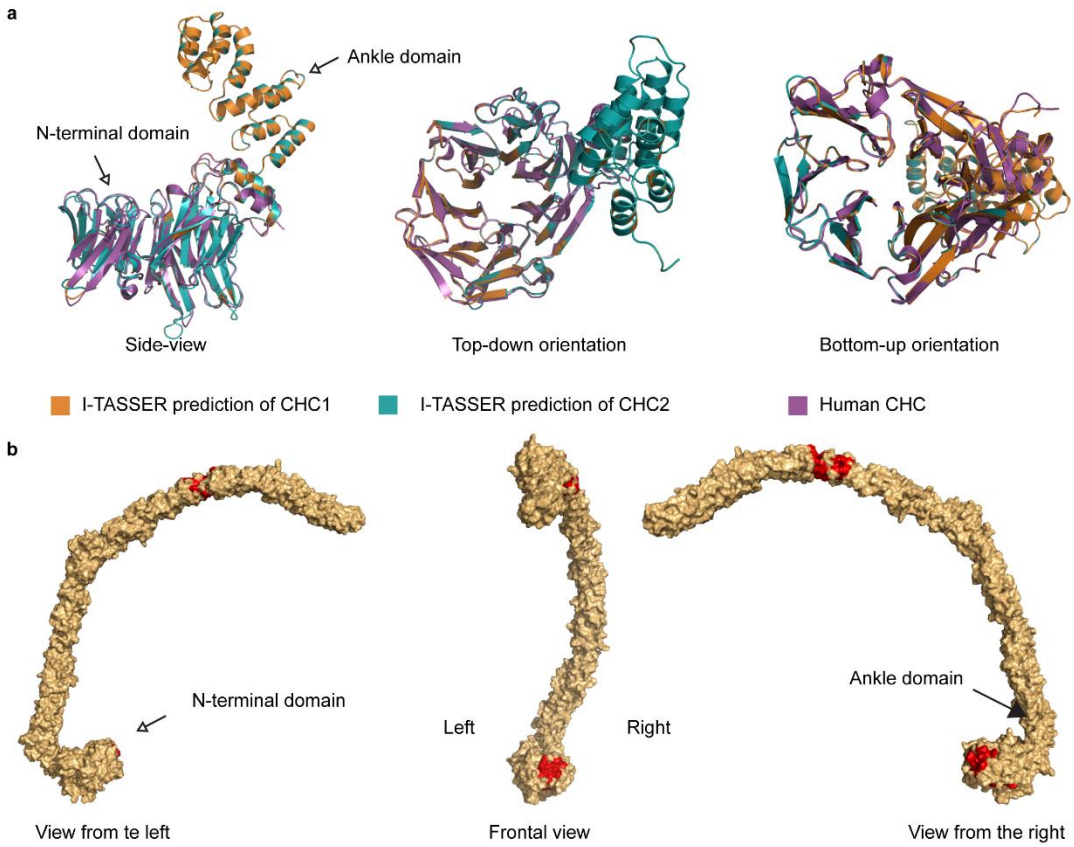

Figure 10. *Arabidopsis* CHC putatively folds as human CHC.

(a) Overlay of I-TASSER[39] predictions for CHC1 and CHC1 with the N-terminal domain of human CHC in complex with Pitstop2 (PDB accession 4G55)[5]. Different views on the overlay are shown. (**b**) I-TASSER prediction of CHC1, showing the N-terminal domain, ankle region and large part of the leg region in different orientations. Red colored areas indicate predicted binding sites. All renders are made with the PyMol application[40]. Pitstop2 is not visualized.

Plant CHC has not been crystallized yet, therefore we relied on the I-TASSER[39] predictions for CHC1 and CHC2. The prediction which resembled best the known overall structure of human CHC was selected for both CHC1 and CHC2. Subsequently we overlaid the predictions with the crystal structure of the N-terminal domain of CHC in complex with Pitstop2 (PDB ID: 4G55)[5]. This resulted in a considerable overlap between all 3 structures, indicating conservation between the human and *Arabidopsis* CHC structure (**Figure 10a**). Submission of CHC sequences to protein BLAST (http://blast.ncbi.nlm.nih.gov/Blast.cgi#alnHdr_4758012) and alignment (**Supplemental Figure 5**) indicated a high sequence similarity between CHC1 and CHC2 in *Arabidopsis* (98%), while comparison with human CHC indicated only about 55% sequence similarity (**Supplemental Figure 6**). Therefore any predictions based on dockings are only indications, which will have to be validated experimentally. Prediction of possible ligand binding sites by I-TASSER, based on known

interactions with CHC in other systems (**Supplemental Figure 5**), resulted in 3 possible regions for ligand binding on CHC in *Arabidopsis*, of which 2 were located in the N-terminal domain, and one in the leg region of CHC (**Figure 10b, Supplemental Figure 5**). Based on these predictions we initiated blind and local docking of ES9-17 and ES9 on the N-terminal domain of human CHC (4G55)[5]. Specifics about the docking procedures are provided in material and methods. Two sites were identified as potential binding pockets of ES9-17 and ES9. The first, which was identified by blind docking, was located in the center of the N-terminal β-barrel (**Figure 11a**). However the bromine of ES9-17 and ES9, which was used as a site for derivatisation, appeared to be orientated towards the blades of the β-barrel, while both small molecules appeared to be buried in the center of the β-barrel (**Figure 11a, arrow**). Based on the prediction it seems unlikely that this particular orientation would allow derivatisation with a linker-biotin moiety for successful affinity purification. The second putative binding pocket is that of Pitstop2[5] (**Figure 11b**). It concerns a local docking, based on the published binding characteristics of Pitstop2[5]. Here the orientation of the bromine is outwards, which would perfectly allow derivatisation with a linker-biotin moiety. However, ES9 adopted a slightly different orientation compared to ES9-17. Currently efforts are ongoing to experimentally determine the possible binding site by swapping domains of CHC1 with the same domain of CHC2. We took into consideration the N-terminal region, the putative binding site in the leg region, and the C-terminal part, which is expected to be a control. If we identify a possible binding region of ES9-17 and ES9, more detailed docking might provide insights into the nature of binding to CHC.

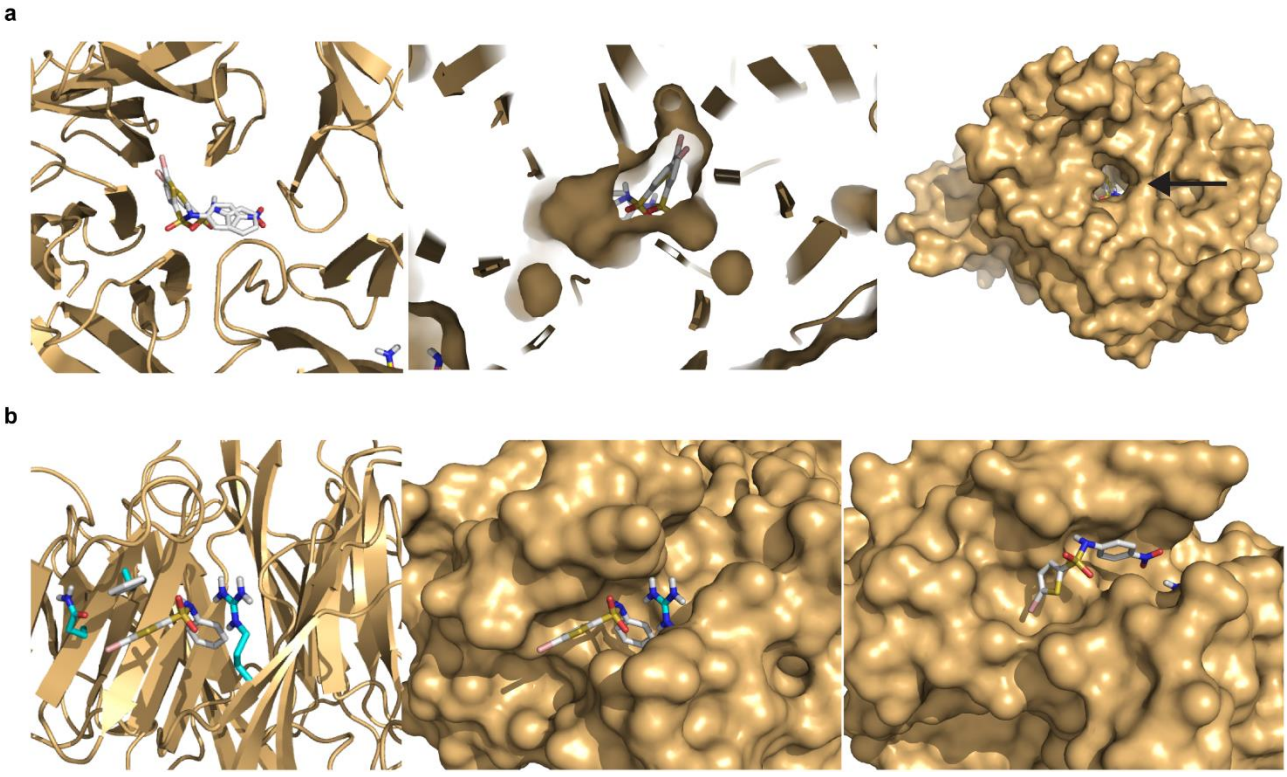

Figure 11 ES9-17 likely binds the Pitstop2 bindings pocket

(a) Blind docking of ES9 and ES9-17 on human CHC in complex with Pitstop2 (PDB accession 45GG)[5]. Both small molecules dock in the central cavity of the β-barrel, but are quite buried. (**b**) Local docking of ES9-17 (central image) and ES9 (right image) or both (left image) on human CHC in complex with Pitstop2 (PDB accession 4G55)[5] in the bindings pocket of Pitstop2. Pitstop2 is not shown.

Discussion

Here, we presented the identification and characterization of a specific small molecule inhibitor of CME in *Arabidopsis*, named ES9-17, which mediated inhibition through binding of clathrin. ES9-17, unlike its parent molecule ES9 (Chapter 3, this thesis), had no effect on ATP depletion and mitochondrial function in *Arabidopsis* at concentrations for which it inhibited FM4-64 uptake. As such ES9-17 lacked the potency to affect general metabolism, a complication which is now generally recognized as a possible side-effect for lead molecules in drug discovery, and a phenotype which is increasingly screened for in small molecule libraries[41-44]. Further characterization highlighted the possible species specificity of ES9-17, as it was much less active in *Drosophila* compared to ES9 (Chapter 3, this thesis), although we cannot exclude that ES9-17 might have been less accessible to *Drosophila* cells. This was corroborated as we observed residual activity related to FM1-43 uptake for much higher concentrations, yet these conditions affected mitochondrial functions.

In *Arabidopsis* the ES9-17 effect appeared to be mainly related to CME as it did not affect the motility and morphology of TGN/EE or Golgi. In addition, both the actin and microtubule cytoskeleton appeared normal, indicating that CME inhibition is likely not due to acute loss of cytoskeleton functionality, as has been reported in yeast, though is of lesser importance for CME in mammalian systems[45]. Moreover, ES9-17 allowed the formation of the BFA body, yet inhibited the accumulation of plasma membrane-derived content into the BFA body. This is unlike its parental molecule ES9 or TyrA23 and CCCP, where the TGN/EE marker Vha-a1-GFP failed to accumulate into BFA bodies, indicating that BFA body formation was prevented because of impaired motility of TGN/EE and Golgi compartments (Chapter 3, this thesis). The formation of the BFA body as visualized by the Vha-a1-GFP[24] marker in presence of ES9-17 therefore indicated that vesicle and compartment dynamics were not affected. This opens as such new opportunities to evaluate the influence of pharmacological CME interference on other endomembrane compartments, and the implications for CME cargo.

The previously reported general freeze in CME components dynamics in the plasma membrane caused by ES9, Tyr23 and CCCP, (Chapter 3, this thesis), was not observed for ES9-17 application. Several CME markers showed an overall increase (2-3 fold) in the life-time in the plasma membrane as compared with the control. This observation is in agreement with life-times measured for endocytic

machinery in presence of Pitstop2[5] where the increase in life-time might reflect non-functional and eventually abortive clathrin coated pits, as the life-time of a molecular component at the plasma membrane depends on the presence and nature of interactors. The least difference was observed between the control and ES9-17 treated CHC1-GFP labeled samples. Here, a possible explanation might be the apparent reduced stability of CHC1-GFP in presence of ES9-17, as measured with CETSA, which might reflect on the overall stability of the clathrin cage *in vivo*. It would therefore be of interest to purify CHC interactors in presence of ES9-17, and compare with control samples, in order to assess if ES9-17 would interfere with any CHC interactor required for proper unfolding of CME.

The purification of ES9 and ES9-17 interactors by affinity purification with different biotinylated ES9 derivatives revealed a remarkable difference between ES9 and ES9-17. As ES9-17 lacked the nitro-group compared with ES9, it became more hydrophobic in nature, which had possibly implications for affinity purification. As ES9-17 became more hydrophobic, interaction with beads might be an explanation as to why it failed to purify CHC. This particular problem is not encountered by ES9, as the nitro-group, which is more hydrophilic, possibly directs the probe away from the beads, thereby facilitating effective purification. The same difference between ES9 and ES9-17 might have implications for CHC binding, as a recent report indicates that even close analogs might bind the same bindings pocket in completely different orientations[46].

For the validation of the putative targets we employed two relatively new, but promising approaches, CETSA[17] and DARTS[18], previously not used in plant systems. Both have been used in numerous studies, reconfirming known small molecule interactions as well as establishing new ones. DARTS has been used in studies including target identification of disulfiram[47], the identification of the ATP synthase β subunit as target of α-ketoglutarate in *C. elegans*[48], and has even been used to identify target proteins of grape seed extract[49]. DARTS is used to identify small molecules which stabilize their protein target by protection from protease digestion. CETSA, on the other hand, can work in both ways, as it can reveal compound binding by stabilization or destabilization of its target protein[37]. Destabilization might indicate binding of protein interfaces, thereby destabilizing protein complexes, which as a consequence disassemble quicker at higher temperatures opposed to control conditions. This type of interactions could be missed by DARTS, as the nature of small molecule binding not necessarily offers enough protection from proteases. CETSA is a relative new approach, yet has already been used in a proteome profiling for interactors of the kinase inhibitor staurosporine, identifying over 50 potential targets[37]. CHC was analyzed as a potential target protein for ES9 and ES9-17, along with control proteins such as γCOPI, AtpB and Tubulin. CETSA revealed a destabilization of CHC and γCOPI in presence of ES9-17 and ES9. Removal of detergent from the extraction buffer, indicated that ES9-17 binds CHC, as is was the only potential target which remained responsive to ES9-17 treatment. Interestingly, the ES9 induced destabilization of γCOPI corresponds

with the ER-Golgi hybrid compartment observed upon ES9 treatment in *Arabidopsis* (Chapter 3, this thesis). Similarly, the absence of a hybrid ER-Golgi compartment upon ES9-17 corresponds with the inability of ES9-17 to destabilize γCOPI.

An even higher degree of ES9-17 specificity towards CHC was revealed when CHC1-GFP and CHC2-GFP were analyzed with CETSA and DARTS. Mainly CHC1-GFP remained responsive to ES9-17, indicating a preferential binding of ES9-17 to CHC1. However, these findings as such are insufficient to conclude that CHC2 is not a target of ES9-17. Indeed, analysis of previously reported mutant lines of CHC[38] indicated that *chc1* and *chc2* mutant lines were sensitive in terms of root growth, whith *chc2-2* the most sensitive. In case ES9-17 would only bind CHC1, one could expect *chc1* mutants to be resistant to ES9-17, while *chc2* mutants would be more sensitive as only CHC1 is functionally available. Though *chc1-1* was not resistant, the sensitivity on ES9-17 was less pronounced compared to Col-0 and *chc2-2*. As such it fits with the hypothesis that ES9-17 binds preferably CHC1. In addition, the sensitivity appears to be ES9-17 specific, as root growth of *chc* mutants on CCCP was less affected compared to Col-0. A further extension to other, unrelated small molecules will strengthen the specificity of ES9-17 towards CHC. Notably the effect on root growth compared to Col-0 is not very strong, which might indicate that ES9-17 mediates root growth inhibition through additional target proteins, and as such could be expected, since predictions indicate small molecules have on average 6 targets[50,51]. As we could not observe major endomembrane disruptions apart from CME, additional protein targets are likely not linked to endomembrane traffic. FM4-64 uptake quantification in mutant lines resulted in a similar pattern in terms of sensitivity, though the apparent resistance of *chc1-1* was more pronounced, confirming our hypothesis of the preferential binding of ES9-17 to CHC1. The *chc2-1* line was found to behave different as expected for all readouts, which might be due to the intronic nature of the insertion[38]. An additional effect of endocytic inhibition by ES9-17 was revealed by the agravitropic response of seedlings grown on ES9-17 without stimulating gravitropic responses. Since presumably proteins implicated in sensing gravity, such as PINs[52], are not taken up and redistributed properly, the plant loses the ability to correctly sense and response to the gravity vector[52]. Again the lack of difference between mutant lines in terms of gravitropic response indicate that both CHC1 and CHC2 are affected by ES9-17 binding. It is the efficiency if binding, and thus the efficiency of endocytic inhibition, which appeared to be different, as shown by FM4-64 uptake and the biochemical validation.

The mechanism by which ES9-17 inhibits CHC function is still very much speculative, however, based on I-TASSER[39] predictions and preliminary docking exercises few possible scenarios can be distinguished. A first possibility is the binding of ES9-17 to the N-terminal domain of CHC, which is involved in recruitment and binding of several accessory proteins required for proper unfolding of CME[1,5]. As such ES9-17 could possibly interfere with proper recruitment, and as a consequence stall

further formation and maturation of the clathrin coated pit. Eventually uncoating mechanisms, which are mostly situated at the C-terminus[1], would disassemble the premature coat. This could be reflected in overall increased life-times of CHC at the PM, a phenotype which is indeed observed upon ES9-17 application. However, none of the differential amino acids between CHC1 and CHC2 correspond to amino acids predicted to be involved in binding pockets (**Supplemental Figure 5**). A second possibility is the binding of ES9-17 in the region which possibly binds CLC. The implications for CLC binding could be two-fold. On the one hand ES9-17 might prevent CLC binding, yet this is not in favor of the cell biological evidence, as CLCs still localize to the PM. On the other hand CLC might still bind, yet is obstructed by ES9-17 in exerting its function, which might result in abortive coated pit formation. The site of CLC binding likely corresponds to the predicted bindings site in the leg region, and contains two differential amino acids between CHC1 and CHC2 (T in CHC1, A in CHC2 on position 1148, and Q in CHC1, H in CHC2 at position 1150) which might account for the difference in binding efficiency of ES9-17 to CHC1 and CHC2. Interestingly, when aligned to human CHC, these two amino acids are not preserved (**Supplemental Figure 6**). In contrast, most of the amino acids predicted to be involved in a binding pocket at the N-terminal domain are conserved. It remains to be seen if ES9-17 is active in human systems in terms of CME inhibition to be able to pinpoint possible binding sites based on activity and conservation of residues between *Arabidopsis* and human systems. Since no structural data of CHC in plants is available, all this remains very much speculation.

In conclusion we present a small molecule inhibitor of CHC, ES9-17, with strong inhibitory effect on CME. As ES9-17 is more specific than any known small molecule effector of CME in *Arabidopsis*, it opens new possibilities to assess CHC function in endomembrane traffic and the implications for developmental, growth and defense responses. Aside a thorough analysis of CHC1 and CHC2 function in CME, ES9-17 might also facilitate a further characterization of CHC function along other endomembrane trafficking routes[53], something which is less explored in plants compared to their role in CME. In addition, it would be highly interesting to see if ES9-17 would have any effect on the recently reported clathrin independent endocytosis in *Arabidopsis*[54]. As such it would be the onset of a thorough analysis of possible non-specific effects of ES9-17 on endomembrane traffic, which is part of the further development of ES9-17 in a highly specific inhibitor of CHC function. Finally, in depth characterization of protein structural requirements for ES9-17 binding, together with mapping of the ES9-17 binding pocket on the CHC protein structure together with crystallization of CHC in presence of ES9-17 would facilitate an in-depth understanding of the molecular events unfolding upon formation of the clathrin cage in *Arabidopsis.*

Acknowledgements

We thank Dr. Steffen Vanneste for useful discussion and material. Ikuko Hara-Nishimura for sending AP2M-GFP, and Jinxing Lin for sending AP2S-GFP. Dr. Yvon Jaillais for sending BKI1-mCitrine and Dr. Daniel Martinez Molina for usefull suggestions on the CETSA protocol and feedback. Also all colleagues who helped with any practical aspects of this work.

Material and methods

Plant material and growth conditions

Arabidopsis thaliana (accession Columbia-0 [Col-0]) seedlings and other lines were stratified for 2 days at 4°C, and grown vertically on agar plates containing ½ strength Murashige and Skoog (½MS) medium supplemented with 1% (w/v) sucrose for 5 days at 22°C in a light/dark cycle of 16 h/ 8 h respectively, prior to use. *Arabidopsis* seedlings were used as control or for labeling of mitochondria and acidic compartments. Following marker lines were used: TML-GFP[25], CLC1-GFP, CHC1-GFP, AP2S-GFP[26], Vha-a1-mRFP[24], SYP22-YFP[55], MAP4-GFP[56], PIN2-GFP, BKI1-mCitrine[35] and Fimbrin-GFP.

Generation of GFP-tagged CHC2 and PSB-D cell culture transformation.

Entry clone generated before[59] was used together with pDONRRP4-1R_RPS5A, pDONRRP2R-P3_GFPstop and pK7m34GW in multisite Gateway reactions (Life technologies) to yield C-terminal tagged CHC2. Both CHC1-GFP (Chapter 3, this thesis) and CHC2-GFP expression vectors were used to transform *Agrobacterium tumefaciens* C58. Subsequent transformation of PSB-D wild type cell cultures was performed as previously described[60].

Chemical treatments, chemical labeling and imaging in *Arabidopsis*

ES9 and analogs were acquired through Chembridge (http://www.chembridge.com/) or synthesized as described below. .Brefeldin A and cycloheximide were acquired through Sigma-Aldrich. All were dissolved in DMSO (Sigma-Aldrich). Visualization of endocytosis was achieved with 2μM N-(3-Triethylammoniumpropyl)-4-(6-(4-(Diethylamino) Phenyl) Hexatrienyl) Pyridinium Dibromide (FM4-64, Life technologies) application. For staining of mitochondria, seedlings were first treated for 30 min in ¼ MS (a 1:1 dilution of ½ MS with water) with the respective small molecules. Subsequently, seedlings are transferred to liquid ¼ MS with 250 nM MitoTracker Red CM-H2XRos (Molecular Probes®, Life Technologies) and the respective small molecules for an additional 30 min. Similarly, acidic compartments were labeled with Lyso Tracker Red DND 99 (Molecular Probes®,

Life Technologies) by treating seedlings with 250 nM Lyso Tracker Red DND 99 in liquid ¼ MS for 30 min. Small molecule treatment was started by adding small molecule at respective concentrations to seedlings in the Lyso Tracker Red DND 99 containing solution for another 30 min. Imaging of seedlings was performed with an Olympus FV10 ASW confocal laser scanning microscope using a 60x water immersion lens (NA 1.2) and 3x digital zoom. Endocytic foci Life-time measurements were determined using a Perkin Elmer Ultra View Vox Spinning disc confocal imaging system running on the Volocity software package mounted on aNikon Eclipse Ti inverted microscope using a Plan Apo Lambda 100x oil (NA 1.45) corrected lens and third generation perfect focus system (PFSIII) for Z-drift compensation. Time series were acquired at 2 time points per second intervals, for 5 minutes. Excitation was done using a solid state 488nm DPSS laser (50mW) and images were acquired using a Hamamatsu ImagEM C9100-13 512x512 BI (16umx16um pixel size) EmCCD camera. Images were processed using the ImageJ (Fiji) software packages.

For quantification of the plasma membrane/cytosol signal intensity ratio, images were converted in ImageJ to 8-bit, and regions of interest (ROIs) were selected based on the plasma membrane or cytosol localization. Histograms listing all intensity values per ROI were generated, and the averages of the 100 most intense pixels were used for calculations.

ATP measurements

Wild type PSB-D Arabidopsis cell cultures were used and maintained as described before[60]. Cell culture of 3 days old was diluted 100 times and mixed thoroughly prior to distribution of 95 µl in 96-well plates. Subsequently, 5 µl of a 1/50 dilution of small molecule stock solution (1000x) in MS medium with Minimal Organics (MSMO) medium was added to cells (final dilution of 1000x) using a Tecan Freedom EVO® robot. ATP levels were detected by addition of 80 µl of ATPlite 1step Luminescence Assay System (Perkin Elmer) after incubation of cells in presence of small molecule for indicated time. Fluorescence was detected using a Perkin Elmer EnVision 2104 multilabel reader with the Wallac Envision manager software package. ATP-lite luminescence was detected with the ultra-sensitive luminescence techonology. Fluorescein diacetate (FDA) stock solution (2% FDA in acetone [w/v], Sigma) was diluted 100x in target medium and 5 µl was added to 95 µl cell culture. Fluorescence was detected with an excitation at 485nm (bandwidth 14nm), and emission at 535nm (bandwidth 25nm).

BES1 dephosphorylation assay

PSB-D wild type cell cultures were used and maintained as described before[60]. Cell cultures three days after sub-culturing were treated with 0,1 µM brassinolide (BL), 10 µM ES9, 50 µM ES9-6, 10 µM ES9-17 (or other as indicated), 10 µM CCCP, 50 µM tyrphostinA23 (TyrA23), 50 µM tyrphostinA51 (TyrA51) and 50 µM antimycin A (AA) for 1 hour while shaking at 130 rpm and harvested and homogenized in liquid nitrogen. Protein extraction was performed with a 20mM Tris-HCl buffer containing 150 mM NaCl, 1% Sodium Dodecyl Sulfate (SDS), 100 mM Dithiothreitol

(DTT) and 1 cOmplete ultra tablet per 10 ml of EDTA free protease inhibitor cocktail (Roche). Samples were run on precast NuPAGE Novex gels (Life Technologies) and transferred to polyvinyl difluoride (PVDF) membrane from iBlot Gel Transfer Stack (Novex, Life Technologies) using the iBlot device (Life technologies). Membranes were blocked for 1 hour in Tris buffered Saline with 0.1 % Tween 20 (TBS-T, Sigma-Aldrich) and 5% Difco Skim milk (Becton, Dickinson and Company). Detection of BES1 occurred with a 1/2000 dilution in TBS-T 5% skim milk of anti-BES1, kindly provided by Yanhai Yin, and anti-rabbit IgG, Horseradish peroxidase (HRP)-linked (GE Healthcare, 1:10000 in TBS-T with 5% skimmed milk) Membrane was developed with application of Western Lightning® Plus–ECL, Enhanced Chemiluminescence Substrate (Perkin-Helmer) and Amersham Hyperfilm ECL (GE Healthcare).

Transmission electron microscopy

Arabidopsis root tips from 5-day-old seedlings were submerged in 200 mM sucrose, 10 mM trehalose, and 10 mM Tris buffer, pH 6.6[61], transferred into planchettes (Leica Microsystems; 3.0x0.5mm, Al, type A and B), and frozen in a high-pressure freezer HPM100 (Leica Microsystems). Freeze substitution was performed in a Leica EM AFS2 unit (Leica Microsystems) in dry acetone supplemented with 0.4% uranyl acetate at −85°C for 16 h, followed by 5 h warm-up to −50°C. After washing with 100% ethanol for 60 min, samples were infiltrated and embedded in Lowicryl HM20 resin at −50°C (intermediate steps of 30%, 50%, 70% HM20 in ethanol, 1 h each). The resin was polymerized with ultraviolet (UV) light for 3 days in the freeze substitution unit. Ultrathin sections were cut on a Leica UC7 (Leica Microsystems) and post-stained with aqueous uranyl acetate/lead citrate. Sections were examined in a JEM 1230 (Jeol) or in a Phillips CM100 transmission electron microscopes, both operating at 80 kV. Micrographs were recorded with a MSC 600CW (Gatan) digital camera or by scanning negatives (MACO EM films TYP S, 6.5x9 cm, ES 206) with an Epson Perfection V750 Pro system.

Drosophila genetics

Fly stocks were maintained on standard maize meal and molasses medium and were obtained from the Bloomington Drosophila Stock Center or from[21].

FM1-43 dye uptake assay and visualization of HA-CHC in Drosophila

FM1-43 labeling was performed as described[62]. Third instar larvae were dissected in HL-3 and prior to a stimulation protocol animals were incubated for 30 minutes in HL-3 supplemented with and without ES9-17 (10 and 100 μM). Next, neurons were stimulated for 5 min in HL-3 with 90 mM KCl and 1.5 mM $CaCl_2$ in the presence of FM 1-43 (4 μM) (Life Technologies) with or without small molecule. After labeling, the preparation was washed several times with HL-3 supplemented with or without small molecule. Images were captured using a confocal microscope (A1R, Nikon) with a 60x

NA 1.0 water dipping lens. The boutonic FM1-43 intensity was quantified using ImageJ and was corrected for background labeling in the muscle.

Immunohistochemistry was performed to visualize HA-CHC as described[21]. Larvae were treated in a similar fashion as for the FM1-43 dye uptake assay without the presence of FM1-43. Next, the treated animals were fixed and stained with a mouse anti-HA antibody (Covance) at 1:500. Alexa 555-conjugated secondary antibodies (Life Technologies) were used at 1:1000. Super resolution structural illumination microscopy images were acquired on a microscope (Elyra S.1; Carl Zeiss) using a 63×, NA 1.4 oil lens and three rotations at room temperature. Next, acquired images were processed and stored using the ZEN 2011 software (Carl Zeiss).

TMRE labeling

Tetramethylrhodamine ethyl ester (TMRE) was used to label the mitochondrial membrane potential as described[63]. D42mitoGFP/+ third instar larvae were dissected in HL-3 and incubated for 30 minutes in HL-3 supplemented with and without ES9-17 (10 µM and 100 µM. Subsequently, larvae were treated for 15 minutes with HL-3 medium supplemented with 50 mM TMRE (Abcam) and the appropriate small molecule at room temperature. Next, fillets were washed with HL-3 with the appropriate small molecule and images were captured using a confocal microscope (A1R, Nikon) with a 60x NA 1.0 water dipping lens. The TMRE labeling intensity was quantified using ImageJ. First, 32-bit image of the mitoGFP channel was thresholded to select the mitochondria of the neuromuscular junction. Subsequently, the TMRE labeling intensity was measured in that region.

Affinity purification with biotinylated small molecules

Cell cultures (PSB-D wild type cells) were harvested by separating cells from medium, flash frozen in liquid nitrogen and grinded using a Retsch® MM400. Cell material was weighed and extraction buffer (50mM Tris-HCl pH 8, 150mM NaCl, 0.1% NP-40 [Sigma] with 1 tablet/10mL cOmplete ULTRA protease inhibitor cocktail, EDTA free [Roche] per 10 ml) was added in 2:1 ratio (200 µl extraction buffer for 100 mg material). Cell material was allowed to thaw on ice for 15 min with occasional mixing. Protein concentration was determined using the Bradford method (Quick start Bradford 1x Dye reagent [Bio-Rad]). Lysate was prepared for affinity purification by removing endogenous biotin. To this end, 50 µl of washed (3x with 500 µl extraction buffer, spun down at 1500 rpm, 4°C) Steptavidin Sepharose High Performance beads (GE Healthcare, referred to as beads in the remainder of the protocol) were applied to 1 ml lysate and incubated at 4°C for 1hr on a rotary wheel. Meanwhile a second batch of beads was prepared in the same way as described above, but biotinylated small molecules (2 µl 50mM stock per 50 µl beads) were added with the last wash. The mixture was left at room temperature for 15 min, and transferred to 4°C until further use. Lysate incubated with beads for the removal of biotin was spun down (1500 rpm, 4°C), supernatant collected, and added to beads incubated with biotinylated small molecules, for which the supernatant was removed after centrifugation (1500 rpm, 4°C) prior to use. The subsequent mixture was incubated for

a minimum of 2 hrs, or overnight at 4°C on a rotary wheel. Next the mixture was spun down (1500 rpm, 4°C), supernatant removed, and washed 3 times (50mM Tris-HCl pH 8, 150mM NaCl). After removal of supernatant from the last wash, appropriate amount of LDS sample buffer (4x LDS sample buffer supplemented with 10x sample reducing agent, Novex, Life Technologies) was added and samples were incubated for 10 min at 70°C and 350 rpm, followed by a 2 min centrifugation at maximum speed. The resulting supernatant was collected and run on 4-12% Bis-Tris protein gels with MES-buffer (NuPage Novex gels and buffer from Life technologies) for 7 min. Gels were stained with SYPRO Ruby protein gel stain (Molecular probes, Invitrogen) according to the rapid staining protocol. Stained gel regions were excised and cut in approximately 9 pieces before submission for LC-MS/MS analysis.

LC−MS/MS Analysis

Gel pieces containing the proteins of interest were cut out of the gel and transferred to Biopure® Eppendorf tubes (Eppendorf AG, Hamburg, Germany). Following two consecutive 15 min wash steps with water/acetonitrile (1/1, v/v) (both Baker HPLC analysed, Mallinckrodt Baker B.V., Deventer, The Netherlands), the gel pieces were dried to complete dryness in a centrifugal vacuum concentrator. They were subsequently re-hydrated in 10 µl of a 0.02 µg/µl of sequencing grade modified trypsin stock solution (Promega Corporation, Madison, WI, USA), 50 mM freshly prepared ammonium bicarbonate solution was added to complete submerge the gel pieces and the digestion proceeded overnight at 37°C. The digestion was stopped by acidification with TFA.

Following centrifugation, the peptide mixture was removed from the gel pieces, transferred to a new Eppendorf tube and completely dried in a centrifugal vacuum concentrator. It was re-dissolved in 20 µl of 0.1% TFA in water/acetonitrile (98/2, v/v) (loading solvent). 10 µl of the obtained peptide mixtures were introduced into an LC−MS/MS system through an Ultimate 3000 RSLC nano LC (Thermo Fisher Scientific, Bremen, Germany) in-line connected to a Q Exactive mass spectrometer (Thermo Fisher Scientific). The sample mixture was first loaded on a trapping column (made in-house, 100 µm internal diameter (I.D.) × 20 mm, 5 µm beads C18 Reprosil-HD, Dr. Maisch, Ammerbuch-Entringen, Germany). After flushing from the trapping column, the sample was loaded on an analytical column (made in-house, 75 µm I.D. × 150 mm, 5 µm beads C18 Reprosil-HD, Dr. Maisch) packed in the needle (PicoFrit SELF/P PicoTip emitter, PF360-75-15-N-5, New Objective, Woburn, MA, USA). Peptides were loaded with loading solvent (0.1% TFA in water/ acetonitrile, 2/98 (v/v)) and separated with a linear gradient from 98% solvent A' (0.1% formic acid in water) to 40% solvent B′ (0.1% formic acid in water/acetonitrile, 20/80 (v/v)) in 30 min at a flow rate of 300 nL/min. This is followed by a 5 min wash reaching 99% solvent B'. Two packing column and two analytical columns were configured in tandem LC mode, and switching between two flow paths – an

analysis flow path and a regeneration flow path – allows column washing and re-equilibration off-line; thus, while one column is re-equilibrated, the system injects a sample on the other column.

The mass spectrometer was operated in data-dependent, positive ionization mode, automatically switching between MS and MS/MS acquisition for the 10 most abundant peaks in a given MS spectrum.

The source voltage was 3.4 kV, and the capillary temperature was 275°C. One MS1 scan (m/z 400−2000, AGC target 3 × 106 ions, maximum ion injection time 80 ms) acquired at a resolution of 70000 (at 200 m/z) was followed by up to 10 tandem MS scans (resolution 17500 at 200 m/z) of the most intense ions fulfilling predefined selection criteria (AGC target 5 × 104 ions , maximum ion injection time 60 ms, isolation window 2 Da, fixed first mass 140 m/z, spectrum data type: centroid, underfill ratio 2%, intensity threshold 1.7xE4, exclusion of unassigned, 1, 5-8, >8 charged precursors, peptide match preferred, exclude isotopes on, dynamic exclusion time 20 s). The HCD collision energy was set to 25% Normalized Collision Energy and the polydimethylcyclosiloxane background ion at 445.120025 Da was used for internal calibration (lock mass).

From the MS/MS data in each LC run, Mascot Generic Files (mgf) were created using the Mascot Distiller software (version 2.4.3.3, Matrix Science). These peak lists were then searched using the Mascot search engine with the Mascot Daemon interface (version 2.4, Matrix Science). Spectra were searched against the TAIR10 database. Variable modifications were set to pyro-glutamate formation of amino-terminal glutamine, acetylation of the protein N-terminus, methionine oxidation and propionaide formation of cysteines. Mass tolerance on precursor ions was set to ± 10 ppm (with Mascot's C13 option set to 1), and on fragment ions to 20 mmu. The instrument setting was on ESI-QUAD. The enzyme was set to trypsin/P, allowing for 1 missed cleavage, and cleavage was also allowed when lysine or arginine is followed by proline. Only peptides that were ranked first and scored above the threshold score, set at 99% confidence, were withheld.

All data management was done by ms_lims , and data analysis was performed using R (http://www.R-project.org) embedded in KNIME . The data were filtered by removing all peptides smaller than eight amino acids and only the proteins containing minimal two peptides in one of experiments were taken into account for data analysis.

CETSA on lysate

The protocol used is based to a large extent on the protocol published earlier[17], with minor adjustments. Cell cultures (PSB-D wild type cell cultures or transformed with the appropriate constructs) were harvested by separating cells from medium, flash frozen in liquid nitrogen and grinded using a Retsch® MM400. Cell material was weighed and extraction buffer (50mM Tris-HCl pH 7.6, 150mM NaCl with 1 tablet/10mL cOmplete ULTRA protease inhibitor cocktail, EDTA free (Roche)) was added in 2:1 ratio (200 µl extraction buffer for 100 mg material). Cell material was allowed to thaw on ice for 15 min with occasional mixing. Next, samples were centrifuged for 30 min

at maximum speed at 4°C, and transferred to new recipients. Lysates were pooled per cell type, and protein concentration was determined using the Bradford method (Quick start Bradford 1x Dye reagent (Bio-Rad)). Pooled lysates were aliquoted according to the number of treatments, treated with small molecules or mock (DMSO, Sigma) at appropriate concentrations and incubated for 30 min at room temperature on a rotary wheel. Next, treated lysates were aliquoted in 60 µl fractions in PCR tubes according to the different temperature treatments, and treated for 2 min at the respective temperature in a Bio-Rad thermal cycler. Samples were allowed to cool down, transferred to new 1.5 ml eppendorf tubes and centrifuged at maximum speed for 30 min at 4°C. After centrifugation, 50 µl of the supernatant was taken and processed for standard western blot analysis.

Detection of proteins was done according to standard western blot procedures. All antibodies were diluted in TBS-T with 5% skimmed milk. Anti CHC (kindly provided by Hwang, 1/3000 dilution), anti AtpB (1/4000, AS05085 Agrisera) and anti Sec21p (1/4000, AS08327 Agrisera) were detected with anti-rabbit IgG, HRP-linked (GE Healthcare, 1:10000) Anti-tubulin (1/15000,) was detected with anti-mouse IgG, Horseradish peroxidase (HRP)-linked (GE Healthcare, 1:10000). GFP was detected with anti-GFP-HRP (1/4000, Miltenyi Biotec). Blots were developed with Western Lightning® Plus–ECL, Enhanced Chemiluminescence Substrate (Perkin-Helmer), and imaging with a Bio-Rad ChemiDoc XRS+ molecular imager. Intensity of bands was measured with the Bio-Rad Image Lab software package.

DARTS

The DARTS protocol was adopted as previously described[18], with the exception of the different used Pronase dilutions. Preparation of lysates was done as described for CETSA. Lysates treated with ES9-17 (100 µM) or mock (DMOS, Sigma) were incubated for 30 minutes on a rotary wheel at room temperature. After incubation lysate was split in equal aliquots for Pronase (Roche, 10 165 921 001) digestion. One aliquot was kept as a non-digested control. Pronase dilutions were prepared from a 10mg/ml stock solution in dH_2O. The 1/100 starting dilution of Pronase, which served to make all subsequent dilutions as indicated, was prepared by dissolving 12.5µl Pronase stock solution in 87.5 µl 1x TNC buffer (500mM Tris-HCl, pH8, 500mM NaCl and 100mM $CaCl_2$, 10X stock). All dilutions were prepared with 1x TNC buffer. Digestion (30 min) was started with 1 min intervals, and stopped by adding sample buffer at a 1x final concentration (4x LDS sample buffer with 10x sample reducing agent, Novex, Life Technologies) in the same sequence as the digestion was started. Western blotting, detection of proteins and quantification as described for CETSA.

Docking of ES9-17 on CHC

All waters and ligands of the protein crystal structures 2XZG (human clathrin terminal domain in complex with pitstop1) and 4G55 (idem with pitstop 2)[5] were manually deleted from the pdb-text file. The emptied structures were subjected to a local minimization with the GROMOS96 (43B1

parameter set)[64] implementation within the Swiss-PdbViewer[65], and polar hydrogens were added. Docking experiments were with AutoDock-Vina[66], using AutoDockTools[67] for pdbqt-format preparations of proteins and ligands. Comparison of the recognition site in respectively 2XZG and 4G55 shows different orientations of the ligand-contacting residues Arg64, Gln89 and Phe91; these were set as flexible during the dockings. Grid-box settings for blind dockings (encompassing the whole protein) on 2XZG were: sizes x, y and z = 60 Å centered at x = 34.3, y = 1.9 and z = 5.6, and on 4G55 were: sizes x, y and z = 60 Å centered at x = 34.2, y = 1.9 and z = 5.6; with docking exhaustiveness set at 256. Grid-box settings for local dockings (encompassing the pitstop recognition site) on 2XZG were: sizes x = 20, y = 24 and z = 20 Å centered at x = 48.4, y = -9.8 and z = 23.3, and on 4G55 were: sizes x = 20, y = 22 and z = 20 Å centered at x = 50.0, y = -10.2 and z = 24.5; with docking exhaustiveness set at 64. Ligands were drawn in 3D with Avogadro[68] and were minimized with the built-in MMFF94s force field[69]. Docking results (20 poses per docking) were visually inspected with PyMOL[40].

Chemical synthesis

All reactions were, unless mentioned otherwise, performed under inert atmosphere in dried glassware with dried teflon stirbars. Thin Layer Chromatography was performed on silica (Macherey-Nagel, pre-coated TLC-plates SIL G-25 UV_{254}, 0.25 mm). TLC plates were visualized by staining with a 5% phosphomolybdic acid-solution in ethanol. Flash chromatography was performed on silica (d=70-200 μm, ±30g silica/1g product). Solvents were used dry unless mentioned otherwise. Anhydric methanol and dimethylformamide were purchased and kept dry on molecular sieves. Solvents were of HPLC quality.

Nuclear magnetic resonance spectra (NMR) were measured in deuterated acetone or deuterated chloroform. Proton (^{1}H) and carbon-13 (^{13}C) spectra were measured at 300MHz (^{13}C: 75MHz) on a Bruker 300MHz Avance II or at 500MHz (^{13}C: 125MHz) on a Bruker 500MHz Avance II or III. Chemical shift (δ) is reported in units ppm relative to residual acetone (^{1}H: δ = 2.05 ppm; ^{13}C = 29.8 and 206.3 ppm) or residual chloroform (^{1}H: δ = 7.26 ppm; ^{13}C = 77.0 ppm). Multiplicites are reported as follows: s = singlet, d = doublet, t = triplet, q = quadruplet, q_5 = quintuplet, m = multiplet, band = multiple overlapping signals, br = broad signal, AB = AB-system with clear roofing. Melting points were measured on an Electrothermal 1900. High Resolution Mass (HRMS) was measured with an Agilent Accurate-Mass Quadrupole Time-of-Flight mass spectrometer.

Synthesis of ES9-10

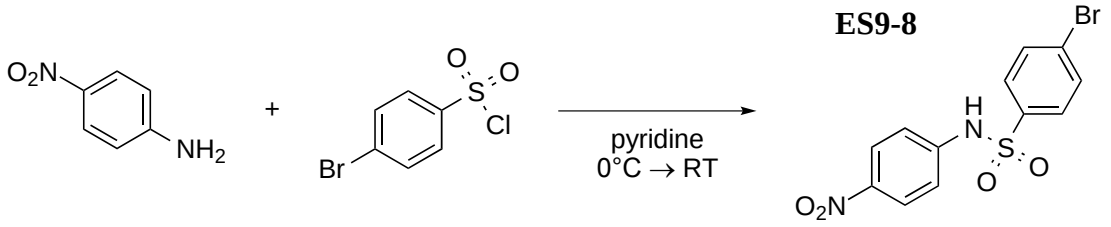

4-nitroaniline (582 mg, 4.22 mmol, 1.08 equiv.) is dissolved in pyridine (8 ml). The mixture is cooled to 0°C and 4-bromobenzenesulfonyl chloride (1 g, 3.91 mmol, 1 equiv.) is added portionwise. The reaction is stirred at room temperature for 17 h. After concentration *in vacuo*, the residue is taken up in water and ethyl acetate (100 ml, 1:1 v/v). The organic phase is washed with hydrochloric acid (6 × 30 ml, 6 M), a saturated sodium bicarbonate solution (30 ml) and a saturated sodium chloride solution (30 ml). The organic phase is dried on sodium sulfate, filtered and concentrated *in vacuo*. The crude solid is recrystallized from 2-propanol to yield sulfonamide **ES9-8** as yellow crystals (1.09 g, 72 %).

Formula: $C_{12}H_9BrN_2O_4S$; M: 357.21 g/mol; TLC (ethyl acetate:petroleum ether, 1:1 v/v): R_f = 0.7; ^{1}H-NMR (500MHz, $(CD_3)_2CO$): δ 8.20 – 8.13 (m, 2H), 7.89 – 7.82 (m, 2H), 7.82 – 7.76 (m, 2H), 7.55 – 7.40 (m, 2H); ^{13}C-NMR (125 MHz, $(CD_3)_2CO$): δ 144.6, 139.6, 133.5, 129.9, 128.7, 126.0, 119.7; HRMS (*m*/*z*): $[M\text{-}H^+]^-$ calcd. for $C_{12}H_8BrN_2O_4S^-$, 354.9394; found, 354.9407

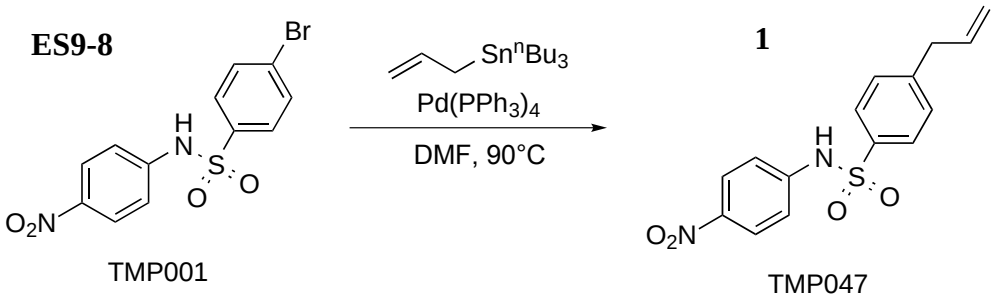

ES9-8 (1g, 2.8mmol, 1.0equiv.) is dissolved in dimethylformamide (20 ml) together with tetrakis(triphenylphosphine)palladium (226 mg, 0.2 mmol, 0.09 equiv.). The mixture is extensively purged with nitrogen gas during 30 min. Allyltributylstannane (1.09 ml, 3.5 mmol, 1.25 equiv.) is added and the mixture is purged for another 5 min. The reaction is heated to 90°C and after stirring for 3.5 h poured into ice water (100 ml). Ethyl acetate (100 ml) is added and the mixture is filtered over a pad of celite. The organic phase is separated and washed with water (30 ml), a saturated sodium bicarbonate solution (30 ml) and a saturated sodium chloride solution (30 ml). After drying on sodium sulfate, the organic phase is concentrated *in vacuo*. The residue is purified by flash chromatography (silica, ethyl acetate:petroleum ether, 3:7 v/v) to yield sulfonamide **1** as a viscous oil. The oil is

dissolved in methyl-*tert*-butylether and petroleum ether is added to give a pale yellow solid, which is recrystallised from carbondisulfide to yield sulfonamide **1** as a bright yellow crystalline solid (563 mg, 1.76 mmol, 63 %).

1

Formula: $C_{15}H_{14}N_2O_4S$; M: 318.35g/mol; TLC (ethyl acetate:petroleum ether, 1:1 v/v): R_f = 0.7; ^{1}H-NMR (500MHz, $(CD_3)_2CO$): δ 8.20 – 8.11 (m, 2H), 7.91 – 7.82 (m, 2H), 7.51 – 7.44 (m, 2H), 7.44 – 7.38 (m, 2 H), 5.93 (ddt, 1 H, *J* = 17.0, 10.1, 7.8 Hz), 5.08 (ddm(AB), 1H, *J* = 17.0,1.6Hz), 5.05 (ddm(AB), 1H, *J* = 10.1,1.6Hz), 3.45 (d, 2H, *J* = 7.8 Hz,); ^{13}C-NMR (125 MHz, $(CD_3)_2CO$): δ 147.4, 145.0, 138.1, 137.1, 130.3, 128.2, 126.0, 119.2, 117.1, 40.3; HRMS (*m*/*z*): $[M\text{-}H^+]^-$ calcd. For $C_{15}H_{13}N_2O_4S^-$, 317.0602; found, 317.0606

ES9-9

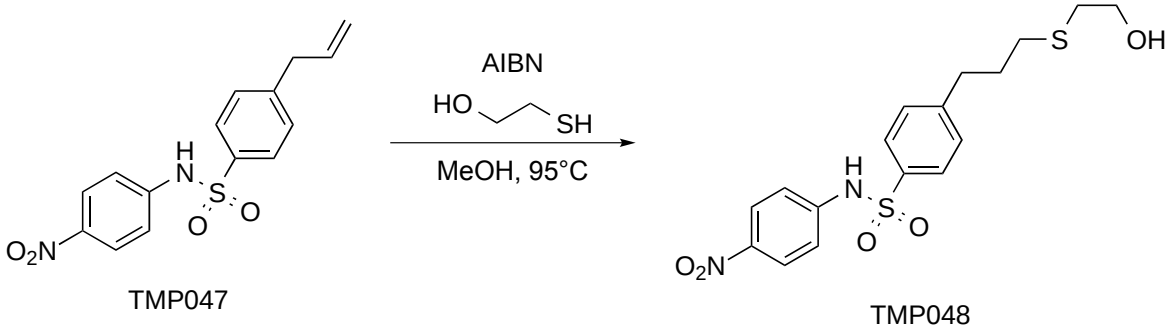

TMP047 TMP048

Sulfonamide **1** (100 mg, 314 µmol, 1.0 equiv.) and 1-mercaptoethanol (220 µl, 3.14 mmol, 10.0 equiv.) is dissolved in methanol (2 ml) together with *N*,*N*'-azobisisobutyronitrile (4 mg, 24 µmol, 0.08 equiv.) in a pressure tube. The mixture is heated to 95°C and stirred. The reaction is monitored with TLC and *N*,*N*'-azobisisobutyronitrile (4 mg) is added with 30 min intervals until complete conversion is observed. The crude mixture is concentrated *in vacuo* and the residue is purified by flash chromatography (silica, ethyl actetate:petroleum ether, 1:1 v/v) to yield **ES9-9** as a yellow oil (68 mg, 59 %).

Formula: $C_{17}H_{20}N_2O_5S_2$; M: 368.48g/mol; TLC (ethylacetate:petroleum ether, 1:1 v/v): R_f = 0.2; ^{1}H-NMR (300MHz, $(CD_3)_2CO$): δ 8.23 – 8.10 (m, 2H), 7.92 – 7.81 (m, 2H), 7.53 – 7.38 (band, 4H), 3.62 (t, 2H, *J* = 6.8Hz), 2.79 (t, 2H, *J* = 7.5Hz), 2.61 (t, 2H, *J* = 6.8Hz), 2.54 (t, 2H, *J* = 7.5Hz), 1.88 (q, 2 H, *J* = 7.5 Hz); ^{13}C-NMR (125 MHz, $CDCl_3$): δ 147.8, 143.5, 143.3, 136.5, 129.4, 127.3, 125.3, 118.2, 60.3, 35.0, 34.4, 30.9, 30.5; HRMS (*m*/*z*): $[M\text{-}H^+]^-$ calcd. for $C_{17}H_{19}N_2O_5S_2^-$, 395.0741; found, 395.0754

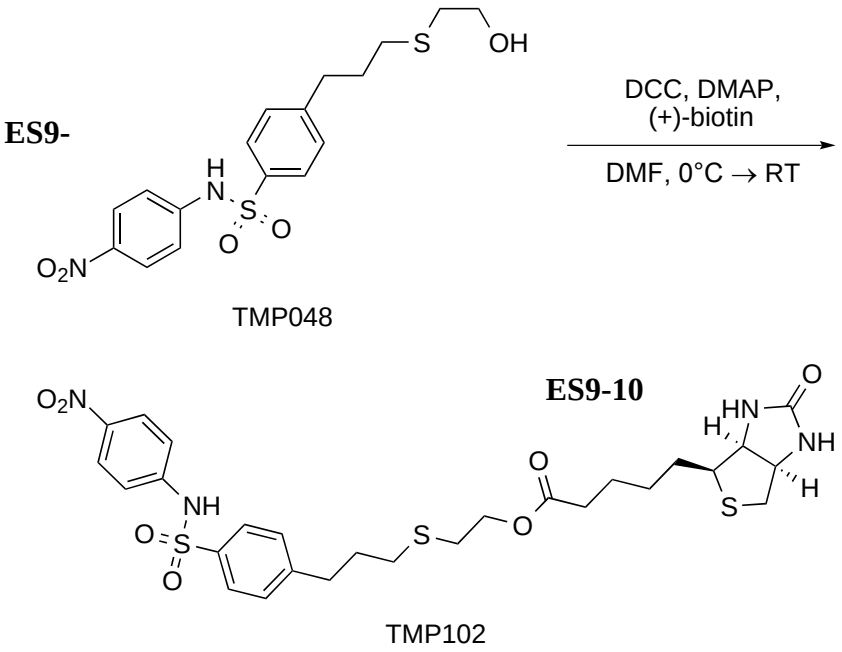

Alcohol **ES9-9** (53.2mg, 144µmol, 1.5equiv.) is dissolved in dimethylformamide (0.5 ml) together with biotin (23.5 mg, 96 µmol, 1.0 equiv.) and 4-dimethylaminopyridine (2 mg, 13 µmol, 0.09 equiv.). The mixture is then stirred until complete dissolution and cooled to 0°C. *N*,*N*'-dicyclohexylcarbodiimide (23.8 mg, 145 µmol, 1.2 equiv.) is added and the mixture is stirred at the same temperature for another 5 min. After heating to room temperature, the reaction is stirred overnight. The mixture is concentrated *in vacuo* and purified by flash chromatography (silica, methanol:chloroform, 3:97 to 6:94 v/v) to yield **ES9-10** as an amorphous yellow solid (63 mg, 74 %).

Formula: $C_{27}H_{34}N_4O_7S_3$; M: 622.78 g/mol; TLC (methanol:chloroform, 1:9 v/v): R_f = 0.35; ^{1}H-NMR (300 MHz, $CDCl_3$): δ 10.88 (s(br), 1 H), 8.10 – 8.02 (m, 2H), 7.90 – 7.81 (m, 2H), 7.39 – 7.27 (band, 4H), 5.90 (s(br), 1 H), 5.12 (s(br), 1H), 4.63 (dd(br), 1 H, *J* = 7.6, 5.5 Hz), 4.42 (ddd(br), 1H, *J* = 7.5, 5.2, 1.1 Hz), 4.18 (t, 2 H, *J* = 6.4 Hz), 3.21 (ddd(br), 1H, *J* = 9.2, 5.6, 4.9 Hz), 2.97 (dd, 1H, *J* = 13.0,4.9Hz), 2.75 (t, 2H, *J* = 6.6Hz), 2.74 (d, 1H, *J* = 12.2 Hz), 2.66 (t, 2H, *J* = 6.4 Hz), 2.49 (t, 2 H, *J* = 7.3 Hz), 2.19 (t, 2 H, *J* = 7.3 Hz), 2.02 – 1.34 (band, 8H+H_2O); ^{13}C-NMR (125 MHz, $CDCl_2$): δ 173.1, 163.8, 147.5, 144.1, 143.3, 136.8, 129.5, 127.4, 125.2, 118.1, 64.1, 62.3, 60.3, 55.7, 40.6, 34.1, 33.6, 31.1, 30.5, 30.3, 28.4, 28.3, 24.8; HRMS (*m*/*z*): $[M\text{-}H^+]^-$ calcd. For $C_{27}H_{33}N_4O_7S_3^-$, 621.1517; found, 621.1512

Synthesis of ES9_6

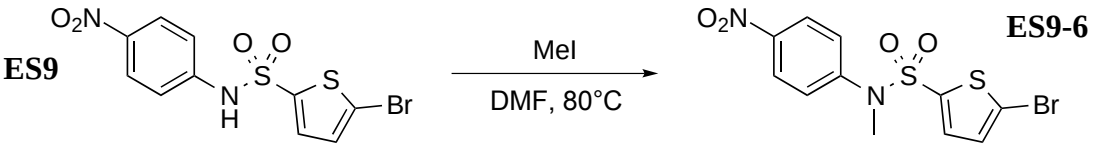

TMP003 TMP335

ES9 (100 mg, 275 µmol, 1.0 equiv.) is dissolved in dimethylformamide (700 µl). Potassium carbonate (76 mg, 550 µmol, 2.0 equiv.) is added and the mixture is stirred for 5 min. Methyl iodide (34 µl, 550 µmol, 2.0 equiv.) is added and the reaction is heated to 80°C and stirred for 1 h. The reaction mixture is cooled down and diluted with ethyl acetate (20 ml) and the organic phase is washed with water (10 ml) and a saturated sodium chloride-solution (7 ml). The organic phase is dried on sodium sulphate, filtered and concentrated *in vacuo* to yield a yellow solid which is recrystallized from 2-propanol to yield **ES9-6** as a yellow crystalline solid (100 mg, 95 %).

Formula: $C_{11}H_9BrN_2O_4S_2$; M: 377.23 g/mol; TLC (ethyl acetate:petroleum ether, 3:7 v/v): R_f = 0.3; ^{1}H-NMR (500MHz, $(CD_3)_2CO$): δ 8.29 – 8.24 (m, 2H), 7.62 – 7.57 (m, 2H), 7.35 – 7.31 (band, 2H), 3.38 (s, 3 H); ^{13}C-NMR (125 MHz, $(CD_3)_2CO$): δ 147.7, 147.1, 138.0, 134.9, 132.5, 127.4, 125.1, 121.0, 38.2; HRMS (*m*/*z*): $[M+OAc^-]^-$ calcd. For $C_{11}H_8BrN_2O_4S_2^-$, 434.9325; found, 434.9319

Synthesis of ES9_17

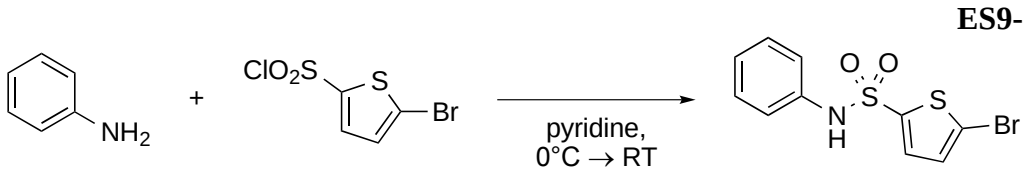

TMP411

Aniline (193 µl, 2.13 mmol, 1.08 equiv.) is dissolved in pyridine (4 ml). The mixture is cooled to 0°C and 4-bromothiophenesulfonyl chloride (0.5 g, 1.95 mmol, 1.0 equiv.) is added portionwise. The reaction is stirred at room temperature for 17 h. After concentration *in vacuo*, the residue is taken up in water and ethyl acetate (50 ml, 1:1 v/v). The organic phase is washed with hydrochloric acid (6 × 30 ml, 6 M), a saturated sodium bicarbonate solution (15 ml) and a saturated sodium chloride solution (15 ml). The organic phase is dried on sodium sulfate, filtered and concentrated *in vacuo*. The crude solid is purified by flash chromatography (silica, ethyl acetate:petroleum ether, 3:5 v/v) and recrystallized from 2-propanol to yield **ES9-17** as yellow crystals (512 mg, 83 %).

Formula: $C_{10}H_8BrNO_2S_2$; M: 318.20 g/mol; TLC (ethyl acetate:petroleum ether, 1:1 v/v): R_f = 0.6; ^{1}H-NMR (500 MHz, $(CD_3)_2CO$): δ 9.21 (s(br), 1 H), 7.36 – 7.30 (band, 3H), 7.30 – 7.25 (m, 2H), 7.20 (d, 1H, *J* = 4.0 Hz), 7.19 – 7.14 (m, 1H); ^{13}C-NMR (125 MHz, $(CD_3)_2CO$): δ 142.4, 138.1, 133.8, 131.9, 130.2, 126.2, 122.3, 119.8; HRMS (*m*/*z*): $[M-H^+]^-$ calcd. For $C_{10}H_7BrNO_2S_2^-$, 315.9107; found,

315.9116

Synthesis of ES9-13

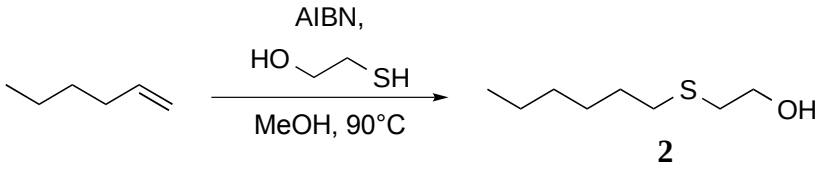

1-hexene (0.5 g, 742 µl, 5.94 mmol, 1.0 equiv.) and 2-mercaptoethanol (414 µl, 59.4 mmol, 10.0 equiv.) are dissolved in methanol (2 ml) together with *N*,*N*'-azobisisobutyronitrile (72 mg, 439 µmol, 0.08 equiv.). The mixture is heated to 95°C and stirred for 1.5 h. After concentration *in vacuo* the residue is purified by flash chromatography (silica, ethyl acetate:petroleum ether, 2:3 v/v) to yield alcohol **2** quantitatively as a colourless oil.

Formula: $C_8H_{18}OS$; M: 162.29 g/mol; TLC (ethyl acetate:petroleum ether, 1:1 v/v): R_f = 0.6; ^{1}H-NMR (500 MHz, $CDCl_3$): δ 3.71 (t, 2 H, *J* = 5.9 Hz), 2.73 (t, 2H, *J* = 5.9Hz), 2.52 (t, 2H, *J* = 7.4Hz), 2.04 (s(br), 1H), 1.58 (q_5, 2H, *J* = 7.4Hz), 1.38 (q_5, 2H, *J* = 7.4Hz), 1.34 – 1.23 (band, 4H), 0.89 (t, 3 H, *J* = 7.0 Hz), ^{13}C-NMR (125 MHz, $CDCl_3$): δ 60.3, 35.5, 31.8, 31.6, 29.9, 28.7, 22.7, 14.2

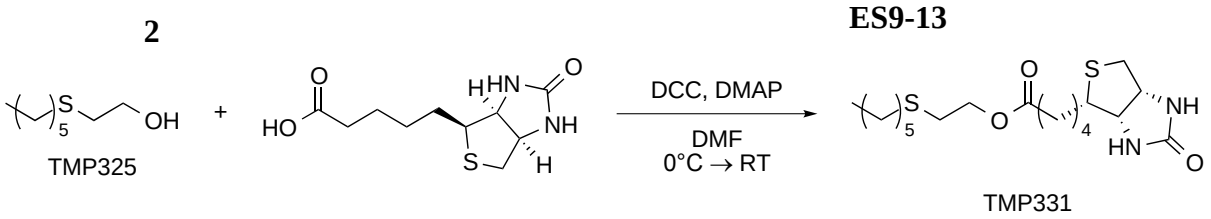

Alcohol **2** (300 mg, 1.85 mmol, 1.0 equiv.) is dissolved in dimethylformamide (4 ml) together with biotin (452 mg, 1.85 mmol, 1.0 equiv.) and 4-dimethylaminopyridine (20 mg, 165 µmol, 0.09 equiv.). The mixture is then stirred until complete dissolution and cooled down to 0°C. A solution of *N*,*N*'-dicyclohexylcarbodiimide (23.8 mg, 145 µmol, 1.2 equiv.) in dimethylformamide (2 ml) is added and the mixture is stirred at the same temperature for 1 h, after which it is heated to room temperature and stirred overnight. The mixture is concentrated *in vacuo* and purified with flash chromatography (silica, methanol:chloroform, 1:9 v/v) to yield **ES9-13** as a white waxy solid (62.9 mg, 9 %).

Formula: $C_{18}H_{32}N_2O_3S_2$; M: 388.59 g/mol; TLC (methanol:dichloromethane, 1:8 v/v): R_f = 0.6; ^{1}H-NMR (300MHz, $CDCl_3$): δ 5.58 (s(br), 1H), 5.13 (s(br), 1 H), 4.51 (dd(br), 1H, *J* = 7.8, 4.9 Hz), 4.32 (dd, 1H, *J* = 7.7, 4.6 Hz), 4.20 (t, 2H, *J* = 6.9 Hz), 3.16 (ddd(br), 1H, *J* = 8.5, 6.6, 5.0 Hz), 2.92 (dd, 1H, *J* = 12.9,5.0 Hz), 2.78 – 2.69 (band, 3H), 2.55 (t, 2H, *J* = 7.3Hz), 2.35 (t, 2H, *J* = 7.3Hz), 1.76 – 1.62 (band, 4H), 1.58 (q_5, 2H, *J* = 7.5Hz), 1.51 – 1.22 (band, 8H+H_2O), 0.89 (t, 3H, *J* = 6.7 Hz); ^{13}C-

NMR (125 MHz, $CDCl_3$): δ 173.5, 163.4, 63.5, 62.1, 60.2, 55.5, 40.7, 33.9, 32.5, 31.6, 30.7, 29.8, 28.7, 28.5, 28.4, 24.9, 22.7, 14.2; HRMS (*m*/*z*): $[M+H^+]^+$ calcd. for $C_{18}H_{33}N_2O_3S_2^+$, 389.1927; found, 389.1933

Synthesis of ES9-15

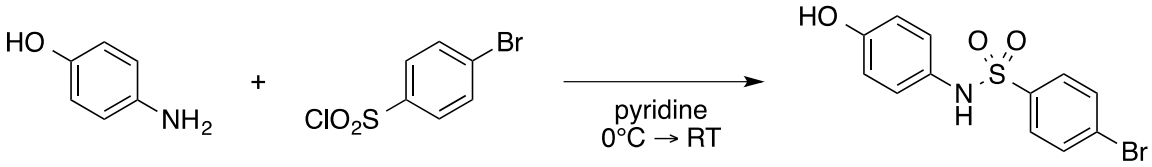

ES9-15

4-aminophenol (230 mg, 2.11 mmol, 1.08 equiv.) is dissolved in pyridine (4 ml). The mixture is cooled to 0°C and 4-bromobenzenesulfonyl chloride (500 mg, 1.95 mmol, 1 equiv.) is added portionwise. The reaction is stirred at room temperature for 17h. After concentration *in vacuo*, the residue is taken up in water and ethyl acetate (75 ml, 1:2 v/v). The organic phase is washed with hydrochloric acid (6 × 15 ml, 6 M), a saturated sodium bicarbonate solution (15 ml) and a saturated sodium chloride solution (15 ml). The organic phase is dried on sodium sulfate, filtered and concentrated *in vacuo* to yield sulfonamide **ES9-15** as a white solid (358.9 mg, 56 %).

Formula: $C_{11}H_9BrN_2O_2S$; M: 313.17 g/mol; TLC (ethyl acetate:petroleum ether, 1:1 v/v): R_f = 0.4; ^{1}H-NMR (300MHz, $(CD_3)_2CO$): δ 8.63 (s(br), 1H), 8.34 (s, 1H), 7.73 – 7.69 (m, 2H), 7.63 – 7.59 (m, 2H), 7.00 – 6.96 (m, 2H), 6.74 – 6.71 (m, 2H); ^{13}C-NMR (125 MHz, $(CD_3)_2CO$): δ 156.5, 140.2, 133.0, 129.9, 129.6, 127.6, 126.0, 116.5; HRMS (*m*/*z*): $[M-H^+]^-$ calcd. for $C_{11}H_8BrN_2O_2S^-$, 325.9492; found, 325.9499

Synthesis of ES9-16

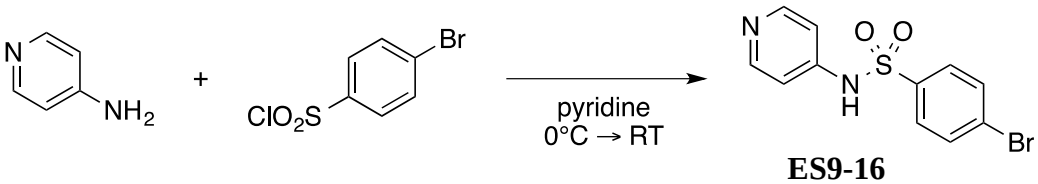

ES9-16

4-aminopyridine (199 mg, 2.11 mmol, 1.08 equiv.) is dissolved in pyridine (4 ml). The mixture is cooled to 0°C and 4-bromobenzenesulfonyl chloride (500 mg, 1.95 mmol, 1 equiv.) is added portionwise. The reaction is stirred at room temperature for 17 h during which a yellow precipitate is formed. After concentration *in vacuo*, the residue is taken up in ethyl acetate (10 ml). The organic phase is washed with sodium hydroxide (3 × 3 ml, 15%). The combined aquous phases are acidified with hydrochloric acid (6 M), until precipitation occurs. The solid is collected, washed with water and dried at 50°C under vacuum ().

Formula: $C_{11}H_9BrN_2O_2S$; M: 313.17 g/mol; ^{1}H-NMR (300MHz, $(CD_3)_2SO$): δ 12.63 (s(br), 1H), 7.99 (d(br), 2H, J = 6.7 Hz), 7.74 – 7.67 (band, 2H), 6.90 (d(br), 2H, J = 7.0 Hz); ^{13}C-NMR (125 MHz, $(CD_3)_2SO$): δ 131.7, 128.1, 124.8, 114.8; HRMS (m/z): $[M+H^+]^+$ calcd. for $C_{11}H_{10}BrN_2O_2S^+$, 312.9641; found, 312.9467

Supplemental information.

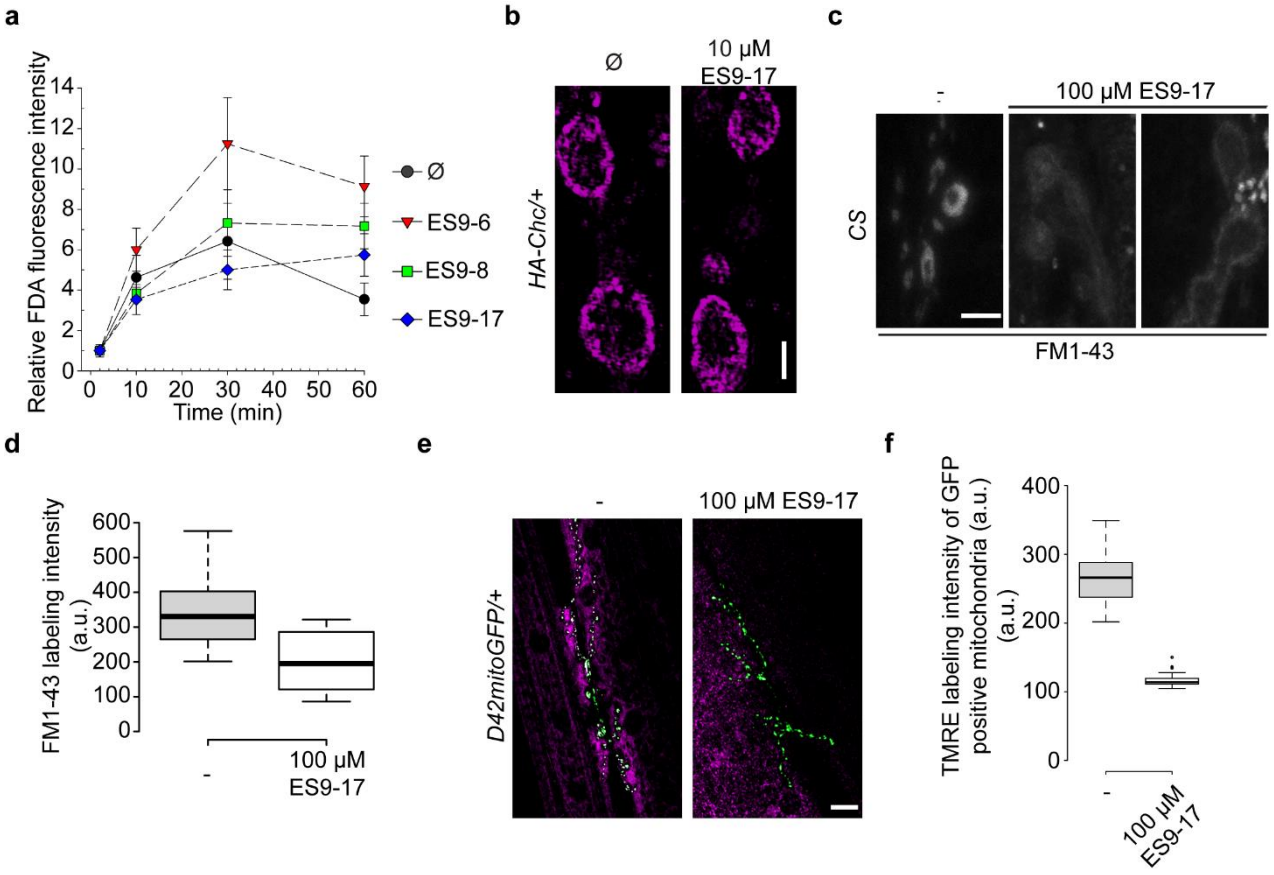

Supplemental Figure 1. Mitochondrial functions and FM1-43 uptake are affected at very high concentrations of ES9-17 in *Drosophila*

(**a**) Relative fluorescein diacetate (FDA) fluorescence intensity for different small molecule treatments of PSB-D wild type cell cultures. Mock treatment (Ø, DMSO), 50 µM ES9-6, 50 µM ES9-8 and 10 µM ES9-17. (**b**) Boutons of the neuromuscular junction in third instar larvae of Drosophila positive for clathrin heavy chain (CHC)-HA for mock or 10 µM ES9-17 in KCl stimulated conditions. (**c**) Tetramethylrhodamine ethyl ester (TMRE) labeling of mitochondria in *D42mitoGFP* positive *Drosophila* neuronal cells for 100 µM ES9-17 and mock treatment. Cells are incubated in the dark for 30 min with ES9-17 or mock, followed by 15 min of TMRE labeling. (**d**) FM1-43 labeling (30 min) of neuromuscular junction boutons in third instar larvae of *Drosophila*, in the control situation (Ø) and in presence of 100 µM ES9-17. Scale bars: 2µm in (b), 5 µm in (c) and 20 µm in (e).

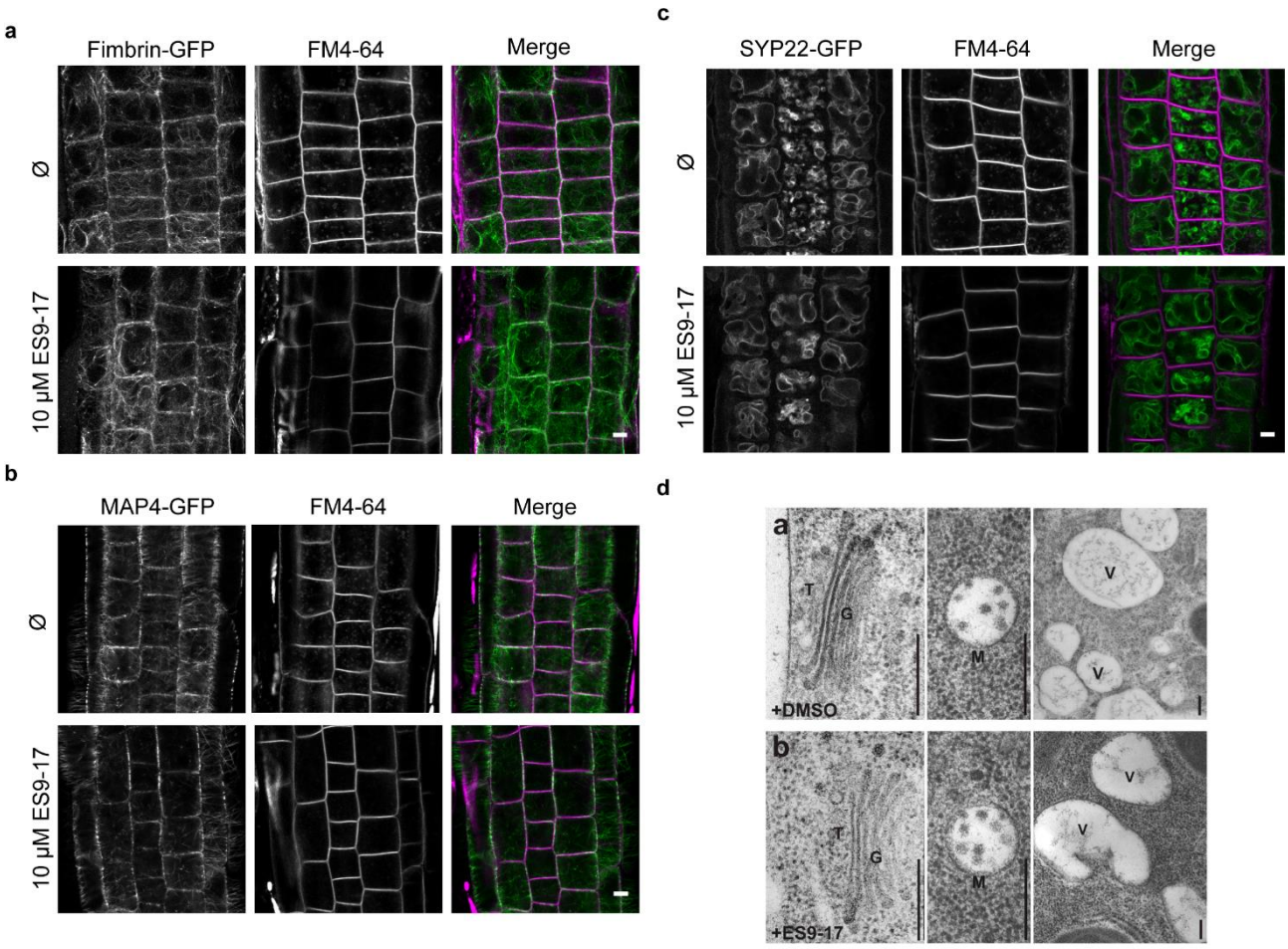

Supplemental Figure 2. ES9-17 had few notable effects on the cytoskeleton and other endomembrane compartments than the plasma membrane.

(**a**) The actin cytoskeleton labeled by Fimbrin-GFP, (**b**) microtubules labeled by MAP4-GFP, and (**c**) vacuolar compartment labeled by SYP22,-GFP were not affected by the ES9-17 treatment. All seedlings were pre-treated for 15 min with ES9-17. Mock (DMSO) treatment, Ø (**d**) Transmission electron microscopy of high-pressure frozen and freeze-substituted Arabidopsis roots. Upon 30 min exposure to 10 µM ES9-17, (a) The Golgi apparatus (G), the trans-Golgi network (T), multivesicular bodies (M), and vacuoles were unaffected. (b) Control cells exposed to DMSO. Scale bars: 5 µm (**a-c**) 200 nm (**d**)

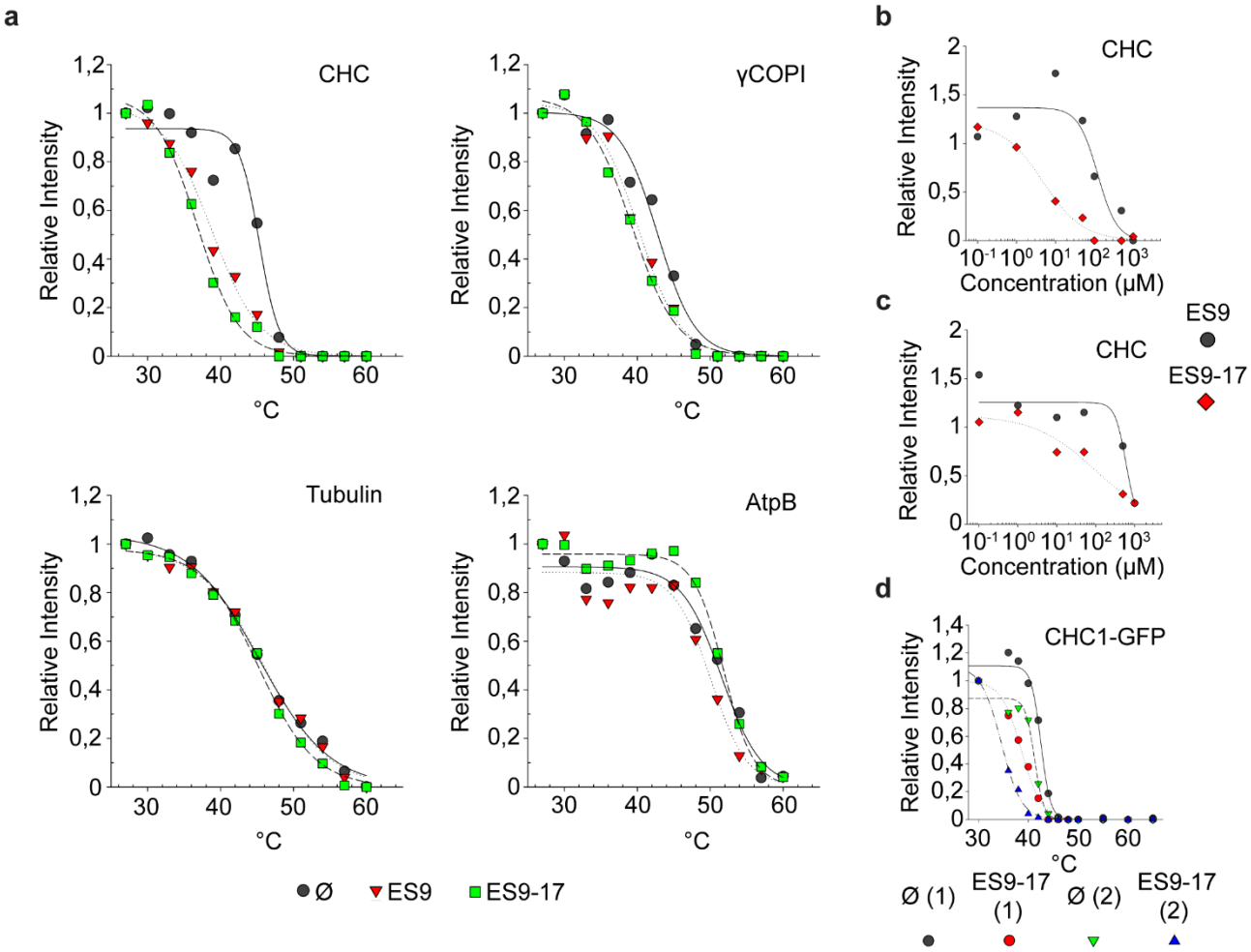

Supplemental Figure 3. ES9-17 targets CHC

(**a**) Representative thermal denaturation for tubulin, clathrin heavy chain (CHC), γCOPI, and the β subunit of ATP synthase (AtpB) respectively in lysate with detergent treated with mock (Ø) or with ES9 (500 μM) and ES9-17 (100 μM). (**b**) Representative isothermal denaturation at 40°C of CHC extracted with detergent in presence of different concentrations of ES9 and ES9-17 or (**c**) extracted without detergent. (**d**) Thermal denaturation for CHC1-GFP expressed in seedlings. 2 biological repeats (indicated by 1 or 2).

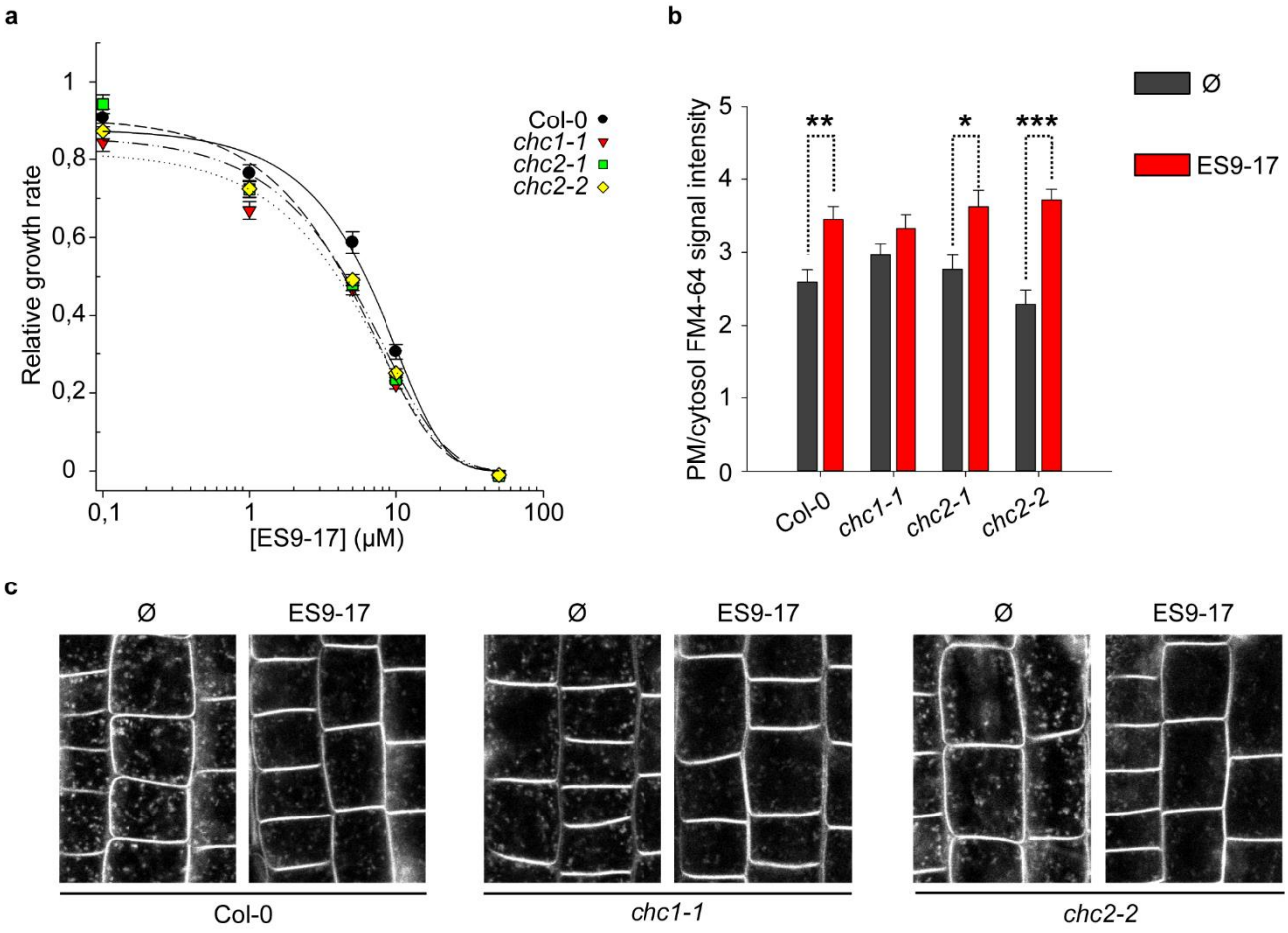

Supplemental Figure 4. *chc1-1* and *chc2-2* are more sensitive to ES9-17

(**a**) Root growth upon transfer to ES9-17 containing medium of 5 days old seedlings as measured after 48 hours. Relative to mock (Ø) treatment. (**b**) Quantification of FM4-64 uptake for seedlings treated for 15 min after pre-treatment with 6 µM ES9-17 for 15 min. *P<0.5 **P<0.01 ***P<0.001 for a two-sided Student's *t*-test. N is at least 9 biological repeats. (**c**) Representative images for FM4-64 uptake in (**b**).

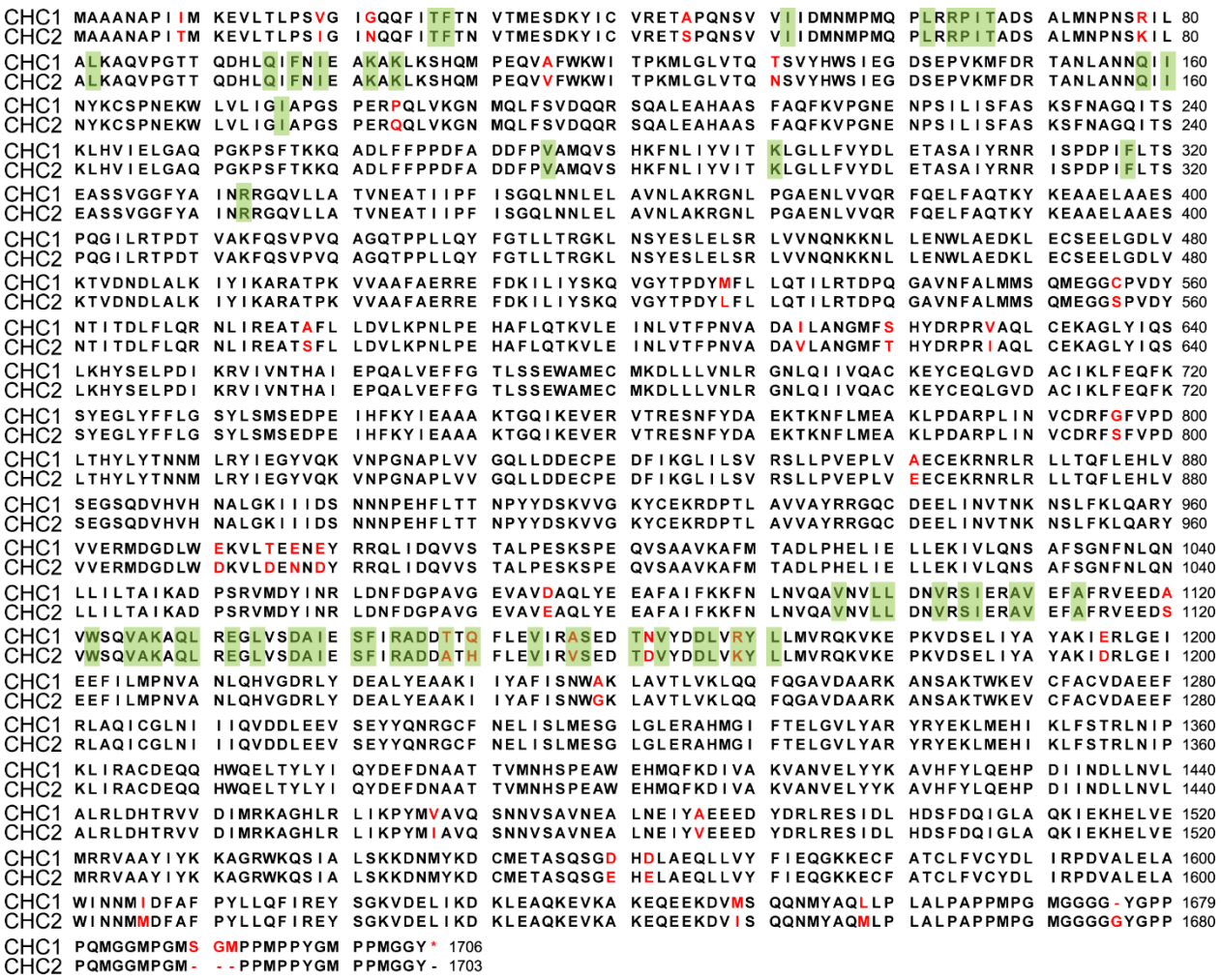

Supplemental Figure 5. CHC1 and CHC2 are very similar in amino acid sequence.

Amino acid sequence alignment of *Arabidopsis* CHC1 and CHC2 sequences. Alignment was performed with CLC workbench. Red residues indicate differences between CHC1 and CHC2. Green highlights the residues which are predicted to be part of a binding pocket, according to I-TASSER.

Supplemental Figure 6. *Arabidopsis* CHC1 and Human CHC amino acid sequence alignment

Amino acid sequence alignment of *Arabidopsis* CHC1 and Human CHC sequences. Alignment was performed with CLC workbench. Different types of amino acids are color coded. Consensus sequence (Cons.) is depicted below the alignment. Pink highlight indicate the ATH CHC1 amino acids predicted to be part of a binding pocket, according to I-TASSER.

Supplemental table 1. List of identified proteins for the ES9-10 affinity purification

Numbers indicate the times a protein is found out of 9 repeats (3 biological repeats, each consisting of 3 technical repeats). Proteins which were not found with the ES9-10 analog, yet were present with the ES9-13 analog, are removed. Similarly all proteins found only once with the ES9-10 analog, but present at least once with the ES9-13 analog were removed.

ACCESSION	DESCRIPTION	ES9-10	ES9-13
AT4G34450	coatomer gamma-2 subunit, putative / gamma-2 coat protein, putative / gamma-2 COP, putative	5	0
AT5G53480	ARM repeat superfamily protein	4	0
AT3G11130	Clathrin, heavy chain	4	0
AT5G40370	Glutaredoxin family protein	4	0
AT2G27600	AAA-type ATPase family protein	3	0
AT4G16760	acyl-CoA oxidase 1	3	0
AT5G26210	alfin-like 4	3	0
AT5G55670	RNA-binding (RRM/RBD/RNP motifs) family protein	3	0
AT5G57870	MIF4G domain-containing protein / MA3 domain-containing protein	3	0
AT2G23350	poly(A) binding protein 4	3	0
AT3G12130	KH domain-containing protein / zinc finger (CCCH type) family protein	3	0
AT1G56190	Phosphoglycerate kinase family protein	3	0
AT2G21390	Coatomer, alpha subunit	3	0
AT3G11830	TCP-1/cpn60 chaperonin family protein	3	0
AT5G07440	glutamate dehydrogenase 2	3	0
AT1G14810	semialdehyde dehydrogenase family protein	3	0
AT1G02090	Proteasome component (PCI) domain protein	2	0
AT1G04690	potassium channel beta subunit 1	2	0
AT1G15710	prephenate dehydrogenase family protein	2	0
AT1G35580	cytosolic invertase 1	2	0
AT1G44835	YbaK/aminoacyl-tRNA synthetase-associated domain	2	0
AT1G64790	ILITYHIA	2	0
AT1G70660	MMS ZWEI homologue 2	2	0
AT1G72730	DEA(D/H)-box RNA helicase family protein	2	0
AT2G28760	UDP-XYL synthase 6	2	0
AT2G33340	MOS4-associated complex 3B	2	0
AT2G47730	glutathione S-transferase phi 8	2	0
AT3G03570	Protein of unknown function (DUF3550/UPF0682)	2	0
AT3G51670	SEC14 cytosolic factor family protein / phosphoglyceride transfer family protein	2	0
AT3G51840	acyl-CoA oxidase 4	2	0
AT3G51950	Zinc finger (CCCH-type) family protein / RNA recognition motif (RRM)-containing protein	2	0
AT4G04020	fibrillin	2	0

AT4G11420	eukaryotic translation initiation factor 3A	2	0
AT4G29480	Mitochondrial ATP synthase subunit G protein	2	0
AT4G31480	Coatomer, beta subunit	2	0
AT4G39230	NmrA-like negative transcriptional regulator family protein	2	0
AT5G11880	Pyridoxal-dependent decarboxylase family protein	2	0
AT5G12040	Nitrilase/cyanide hydratase and apolipoprotein N-acyltransferase family protein	2	0
AT5G19990	regulatory particle triple-A ATPase 6A	2	0
AT5G58110	chaperone binding*ATPase activators	2	0
AT1G10270	glutamine-rich protein 23	2	0
AT1G31730	Adaptin family protein	2	0
AT1G35620	PDI-like 5-2	2	0
AT1G48030	mitochondrial lipoamide dehydrogenase 1	2	0
AT1G48170	unknown protein.	2	0
AT1G62740	stress-inducible protein, putative	2	0
AT2G20860	lipoic acid synthase 1	2	0
AT2G42500	protein phosphatase 2A-3	2	0
AT3G07720	Galactose oxidase/kelch repeat superfamily protein	2	0
AT4G20890	tubulin beta-9 chain	2	0
AT5G19820	ARM repeat superfamily protein	2	0
AT5G27640	translation initiation factor 3B1	2	0
AT5G44780	unknown protein	2	0
AT1G06220	Ribosomal protein S5/Elongation factor G/III/V family protein	2	0
AT1G07890	ascorbate peroxidase 1	2	0
AT1G08200	UDP-D-apiose/UDP-D-xylose synthase 2	2	0
AT1G20950	Phosphofructokinase family protein	2	0
AT1G43690	ubiquitin interaction motif-containing protein	2	0
AT1G50200	Alanyl-tRNA synthetase	2	0
AT1G62380	ACC oxidase 2	2	0
AT2G16060	hemoglobin 1	2	0
AT2G18040	peptidylprolyl cis/trans isomerase, NIMA-interacting 1	2	0
AT2G20420	ATP citrate lyase (ACL) family protein	2	0
AT2G43360	Radical SAM superfamily protein	2	0
AT2G47470	thioredoxin family protein	2	0
AT3G09810	isocitrate dehydrogenase VI	2	0
AT3G13460	evolutionarily conserved C-terminal region 2	2	0
AT3G47520	malate dehydrogenase	2	0
AT3G52880	monodehydroascorbate reductase 1	2	0
AT4G16130	arabinose kinase	2	0
AT4G30010	unknown protein	2	0
AT5G20830	sucrose synthase 1	2	0

AT5G26710	Glutamyl/glutaminyl-tRNA synthetase, class Ic	2	0
AT5G52520	Class II aaRS and biotin synthetases superfamily protein	2	0
AT5G66680	dolichyl-diphosphooligosaccharide-protein glycosyltransferase 48kDa subunit family protein	2	0
AT3G23990	heat shock protein 60	2	0
AT5G49910	chloroplast heat shock protein 70-2	2	0
AT1G01470	Late embryogenesis abundant protein	1	0
AT1G01960	SEC7-like guanine nucleotide exchange family protein	1	0
AT1G06060	LisH and RanBPM domains containing protein	1	0
AT1G07170	PHF5-like protein	1	0
AT1G11580	methylesterase PCR A	1	0
AT1G12270	stress-inducible protein, putative	1	0
AT1G13190	RNA-binding (RRM/RBD/RNP motifs) family protein	1	0
AT1G15280	CASC3/Barentsz eIF4AIII binding	1	0
AT1G24280	glucose-6-phosphate dehydrogenase 3	1	0
AT1G29150	non-ATPase subunit 9	1	0
AT1G29900	carbamoyl phosphate synthetase B	1	0
AT1G31780	Protein coding	1	0
AT1G32440	plastidial pyruvate kinase 3	1	0
AT1G33120	Ribosomal protein L6 family	1	0
AT1G36280	L-Aspartase-like family protein	1	0
AT1G48760	delta-adaptin	1	0
AT1G48900	Signal recognition particle, SRP54 subunit protein	1	0
AT1G53310	phosphoenolpyruvate carboxylase 1	1	0
AT1G53750	regulatory particle triple-A 1A	1	0
AT1G59960	NAD(P)-linked oxidoreductase superfamily protein	1	0
AT1G69740	Aldolase superfamily protein	1	0
AT1G70520	cysteine-rich RLK (RECEPTOR-like protein kinase) 2	1	0
AT1G72010	TCP family transcription factor	1	0
AT1G76150	enoyl-CoA hydratase 2	1	0
AT1G76810	eukaryotic translation initiation factor 2 (eIF-2) family protein	1	0
AT1G77670	Pyridoxal phosphate (PLP)-dependent transferases superfamily protein	1	0
AT1G80720	Mitochondrial glycoprotein family protein	1	0
AT2G06530	SNF7 family protein	1	0
AT2G14260.2	proline iminopeptidase	1	0
AT2G15430	DNA-directed RNA polymerase family protein	1	0
AT2G15620	nitrite reductase 1	1	0
AT2G16485	nucleic acid binding*zinc ion binding*DNA binding	1	0
AT2G17130	isocitrate dehydrogenase subunit 2	1	0
AT2G17390	ankyrin repeat-containing 2B	1	0
AT2G20190	CLIP-associated protein	1	0
AT2G20690	lumazine-binding family protein	1	0

AT2G23890	HAD-superfamily hydrolase, subfamily IG, 5'-nucleotidase	1	0
AT2G31240	Tetratricopeptide repeat (TPR)-like superfamily protein	1	0
AT2G31810	ACT domain-containing small subunit of acetolactate synthase protein	1	0
AT2G34970	Trimeric LpxA-like enzyme	1	0
AT2G35690	acyl-CoA oxidase 5	1	0
AT2G36160	Ribosomal protein S11 family protein	1	0
AT2G37790	NAD(P)-linked oxidoreductase superfamily protein	1	0
AT2G40765	unknown protein	1	0
AT2G42120	DNA polymerase delta small subunit	1	0
AT2G42810	protein phosphatase 5.2	1	0
AT2G44350	Citrate synthase family protein	1	0
AT2G45980	unknown protein	1	0
AT3G02360	6-phosphogluconate dehydrogenase family protein	1	0
AT3G05780	lon protease 3	1	0
AT3G06350	dehydroquinate dehydratase, putative / shikimate dehydrogenase, putative	1	0
AT3G06650	ATP-citrate lyase B-1	1	0
AT3G07630	arogenate dehydratase 2	1	0
AT3G13300	Transducin/WD40 repeat-like superfamily protein	1	0
AT3G15590	Tetratricopeptide repeat (TPR)-like superfamily protein	1	0
AT3G17210	heat stable protein 1	1	0
AT3G19170	presequence protease 1	1	0
AT3G22980	Ribosomal protein S5/Elongation factor G/III/V family protein	1	0
AT3G52230	unknown protein	1	0
AT3G54540	general control non-repressible 4	1	0
AT3G55610	delta 1-pyrroline-5-carboxylate synthase 2	1	0
AT3G62010	unknown protein	1	0
AT3G63250	homocysteine methyltransferase 2	1	0
AT4G10320	tRNA synthetase class I (I, L, M and V) family protein	1	0
AT4G24840	Protein coding	1	0
AT4G26840	small ubiquitin-like modifier 1	1	0
AT4G27070	tryptophan synthase beta-subunit 2	1	0
AT4G27490	3'-5'-exoribonuclease family protein	1	0
AT4G28400	Protein phosphatase 2C family protein	1	0
AT4G32050	neurochondrin family protein	1	0
AT4G34040	RING/U-box superfamily protein	1	0
AT4G34110	poly(A) binding protein 2	1	0
AT5G06770	KH domain-containing protein / zinc finger (CCCH type) family protein	1	0
AT5G10470	kinesin like protein for actin based chloroplast movement 1	1	0
AT5G12860	dicarboxylate transporter 1	1	0

AT5G17060	ADP-ribosylation factor B1B	1	0
AT5G22770	alpha-adaptin	1	0
AT5G23060	calcium sensing receptor	1	0
AT5G42970	Proteasome component (PCI) domain protein	1	0
AT5G43940	GroES-like zinc-binding dehydrogenase family protein	1	0
AT5G46280	Minichromosome maintenance (MCM2/3/5) family protein	1	0
AT5G47880	eukaryotic release factor 1-1	1	0
AT5G51430	conserved oligomeric Golgi complex component-related / COG complex component-related	1	0
AT5G53460	NADH-dependent glutamate synthase 1	1	0
AT5G54900	RNA-binding protein 45A	1	0
AT5G58040	homolog of yeast FIP1 [V]	1	0
AT5G58220.3	transthyretin-like protein	1	0
AT5G58410	HEAT/U-box domain-containing protein	1	0
AT5G58490	NAD(P)-binding Rossmann-fold superfamily protein	1	0
AT5G61220	LYR family of Fe/S cluster biogenesis protein	1	0
AT5G65270	RAB GTPase homolog A4A	1	0
ATMG00510	NADH dehydrogenase subunit 7	1	0
AT1G09080	Heat shock protein 70 (Hsp 70) family protein	1	0
AT1G11180	Secretory carrier membrane protein (SCAMP) family protein	1	0
AT1G12310	Calcium-binding EF-hand family protein	1	0
AT1G14510	alfin-like 7	1	0
AT1G23190	Phosphoglucomutase/phosphomannomutase family protein	1	0
AT1G35460	basic helix-loop-helix (bHLH) DNA-binding superfamily protein	1	0
AT1G45000	AAA-type ATPase family protein	1	0
AT1G53260	Protein coding	1	0
AT1G53850	20S proteasome alpha subunit E1	1	0
AT1G66080	unknown protein	1	0
AT1G66240	homolog of anti-oxidant 1	1	0
AT1G69830	alpha-amylase-like 3	1	0
AT1G72550	tRNA synthetase beta subunit family protein	1	0
AT1G80270	PENTATRICOPEPTIDE REPEAT 596	1	0
AT1G80410	tetratricopeptide repeat (TPR)-containing protein	1	0
AT1G80670	Transducin/WD40 repeat-like superfamily protein	1	0
AT2G17630	Pyridoxal phosphate (PLP)-dependent transferases superfamily protein	1	0
AT2G21150	XAP5 family protein	1	0
AT2G22300	signal responsive 1	1	0
AT2G45300	RNA 3'-terminal phosphate cyclase/enolpyruvate transferase, alpha/beta	1	0
AT3G02020	aspartate kinase 3	1	0
AT3G03250	UDP-GLUCOSE PYROPHOSPHORYLASE 1	1	0
AT3G10360	pumilio 4	1	0

AT3G12500	basic chitinase	1	0
AT3G25530	glyoxylate reductase 1	1	0
AT3G47340	glutamine-dependent asparagine synthase 1	1	0
AT3G49680	branched-chain aminotransferase 3	1	0
AT3G52140	tetratricopeptide repeat (TPR)-containing protein	1	0
AT3G57610	adenylosuccinate synthase	1	0
AT3G61960	Protein kinase superfamily protein	1	0
AT4G00620	Amino acid dehydrogenase family protein	1	0
AT4G02350	exocyst complex component sec15B	1	0
AT4G02570	cullin 1	1	0
AT4G04770	ATP binding cassette protein 1	1	0
AT4G09000	general regulatory factor 1	1	0
AT4G11150	vacuolar ATP synthase subunit E1	1	0
AT4G17520	Hyaluronan / mRNA binding family	1	0
AT5G21160	LA RNA-binding protein	1	0
AT5G22480	ZPR1 zinc-finger domain protein	1	0
AT5G43330	Lactate/malate dehydrogenase family protein	1	0
AT5G43830	Aluminium induced protein with YGL and LRDR motifs	1	0
AT5G63620	GroES-like zinc-binding alcohol dehydrogenase family protein	1	0
AT5G64290	dicarboxylate transport 2	1	0
AT5G66420	Uncharacterised conserved protein	1	0
AT1G01620	plasma membrane intrinsic protein 1C	1	0
AT1G07670	endomembrane-type CA-ATPase 4	1	0
AT1G18450	actin-related protein 4	1	0
AT1G64190	6-phosphogluconate dehydrogenase family protein	1	0
AT1G79500	Aldolase-type TIM barrel family protein	1	0
AT1G80480	plastid transcriptionally active 17	1	0
AT2G01350.4	quinolinate phoshoribosyltransferase	1	0
AT2G07640	NAD(P)-binding Rossmann-fold superfamily protein	1	0
AT2G20630	PP2C induced by AVRRPM1	1	0
AT2G36250	Tubulin/FtsZ family protein	1	0
AT2G40290	Eukaryotic translation initiation factor 2 subunit 1	1	0
AT2G40620	Basic-leucine zipper (bZIP) transcription factor family protein	1	0
AT2G41100	Calcium-binding EF hand family protein	1	0
AT3G05530	regulatory particle triple-A ATPase 5A	1	0
AT3G13222	GBF-interacting protein 1	1	0
AT4G01050	thylakoid rhodanese-like	1	0
AT4G02060	Minichromosome maintenance (MCM2/3/5) family protein	1	0
AT4G18480	P-loop containing nucleoside triphosphate hydrolases superfamily protein	1	0
AT4G19540	IND1(iron-sulfur protein required for NADH dehydrogenase)-like	1	0

AT4G31300	N-terminal nucleophile aminohydrolases (Ntn hydrolases) superfamily protein	1	0
AT4G38630	regulatory particle non-ATPase 10	1	0
AT5G10940	transducin family protein / WD-40 repeat family protein	1	0
AT5G16510	Alpha-1,4-glucan-protein synthase family protein	1	0
AT5G24520	Transducin/WD40 repeat-like superfamily protein	1	0
AT5G39570	Protein coding	1	0
AT5G50920	CLPC homologue 1	1	0
AT5G54430	Adenine nucleotide alpha hydrolases-like superfamily protein	1	0
AT5G60980	Nuclear transport factor 2 (NTF2) family protein with RNA binding (RRM-RBD-RNP motifs) domain	1	0
AT5G62690	tubulin beta chain 2	1	0
AT1G66410	calmodulin 4	1	0
AT1G51710	ubiquitin-specific protease 6	6	1
AT2G42520	P-loop containing nucleoside triphosphate hydrolases superfamily protein	6	1
AT1G79920	Heat shock protein 70 (Hsp 70) family protein	6	1
AT1G56410	heat shock protein 70 (Hsp 70) family protein	5	1
AT1G49760	poly(A) binding protein 8	4	1
AT1G09640	Translation elongation factor EF1B, gamma chain	4	1
AT1G14980	chaperonin 10	4	1
AT5G20890	TCP-1/cpn60 chaperonin family protein	4	1
AT5G13110	glucose-6-phosphate dehydrogenase 2	4	1
AT1G42970	glyceraldehyde-3-phosphate dehydrogenase B subunit	3	1
AT2G31660	ARM repeat superfamily protein	3	1
AT3G03910	glutamate dehydrogenase 3	3	1
AT2G47510	fumarase 1	3	1
AT3G43190	sucrose synthase 4	3	1
AT5G50850	Transketolase family protein	3	1
AT1G07370	proliferating cellular nuclear antigen 1	3	1
AT1G52760	lysophospholipase 2	3	1
AT2G32730	26S proteasome regulatory complex, non-ATPase subcomplex, Rpn2/Psmd1 subunit	3	1
AT2G45620	Nucleotidyltransferase family protein	3	1
AT3G07770	HEAT SHOCK PROTEIN 89	3	1
AT3G59820	LETM1-like protein	3	1
AT4G15410	serine/threonine protein phosphatase 2A 55 kDa regulatory subunit B prime gamma	3	1
AT4G24190	Chaperone protein htpG family protein	3	1
AT4G39260	cold, circadian rhythm, and RNA binding 1	3	1
AT5G10860	Cystathionine beta-synthase (CBS) family protein	3	1
AT5G26360	TCP-1/cpn60 chaperonin family protein	3	1
AT5G65430	general regulatory factor 8	3	1

AT5G67630	P-loop containing nucleoside triphosphate hydrolases superfamily protein	3	1
AT1G18500	methylthioalkylmalate synthase-like 4	3	1
AT3G13920	eukaryotic translation initiation factor 4A1	3	1
AT5G22060	DNAJ homologue 2	3	1
AT5G15530	biotin carboxyl carrier protein 2	3	1
AT3G50370	unknown protein	3	1
AT4G33030	sulfoquinovosyldiacylglycerol 1	3	1
AT1G17720	Protein phosphatase 2A, regulatory subunit PR55	2	1
AT1G60690	NAD(P)-linked oxidoreductase superfamily protein	2	1
AT1G65220	ARM repeat superfamily protein	2	1
AT1G71220	UDP-glucose:glycoprotein glucosyltransferases	2	1
AT2G01140	Aldolase superfamily protein	2	1
AT2G36060	MMS ZWEI homologue 3	2	1
AT2G44100	guanosine nucleotide diphosphate dissociation inhibitor 1	2	1
AT3G02260	auxin transport protein (BIG)	2	1
AT4G05530	indole-3-butyric acid response 1	2	1
AT5G05990	Mitochondrial glycoprotein family protein	2	1
AT5G17000	Zinc-binding dehydrogenase family protein	2	1
AT5G17270	Protein prenylyltransferase superfamily protein	2	1
AT5G35790	glucose-6-phosphate dehydrogenase 1	2	1
AT5G44720	Molybdenum cofactor sulfurase family protein	2	1
AT5G51110	Transcriptional coactivator/pterin dehydratase	2	1
AT5G67560	ADP-ribosylation factor-like A1D	2	1
AT1G52360	Coatomer, beta' subunit	2	1
AT1G62020	Coatomer, alpha subunit	2	1
AT1G78650	DNA-directed DNA polymerases	2	1
AT2G01190	Octicosapeptide/Phox/Bem1p family protein	2	1
AT2G18510	RNA-binding (RRM/RBD/RNP motifs) family protein	2	1
AT2G25970	KH domain-containing protein	2	1
AT2G41220	glutamate synthase 2	2	1
AT3G05790	lon protease 4	2	1
AT3G09840	cell division cycle 48	2	1
AT3G52180	dual specificity protein phosphatase (DsPTP1) family protein	2	1
AT3G54360	zinc ion binding	2	1
AT3G55380	ubiquitin-conjugating enzyme 14	2	1
AT3G60240.2	eukaryotic translation initiation factor 4G	2	1
AT4G01100	adenine nucleotide transporter 1	2	1
AT4G20850	tripeptidyl peptidase ii	2	1
AT5G23140	nuclear-encoded CLP protease P7	2	1
AT5G37510	NADH-ubiquinone dehydrogenase, mitochondrial, putative	2	1

AT5G41210	glutathione S-transferase THETA 1	2	1
AT5G42220	Ubiquitin-like superfamily protein	2	1
AT1G04810	26S proteasome regulatory complex, non-ATPase subcomplex, Rpn2/Psmd1 subunit	2	1
AT1G07360	CCCH-type zinc fingerfamily protein with RNA-binding domain	2	1
AT1G10200	GATA type zinc finger transcription factor family protein	2	1
AT1G11840	glyoxalase I homolog	2	1
AT1G13870	calmodulin binding*purine nucleotide binding	2	1
AT1G15870	Mitochondrial glycoprotein family protein	2	1
AT1G16300	glyceraldehyde-3-phosphate dehydrogenase of plastid 2	2	1
AT1G20010	tubulin beta-5 chain	2	1
AT1G24360	NAD(P)-binding Rossmann-fold superfamily protein	2	1
AT1G28200	FH interacting protein 1	2	1
AT1G34430	2-oxoacid dehydrogenases acyltransferase family protein	2	1
AT1G35160	GF14 protein phi chain	2	1
AT1G51690	protein phosphatase 2A 55 kDa regulatory subunit B alpha isoform	2	1
AT1G69230	SPIRAL1-like2	2	1
AT1G71270	Vps52 / Sac2 family	2	1
AT1G79550	phosphoglycerate kinase	2	1
AT2G03680	spiral1	2	1
AT2G07690	Minichromosome maintenance (MCM2/3/5) family protein	2	1
AT2G07727	Di-haem cytochrome, transmembrane*Cytochrome b/b6, C-terminal	2	1
AT2G17980	Sec1/munc18-like (SM) proteins superfamily	2	1
AT2G31390	pfkB-like carbohydrate kinase family protein	2	1
AT3G08590	Phosphoglycerate mutase, 2,3-bisphosphoglycerate-independent	2	1
AT3G13860	heat shock protein 60-3A	2	1
AT3G19760	eukaryotic initiation factor 4A-III	2	1
AT3G20250	pumilio 5	2	1
AT3G48750	cell division control 2	2	1
AT3G48870	Clp ATPase	2	1
AT3G52300	ATP synthase D chain, mitochondrial	2	1
AT4G09320	Nucleoside diphosphate kinase family protein	2	1
AT4G27585	SPFH/Band 7/PHB domain-containing membrane-associated protein family	2	1
AT4G31790	Tetrapyrrole (Corrin/Porphyrin) Methylases	2	1
AT5G06460	ubiquitin activating enzyme 2	2	1
AT5G10240	asparagine synthetase 3	2	1
AT5G11670	NADP-malic enzyme 2	2	1
AT5G12850	CCCH-type zinc finger protein with ARM repeat domain	2	1
AT5G13420	Aldolase-type TIM barrel family protein	2	1
AT5G16050	general regulatory factor 5	2	1

AT5G16290	VALINE-TOLERANT 1	2	1
AT5G17310.2	UDP-glucose pyrophosphorylase 2	2	1
AT5G27600	long-chain acyl-CoA synthetase 7	2	1
AT5G38480	general regulatory factor 3	2	1
AT5G40190	RNA ligase/cyclic nucleotide phosphodiesterase family protein	2	1
AT5G54770	thiazole biosynthetic enzyme, chloroplast (ARA6) (THI1) (THI4)	2	1
AT1G72370	40s ribosomal protein SA	2	1
AT3G29360	UDP-glucose 6-dehydrogenase family protein	2	1
AT5G12110	Glutathione S-transferase, C-terminal-like*Translation elongation factor EF1B/ribosomal protein S6	2	1
AT5G60170	RNA binding (RRM/RBD/RNP motifs) family protein	2	1
AT2G22250	aspartate aminotransferase	2	1
AT5G66760	succinate dehydrogenase 1-1	2	1
AT3G03780	methionine synthase 2	6	2
AT4G27440	protochlorophyllide oxidoreductase B	6	2
AT3G09440	Heat shock protein 70 (Hsp 70) family protein	6	2
AT2G25140	casein lytic proteinase B4	6	2
AT1G52670	Single hybrid motif superfamily protein	5	2
AT3G60750	Transketolase	5	2
AT3G63460	transducin family protein / WD-40 repeat family protein	5	2
AT1G27450.2	adenine phosphoribosyl transferase 1	5	2
AT5G17920	Cobalamin-independent synthase family protein	5	2
AT2G16600	rotamase CYP 3	4	2
AT3G22330	putative mitochondrial RNA helicase 2	4	2
AT3G18190	TCP-1/cpn60 chaperonin family protein	4	2
AT3G22200	Pyridoxal phosphate (PLP)-dependent transferases superfamily protein	4	2
AT3G16950	lipoamide dehydrogenase 1	4	2
AT1G71380	cellulase 3	4	2
AT1G12410	CLP protease proteolytic subunit 2	3	2
AT1G22920	COP9 signalosome 5A	3	2
AT1G26570	UDP-glucose dehydrogenase 1	3	2
AT2G44310	Calcium-binding EF-hand family protein	3	2
AT3G22430	Protein coding	3	2
AT3G02520	general regulatory factor 7	3	2
AT3G56150	eukaryotic translation initiation factor 3C	3	2
AT4G19880	Glutathione S-transferase family protein	3	2
AT1G15140	FAD/NAD(P)-binding oxidoreductase	3	2
AT1G27970	nuclear transport factor 2B	3	2
AT1G70770	Protein of unknown function DUF2359, transmembrane	3	2
AT1G79340	metacaspase 4	3	2
AT1G79530	glyceraldehyde-3-phosphate dehydrogenase of plastid 1	3	2

AT2G45140	plant VAP homolog 12	3	2
AT3G22890	ATP sulfurylase 1	3	2
AT3G43300	HOPM interactor 7	3	2
AT3G55440	triosephosphate isomerase	3	2
AT5G11340	Acyl-CoA N-acyltransferases (NAT) superfamily protein	3	2
AT5G15770	glucose-6-phosphate acetyltransferase 1	3	2
AT5G20720	chaperonin 20	3	2
AT5G42790	proteasome alpha subunit F1	3	2
AT5G45130	RAB homolog 1	3	2
AT5G65020	annexin 2	3	2
AT1G53240	Lactate/malate dehydrogenase family protein	3	2
AT1G73010	phosphate starvation-induced gene 2	3	2
AT3G46060	RAB GTPase homolog 8A	3	2
AT3G51160	NAD(P)-binding Rossmann-fold superfamily protein	3	2
AT4G20020	unknown protein	3	2
AT4G28440	Nucleic acid-binding, OB-fold-like protein	3	2
AT4G34870	rotamase cyclophilin 5	3	2
AT5G13260	unknown protein	3	2
AT5G17380	Thiamine pyrophosphate dependent pyruvate decarboxylase family protein	3	2
AT5G56030	heat shock protein 81-2	3	2
AT5G58290	regulatory particle triple-A ATPase 3	3	2
AT5G59710	VIRE2 interacting protein 2	3	2
AT1G36160	acetyl-CoA carboxylase 1	3	2
AT2G16440	Minichromosome maintenance (MCM2/3/5) family protein	3	2
AT2G38940	phosphate transporter 1*4	3	2
AT2G43140	basic helix-loop-helix (bHLH) DNA-binding superfamily protein	3	2
AT2G05990	NAD(P)-binding Rossmann-fold superfamily protein	3	2
AT3G07810	RNA-binding (RRM/RBD/RNP motifs) family protein	3	2
AT5G64260	EXORDIUM like 2	3	2
AT1G49600	RNA-binding protein 47A	2	2
AT3G42790	alfin-like 3	2	2
AT5G16730	Plant protein of unknown function (DUF827)	2	2
AT1G16890.2	ubiquitin-conjugating enzyme 36	2	2
AT1G32580	plastid developmental protein DAG, putative	2	2
AT2G03230	GCK domain-containing protein	2	2
AT2G20140	AAA-type ATPase family protein	2	2
AT3G02090	Insulinase (Peptidase family M16) protein	2	2
AT4G17510	ubiquitin C-terminal hydrolase 3	2	2
AT5G03290	isocitrate dehydrogenase V	2	2
AT5G12370	exocyst complex component sec10	2	2
AT5G25940	early nodulin-related	2	2

AT5G27770	Ribosomal L22e protein family	2	2
AT1G09100	26S proteasome AAA-ATPase subunit RPT5B	2	2
AT1G16520	unknown protein	2	2
AT1G30890	Integral membrane HRF1 family protein	2	2
AT1G43190	polypyrimidine tract-binding protein 3	2	2
AT2G02470	alfin-like 6	2	2
AT2G02740	ssDNA-binding transcriptional regulator	2	2
AT2G41530	S-formylglutathione hydrolase	2	2
AT2G46520	cellular apoptosis susceptibility protein, putative / importin-alpha re-exporter, putative	2	2
AT3G03660	WUSCHEL related homeobox 11	2	2
AT3G10380	subunit of exocyst complex 8	2	2
AT3G45770	Polyketide synthase, enoylreductase family protein	2	2
AT3G52560	ubiquitin E2 variant 1D-4	2	2
AT3G55620	Translation initiation factor IF6	2	2
AT3G60830	actin-related protein 7	2	2
AT4G11380	Adaptin family protein	2	2
AT4G23650	calcium-dependent protein kinase 6	2	2
AT4G27270	Quinone reductase family protein	2	2
AT4G34200	D-3-phosphoglycerate dehydrogenase	2	2
AT4G37190	Protein coding	2	2
AT4G38740	rotamase CYP 1	2	2
AT5G02500	heat shock cognate protein 70-1	2	2
AT5G08300	Succinyl-CoA ligase, alpha subunit	2	2
AT5G12150	Rho GTPase activation protein (RhoGAP) with PH domain	2	2
AT5G16300	Vps51/Vps67 family (components of vesicular transport) protein	2	2
AT5G55280	homolog of bacterial cytokinesis Z-ring protein FTSZ 1-1	2	2
AT5G56290	peroxin 5	2	2
AT1G51980	Insulinase (Peptidase family M16) protein	2	2
AT2G39770	Glucose-1-phosphate adenylyltransferase family protein	2	2
AT4G33070	Thiamine pyrophosphate dependent pyruvate decarboxylase family protein	2	2
AT5G12250	beta-6 tubulin	2	2
AT5G52920	plastidic pyruvate kinase beta subunit 1	2	2
AT2G29550	tubulin beta-7 chain	2	2
AT4G34030	3-methylcrotonyl-CoA carboxylase	2	2
AT5G23540	Mov34/MPN/PAD-1 family protein	2	2
AT5G52640	heat shock protein 90	6	3
AT3G48560	chlorsulfuron/imidazolinone resistant 1	6	3
AT2G02560	cullin-associated and neddylation dissociated	6	3
AT3G02530	TCP-1/cpn60 chaperonin family protein	6	3

AT2G39730	rubisco activase	5	3
AT2G21330	fructose-bisphosphate aldolase 1	5	3
AT1G16030	heat shock protein 70B	4	3
AT1G12000	Phosphofructokinase family protein	4	3
AT1G13440	glyceraldehyde-3-phosphate dehydrogenase C2	4	3
AT3G04880	DNA-damage-repair/toleration protein (DRT102)	3	3
AT1G30630	Coatomer epsilon subunit	3	3
AT1G79230	mercaptopyruvate sulfurtransferase 1	3	3
AT2G43090	Aconitase/3-isopropylmalate dehydratase protein	3	3
AT3G22850	Aluminium induced protein with YGL and LRDR motifs	3	3
AT3G44110	DNAJ homologue 3	3	3
AT1G04410	Lactate/malate dehydrogenase family protein	3	3
AT1G07705	NOT2 / NOT3 / NOT5 family	3	3
AT1G32500	non-intrinsic ABC protein 6	3	3
AT2G36530	Enolase	3	3
AT3G15660	glutaredoxin 4	3	3
AT3G20050	T-complex protein 1 alpha subunit	3	3
AT3G56240	copper chaperone	3	3
AT3G62120	Class II aaRS and biotin synthetases superfamily protein	3	3
AT5G22650	histone deacetylase 2B	3	3
AT1G50570	Calcium-dependent lipid-binding (CaLB domain) family protein	3	3
AT2G05710	aconitase 3	3	3
AT1G35720	annexin 1	3	3
AT1G53500	NAD-dependent epimerase/dehydratase family protein	3	3
AT1G69410	eukaryotic elongation factor 5A-3	3	3
AT3G54470	uridine 5'-monophosphate synthase / UMP synthase (PYRE-F) (UMPS)	3	3
AT4G29840	Pyridoxal-5'-phosphate-dependent enzyme family protein	2	3
AT1G22840	CYTOCHROME C-1	2	3
AT1G52730	Transducin/WD40 repeat-like superfamily protein	2	3
AT3G53580	diaminopimelate epimerase family protein	2	3
AT4G25130	peptide met sulfoxide reductase 4	2	3
AT5G20060	alpha/beta-Hydrolases superfamily protein	2	3
AT1G20110	RING/FYVE/PHD zinc finger superfamily protein	2	3
AT3G08530	Clathrin, heavy chain	2	3
AT5G15490	UDP-glucose 6-dehydrogenase family protein	2	3
AT5G55530	Calcium-dependent lipid-binding (CaLB domain) family protein	2	3
AT1G63000	nucleotide-rhamnose synthase/epimerase-reductase	2	3
AT4G24280	chloroplast heat shock protein 70-1	7	4
AT1G77120	alcohol dehydrogenase 1	6	4
AT1G03090.2	methylcrotonyl-CoA carboxylase alpha chain, mitochondrial / 3-methylcrotonyl-CoA carboxylase 1 (MCCA)	6	4
AT2G16570	GLN phosphoribosyl pyrophosphate amidotransferase 1	6	4

AT5G14040	phosphate transporter 3*1	5	4
AT2G27730	copper ion binding	4	4
AT2G21660	cold, circadian rhythm, and rna binding 2	4	4
AT1G24510	TCP-1/cpn60 chaperonin family protein	4	4
AT3G12050	Aha1 domain-containing protein	4	4
AT5G28540	heat shock protein 70 (Hsp 70) family protein	4	4
AT5G16710	dehydroascorbate reductase 1	4	4
AT5G44340	tubulin beta chain 4	3	4
AT5G20010	RAS-related nuclear protein-1	3	4
AT5G02490	Heat shock protein 70 (Hsp 70) family protein	2	4
AT5G09810	actin 7	2	4
AT3G62530	ARM repeat superfamily protein	9	5
AT2G37620	actin 1	8	5
AT1G49240	actin 8	7	5
AT5G56000	HEAT SHOCK PROTEIN 81.4	6	5
AT2G44060	Late embryogenesis abundant protein, group 2	6	5
AT3G25860	2-oxoacid dehydrogenases acyltransferase family protein	6	5
AT2G04030	Chaperone protein htpG family protein	5	5
AT2G36460	Aldolase superfamily protein	4	5
AT3G08580	ADP/ATP carrier 1	4	5
AT2G20580	26S proteasome regulatory subunit S2 1A	4	5
AT3G56130	biotin/lipoyl attachment domain-containing protein	4	5
AT5G13280	aspartate kinase 1	3	5
AT1G55490	chaperonin 60 beta	9	6
AT3G12580	heat shock protein 70	8	6
AT1G54270	eif4a-2	8	6
AT1G78900	vacuolar ATP synthase subunit A	8	6
AT5G65720	nitrogen fixation S (NIFS)-like 1	7	6
AT1G56070	Ribosomal protein S5/Elongation factor G/III/V family protein	7	6
AT3G52930	Aldolase superfamily protein	7	6
AT1G43800	Plant stearoyl-acyl-carrier-protein desaturase family protein	6	6
AT5G35360	acetyl Co-enzyme a carboxylase biotin carboxylase subunit	6	6
AT5G18230	transcription regulator NOT2/NOT3/NOT5 family protein	6	6
AT2G45290	Transketolase	6	6
AT1G24300	GYF domain-containing protein	5	6
AT5G16390	chloroplastic acetylcoenzyme A carboxylase 1	5	6
AT4G02930	GTP binding Elongation factor Tu family protein	9	7
AT4G20360	RAB GTPase homolog E1B	9	7
AT5G08670	ATP synthase alpha/beta family protein	9	7
AT2G07698	ATPase, F1 complex, alpha subunit protein	9	7
AT3G17390	S-adenosylmethionine synthetase family protein	9	7

AT5G09590	mitochondrial HSO70 2	9	7
AT1G26630	Eukaryotic translation initiation factor 5A-1 (eIF-5A 1) protein	6	7
AT1G27430	GYF domain-containing protein	6	7
AT2G28000	chaperonin-60alpha	6	7
AT1G07920	GTP binding Elongation factor Tu family protein	9	8
AT3G04120	glyceraldehyde-3-phosphate dehydrogenase C subunit 1	8	8
AT5G19550	aspartate aminotransferase 2	8	8
AT3G03960	TCP-1/cpn60 chaperonin family protein	7	8
AT4G37910	mitochondrial heat shock protein 70-1	9	9
AT1G04820	tubulin alpha-4 chain	8	9

Supplemental table 2. List of identified proteins for the ES9-18 affinity purification

Numbers indicate the times a protein is found out of 3 biological repeats. Proteins which were not found with the ES9-18 analog, yet were present with the ES9-13 analog, are removed. Similarly all proteins found only once with the ES9-18 analog, but present at least once with the ES9-13 analog were removed.

ACCESSION	DESCRIPTION	ES9-18	ES9-13
AT3G01540	DEAD box RNA helicase 1	3	0
AT4G36210.3	Protein of unknown function (DUF726)	3	0
AT1G09870	histidine acid phosphatase family protein	2	0
AT1G22840	CYTOCHROME C-1	2	0
AT1G31910	GHMP kinase family protein	2	0
AT1G34430	2-oxoacid dehydrogenases acyltransferase family protein	2	0
AT1G70660	MMS ZWEI homologue 2	2	0
AT1G72150	PATELLIN 1	2	0
AT1G73430	sec34-like family protein	2	0
AT2G05990	NAD(P)-binding Rossmann-fold superfamily protein	2	0
AT3G04120	glyceraldehyde-3-phosphate dehydrogenase C subunit 1	2	0
AT4G18480	P-loop containing nucleoside triphosphate hydrolases superfamily protein	2	0
AT4G29840	Pyridoxal-5'-phosphate-dependent enzyme family protein	2	0
AT5G05980	DHFS-FPGS homolog B	2	0
AT5G19990	regulatory particle triple-A ATPase 6A	2	0
AT5G48300	ADP glucose pyrophosphorylase 1	2	0
AT1G01960	SEC7-like guanine nucleotide exchange family protein	1	0
AT1G03630	protochlorophyllide oxidoreductase C	1	0
AT1G04620	coenzyme F420 hydrogenase family / dehydrogenase, beta subunit family	1	0
AT1G06410	trehalose-phosphatase/synthase 7	1	0
AT1G07360	CCCH-type zinc fingerfamily protein with RNA-binding domain	1	0
AT1G07370	proliferating cellular nuclear antigen 1	1	0
AT1G07790	Histone superfamily protein	1	0

AT1G08200	UDP-D-apiose/UDP-D-xylose synthase 2	1	0
AT1G09430	ATP-citrate lyase A-3	1	0
AT1G11840	glyoxalase I homolog	1	0
AT1G12775	Pentatricopeptide repeat (PPR) superfamily protein	1	0
AT1G13450	Homeodomain-like superfamily protein	1	0
AT1G14360	UDP-galactose transporter 3	1	0
AT1G15210	pleiotropic drug resistance 7	1	0
AT1G15710	prephenate dehydrogenase family protein	1	0
AT1G15910	XH/XS domain-containing protein	1	0
AT1G16520	unknown protein	1	0
AT1G18450	actin-related protein 4	1	0
AT1G18500	methylthioalkylmalate synthase-like 4	1	0
AT1G20260	ATPase, V1 complex, subunit B protein	1	0
AT1G20950	Phosphofructokinase family protein	1	0
AT1G23260	MMS ZWEI homologue 1	1	0
AT1G30890	Integral membrane HRF1 family protein	1	0
AT1G31230	aspartate kinase-homoserine dehydrogenase i	1	0
AT1G31800	cytochrome P450, family 97, subfamily A, polypeptide 3	1	0
AT1G32350	alternative oxidase 1D	1	0
AT1G42550	plastid movement impaired1	1	0
AT1G42970	glyceraldehyde-3-phosphate dehydrogenase B subunit	1	0
AT1G74310	heat shock protein 101	1	0
AT1G77730	Pleckstrin homology (PH) domain superfamily protein	1	0
AT2G14120	dynamin related protein	1	0
AT2G23370	unknown protein	1	0
AT2G26660	SPX domain gene 2	1	0
AT2G29470	glutathione S-transferase tau 3	1	0
AT2G33040	gamma subunit of Mt ATP synthase	1	0
AT2G42890	MEI2-like 2	1	0
AT2G42910	Phosphoribosyltransferase family protein	1	0
AT2G47730	glutathione S-transferase phi 8	1	0
AT3G02080	Ribosomal protein S19e family protein	1	0
AT3G03570	Protein of unknown function (DUF3550/UPF0682)	1	0
AT3G05590	ribosomal protein L18	1	0
AT3G08943	ARM repeat superfamily protein	1	0
AT3G09200	Ribosomal protein L10 family protein	1	0
AT3G10950	Zinc-binding ribosomal protein family protein	1	0
AT3G11510	Ribosomal protein S11 family protein	1	0
AT3G16950	lipoamide dehydrogenase 1	1	0
AT3G22270	Topoisomerase II-associated protein PAT1	1	0
AT3G29360	UDP-glucose 6-dehydrogenase family protein	1	0
AT3G48850	phosphate transporter 3*2	1	0

AT3G48860	unknown protein	1	0
AT3G50370	unknown protein	1	0
AT3G51550	Malectin/receptor-like protein kinase family protein	1	0
AT3G62010	unknown protein	1	0
AT4G02570	cullin 1	1	0
AT4G04910	AAA-type ATPase family protein	1	0
AT4G13890	Pyridoxal phosphate (PLP)-dependent transferases superfamily protein	1	0
AT4G21710	DNA-directed RNA polymerase family protein	1	0
AT4G22000	unknown protein	1	0
AT4G22380	Ribosomal protein L7Ae/L30e/S12e/Gadd45 family protein	1	0
AT4G34450	coatomer gamma-2 subunit, putative / gamma-2 coat protein, putative / gamma-2 COP, putative	1	0
AT5G01010	Protein coding	1	0
AT5G02490	Heat shock protein 70 (Hsp 70) family protein	1	0
AT5G06970	Protein of unknown function (DUF810)	1	0
AT5G08300	Succinyl-CoA ligase, alpha subunit	1	0
AT5G08740	NAD(P)H dehydrogenase C1	1	0
AT5G09810	actin 7	1	0
AT5G10860	Cystathionine beta-synthase (CBS) family protein	1	0
AT5G16210	HEAT repeat-containing protein	1	0
AT5G16730	Plant protein of unknown function (DUF827)	1	0
AT5G20650	copper transporter 5	1	0
AT5G25270	Ubiquitin-like superfamily protein	1	0
AT5G26040	histone deacetylase 2	1	0
AT5G43010	regulatory particle triple-A ATPase 4A	1	0
AT5G49830	exocyst complex component 84B	1	0
AT5G50210	quinolinate synthase	1	0
AT5G50870	ubiquitin-conjugating enzyme 27	1	0
AT5G53930	unknown protein	1	0
AT5G62690	tubulin beta chain 2	1	0
AT5G67630	P-loop containing nucleoside triphosphate hydrolases superfamily protein	1	0
AT1G29150	non-ATPase subunit 9	3	1
AT1G53500	NAD-dependent epimerase/dehydratase family protein	3	1
AT1G56500	haloacid dehalogenase-like hydrolase family protein	3	1
AT1G70770	Protein of unknown function DUF2359, transmembrane	3	1
AT3G14390	Pyridoxal-dependent decarboxylase family protein	3	1
AT3G55620	Translation initiation factor IF6	3	1
AT5G16300	Vps51/Vps67 family (components of vesicular transport) protein	3	1
AT5G52520	Class II aaRS and biotin synthetases superfamily protein	3	1
AT5G60980	Nuclear transport factor 2 (NTF2) family protein with RNA binding (RRM-RBD-RNP motifs) domain	3	1

ATCG00470	ATP synthase epsilon chain	3	1
AT1G02690	importin alpha isoform 6	2	1
AT1G04750	vesicle-associated membrane protein 721	2	1
AT1G07180	alternative NAD(P)H dehydrogenase 1	2	1
AT1G24510	TCP-1/cpn60 chaperonin family protein	2	1
AT1G36160	acetyl-CoA carboxylase 1	2	1
AT1G37130	nitrate reductase 2	2	1
AT1G51980	Insulinase (Peptidase family M16) protein	2	1
AT1G71820	SEC6	2	1
AT1G76810	eukaryotic translation initiation factor 2 (eIF-2) family protein	2	1
AT1G78650	DNA-directed DNA polymerases	2	1
AT1G79920	Heat shock protein 70 (Hsp 70) family protein	2	1
AT2G15620	nitrite reductase 1	2	1
AT2G21790	ribonucleotide reductase 1	2	1
AT2G43160	ENTH/VHS family protein	2	1
AT3G02260	auxin transport protein (BIG)	2	1
AT3G05560	Ribosomal L22e protein family	2	1
AT3G05680	embryo defective 2016	2	1
AT3G08530	Clathrin, heavy chain	2	1
AT3G12760	Protein coding	2	1
AT3G15450	Aluminium induced protein with YGL and LRDR motifs	2	1
AT3G21110	purin 7	2	1
AT3G22310	putative mitochondrial RNA helicase 1	2	1
AT3G57350	Nucleoporin interacting component (Nup93/Nic96-like) family protein	2	1
AT3G62460	Putative endonuclease or glycosyl hydrolase	2	1
AT3G63460	transducin family protein / WD-40 repeat family protein	2	1
AT4G02060	Minichromosome maintenance (MCM2/3/5) family protein	2	1
AT5G04910	unknown protein	2	1
AT5G09890	Protein kinase family protein	2	1
AT5G11060	KNOTTED1-like homeobox gene 4	2	1
AT5G13260	unknown protein	2	1
AT5G13280	aspartate kinase 1	2	1
AT5G15770	glucose-6-phosphate acetyltransferase 1	2	1
AT5G16050	general regulatory factor 5	2	1
AT5G44720	Molybdenum cofactor sulfurase family protein	2	1
AT5G58290	regulatory particle triple-A ATPase 3	2	1
AT5G64270	splicing factor, putative	2	1
AT5G65020	annexin 2	2	1
AT1G04290	Thioesterase superfamily protein	3	2
AT1G22410	Class-II DAHP synthetase family protein	3	2
AT1G33120	Ribosomal protein L6 family	3	2

AT1G51710	ubiquitin-specific protease 6	3	2
AT2G04030	Chaperone protein htpG family protein	3	2
AT2G07727	Di-haem cytochrome, transmembrane*Cytochrome b/b6, C-terminal	3	2
AT2G15860	unknown protein	3	2
AT2G16440	Minichromosome maintenance (MCM2/3/5) family protein	3	2
AT2G16570	GLN phosphoribosyl pyrophosphate amidotransferase 1	3	2
AT2G20140	AAA-type ATPase family protein	3	2
AT2G21600	endoplasmatic reticulum retrieval protein 1B	3	2
AT2G22170	Lipase/lipooxygenase, PLAT/LH2 family protein	3	2
AT2G31660	ARM repeat superfamily protein	3	2
AT2G36530	Enolase	3	2
AT2G39770	Glucose-1-phosphate adenylyltransferase family protein	3	2
AT2G45140	plant VAP homolog 12	3	2
AT3G02530	TCP-1/cpn60 chaperonin family protein	3	2
AT3G04880	DNA-damage-repair/toleration protein (DRT102)	3	2
AT3G05790	lon protease 4	3	2
AT3G09840	cell division cycle 48	3	2
AT3G12580	heat shock protein 70	3	2
AT3G15410	Leucine-rich repeat (LRR) family protein	3	2
AT3G20050	T-complex protein 1 alpha subunit	3	2
AT3G22200	Pyridoxal phosphate (PLP)-dependent transferases superfamily protein	3	2
AT3G23400	Plastid-lipid associated protein PAP / fibrillin family protein	3	2
AT3G45190	SIT4 phosphatase-associated family protein	3	2
AT3G51140	Protein of unknown function (DUF3353)	3	2
AT3G62120	Class II aaRS and biotin synthetases superfamily protein	3	2
AT4G24840	Protein coding	3	2
AT4G28440	Nucleic acid-binding, OB-fold-like protein	3	2
AT4G34490	cyclase associated protein 1	3	2
AT5G03290	isocitrate dehydrogenase V	3	2
AT5G17380	Thiamine pyrophosphate dependent pyruvate decarboxylase family protein	3	2
AT5G18230	transcription regulator NOT2/NOT3/NOT5 family protein	3	2
AT5G27770	Ribosomal L22e protein family	3	2
AT5G28540	heat shock protein 70 (Hsp 70) family protein	3	2
AT5G35360	acetyl Co-enzyme a carboxylase biotin carboxylase subunit	3	2
AT5G42150	Glutathione S-transferase family protein	3	2
AT5G43970	translocase of outer membrane 22-V	3	2
AT5G62810	peroxin 14	3	2
AT5G66760	succinate dehydrogenase 1-1	3	2
AT1G10270	glutamine-rich protein 23	2	2
AT1G21770	Acyl-CoA N-acyltransferases (NAT) superfamily protein	2	2

AT1G28200	FH interacting protein 1	2	2
AT1G31780	Protein coding	2	2
AT1G32500	non-intrinsic ABC protein 6	2	2
AT1G32580	plastid developmental protein DAG, putative	2	2
AT1G43190	polypyrimidine tract-binding protein 3	2	2
AT1G44900	minichromosome maintenance (MCM2/3/5) family protein	2	2
AT1G48760	delta-adaptin	2	2
AT1G50670	OTU-like cysteine protease family protein	2	2
AT1G55840	Sec14p-like phosphatidylinositol transfer family protein	2	2
AT1G62020	Coatomer, alpha subunit	2	2
AT1G71270	Vps52 / Sac2 family	2	2
AT1G71380	cellulase 3	2	2
AT1G77120	alcohol dehydrogenase 1	2	2
AT2G20580	26S proteasome regulatory subunit S2 1A	2	2
AT2G20790	clathrin adaptor complexes medium subunit family protein	2	2
AT2G21390	Coatomer, alpha subunit	2	2
AT2G27600	AAA-type ATPase family protein	2	2
AT2G32730	26S proteasome regulatory complex, non-ATPase subcomplex, Rpn2/Psmd1 subunit	2	2
AT2G41620	Nucleoporin interacting component (Nup93/Nic96-like) family protein	2	2
AT2G42520	P-loop containing nucleoside triphosphate hydrolases superfamily protein	2	2
AT2G43140	basic helix-loop-helix (bHLH) DNA-binding superfamily protein	2	2
AT3G01290	SPFH/Band 7/PHB domain-containing membrane-associated protein family	2	2
AT3G02360	6-phosphogluconate dehydrogenase family protein	2	2
AT3G05040	ARM repeat superfamily protein	2	2
AT3G12050	Aha1 domain-containing protein	2	2
AT3G20250	pumilio 5	2	2
AT3G26650	glyceraldehyde 3-phosphate dehydrogenase A subunit	2	2
AT3G45450	Double Clp-N motif-containing P-loop nucleoside triphosphate hydrolases superfamily protein	2	2
AT3G45770	Polyketide synthase, enoylreductase family protein	2	2
AT3G46060	RAB GTPase homolog 8A	2	2
AT3G52180	dual specificity protein phosphatase (DsPTP1) family protein	2	2
AT3G52300	ATP synthase D chain, mitochondrial	2	2
AT3G59820	LETM1-like protein	2	2
AT4G16130	arabinose kinase	2	2
AT4G20260	plasma-membrane associated cation-binding protein 1	2	2
AT4G21150	ribophorin II (RPN2) family protein	2	2
AT4G24190	Chaperone protein htpG family protein	2	2

AT4G27270	Quinone reductase family protein	2	2
AT4G39220	Rer1 family protein	2	2
AT5G02500	heat shock cognate protein 70-1	2	2
AT5G06460	ubiquitin activating enzyme 2	2	2
AT5G13110	glucose-6-phosphate dehydrogenase 2	2	2
AT5G15450	casein lytic proteinase B3	2	2
AT5G15490	UDP-glucose 6-dehydrogenase family protein	2	2
AT5G23060	calcium sensing receptor	2	2
AT5G27600	long-chain acyl-CoA synthetase 7	2	2
AT5G41210	glutathione S-transferase THETA 1	2	2
AT5G45130	RAB homolog 1	2	2
AT5G46630	Clathrin adaptor complexes medium subunit family protein	2	2
AT5G52920	plastidic pyruvate kinase beta subunit 1	2	2
AT5G53480	ARM repeat superfamily protein	2	2
AT5G58070	temperature-induced lipocalin	2	2
AT5G59710	VIRE2 interacting protein 2	2	2
AT5G65720	nitrogen fixation S (NIFS)-like 1	2	2
ATCG00120	ATP synthase subunit alpha	2	2
AT1G03090.2	methylcrotonyl-CoA carboxylase alpha chain, mitochondrial / 3-methylcrotonyl-CoA carboxylase 1 (MCCA)	3	3
AT1G04820	tubulin alpha-4 chain	3	3
AT1G07920	GTP binding Elongation factor Tu family protein	3	3
AT1G12000	Phosphofructokinase family protein	3	3
AT1G13440	glyceraldehyde-3-phosphate dehydrogenase C2	3	3
AT1G22920	COP9 signalosome 5A	3	3
AT1G24300	GYF domain-containing protein	3	3
AT1G26630	Eukaryotic translation initiation factor 5A-1 (eIF-5A 1) protein	3	3
AT1G27450.2	adenine phosphoribosyl transferase 1	3	3
AT1G30630	Coatomer epsilon subunit	3	3
AT1G55490	chaperonin 60 beta	3	3
AT1G56070	Ribosomal protein S5/Elongation factor G/III/V family protein	3	3
AT1G64190	6-phosphogluconate dehydrogenase family protein	3	3
AT1G78900	vacuolar ATP synthase subunit A	3	3
AT1G79230	mercaptopyruvate sulfurtransferase 1	3	3
AT2G02560	cullin-associated and neddylation dissociated	3	3
AT2G07698	ATPase, F1 complex, alpha subunit protein	3	3
AT2G21470	SUMO-activating enzyme 2	3	3
AT2G21640	Encodes a protein of unknown function that is a marker for oxidative stress response.	3	3
AT2G21660	cold, circadian rhythm, and rna binding 2	3	3
AT2G27730	copper ion binding	3	3
AT2G28000	chaperonin-60alpha	3	3

AT2G39730	rubisco activase	3	3
AT2G44060	Late embryogenesis abundant protein, group 2	3	3
AT2G45290	Transketolase	3	3
AT3G02090	Insulinase (Peptidase family M16) protein	3	3
AT3G03780	methionine synthase 2	3	3
AT3G03960	TCP-1/cpn60 chaperonin family protein	3	3
AT3G08580	ADP/ATP carrier 1	3	3
AT3G11270	Mov34/MPN/PAD-1 family protein	3	3
AT3G17390	S-adenosylmethionine synthetase family protein	3	3
AT3G22330	putative mitochondrial RNA helicase 2	3	3
AT3G43300	HOPM interactor 7	3	3
AT3G52230	unknown protein	3	3
AT3G56130	biotin/lipoyl attachment domain-containing protein	3	3
AT3G58610	ketol-acid reductoisomerase	3	3
AT3G60240.2	eukaryotic translation initiation factor 4G	3	3
AT3G62530	ARM repeat superfamily protein	3	3
AT4G02930	GTP binding Elongation factor Tu family protein	3	3
AT4G11380	Adaptin family protein	3	3
AT4G11420	eukaryotic translation initiation factor 3A	3	3
AT4G20360	RAB GTPase homolog E1B	3	3
AT4G24280	chloroplast heat shock protein 70-1	3	3
AT4G37910	mitochondrial heat shock protein 70-1	3	3
AT5G09590	mitochondrial HSO70 2	3	3
AT5G15530	biotin carboxyl carrier protein 2	3	3
AT5G16390	chloroplastic acetylcoenzyme A carboxylase 1	3	3
AT5G17920	Cobalamin-independent synthase family protein	3	3
AT5G28840	GDP-D-mannose 3',5'-epimerase	3	3
AT5G41670	6-phosphogluconate dehydrogenase family protein	3	3
AT5G52640	heat shock protein 90	3	3
AT5G53620	unknown protein	3	3
AT5G56000	HEAT SHOCK PROTEIN 81.4	3	3
AT5G56030	heat shock protein 81-2	3	3
AT5G59720	heat shock protein 18.2	3	3
AT5G64260	EXORDIUM like 2	3	3
AT1G27970	nuclear transport factor 2B	2	3
AT1G49240	actin 8	2	3
AT1G50200	Alanyl-tRNA synthetase	2	3
AT1G69410	eukaryotic elongation factor 5A-3	2	3
AT2G25140	casein lytic proteinase B4	2	3
AT3G09440	Heat shock protein 70 (Hsp 70) family protein	2	3
AT3G13920	eukaryotic translation initiation factor 4A1	2	3
AT3G16400	nitrile specifier protein 1	2	3

AT3G18190	TCP-1/cpn60 chaperonin family protein	2	3
AT3G56150	eukaryotic translation initiation factor 3C	2	3
AT3G60750	Transketolase	2	3
AT4G13930	serine hydroxymethyltransferase 4	2	3
AT4G27440	protochlorophyllide oxidoreductase B	2	3
AT4G34030	3-methylcrotonyl-CoA carboxylase	2	3
AT5G08670	ATP synthase alpha/beta family protein	2	3
AT5G19550	aspartate aminotransferase 2	2	3
AT5G22650	histone deacetylase 2B	2	3
AT5G24810	ABC1 family protein	2	3
AT5G27640	translation initiation factor 3B1	2	3
AT5G55280	homolog of bacterial cytokinesis Z-ring protein FTSZ 1-1	2	3
AT5G56010	heat shock protein 81-3	2	3

References

1. Kirchhausen, T., Owen, D. & Harrison, S. C. Molecular structure, function, and dynamics of clathrin-mediated membrane traffic. *Cold Spring Harb Perspect Biol* **6**, a016725 (2014).
2. Baisa, G. A., Mayers, J. R. & Bednarek, S. Y. Budding and braking news about clathrin-mediated endocytosis. *Curr Opin Plant Biol* **16**, 718–725 (2013).
3. Zhang, Y. et al. Change your Tplate, change your fate: plant CME and beyond. *Trends Plant Sci* **20**, 41–48 (2015).
4. McMahon, H. T., McMahon, H. T., Boucrot, E. & Boucrot, E. Molecular mechanism and physiological functions of clathrin-mediated endocytosis. *Nat Rev Mol Cell Biol* **12**, 517–533 (2011).
5. Kleist, von, L. et al. Role of the clathrin terminal domain in regulating coated pit dynamics revealed by small molecule inhibition. *Cell* **146**, 471–484 (2011).
6. Macia, E. et al. Dynasore, a cell-permeable inhibitor of dynamin. *Dev Cell* **10**, 839–850 (2006).
7. Dutta, D., Williamson, C. D., Cole, N. B. & Donaldson, J. G. Pitstop 2 is a potent inhibitor of clathrin-independent endocytosis. *PLoS ONE* **7**, e45799 (2012).
8. Willox, A. K., Sahraoui, Y. M. E. & Royle, S. J. Non-specificity of Pitstop 2 in clathrin-mediated endocytosis. *Biol Open* **3**, 326–331 (2014).
9. Stahlschmidt, W., Robertson, M. J., Robinson, P. J., McCluskey, A. & Haucke, V. Clathrin terminal domain-ligand interactions regulate sorting of mannose 6-phosphate receptors mediated by AP-1 and GGA adaptors. *J Biol Chem* **289**, 4906–4918 (2014).
10. McCluskey, A. et al. Building a better dynasore: the dyngo compounds potently inhibit dynamin and endocytosis. *Traffic* **14**, 1272–1289 (2013).
11. Hill, T. A. et al. Inhibition of dynamin mediated endocytosis by the dynoles--synthesis and functional activity of a family of indoles. *J. Med. Chem.* **52**, 3762–3773 (2009).
12. Sharfman, M. et al. Endosomal signaling of the tomato leucine-rich repeat receptor-like protein LeEix2. *Plant J* **68**, 413–423 (2011).
13. Yaish, P., Gazit, A., Gilon, C. & Levitzki, A. Blocking of EGF-dependent cell proliferation by EGF receptor kinase inhibitors. *Science* **242**, 933–935 (1988).
14. Crump, C. M., Williams, J. L., Stephens, D. J. & Banting, G. Inhibition of the interaction between tyrosine-based motifs and the medium chain subunit of the AP-2 adaptor complex by specific tyrphostins. *J Biol Chem* **273**, 28073–28077 (1998).
15. Banbury, D. N., Oakley, J. D., Sessions, R. B. & Banting, G. Tyrphostin A23 inhibits internalization of the transferrin receptor by perturbing the interaction between tyrosine motifs

and the medium chain subunit of the AP-2 adaptor complex. *J Biol Chem* **278**, 12022–12028 (2003).

16. Ortiz-Zapater, E., Soriano-Ortega, E., Marcote, M. J., Ortiz-Masiá, D. & Aniento, F. Trafficking of the human transferrin receptor in plant cells: effects of tyrphostin A23 and brefeldin A. *Plant J* **48**, 757–770 (2006).
17. Martinez Molina, D. et al. Monitoring drug target engagement in cells and tissues using the cellular thermal shift assay. *Science* **341**, 84–87 (2013).
18. Lomenick, B. et al. Target identification using drug affinity responsive target stability (DARTS). *Proc Natl Acad Sci USA* **106**, 21984–21989 (2009).
19. Kasprowicz, J. et al. Inactivation of clathrin heavy chain inhibits synaptic recycling but allows bulk membrane uptake. *J Cell Biol* **182**, 1007–1016 (2008).
20. Heerssen, H., Fetter, R. D. & Davis, G. W. Clathrin dependence of synaptic-vesicle formation at the Drosophila neuromuscular junction. *Curr Biol* **18**, 401–409 (2008).
21. Kasprowicz, J., Kuenen, S., Swerts, J., Miskiewicz, K. & Verstreken, P. Dynamin photoinactivation blocks Clathrin and α-adaptin recruitment and induces bulk membrane retrieval. *J Cell Biol* **204**, 1141–1156 (2014)
22. Poot, M. et al. Analysis of mitochondrial morphology and function with novel fixable fluorescent stains. *J. Histochem. Cytochem.* **44**, 1363–1372 (1996).
23. Scaduto, R. C. & Grotyohann, L. W. Measurement of mitochondrial membrane potential using fluorescent rhodamine derivatives. *Biophys. J.* **76**, 469–477 (1999).
24. Dettmer, J., Hong-Hermesdorf, A., Stierhof, Y.-D. & Schumacher, K. Vacuolar H+-ATPase activity is required for endocytic and secretory trafficking in Arabidopsis. *Plant Cell* **18**, 715–730 (2006).
25. Gadeyne, A. et al. The TPLATE adaptor complex drives clathrin-mediated endocytosis in plants. *Cell* **156**, 691–704 (2014).
26. Fan, L. et al. Dynamic analysis of Arabidopsis AP2 σ subunit reveals a key role in clathrin-mediated endocytosis and plant development. *Development* **140**, 3826–3837 (2013).
27. Irani, N. G. et al. Fluorescent castasterone reveals BRI1 signaling from the plasma membrane. *Nat Chem Biol* **8,** 583–589 (2012).
28. Di Rubbo, S. et al. The clathrin adaptor complex AP-2 mediates endocytosis of brassinosteroid insensitive1 in Arabidopsis. *Plant Cell* **25**, 2986–2997 (2013).
29. Yin, Y. et al. BES1 accumulates in the nucleus in response to brassinosteroids to regulate gene expression and promote stem elongation. *Cell* **109**, 181–191 (2002).
30. Zhu, J.-Y., Sae-Seaw, J. & Wang, Z.-Y. Brassinosteroid signalling. *Development* **140**, 1615–1620 (2013).

31. Kasianowicz, J., Benz, R. & McLaughlin, S. The kinetic mechanism by which CCCP (carbonyl cyanide m-chlorophenylhydrazone) transports protons across membranes. *J. Membr. Biol.* **82**, 179–190 (1984).
32. Heytler, P. G. uncoupling of oxidative phosphorylation by carbonyl cyanide phenylhydrazones. I. Some characteristics of m-Cl-CCP action on mitochondria and chloroplasts. *Biochemistry* **2**, 357–361 (1963).
33. Potter, V. R. & Reif, A. E. Inhibition of an electron transport component by antimycin A. *J Biol Chem* **194**, 287–297 (1952).
34. Wang, X. & Chory, J. Brassinosteroids regulate dissociation of BKI1, a negative regulator of BRI1 signaling, from the plasma membrane. *Science* **313**, 1118–1122 (2006).
35. Jaillais, Y. et al. Tyrosine phosphorylation controls brassinosteroid receptor activation by triggering membrane release of its kinase inhibitor. *Genes Dev* **25**, 232–237 (2011).
36. Popoff, V., Adolf, F., Brügger, B. & Wieland, F. COPI budding within the Golgi stack. *Cold Spring Harb Perspect Biol* **3**, a005231 (2011).
37. Savitski, M. M. et al. Tracking cancer drugs in living cells by thermal profiling of the proteome. *Science* **346**, 1255784 (2014).
38. Kitakura, S. et al. Clathrin mediates endocytosis and polar distribution of PIN auxin transporters in Arabidopsis. Plant Cell **23**, 1920–1931 (2011).
39. Roy, A., Kucukural, A. & Zhang, Y. I-TASSER: a unified platform for automated protein structure and function prediction. *Nat. Protoc* **5**, 725–738 (2010).
40. DeLano, W. L., The PyMOL Molecular Graphics System, 0.99rc6.; DeLano Scientific LLC: San Carlos, CA, USA 41. Chan, K., Truong, D., Shangari, N. & O'Brien, P. J. Drug-induced mitochondrial toxicity. *Expert Opin. Drug Metab. Toxicol.* **1**, 655–669 (2005).
41. Chan, K., Truong, D., Shangari, N. & O'Brien, P. J. Drug-induced mitochondrial toxicity. *Expert Opin. Drug Metab. Toxicol*. **1**, 655–669 (2005).
42. Swiss, R., Niles, A., Cali, J. J., Nadanaciva, S. & Will, Y. Validation of a HTS-amenable assay to detect drug-induced mitochondrial toxicity in the absence and presence of cell death. *Toxicol In Vitro* **27**, 1789–1797 (2013).
43. Moffat, J. G., Rudolph, J. & Bailey, D. Phenotypic screening in cancer drug discovery - past, present and future. *Nat Rev Drug Discov* **13**, 588–602 (2014).
44. O'Brien, P. J. High-content analysis in toxicology: screening substances for human toxicity potential, elucidating subcellular mechanisms and in vivo use as translational safety biomarkers. *Basic Clin. Pharmacol. Toxicol*. **115**, 4–17 (2014).

45. Mooren, O. L., Galletta, B. J. & Cooper, J. A. Roles for actin assembly in endocytosis. *Annu. Rev. Biochem*. **81**, 661–686 (2012).

46. Kuhnert, M. et al. Tracing binding modes in hit-to-lead optimization: chameleon-like poses of aspartic protease inhibitors. *Angew. Chem. Int. Ed.* **54**, 2849–2853 (2015).

47. Robinson, T. J. W. et al. High-throughput screen identifies disulfiram as a potential therapeutic for triple-negative breast cancer cells: interaction with IQ motif-containing factors. *Cell Cycle* **12**, 3013–3024 (2013).

48. Chin, R. M. et al. The metabolite α-ketoglutarate extends lifespan by inhibiting ATP synthase and TOR. *Nature* **510**, 397–401 (2014).

49. Derry, M. M. et al. Target identification of grape seed extract in colorectal cancer using drug affinity responsive target stability (DARTS) technique: role of endoplasmic reticulum stress response proteins. *Curr Cancer Drug Targets* **14**, 323–336 (2014).

50. Mestres, J., Gregori-Puigjané, E., Valverde, S. & Solé, R. V. The topology of drug-target interaction networks: implicit dependence on drug properties and target families. *Mol Biosyst* **5**, 1051–1057 (2009).

51. Arooj, M. et al. Finding off-targets, biological pathways & target diseases for chymase inhibitors via structure-based systems biology approach. *Proteins* (2014).

52. Luschnig, C. & Vert, G. The dynamics of plant plasma membrane proteins: PINs and beyond. *Development* **141**, 2924–2938 (2014).

53. Kirchhausen, T., Owen, D. & Harrison, S. C. Molecular structure, function, and dynamics of clathrin-mediated membrane traffic. *Cold Spring Harb Perspect Biol* **6**, a016725 (2014).

54. Baral, A. et al. Salt-induced remodeling of spatially restricted clathrin-independent endocytic pathways in Arabidopsis root. *Plant Cell* **27**, 1297–1315 (2015).

55. Robert, S. et al. Endosidin1 defines a compartment involved in endocytosis of the brassinosteroid receptor BRI1 and the auxin transporters PIN2 and AUX1. *Proc Natl Acad Sci USA* **105**, 8464–8469 (2008).

56. Marc, J. et al. A GFP-MAP4 reporter gene for visualizing cortical microtubule rearrangements in living epidermal cells. *Plant Cell* **10**, 1927–1940 (1998).

59. Van Damme, D. et al. Adaptin-like protein TPLATE and clathrin recruitment during plant somatic cytokinesis occurs via two distinct pathways. *Proc Natl Acad Sci USA* **108**, 615–620 (2011).

60. Van Leene, J. et al. A tandem affinity purification-based technology platform to study the cell cycle interactome in Arabidopsis thaliana. *Mol Cell Proteomics* **6**, 1226–1238 (2007).

61. Hillmer, S., Viotti, C. & Robinson, D. G. An improved procedure for low-temperature embedding of high-pressure frozen and freeze-substituted plant tissues resulting in excellent structural preservation and contrast. J Microsc 247, 43–47 (2012).
62. Verstreken, P., Ohyama, T. & Bellen, H. J. FM 1-43 labeling of synaptic vesicle pools at the Drosophila neuromuscular junction. *Methods Mol Biol* **440**, 349–369 (2008).
63. Shidara, Y. & Hollenbeck, P. J. Defects in mitochondrial axonal transport and membrane potential without increased reactive oxygen species production in a Drosophila model of Friedreich ataxia. *J. Neurosci*. **30**, 11369–11378 (2010).
64. Van Gunsteren, W. F.; Billeter, S. R.; Eising, A. A.; Hünenberger, P. H.; Krüger, P.; Mark, A. E.; Scott, W. R. P.; Tironi, I. G., Bi2omolecular Simulation: The GROMOS96 Manual and User Guide. *vdf Hochschulverlag AG an der ETH Zürich and BIOMOS b.v.*: Zürich, Groningen, 1996
65. Guex, N.; Peitsch, M. C., Swiss-Model and the Swiss-PdbViewer: An environment for comparative protein modeling. *Electrophoresis* **18**, 2714-2723 (1997).
66. Trott, O.; Olson, A. J., AutoDock Vina: Improving the speed and accuracy of docking with a new scoring function, efficient optimization, and multithreading. *J. Comp. Chem.*, **31(2)**, 455–461 (2010).
67. Sanner, M. F., Using the Python programming language for bioinformatics. *J. Mol. Graphics Mod.* **17(1)**, 57–61 (1999).
68. Avogadro: an open-source molecular builder and visualization tool. Version 1.01. http://avogadro.openmolecules.net/.
69. Halgren, T. A., Merck molecular force field. I. Basis, form, scope, parameterization, and performance of MMFF94. *J. Comp. Chem*. **17**, 490–519 (1996).

Chapter V: Identification of a trans-membrane protein family through computational target prediction

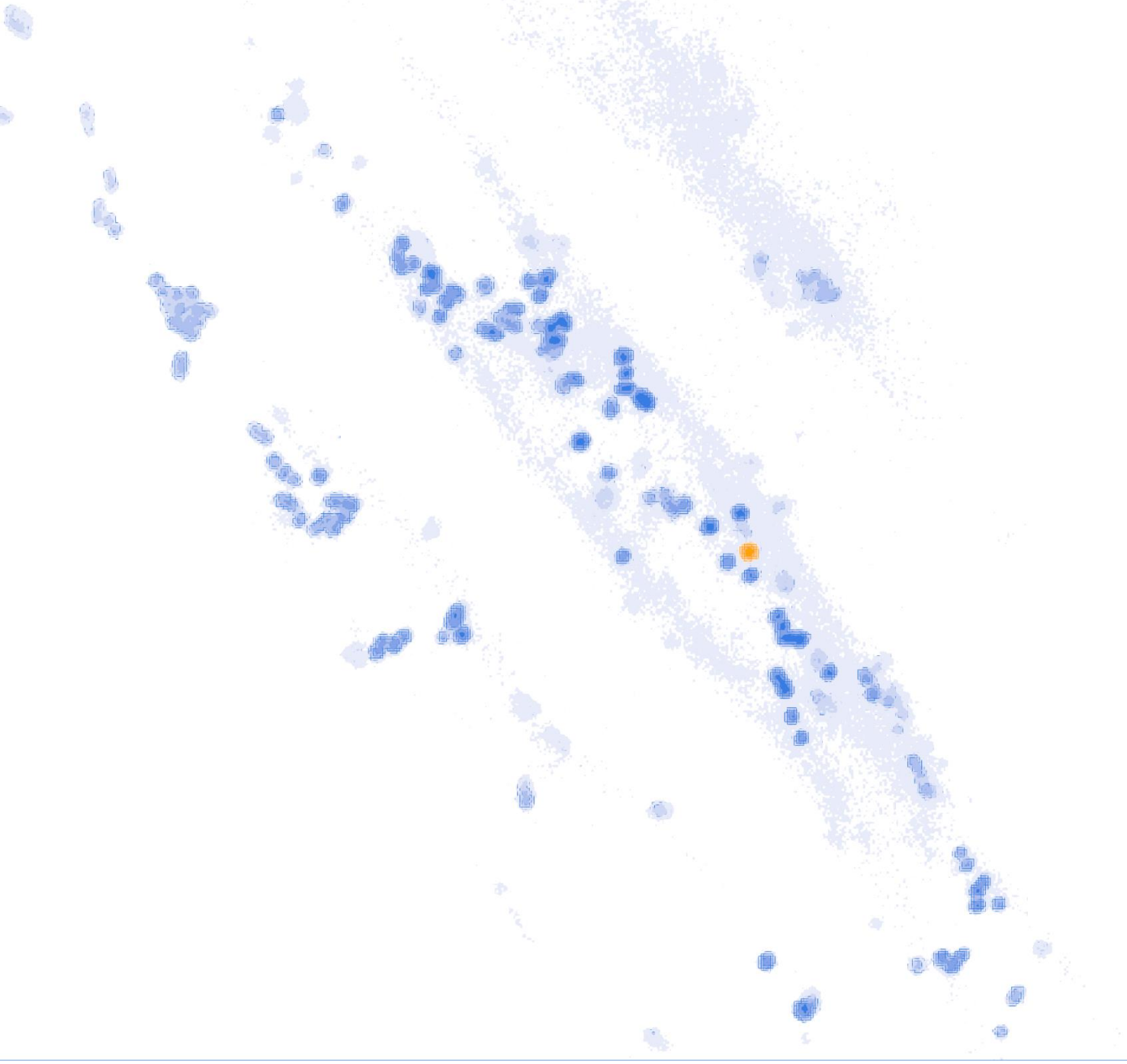

Identification of a trans-membrane protein family through computational target prediction

Wim Dejonghe[1,2], Evelien Mylle[1,2] Isabelle Van Houtte[1,2], Rahul Kumar[1,2], Bram Denoo[3], Johan Winne[3] and Eugenia Russinova[1,2]

[1]Department of Plant Systems Biology, VIB, 9052 Ghent, Belgium
[2]Department of Plant Biotechnology and Bioinformatics, Ghent University, 9052 Ghent, Belgium
[3]Department of Organic Chemistry, Polymer Chemistry Research Group and Laboratory for Organic Synthesis, Ghent University, Krijgslaan 281 S4-bis, B-9000 Ghent, Belgium.

Author contribution: W. D. did the genotyping, generation and characterization of mutants, and was involved in cloning and confocal microscopy. W. D. wrote the manuscript and made the figures.

Abstract

Computational prediction of small molecule target proteins is not well established in plant chemical biology, despite its success in mammalian drug discovery. In this study we attempt to identify target proteins in *Arabidopsis* of a small molecule effector of endomembrane traffic based on its chemical similarities with the know drug Rosiglitazone and protein structural data of Rosiglitazone in complex with its target in human systems. We identified a family of trans-membrane proteins with unknown function, and tried to validate the computational prediction by mutant growth on the small molecule hit. In addition, we initialize the characterization of the trans-membrane protein family, and found indications of involvement in sterol metabolism or transport and possibly defense responses.

Introduction

The majority of target identification strategies in drug discovery and plant chemical biology employ affinity purification based approaches, biochemical or genetic tools and phenotype-based selection of target proteins[1-3]. A much less explored target identification strategy includes the use of computational strategies to predict target proteins. Though in recent years the mammalian drug discovery field witnessed a surge in novel prediction algorithms[4], plant chemical biology has yet to see this field of target prediction to emerge fully. Examples exist[3], including the design of a novel auxin antagonist auxinole[5]. Alternatively, molecular design of target proteins might repurpose small molecules, as exemplified by mandipropamid binding to the abscisic acid (ABA) receptor PYRABACTIN RESISTANCE 1 (PYR1)[6], which itself was identified through a chemical genetics screen for Pyrabactin resistant mutants[6]. One of the main reasons for the backlog in computational approaches in the plant field is the absence of internationally recognized large data collections containing protein structural, chemical and biological data related to small molecules used in the plant field[7]. In drug discovery, large depositories of small molecule related data such as ChEMBL[8] and PubChem[9] are the backbone for computational target prediction strategies, which can be ligand or target based[4,10,11]. Often, computational prediction is aimed at finding new interactions for small molecules or proteins of interest, yet an increasing number of studies are geared towards the identification of additional target proteins for known small molecule drugs[10,12]. These efforts fit into the current increasingly accepted view that the old 'lock and key' model[13] is outdated for most small molecules, while a polypharmacology model, or the ability of a small molecule to bind multiple target proteins, is more suited[4,10,12]. This is supported by the prediction that, on average, small molecules in drug discovery bind to six target proteins[14,15]. As small molecules, or certain substructures thereof, can bind different target proteins, which probably offer a similar binding environment in their tertiary and quaternary structure in one system, it becomes conceivable that this principle is applicable across different systems.

The latter hypothesis is the starting point of this chapter as we report on attempts to identify target proteins in *Arabidopsis* for a small molecule hit. The idea of transferability is not new as several small molecules used in plant biology with known mode of action have their origin in mammalian systems. The best known example, and one of the few well characterized small molecule effectors of endomembrane traffic in plants, is Brefeldin A (BFA). BFA was identified as an inhibitor of ADP-ribosylation factor (ARF) proteins in association with guanine exchange factors (GEFs), through binding the Sec7 domain, which determines BFA sensitivity[16-20]. The result is a heavily affected ER-Golgi traffic through a failed recruitment of vesicle coat proteins[21]. BFA has been show to affect ARF-GEFS in plants through genetic means[22], thereby successfully translating the mode of action in

mammalian and other systems to plant, despite a detailed biochemical characterization of BFA target proteins in plants.

However, in our study it concerns the attempt to identify target proteins of a small molecule hit, based on data from the mammalian field, which does not necessarily have the same mode of action across different systems. It therefore potentially deals with the transferability of protein structural and chemical data, rather than biological data. The small molecule was identified through a screen for inhibitors of clathrin mediated endocytosis (CME) (Chapter 2, this thesis), and shared a chemical group with the known drug Rosiglitazone. Rosiglitazone is well known as drug against diabetes type 2[23,24]. Though on the market for a number of years, popularity and availability have decreased as a result of undesired side effects, including heart failure, weight gain through water retention and even the increased risk for bladder cancer[23,24]. In addition, a recent report suggests a dysfunction of mitochondria at higher concentrations[25]. As a consequence, Rosiglitazone has been withdrawn from European markets, while under strict regulations in the United States[24]. The protein target of Rosiglitazone is known as peroxisome proliferator-activated receptor γ (PPARγ)[26], for which a crystal structure has been reported in complex with Rosiglitazone[27]. PPARγ belongs to the ligand-activated nuclear receptor transcription factor family. Its domain architecture includes, from N- to C-terminus, a trans activation domain, highly conserved DNA binding domain and ligand binding domain (LBD)[28].

Given that Rosiglitazone and our small molecule hit share a chemical group involved in target binding, and the reported crystal structure of Rosiglitazone in complex with its target protein[27,28] , we adopt a strategy combining aspects of both the ligand and target orientated computational strategies to identify possible target proteins of our small molecule of interest in *Arabidopsis*. To this end, structural data of the PPARγ LBD in complex with Rosiglitazone was used to query the *Arabidopsis* genome with BackPhyre[29] (http://www.sbg.bio.ic.ac.uk/phyre2/html/page.cgi?id=index_advanced), in search of proteins which possibly adopt a similar tertiary or quaternary structure such that it could accommodate our small molecule in a similar way as the PPARγ LBD Rosiglitazone. We identified a plant specific transmembrane protein family with unknown function as possible targets. The main goal is to assess possible binding between the small molecule hit and identified proteins in what is a proof of concept study. In addition, as the identified protein family has an unknown function, we initiate their characterization in terms of biological function, and speculate on their possible connection with brassinosteroid transport and signaling aside a possible role in endomembrane traffic.

Results

Structure-activity relation analysis reveals the core structure of small molecule 39

Small molecule 39 (**Figure 1a**) was identified as a hit since it retained the ability to de-phosphorylate BRI1 EMS-SUPPRESSOR1 (BES1)[30], while inhibiting FM4-64 uptake at relative low concentration (**Figure 2a,b**) (Chapter 2, this thesis). De-phosphorylation of BES1 was used as a measure of active brassinosteroid (BR) signaling[30,31], while FM4-64 is frequently used as a dye to visualize CME in Arabidopsis[32]. Small molecule 39 therefore inhibited CME, yet activated BR signaling at a concentration of 25 μM. In addition, compound 39 caused depolymerization of the microtubules, seen as diffuse cytosolic signal of MAP4-GFP[33] (**Figure 2b**). Structure-activity relation (SAR) analysis of several 39 analogs aimed at mapping the essential chemical moieties for activity. Analogs were tested for FM4-64 uptake and MAP4-GFP destabilization as readouts for activity. Small molecules 39-1 and 39-2 (**Figure 1a**) were active in terms of FM4-64 uptake inhibition and partial depolymerization of MAP4-GFP (**Figure 2b**) at 25 μM, and therefore showed hardly any loss in activity compared to 39. Analogues 39-3, 39-4 and 39-5 (**Figure 1a**) were not active in terms of FM4-64 uptake and MAP4-GFP at 50 μM (**Figure 2b**). Our SAR analysis revealed 39-2 as the core chemical structure. The reason lies in the relative instability in aqueous solution of the carbon bond between the tertiary amine of the thiazolidinedione (TZD) moiety and the secondary amine linked to the toluene moiety. This type of bond is present in 39, 39-1, 39-4 and 39-5. Hydrolysis results in the conversion of the formaldehyde-aminal derived imide of the TZD moiety into a free imide, which now can form hydrogen bonds, and might be required for protein binding. Small molecule 39-3 lacks such unstable carbon bond, therefore retains the tertiary amine of the TZD moiety, and remains inactive. Both 39 and 39-1 are thus most likely converted into 39-2 *in vivo*, while 39-4 and 39-5 illustrate the necessity of the fluorobenzene moiety for activity, as both are probably converted into TZD, which as such appeared inactive.

The TZD moiety of 39-2 appeared essential for activity and is shared with Rosiglitazone (**Figure 1b**). In fact, Rosiglitazone contains a substructure which largely resembles 39-2 (**Figure 1b, box**), lacking the fluorine and double bond between the TZD and fluorobenzene moieties of 39-2. Although both the double bond, dictating the orientation of the fluorobenzene moiety, and the fluorine might have important implications for 39-2 activity in *Arabidopsis*, the overall similarity with the Rosiglitazone substructure was the incentive to use the available structural data of Rosiglitazone in complex with its target protein to predict possible targets of 39, and by extension 39-2, in *Arabidopsis*.

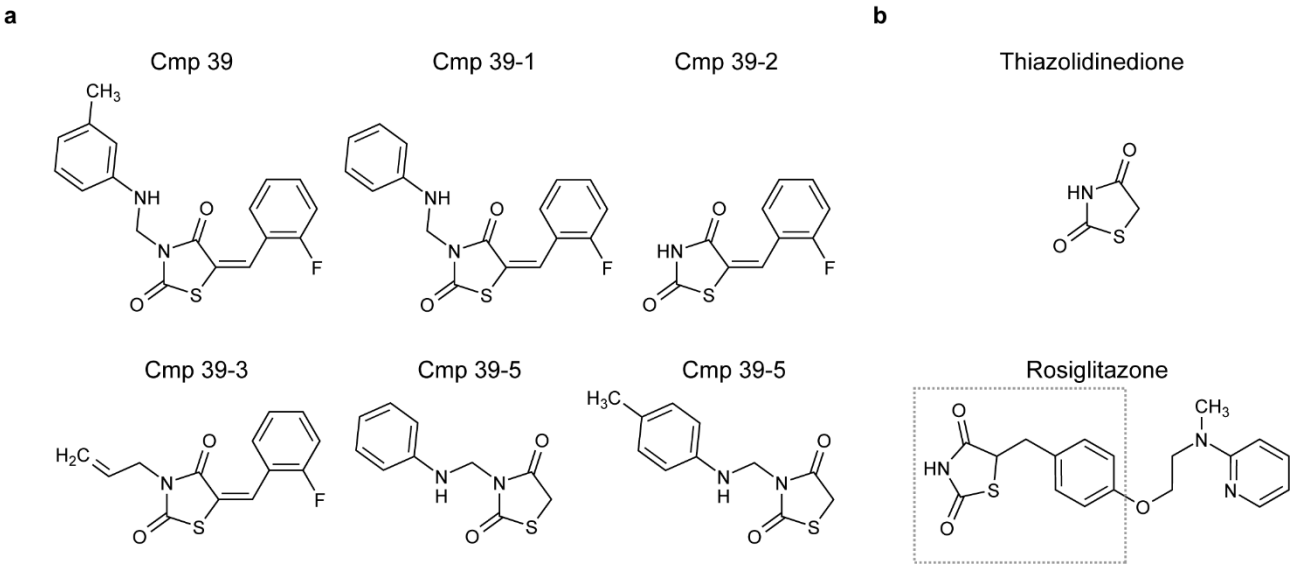

Figure 1. Analogues of small molecule 39, and the similarity with Rosiglitazone.

(**a**) Original structure of 39 and tested commercial analogues. (**b**) Structure of the thiazolidinedione moiety and Rosiglitazone.

Small molecule 39 potentially binds a family of 4 membrane proteins in *Arabidopsis*

Since PPARγ, the target of Rosiglitazone, would be used as a template to identify possible target proteins of 39 in *Arabidopsis*, both nucleotide and protein sequences of human PPARγ were used to query for paralogues genes in *Arabidopsis*. However, only alignments with very low scores were retrieved, even for the LBD as a template, indicating little conservation. We therefore relied solely on structural protein data for prediction. We used BackPhyre, part of the Protein Homology/analogY Recognition Engine V 2.0 (Phyre2)[29] expert mode module, to perform this prediction. BackPhyre uses a Protein Data Bank (PDB) entry as template to query a genome of choice for protein sequences which might fold into similar tertiary or quaternary structure. As template we used the PDB entry 2PRG[27], which represents the LBD of PPARγ in complex with Rosiglitazone (**Figure 3a**). The figure depicts a render generated by PyMol[34], and shows a selection of LBD secondary structure elements engaged in Rosiglitazone binding. A schematic representation of the binding pocket[28] (**Figure 3b**) provides a better view on amino acids involved in Rosiglitazone binding. Only the LBD was considered to avoid added complexity of the DNA binding and transactivation domain, which could increase the risk of false positives. Interestingly, only 10 hits were retrieved (**Supplemental Table 1**) of which the first 4 are of the same protein family with unknown function in *Arabidopsis*.

A closer look revealed that all four are members of the same land plant specific gene family, according to the online comparative genomics platform PLAZA 3[35]. In addition, the top two hits, AT5G40640 and AT3G27390 were closest related, while AT4G37030 and AT4G12680 were more distant (**Figure 4a**). As possible target proteins of 39, we named this gene family *PTE* (*Putative Target of Endosidin*), since 39 belongs to the collection of small molecules following the endosidin nomenclature[36]. The

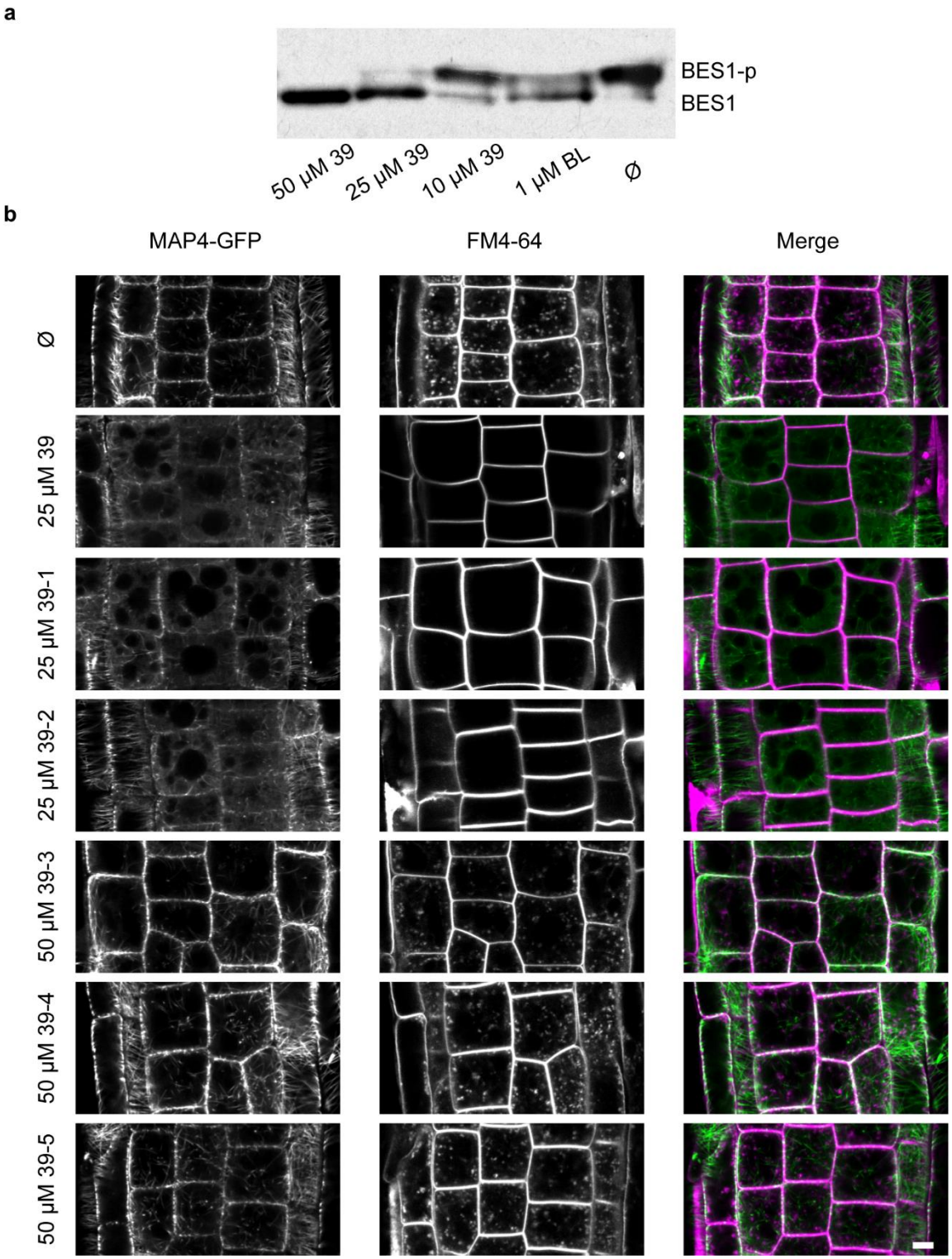

Figure 2. BR signaling in presence of 39, and FM4-64 based structure activity relation analysis.

(**a**) BES1 phosphorylation as measured in PSB-D cell cultures expressing BES1-TAP, incubated for 1 hour with appropriate concentration of 39. (**b**) MAP4-GFP seedlings of 5 days old treated with 39 and analogues for 15 min, followed by a 2µM FM4-64 pulse for 30 min. Scale bar: 5 µm

numbering of the genes is according to the BackPhyre ranking, therefore *PTE1* represents AT5G40640, *PTE2* AT3G27390, *PTE3* AT4G37030 and *PTE4* AT4G12680. Further classification by PLAZA revealed that the *PTE* genes belong to the ligand binding nuclear hormone receptor gene family (HOM03D001281), while gene ontology terms based on experimental evidence indicated

plasma membrane localization (GO:0005886)[37]. Gene ontology for biological process or molecular function were unknown. In addition, PTE proteins were predicted to contain up to eight trans-membrane regions, while possibly situated in the secretory pathway according to the plant membrane protein database ARAMEMNON[38].

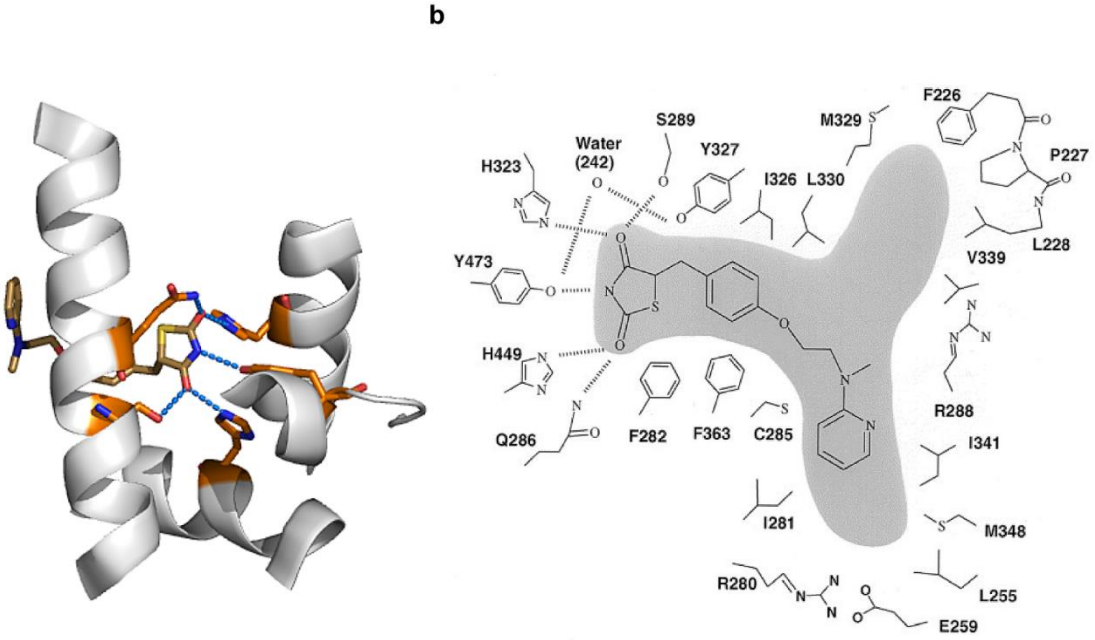

Figure 3 Structural aspects of Peroxisome Proliferator-activated Receptor γ interaction with Rosiglitazone.

(**a**) 3-dimensional representation of the Rosiglitazone binding site, as depicted by partial alpha helices of the Peroxisome Proliferator-activated Receptor γ (PPARγ) ligand binding domain (grey) contributing amino acids participating in Rosiglitazone binding (orange). Brown structure represents Rosiglitazone. Yellow indicates Sulfur, blue nitrogen and red oxygen. Dotted blue lines indicate hydrogen bonds between Rosiglitazone and PPARγ. Crystal structure 2PRG[27], obtained through the protein data bank and visualized using PyMOL molecular viewer (http://www.pymol.org/). (**b**) Adopted[27] schematic representation of the Rosiglitazone binding site, and amino acids involved in binding.

Higher order mutants of the *PTE* gene family were sensitive to 39

The strategy to assess the possibility of compound 39 binding to the PTE proteins included growth analysis of *pte* mutant lines on medium containing 39. Increased resistance or sensitivity could be a first indication of binding. Initial efforts were focused on *PTE1* and *PTE2* mutant lines, as the likelihood of 39 binding was the highest. Several insertion mutants were acquired per gene to test the hypothesis above. Two SALK lines for *PTE1* were characterized in terms of insertion site and transcript levels: SALK_099018 and SALK_142384. While SALK_142384 contained an insertion approximately in the middle of the first intron, SALK 099018 appeared to have an insertion situated in the beginning of the second exon (**Figure 5a**). Amplification products for genotyping purposes were normal, without presence of surplus bands or other aberrant amplification products (**Figure 5b-**

c). The SALK_142384 mutant had reduced transcript levels of *PTE1*, to about 30% as compared to the wild type, whereas SALK_099018 transcript levels were decreased to about 10% as compared to the wild type (**Figure 5d**). A more detailed analysis of the SALK_099018 lines revealed that the 5' and 3' transcripts of *PTE1* were down regulated to about 10%, while transcription over the insertion was absent (**Figure 5e**). Therefore, SALK_099018 (*pte1-1*) was considered as a null mutant and selected for further characterization.

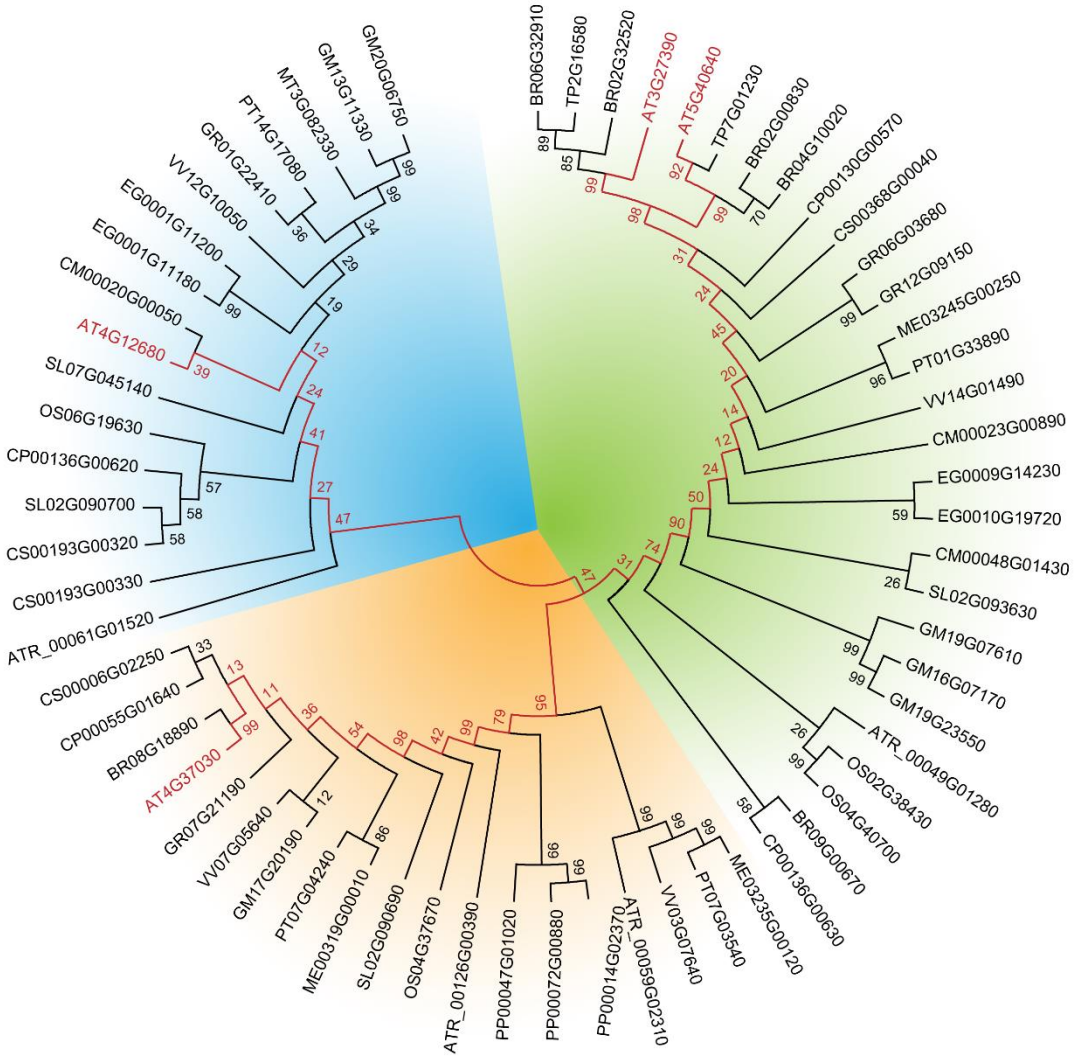

Figure 4. Evolutionary relationship of plant nuclear hormone receptor orthologues

Multiple sequence alignment, including 64 complete protein sequences from 17 plant species. Based on their relative sequence relatedness, protein sequences clustered in three different groups. Four members are encoded by Arabidopsis whereas at least six members are encoded by its close relative *Brassica rapa*. At5g40640 and At3g27390 sequences were found to be relatively more conserved than the remaining Arabidopsis homologs. Bootstrap supports are indicated at each branch.

Only one insertion mutant was found for the *PTE2* gene: WiscDsLox320E02 (*pte2*). The insertion was in the second intron, just upstream of the third exon (**Figure 6a**). Probably because of the intronic

nature of the insertion, genotyping revealed a weak PCR product for homozygous mutants which was slightly smaller in size compared to PCR products obtained with the same primers in heterozygous or wild type plants (**Figure 6b**). Overall expression was substantially reduced (**Figure 6c**), yet more detailed analysis revealed still some 5' transcripts, while the expression of 3' transcripts were virtually absent (**Figure 6d**). In contrast to the *pte1-1* allele, *pte2* showed residual transcript levels over the insertion (**Figure 6d**), which could be due to aberrant splicing events.

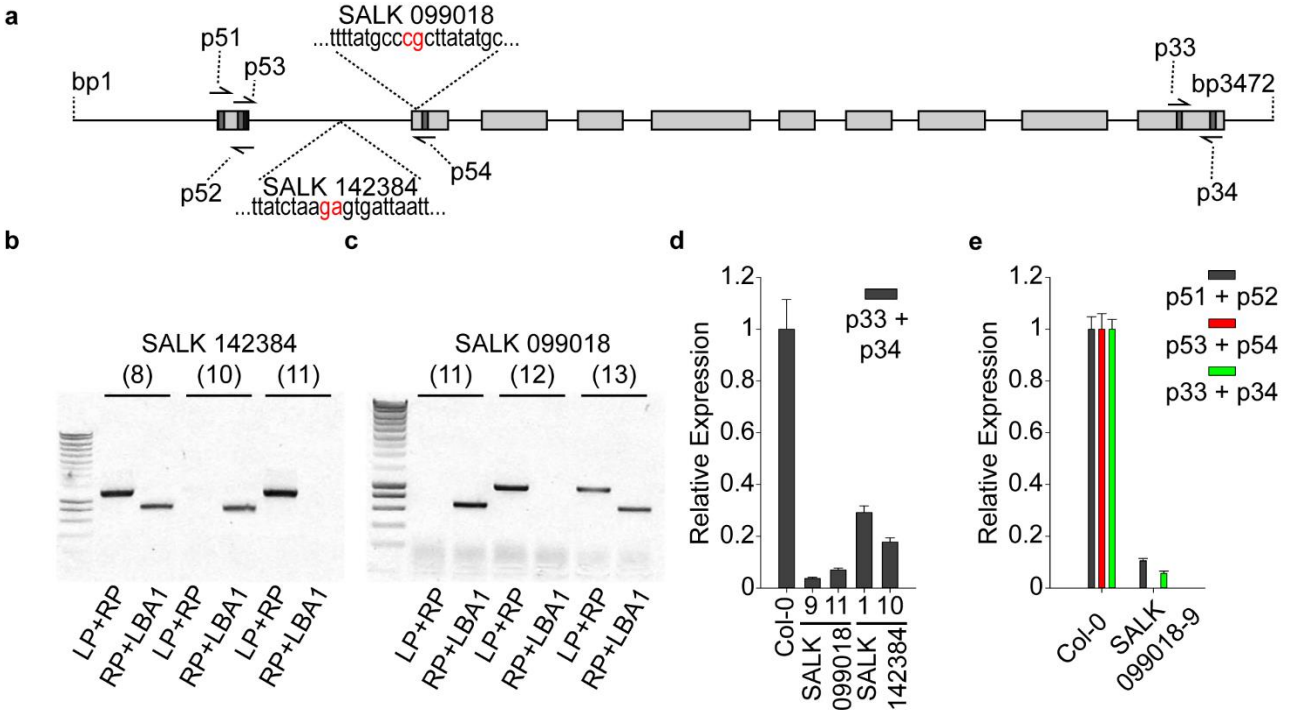

Figure 5. Characterization of *PTE1* mutants.

(**a**) Schematic representation of the *PTE1* genomic region (black line), with light grey boxes representing exons and dark grey regions primer binding sites (e.g. p54). Remaining regions represent sequences upstream and downstream of the *PTE1* gene, as well as introns. SALK insertions are indicated by triangular structures, with relevant sequence. Insertion site is situated between both nucleotides colored red. (**b-c**) Representative gels showing amplification products seen with combinations of the left primer (LP) flanking the SALK insertion, right primer (RP) and TDNA specific primer (LBA1). (**d**) Results of quantitative PCR (qPCR) for both SALK lines, and (**e**) more detailed qPCR results for selected SALK line. SALK 099018: *pte1*

To assess the sensitivity of the *pte* mutants to compound 39, mutant seedlings grown on normal medium for 5 days were transferred to medium complemented with different concentrations of compound 39. Seedlings were gravistimulated in early experiments, as inhibition of endocytosis would be reflected in gravitropic resonses[39]. In addition, seedlings were grown in the dark to avoid possible interference of phototropism with gravitropic responses[41]. Root growth was measured after 48 hours. Both *pte1-1* and *pte2* mutants were not significantly affected when compared to wild type Col-0 seedlings (**Figure 7a**). In fact, both seemed to be slightly resistant, with *pte1-1* showing the strongest effect. As *PTE1* and *PTE2* genes might be redundant we generated a double mutant *pte1-*

1pte2, and three independent homozygous mutant lines were selected. Transcript levels for *PTE1* and *PTE2* remained residual for all three mutants (**Figure 7b**), while *PTE3* and *PTE4* expression was partially down regulated in the *pte1-1pte2* double mutant with number 27 (**Figure 7b**). The two other *pte1-1pte2* mutant lines, with numbers 11 and 33, appeared to have normal *PTE3* and *PTE4* expression. Root growth of the three independent mutant lines was evaluated in the same conditions as for the single mutants. The initially observed resistance was not reproduced, instead all three *pte1-1pte2* mutant lines showed higher sensitivity to compound 39 (**Figure 7c**). The highest sensitivity was observed for the *pte1-1pte2* line with number 27, which therefore was selected as the mutant line for further experimental work. The obtained results were the first indication of a possible connection between the mode of action of compound 39 and the PTE protein family. Further triple and quadruple mutants were generated to strengthen these observations.

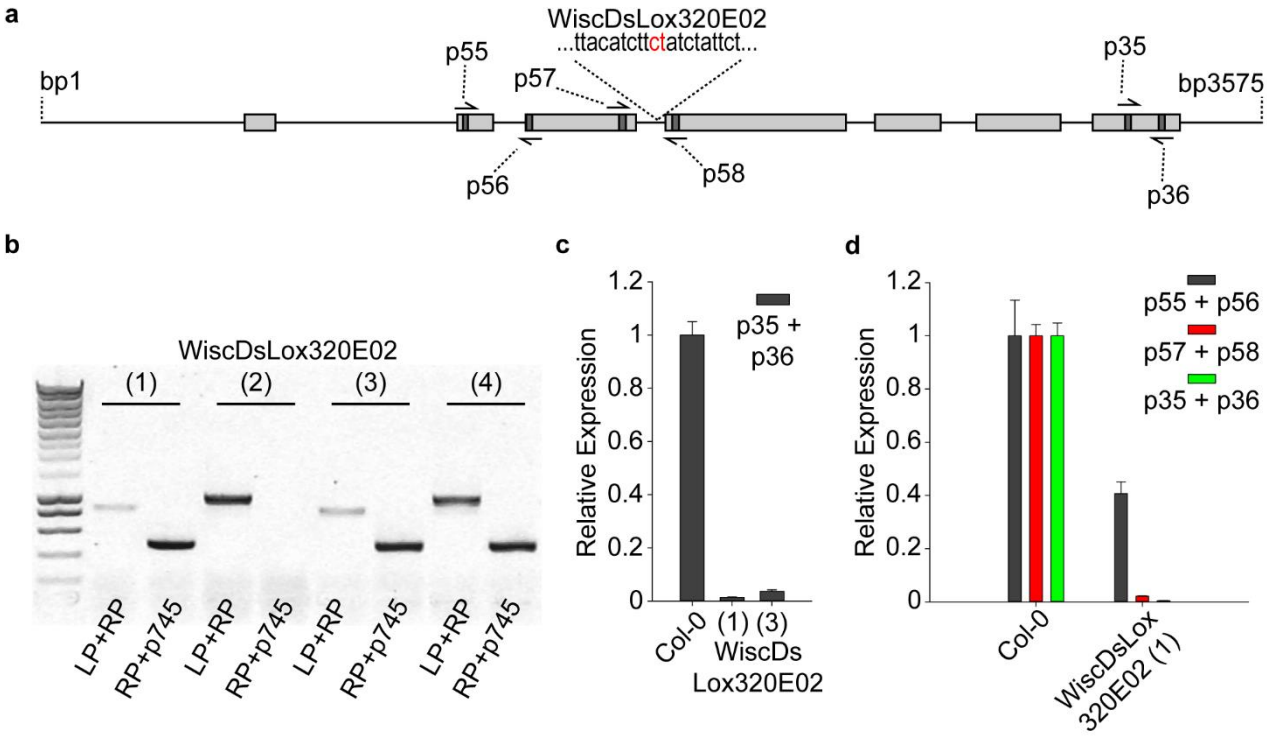

Figure 6. Characterization of *PTE2* mutant.

(**a**) Schematic representation of the *PTE2* genomic region (black line), with light grey boxes representing exons and dark grey regions primer binding sites (e.g. p58). Remaining regions represent sequences upstream and downstream of the *PTE2* gene, as well as introns. WiscDsLox insertion is indicated by triangular structure, with relevant sequence. Insertion site is situated between both nucleotides colored red. (**b**) Representative gels showing amplification products seen with combinations of the left primer (LP) flanking the WiscDsLox insertion, right primer (RP) and TDNA specific primer (p745). (**c**) Results of quantitative PCR (qPCR) for two homozygous lines, and (**d**) more detailed qPCR results for selected mutant line. WiscDsLox320E02: *pte2* mutant

To this end two additional SALK lines were tested, representing the remaining two members from the *PTE* family: SALK_133576 (*pte3*) and SALK_025092 (*pte4*). The *pte3* mutant contained a double insertion in the fourth exon (**Figure 8a**), which is probably an inverted repeat as both the left and right primer flanking the insertion yielded PCR product in combination with the SALK primer LBA1.

Only the combination with the right flanking primer is depicted (**Figure 8b**). The insertion for SALK_025092 was situated at the very end of the first exon (**Figure 8a**), and no aberrant amplification products were observed (**Figure 8c**). No gene specific qPCR primer pair could be designed spanning the insertion site for SALK_133576, therefore transcript analysis is only represented by primer pairs 5' and 3' from the insertion (**Figure 8d**). In contrast to SALK_099018 (*pte1-1*) and WiscDsLox320E02 (*pte2*), 3' transcript levels of At4g37030 (*PTE3*) increased in SALK_133576, likely as a result of transcription driven from the T-DNA insertion. A similar result was obtained for SALK_025092, where an even higher increase of transcript was observed at the 5' and 3' ends of the gene, while absent over the insertion (**Figure 8e**).

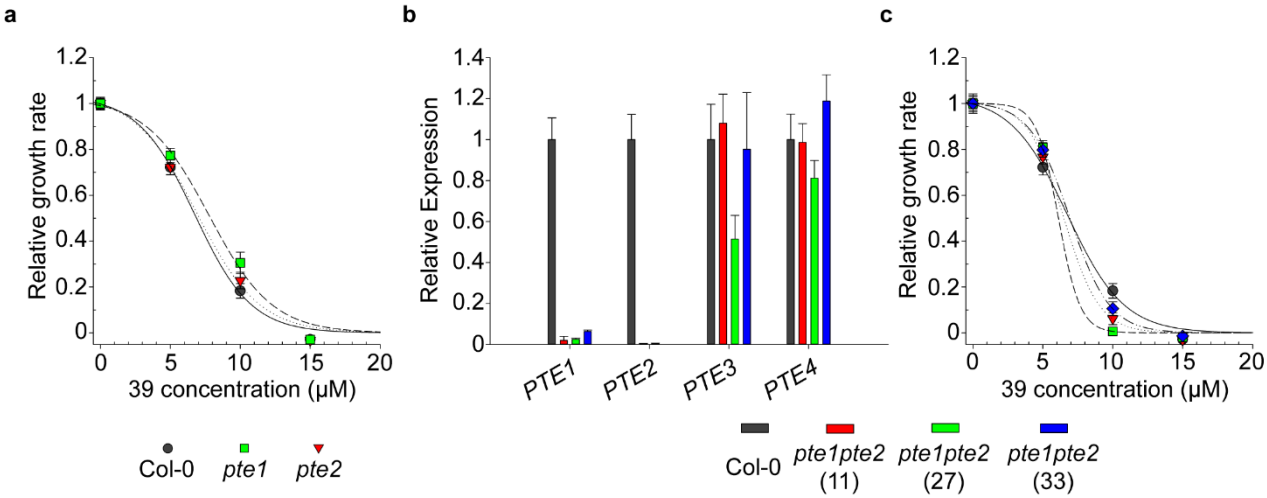

Figure 7. Growth of single and double mutants on small molecule 39.

(**a**) Relative root growth rate of 5 days old seedlings, transferred to new growth medium supplemented with small molecule 39, and left to grow for 48h hours in the dark. (**b**) Quantitative PCR analysis of *PTE* gene expression in different independent *pte1pte2* double mutants. (**c**) Relative root growth rate for different independent *pte1pte2* double mutants as described in (**a**). PTE: putative target of endosidin. Error bars: Standard error of the mean in (a) and (c), standard deviation in (b). n is at least 20 in (a) and (c), 3 in (b)

The *pte3* and *pte4* mutants were first grown on medium containing compound 39 as was done for the other mutant lines in order to evaluate possible resistance or sensitivity to the compound (**Figure 9a**). Both *pte3* and *pte4* single mutants behaved similar to Col-0 and *pte1-1* and *pte2* mutants. Subsequently each single *pte3* and *pte4* mutant was crossed with the *pte1-1pte2* double mutant to generate triple mutants. The resulting *pte1-1pte2pte3* and *pte1-1pte2pte4* triple mutants were crossed in order to generate a quadruple mutant *pte1-1pte2pte3pte4* (referred to in the rest of the manuscript as *pte1to4*). We identified only 2 potential quadruple mutants from the more than 100 F2 plants used for genotyping, of which only one was confirmed by genotyping and qPCR (**Figure 9b**). Though we used the same primers as for the *pte1-1pte2* qPCR analysis, we noted an unexpected reduction in transcripts for *PTE3* and *PTE4*. Upon evaluation of root growth in presence of 39, a similar trend

emerged as seen for the *pte1-1pte2* double mutant, though sensitivity appeared to be spread over a wider concentration range (**Figure 9c**).

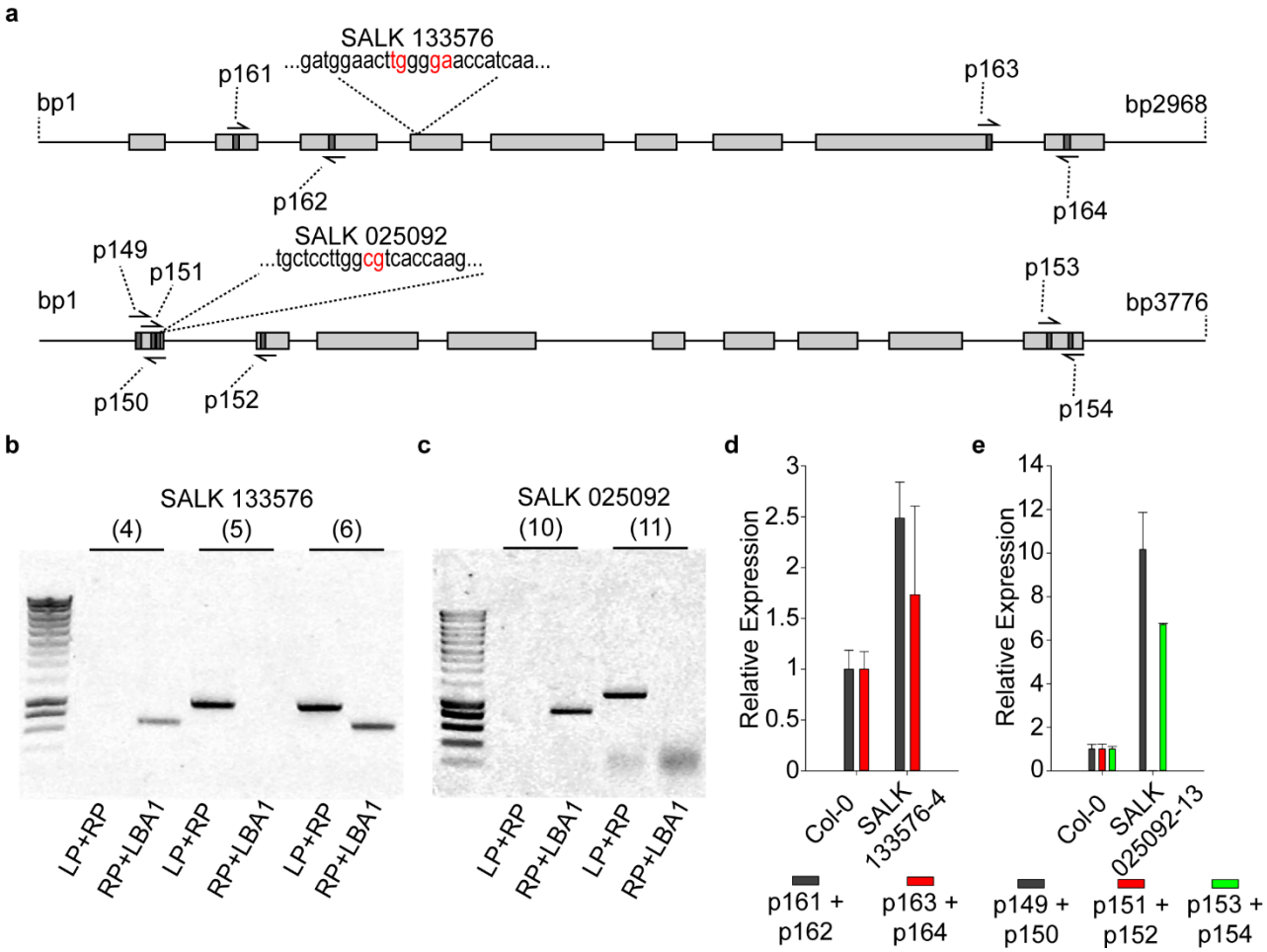

Figure 8. Characterization of *PTE3 and PTE4* mutants.

(**a**) Schematic representation of the *PTE3 and PTE4* genomic region (black line), with light grey boxes representing exons and dark grey regions primer binding sites (e.g. p152). Remaining regions represent sequences upstream and downstream of the *PTE3 and PTE4* genes, as well as introns. SALK insertions are indicated by triangular structure, with relevant sequence. Insertion site is situated between both nucleotides colored red. (**b-c**) Representative gels showing amplification products seen with combinations of the left primer (LP) flanking the SALK insertion, right primer (RP) and TDNA specific primer (LBA1). (**d**) Detailed quantitative PCR (qPCR) result for the *pte3* mutant, and (**e**) detailed qPCR results for the *pte4* mutant. SALK 133576: *pte3* mutant. SALK02592: *pte4* mutant

Sensitivity of mutant lines appeared to be 39 specific.

In order to evaluate if compound 39 affects energy metabolism, PSB-D wild type cell cultures were tested for ATP depletion in the presence of compound. Surprisingly, 39 was able to deplete ATP (**Figure 10a**), though the depletion signature was quite different compared to the protonophore compounds (Chapter 3, this thesis) While the initial ATP levels dropped with about 20%, they remained constant during the remainder measuring time. A similar trend emerged for 39-2 (**Figure 10a**). The observation that 39 could deplete ATP to a certain extent, might indicate that compound 39 is a protonophore. However, ATP production can be affected through a different mode of action, as the ATP depletion signature differed from the one described for protonophore compounds. We

next tested if the increased sensitivity of the *pte1to4* mutant to compound 39 is also retained in the presence of protonophore compounds, thus if the observed sensitivity on 39 was specific. For this, *pte1-1pte2* and *pte1to4* mutant lines were grown in dark on different concentrations of CCCP and compared to Col-0 (**Figure 10b**). We observed a similar sensitivity on 39 appeared for mutant lines compared to Col-0, and suggests a general increase of sensitivity of mutant lines towards small molecules with protonophore mode of action. However, to extend the root growth assays further, *pte1-1pte2* and *pte1to4* mutant lines were grown on 39 and CCCP in the light (**Figure 10c**). Here a different situation emerged. While *pte1-1pte2* seemed to have lost its sensitivity on 39 in the light, *pte1to4* appeared to have an even higher sensitivity on 39 (**Figure 10c**). Surprisingly, this behavior on 39 was not repeated for growth on CCCP, in contrast to the situation in the dark, as both *pte1pte2* and *pte1to4* behaved much like Col-0 on CCCP in the light (**Figure 10c**).

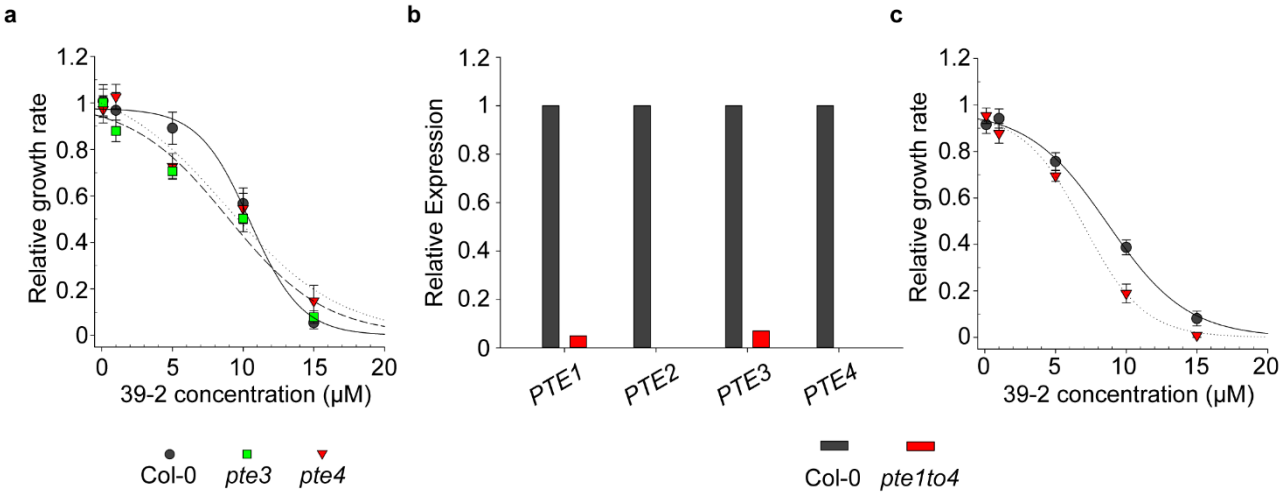

Figure 9. Growth of single and quadruple mutants on small molecule 39-2.

(**a**) Relative root growth rate of 5 days old seedlings, transferred to new growth medium supplemented with small molecule 39-2, and left to grow for 48h hours in the dark. (**b**) Quantitative PCR analysis of *PTE* gene expression in the *pte1to4* quadruple mutant. (**c**) Relative root growth rate of the *pte1to4* quadruple mutant on 39-2 as described in (**a**). PTE: putative target of endosidin. Error bars: Standard error of the mean. N is at least 20.

In conclusion we showed that, although *pte1-1pte2* and *pte1to4* appear slightly sensitive on 39 and possibly protonophores in general, only *pte1to4* retained its increased sensitivity towards compound 39 in the light. The sensitivity of *pte1pte2* on 39 and CCCP was largely gone. This is possibly a first indication that 39 can bind PTE proteins, as the sensitivity of *pte1to4* on 39 appeared to be specific.

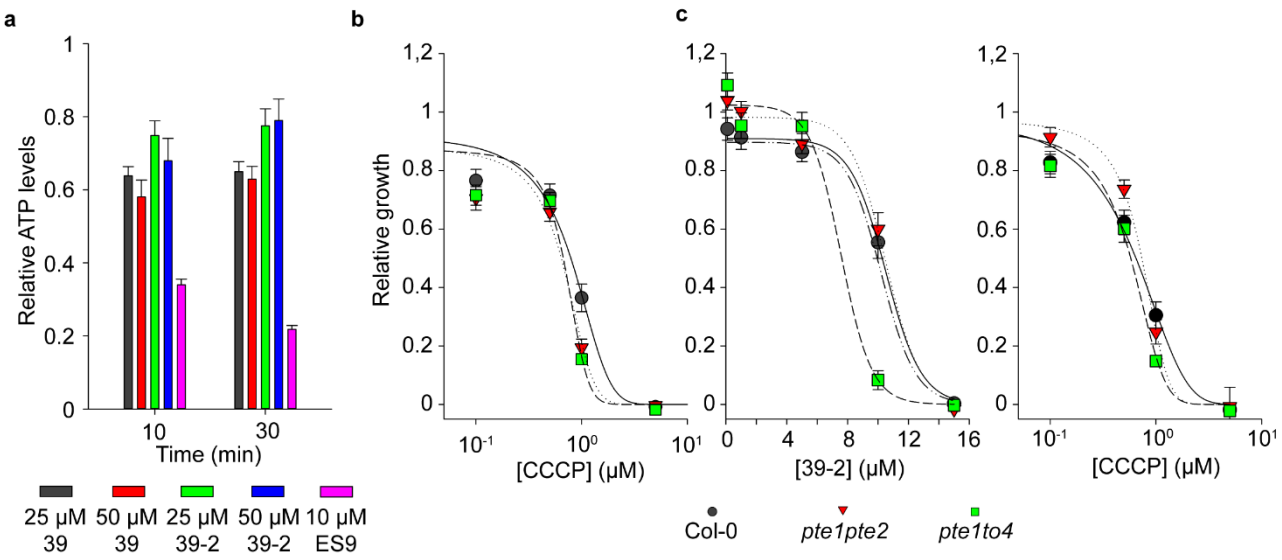

Figure 10. Compound 39 possibly acts as a weak protonophore.

(**a**) Relative (to mock, DMSO) ATP levels in PSB-D wild type cell cultures for ES9 and ES9-2 treatments at the indicated concentration and time-points compared to ES9 mediated ATP depletion. (**b**) Wild type *Arabidopsis* seedlings (Col-0, 5 days) grown in the dark for 48 hour on different concentrations of carbonyl cyanide m-chlorophenyl hydrazone (CCCP), relative to mock (DMSO). Note the higher sensitivity compared to Col-0 of *pte1to4* on CCCP. (**c**) Wild type *Arabidopsis* seedlings (Col-0, 5 days) grown in the light for 48 hour on different concentrations of ES9-2 and CCCP, relative to mock (DMSO). Note the difference in sensitivity compared to Col-0 of *pte1to4* on CCCP and ES9-2. Error bars: standard error of the mean. N is 8 in (a), and at least 20 in (b) and (c).

PTE proteins localize mainly to the plasma membrane.

In a first attempt to characterize the function of the PTE family in Arabidopsis we set out to evaluate the localization of the PTE proteins. The PTE proteins were predicted to be located in the PM, according to gene ontology terms. Based on the plant membrane database ARAMAMNON[38], all four members of the PTE family are predicted to have a total of 5-6 transmembrane domains (**Figure 11a**). The putative transmembrane regions are assigned a score between 0 and 1, with 1 the highest probability, according to AramTmCon, a consensus transmembrane region prediction based on 18 individual algorithms (**Figure 11a**). As PTE1 and PTE2 appear to be the two most important PTE family members, efforts were first focused on them, and several tagged versions of PTE1 and PTE2 were made in to visualize the protein family. In an attempt to determine the topology we inserted GFP in predicted loop regions for PTE1 and PTE2 (**Figure 11a**). From tobacco infiltration experiments we found that only constructs with GFP inserted in the second loop resulted in fluorescence, while the other two GFP insertions were not fluorescent in all experiments (**Figure 11b**). Although the possibility exists that GFP was inserted too close to, or in the actual transmembrane region, it is tempting to speculate that this situation reflects the topology of the PTE protein family. That would mean the N-terminus is oriented towards the cytosol, the first loop to the apoplast, while the second again towards the cytosol (**Figure 11c**). Further experiments are needed to conclude in favor of such situation.

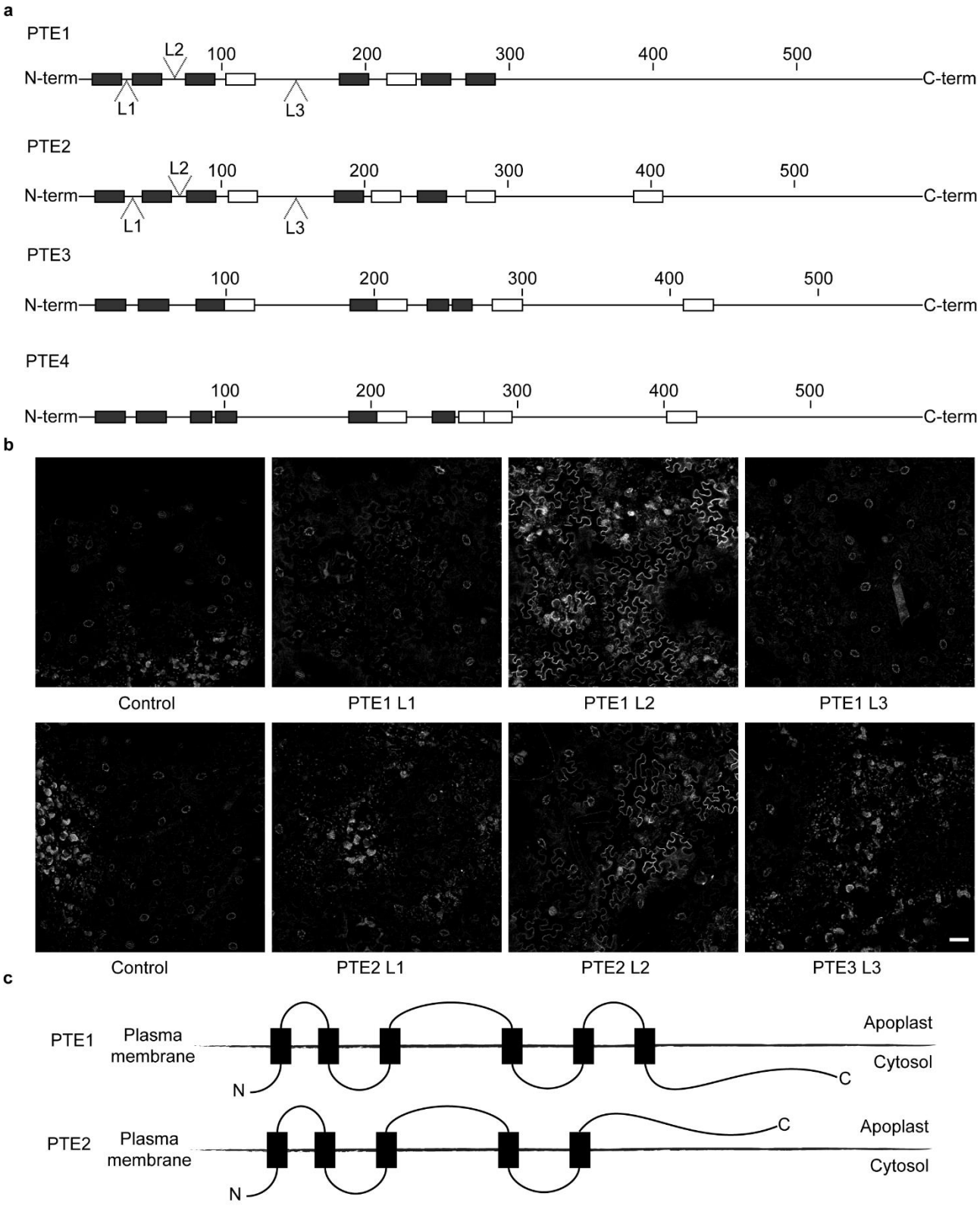

Figure 11 Loop 2 of PTE1 and PTE2 is likely oriented into the cytosol.

(**a**) Schematic representation of predicted trans-membrane regions for PTE proteins according to ARAMEMNON(ref). Dark grey boxes indicate trans-membrane regions with a score above 0.5, while white boxes are predicted trans-membrane regions with a score below 0,5 Triangles indicate the insertion positions of GFP in predicted loop regions between two trans-membrane domains. (**b**) *Nicotiana benthamiana* leaf infiltration with different constructs representing the GFP insertions in loops regions of PTE1 and PTE2. Control represents non-infiltrated leaf. Scale bar 50 µm. (**c**)

Schematic representation of the possible PTE1 and PTE2 topology. Only transmembrane regions with a prediction score above 0.5 (black boxes) are depicted.

Next, classical C-terminal GFP fusions were generated for all four members and visualized when stably expressed in *Arabidopsis* (**Figure 12**). As expected, both PTE1 and PTE2 localized mainly to the plasma membrane, while a weaker cytosolic signal was present. Though the cytosolic signal resembled ER localization, it is preliminary to conclude to such localization as no co-localization experiments with ER markers or dyes were performed. In addition, PTE1-GFP localized to distinct spots in the cytosol (**Figure 12 inset**), which are of unknown nature. The localization of the other two members, PTE3-GFP and PTE4-GFP is ongoing.

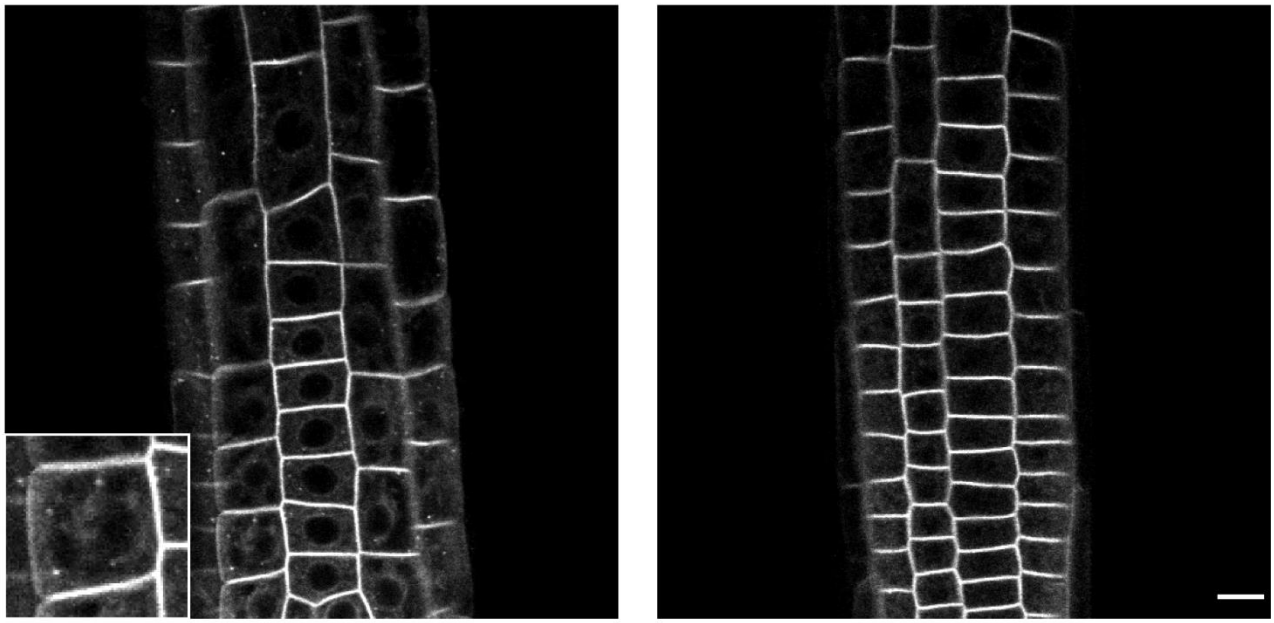

Figure 12. PTE1 and PTE2 localized mainly at the plasma membrane

C-terminal tagged PTE1-GFP (left) and PTE2-GFP (right) localized mainly at the plasma membrane, in addition to a weaker cytosolic signal. Note the spot-like structures observed for PTE1-GFP (inset), likely of endosomal nature. Scale bar: 15 µM

PTE1 interacts with MSBP2

In search for more information on the different PTE proteins, all members of the family were queried against the Membrane-based Interactome Network Database (MIND, http://cas-biodb.cas.unt.edu/project/mind/index.php)[41]. Only PTE1 was found to interact with a number of proteins. Interactions were scored based on the number of positive split-ubiquitin interaction in the 2 primary and 2 secondary screens. Amongst interactors of PTE1 with the highest score (i.e. scored in all 4 assays positive) were a considerable amount of proteins involved in sterol binding and metabolism. These include a member of the sterol methyl oxidase (SMO) family (AT4G22756), MEMBRANE-ASSOCIATED PROGESTERONE BINDING PROTEIN 2 (MAPR2; AT2G24940) and MEMBRANE STEROID BINDING PROTEIN 2 (MSBP2; AT3G48890). A related interactor

which was only confirmed in 3 out of 4 experiments was the MEMBRANE STEROID BINDING PROTEIN 1 (MSBP1; AT5G52240). It is worth mentioning that also BRASSINOSTEROID INSENSITIVE 1 (BRI1; AT4G39400) was found, yet only in one out of four experiments. As MSBP2 was one of the best interactors in the initial release of the MIND database we decided to confirm the PTE1-MSBP2 interaction by bimolecular fluorescence complementation (BiFC). As expected, PTE1 and MSBP2 fused to head GFP (hGFP) or tail GFP (tGFP) alone were not able to fluoresce (**Figure 13a**). PTE1 fused to tGFP combined with hGFP induced fluorescence (**Figure 13b**), though PTE1-hGFP with tGFP could not. The latter is probably be due to very weak tGFP expression, as evaluated by the weak RFP signal. Both hGFP and tGFP constructs contain RFP in the backbone, which serves as a control for efficient infiltration. For that reason, both hGFP and tGFP alone were not able to induce fluorescence (**Figure 13b**). When MSBP2 and PTE1 constructs were combined, both orientations induced fluorescence (**Figure 13c**), similar as the PTE1-hGFP and PTE1-tGFP combination. The former indicates binding, especially because both are transmembrane proteins, while the latter hints towards the ability of PTE1 proteins to homodimerize. The above results therefore indicate binding between MSBP2 and PTE1, though this interaction would need to be validated with independent experimental readouts.

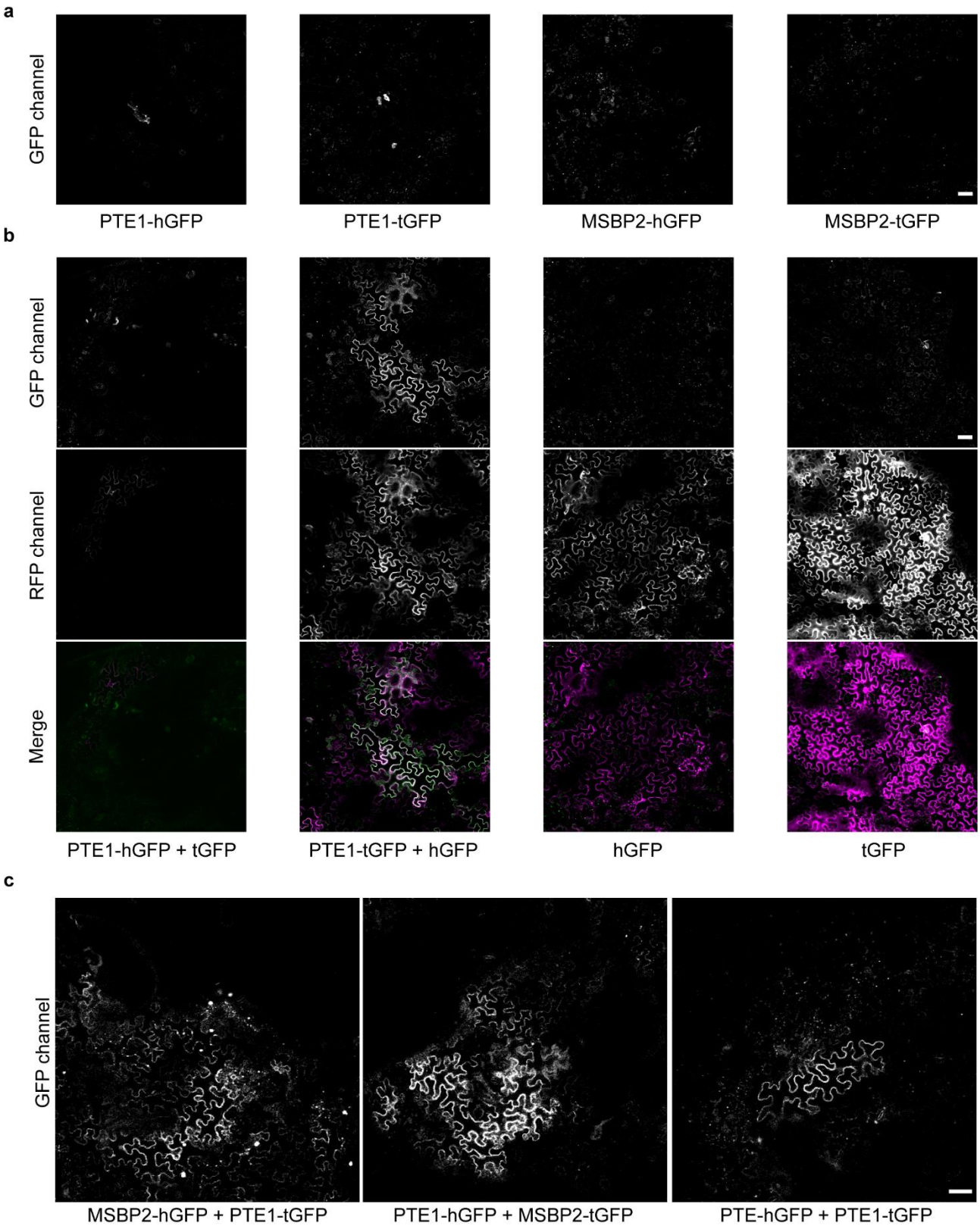

Figure 13. PTE1 interacts with MSBP2 through BiFC in *Nicotiana benthamiana*

(**a**) Infiltration of bimolecular fluorescence complementation (BiFC) constructs for PTE1 and MSBP2 alone fail to induce fluorescence. (**b**) Combination of PTE1 BiFC constructs with either hGFP or tGFP constructs induced GFP signal, though the PTE1-hGFP and tGFP combination induced very weak signal. No GFP signal was observed for hGFP or tGFP alone, while infiltration was successful, judged from the RFP signal originating from the vector backbone. (**c**) Combination of MSBP2 and PTE1 constructs induced GFP signal, in addition to the PTE1-hGFP and PTE1-tGFP combination, indicating possible homodimerization. Head GFP (hGFP), tail gfp (tGFP). Scale bar: 5 µm

Discussion

Protein function annotation based on structural homology searches and predictions is a field of computational biology which is increasingly used as proteins can lack orthologs in other systems based on primary sequence alone[42], yet might share a similar tertiary or quaternary protein structure. Although several computational strategies exist to identify possible target proteins for selected ligands[43], or explore possible ligands for a given target protein, we chose an approach within reach of our limited knowledge on computational prediction to find putative target proteins of 39 in *Arabidopsis.* To this end we used BackPhyre as part of the Phyre2[29]. We identified four putative target proteins of 39, based on the LBD of PPARγ in complex with Rosiglitazone[27]. However, BackPhyre seems to be rarely used, as only one report was found which used BackPhyre[44], and therefore might indicate a poor performance in terms of prediction. This could, in combination with the unconventional target fishing result in unreliable target prediction for 39. An independent search with the same parameters however, using a similar an frequently used search engine called HHpred[45], resulted in the identification of the same set of proteins in *Arabidopsis* (data not shown), indicating the BackPhyre predictions are valid. Interestingly the HHpred structural alignment was located at the C-terminal part of the PTE protein family.

As the entire PTE protein family has unknown function, little is found on either PTE protein in literature. The most information can be found on PTE1 and PTE2, which have been localized on the PM based on a study which evaluated phosphorylation events of PM proteins after 10 min of flagellin22 (flg22) or xylanase[37]. A phosphorylation on S223 was identified for PTE2, located in the C-terminal cytosolic domain for samples treated with flg22, but not with xylanase. While the identified phosphorylation on the PTE2 peptide was considered significant, the phosphorylated peptide for PTE1 was found only once, and thus not significant. Another study indicated that PTE2 can be phosphorylated on S560, further towards the C-terminus compared to the flg22 induced phosphorylation, by Ca^{2+}-dependent protein kinase 16 (CPK16)[46]. These results suggest a role for PTE2 in flg22-induced defense responses, which might be mediated through Ca^{2+} signaling. The only report where PTE1 is mentioned[37] indicates it is probably not involved in defense responses, at least not through flg22 or xylanase induced signaling events. Therefore PTE1 might have a different function, which might be linked with sterol metabolism and transport, as PTE1 seems to interact with sterol binding proteins such as MSBP2. Although these observations have to be further strengthened and validated, it is probable that PTE proteins interact with different kinds of sterol binding proteins. One could therefore speculate that PTE proteins are the link between defense induced signaling and adaptation of the plasma membrane through altered sterol composition in order to properly respond to pathogen attack.

Currently, substantial efforts go into the characterization of the PTE protein family in terms of mutant phenotype, interaction with proteins such as MSBP1 and MSBP2, and the implications for cell biology and endomembrane traffic. Importantly though, because *pte* mutants are still viable and show hardly any obvious phenotype, inhibition of CME by 39 application is likely not mediated by the PTE protein family. It might therefore be established through an non-specific mechanism, or through different protein targets of 39. Here the reduction in ATP content comes into view, together with the slight sensitivity of *pte* mutants on CCCP. Indeed, it is conceivable that 39 would possess protonophoric characteristics, though much less potent compared to ES9 (Chapter 3, this thesis), as judged from the ATP depletion in PSB-D wild type cell cultures. The observations concerning the *pte1-1pte2* and *pte1to4* sensitivity on CCCP and 39 are in support of the above hypothesis. In dark grown seedlings the only source of ATP is derived from the mitochondria, while chloroplast provide an important contribution in the light. Any interference with mitochondrial function which reflects on ATP production will be therefore more pronounced in the dark. As such the slight increase in sensitivity on 39 can be explained, given that the mutants display a similar sensitivity on the known protonophore CCCP. How the PTE protein family is linked to a higher sensitivity on protonophoric small molecules is unclear. Furthermore, the marked increase in sensitivity on 39 of the *pte1to4* quadruple mutant, which was not repeated on CCCP, indicates that this particular increase in sensitivity is likely linked to PTE proteins, either directly or indirectly, and possibly reflects 39 binding. It would be interesting to see how all other possible mutant combination behave on 39, (i.e. the *pte3pte4* double mutant), in order to fully dissect the individual contribution of PTE proteins in terms of 39 binding, in addition to a thorough analysis of CME in the quadruple mutant.

Initial SAR analysis was based on the ability to inhibit FM4-64 uptake, but given the discussion above, might be an insufficient assessment of 39 and related analogs in terms of activity towards the PTE protein family. It would therefore be essential to re-assess analog activity by evaluating effects on *pte1to4* root growth.

As the PTE protein family is not essential for cell survival, sensitivity of the *pte1to4* mutant to compound 39 indicated that growth inhibition is not established through possible 39 binding to the PTE protein family alone. It therefore confirms the existence of additional target proteins, and thus a polypharmacological binding nature. The opposite situation, in which the *pte1to4* mutant is completely resistant to 39, would be indicative of the sole contribution of the PTE protein family to growth inhibition, and would indicate that 39 only targets PTE proteins which mediate the growth inhibition. Other protein targets which are not contributing to growth inhibition cannot be excluded in that situation however.

Further dissection of chemical structure requirements for 39 activity towards PTE proteins would allow a better understanding on 39 association with PTE proteins, and would facilitate the development of a more specific inhibitor for the PTE protein family through abolishing non-specific

effects such as the presumed protonophore characteristics. To this end a continuation of 39 SAR has been initiated, for which the chemical synthesis is described in the methods section.

In conclusion we identified a small molecule which has the potential to be confirmed as an inhibitor of the PTE protein family with unknown function in *Arabidopsis.* Identification was mediated through computational prediction of putative targets, based on a known small molecule with similar chemical characteristics as 39, in complex with its target in human systems. Although we don't have a clear image yet on the contribution of the PTE protein family in plant biology, evidence suggests a role in defense responses and sterol metabolism or transport.

Material and methods

Plant material and growth conditions

Arabidopsis thaliana (accession Columbia-0 [Col-0]) seedlings and other lines were stratified for 2 days at 4°C, and grown vertically on agar plates containing ½ strength Murashige and Skoog (½MS) medium supplemented with 1% (w/v) sucrose for 5 days at 22°C in a light/dark cycle of 16 h/ 8 h respectively, prior to use. Following marker line was used: MAP4-GFP[47]. SALK_099018 (N599018), SALK_142384 (N642384), SALK_133576 (N679117), SALK_025092 (N525092) and WiscDsLox320E02 (N851129) were acquired through the European Arabidopsis Stock Centre NASC.

Genotyping of insertion mutants and preparation of constructs.

All primers used for genotyping of insertion mutants (single mutants and higher order mutants) can be found in Supplemental table 1. The LBA1 and p745 primers were used for SALK and WiscDsLox insertion mutant respectively.

At5g40640 (attB1F_40640, attB2R_40640, attB2R_40640_nostop), At3g27390 (attB1F_27390, attB2R_27390, attB2R_27390_nostop), At4g37030 (attB1F_37030, attB2R_37030, attB2R_37030_nostop) and At4g12680 (attB1F_12680, attB2R_12680, attB2R_12680_nostop) were amplified from *Arabidopsis* Col-0 cDNA with indicated primers to yield coding sequence (CDS) with stop and without stop flanked by attB-sites (Invitrogen). Amplified fragments were cloned in the pDONR221 vector (Life Technologies). The resulting entry vectors were used in subsequent cloning. In order to insert GFP in the different loops of At5g40640 and At3g27390 we adopted a cloning strategy as previously described[48]. The general strategy consisted of the GFP CDS insertion in the middle of each loop region, as identified through the consensus prediction of trans-membrane regions (**Figure 11a**, ARAMEMNON[38]. Predictions with a score below 0.5 were not considered as potential trans-membrane region. On each side, between GFP and the protein sequence, a linker region was inserted (amino acid composition SGGGGS) to allow flexibility for GFP and the protein to fold properly. The nucleotide sequence of each linker used a different codon for serine (TCTGGAGGCGGCGGATCT and TCAGGCGGAGGAGGCTCA) to control directionality of the GFP insertion. Briefly, each CDS was amplified in two fragments: one from the start codon to insertion site (primers attB1F_40640/27390 and 40640/27390_L1rev), the second from the insertion site to the stop codon (primers attB2R_40640/27390 and 40640/27390_L1fw). The GFP CDS was amplified from any GFP (without stop) containing vector with primers eGFP_Lxfw and eGFP_Lxrev. DNA was purified from resulting gel-pieces and combined in a standard PCR reaction without added primers. As such the total CDS with inserted GFP sequence was generated through annealing of the linker sequence overhangs of each fragment. A final PCR reaction with attB containing primers (attB1F_40640/27390, attB2R_40640/27390) ensured amplification of enough product to insert in a

pDONR221 vector. Entry vectors were used for subsequent cloning into several destination constructs, including pH2GW7 (for constructs with GFP insertion) and pDONRRP4-1R_RPS5A, pDONRRP2R-P3_GFPstop and pK7m34GW for C-terminal GFP-tagged versions.

Generation of clones for bimolecular fluorescence complementation was done as described before[49].

qPCR

Seedlings (5 days) were flash frozen in liquid N_2, grinded using a Retsch® MM400, and 1 ml Trizol reagent (Molecular Research Center) was applied per sample. Next, 0.2 ml chloroform was added prior to centrifugation for 15 min at 12000 g and 4°C. The top phase was transferred to a new recipient and supplemented with 0.5 ml isopropanol. From there on, samples were applied on RNeasy mini kit columns (Qiagen) and the protocol was finished according to manufacturer's instructions. Concentration of purified RNA was determined with a NanoDrop spectrophotometer (Thermo Scientific), after which all samples were brought to a concentration of approximately 100 ng/µl. For each sample 1 µg of RNA was subsequently used for cDNA synthesis (iScript, Bio-Rad, according to manufacturer's instructions), and cDNA was diluted 10 times. Samples and primers (Supplemental table 1) were distributed and mixed with SYBR green I master mix (Roche Diagnostics) and run on a Light Cycler 480 (Roche Diagnostics).

Tobacco infiltration and bimolecular fluorescence complementation

Nicotiana benthamiana infiltration with *Agrobacterium tumefaciens* culture was performed as described earlier[49]. *Agrobacterium* transformed with appropriate constructs was cultured in yeast extract broth (YEB) medium for 2 days with applicable antibiotics. Culture was washed and re-suspended in infiltration medium (0.5 mM methyl esther sulfonate [MES], 1 mM $MgCl_2$ and 100 µM acetosyringone) with a final optical density at 600 nm (OD600) of 1. Leaves of four weeks old *N. bentamiana* plants were infiltrated with a syringe, and imaged 3-4 days after.

Chemical treatments and imaging

Compound 39 and analogs were acquired through Chembridge (http://www.chembridge.com/) or synthesized as described below. Carbonyl cyanide 3-chlorophenylhydrazone was acquired through Sigma-Aldrich. All were dissolved in DMSO (Sigma-Aldrich). Visualization of endocytosis was achieved with 2µM N-(3-Triethylammoniumpropyl)-4-(6-(4-(Diethylamino) Phenyl) Hexatrienyl) Pyridinium Dibromide (FM4-64, Life technologies) application. Imaging of seedlings and *N. benthamiana* leaves was performed with an Olympus FV10 ASW confocal laser scanning microscope using a 60x water immersion lens (NA 1.2) and 3x digital zoom. Images were processed using the imageJ (Fiji) software packages.

BES1 dephosphorylation assay

PSB-D cell cultures expressing BES1-TAP were generated and maintained as described before[50,51]. Cell cultures were treated with different concentrations of 39 as indicated, brassinolide (BL, 1 μM) for 1 hour while shaking at 130 rpm and harvested and homogenized in liquid nitrogen. Protein extraction was performed with a 20mM Tris-HCl buffer containing 150 mM NaCl, 1% Sodium Dodecyl Sulfate (SDS), 100 mM Dithiothreitol (DTT) and 1 cOmplete ultra tablet per 10 ml of EDTA free protease inhibitor cocktail (Roche). Protein concentration was determined with the Quick start Bradford 1x Dye reagent (Bio-Rad). Samples (30 μg) were run on a 10% SDS-PAGE gel and transferred to polyvinyl difluoride (PVDF) membrane from iBlot Gel Transfer Stack (Novex, Life Technologies) using the iBlot device (Life technologies). Membranes were blocked for 1 hour in Tris buffered Saline with 0.1 % Tween 20 (TBS-T, Sigma-Aldrich) and 3% Difco Skim milk (Becton, Dickinson and Company). Detection of BES1-TAP occurred with a 1/5000 dilution in TBS-T 3% skim milk of Horseradish peroxidase (HRP) conjugated Peroxidase Anti-Peroxidase (PAP) Soluble Complex antibody produced in rabbit (P1291, Sigma) for 1 hour. Membrane was developed with application of Western Lightning® Plus–ECL, Enhanced Chemiluminescence Substrate (Perkin-Helmer) and Amersham Hyperfilm ECL (GE Healthcare).

ATP measurements

Wild type PSB-D Arabidopsis cell cultures were used and maintained as described beforeVan Leene, 2007. Cell culture of 3 days old was diluted 5 times and mixed thoroughly prior to distribution of 95 μl in 96-well plates. Subsequently, 5 μl of a 1/50 dilution of small molecule stock solution (1000x) in MS medium with Minimal Organics (MSMO) medium was added to cells (final dilution of 1000x) using a Tecan Freedom EVO® robot. ATP levels were detected by addition of 80 μl of ATPlite 1step Luminescence Assay System (Perkin Elmer) after incubation of cells in presence of small molecule for indicated time. Fluorescence was detected using a Perkin Elmer EnVision 2104 multilabel reader with the Wallac Envision manager software package. ATP-lite luminescence was detected with the ultra-sensitive luminescence techonology.

Phylogenetic tree generation

Complete protein sequences (64) from algae (*chlamydomonas reinhardtii*), lower plants (*Physcomitrella patens*) and higher plants including both monocots and dicots, covering in total 17 species, were down loaded from PLAZA v3.0[35]. A ClustalX v2.0 multiple sequence alignment[52] was generated, which was subsequently used for the Molecular Evolutionary Genetic Analysis (MEGA 6) tool. A Neighbor-joining (NJ) algorithm with p-distance method and pair wise deletion of gaps, using default parameters was adopted to generate an un-rooted phylogenetic tree. A total number of 1000 replicates were tested per analysis and bootstrap statistical analysis for these replicates was employed to test the phylogeny[53].

Chemical syntheses

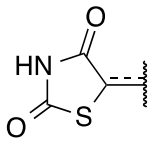

a	b	c	d	e
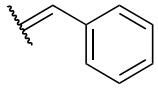	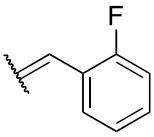	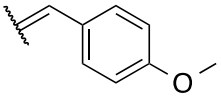	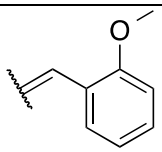	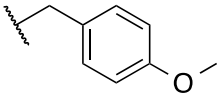

Compounds a-d (Knoevenagel condensation)

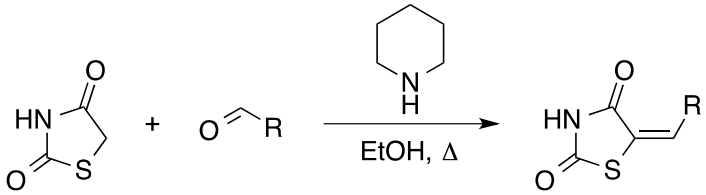

2,4-thiazolidinedione (1g, 8.5 mmol, 1.0 equiv.) together with the appropriate aldehyde (1.0 equiv.) is dissolved in ethanol (85 ml). Piperidine (672 µL, 0.8 equiv.) is added and the mixture is refluxed for 20h. After cooling, the mixture is poured into water (50 mL) and acetic acid is added until precipitation occurs. The solid is collected and dried at 50°C under vacuum. The resulting amorphous solid is recrystallized from methanol.

Compound e

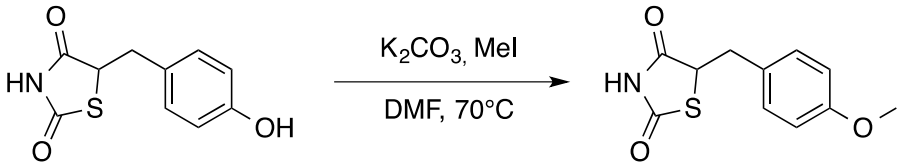

5-(4-hydroxybenzyl)-2,4-thiazolidinedione (500 mg, 2.2 mmol, 1.0 equiv.) is dissolved in dimethylformamide (5 mL). Potassium carbonate (588 mg, 4.1 mmol, 1.9 equiv.) is added and the mixture is stirred for 5 min. Methyl iodide (164 µL, 2.6 mmol, 1.2 equiv.) is added and the reaction is heated to 70°C and stirred until judged complete by TLC. The mixture is concentrated *in vacuo* and the residue is taken up in an ethyl acetate-ammonium chloride mixture (60 mL, 1:1 v/v). The organic phase is washed with water (3×10 mL) and a saturated sodium chloride solution (10 mL). The organic phase is dried on sodium sulfate, filtered and concentrated *in vacuo*. The resulting solid is dried at 50°C under vacuum and subsequently purified by flash chromatography (silica, methanol: chloroform, 6:94 v/v) to yield **e** as a pale yellow solid (245.9 mg, 1.1 mmol, 47%).

a: Formula: $C_{10}H_7NO_2S$; M: 205.23 g/mol; ^{1}H-NMR (300MHz, $(CD_3)_2SO$): δ 12.62 (s(br), 1H), 7.80 (s, 1H), 7.60 (d(br), 2H, J = 7.4 Hz), 7.54 (d(br), 2H, J = 7.4 Hz), 7.48 (d(br), 2H, J = 7.4 Hz); ^{13}C-NMR (125 MHz, $(CD_3)_2SO$): δ 167.9, 167.3, 133.0, 131.8, 130.4, 130.0, 129.3, 123.5; HRMS (m/z): $[M\text{-}H^+]^-$ calcd. for $C_{10}H_6NO_2S^-$, 204.0125; found, 204.0131

b: Formula: $C_{10}H_6FNO_2S$; M: 223.22 g/mol; ^{1}H-NMR (300MHz, $(CD_3)_2SO$): δ 12.70 (s(br), 1H), 7.97 (s, 1H)), 7.59 – 7.51 (band, 2H), 7.42 – 7.35 (band, 2H); ^{13}C-NMR (125 MHz, $(CD_3)_2SO$): δ 167.6, 167.0, 160.5 (d, $^1J_{CF}$ = 250.0 Hz), 132.8 (d, $^3J_{CF}$ = 8.8 Hz), 128.8, 126.3, 125.4, 122.7 (d, $^3J_{CF}$ = 6.5 Hz), 121.0 (d, $^3J_{CF}$ = 11.9 Hz), 116.2 (d, $^2J_{CF}$ = 21.7 Hz); HRMS (m/z): $[M\text{-}H^+]^-$ calcd. for $C_{10}H_5FNO_2S^-$, 222.0031; found, 222.0038

c: Formula: $C_{11}H_9NO_3S$; M: 235.26 g/mol; ^{1}H-NMR (300MHz, $(CD_3)_2SO$): δ 11.01 (s(br), 1H), 7.75 (s, 1H), 7.62 – 7.57 (m, 2H), 7.14 – 7.09 (m, 2H), 3.89 (s, 3H); ^{13}C-NMR (125 MHz, $(CD_3)_2SO$): δ 132.1, 132.0, 125.9, 114.8, 55.0; HRMS (m/z): $[M\text{-}H^+]^-$ calcd. for $C_{11}H_8NO_3S^-$, 234.0230; found, 234.0228

d: Formula: $C_{11}H_9NO_3S$; M: 235.26 g/mol; ^{1}H-NMR (300MHz, $(CD_3)_2SO$): δ 12.55 (s, 1H), 7.97 (s, 1H), 7.50 – 7.46 (m, 1H), 7.43 – 7.40 (m, 1H), 7.16 (d(br), 1H, J = 8.4 Hz), 7.10 (d(br), 1H, J = 8.4 Hz), 3.89 (s, 3H); ^{13}C-NMR (125 MHz, $(CD_3)_2SO$): δ 168.1, 167.4, 158.0, 132.4, 128.6, 126.5, 123.5, 121.4, 121.0, 111.9, 55.8; HRMS (m/z): $[M\text{-}H^+]^-$ calcd. for $C_{11}H_8NO_3S^-$, 234.0230; found, 234.0231

e: Formula: $C_{11}H_{11}NO_3S$; M: 237.27 g/mol; TLC (methanol:chloroform, 1:9 v/v): R_f = 0.7; ^{1}H-NMR (300MHz, $(CD_3)_2SO$): δ 9.33 (s, 1H), 7.10 – 6.99 (m, 2H), 6.72 – 6.66 (m, 2H), 4.82 (dd, 1H, J = 9.4, 4.3 Hz), 3.31 (dd, 1H, J = 14.1, 4.3 Hz), 2.98 (dd, 1H, J = 14.1, 9.4 Hz); ^{13}C-NMR (125 MHz, $(CD_3)_2SO$): δ 174.0, 171.2, 156.4, 130.2, 126.6, 115.2, 51.4, 36.5, 27.5; HRMS (m/z): $[M\text{-}H^+]^-$ calcd. for $C_{11}H_{10}NO_3S^-$, 236.0387; found, 236.0379

Supplemental information

Supplemental Table 1. Putative interactors of 39 as identified through BackPhyre

Rank	Description	Organism	Gene name	Alignment	Confidence	% i.d.
1	gi|30693640|ref|NP_198880.2| unknown protein	*A. thaliana*	AT5G40640	105-225	86.6	19
2	gi|30688768|ref|NP_189375.2| unknown protein	*A. thaliana*	AT3G27390	105-225	80	17
3	gi|79497780|ref|NP_195420.2| unknown protein	*A. thaliana*	AT4G37030	105-225	77	15
4	gi|15235450|ref|NP_193004.1| unknown protein	*A. thaliana*	AT4G12680	105-223	74.6	13
5	gi|15220546|ref|NP_176947.1| unknown protein	*A. thaliana*	AT1G67810	78-222	65.3	11
6	gi|15220831|ref|NP_178196.1| unknown protein	*A. thaliana*	AT1G80810	169-256	57.1	9
7	gi|18409259|ref|NP_564964.1| unknown protein	*A. thaliana*	AT1G69390	174-206	49.1	26
8	gi|15223907|ref|NP_172353.1| unknown protein	*A. thaliana*	AT1G08760	110-207	29.6	9
9	gi|15234115|ref|NP_192035.1| transcription regulator	*A. thaliana*	AT4G01260	82-104	21.5	36
10	gi|42564175|ref|NP_188107.3| DNA binding / catalytic	*A. thaliana*	AT3G14890	86-103	20	33

Supplemental Table 2. List of used primers.

Primers used for genotyping	
SALK_099018_LP	AATCACAGCACCTGGAATTTG
SALK_099018_RP	GCGATCTTCAATGCCATAAAG
SALK_142384_LP	ACCGATCACCAAGAAACACAC
SALK_142384_RP	GCCAGAGAATGACACCAAGAG
SALK_133576_LP	CATCTTTGCCTTTTGTTCTGC
SALK_133576_RP	CTCGATTAATCGCGTCTTGAG
SALK_025092_LP	GAACCATCAACAAAGCAATGG
SALK_025092_RP	ATTTGTATGTCCTCGGCAATG
WiscDsLox320E02_LP	ACTCGTATGCCTCGTTGTGAC
WiscDsLox320E02_RP	GGTACAGGACCAGAAAAAGGC

LBA1	TGGTTCACGTAGTGGGCCATC
P745	AACGTCCGCAATGTGTTATTAAGTTGTC
Primers used for cloning	
attB1F_40640	GGGGACAAGTTTGTACAAAAAAGCAGGCTCAATGGAGCCTCCAACGGGA
attB2R_40640	GGGGACCACTTTGTACAAGAAAGCTGGGTTTTACACAATATCAATGTCTCTTAAC
attB2R_40640_nostop	GGGGACCACTTTGTACAAGAAAGCTGGGTTCACAATATCAATGTCTCTTAACC
attB1F_27390	GGGGACAAGTTTGTACAAAAAAGCAGGCTCAATGGAGCCTCCAATAGGATT
attB2R_27390	GGGGACCACTTTGTACAAGAAAGCTGGGTTTTAAACTATATCTACATTCCTTGA
attB2R_27390_nostop	GGGGACCACTTTGTACAAGAAAGCTGGGTTAACTATATCTACATTCCTTGAGA
attB1F_37030	GGGGACAAGTTTGTACAAAAAAGCAGGCTCAATGGCTGTCGTCGTCACT
attB2R_37030	GGGGACCACTTTGTACAAGAAAGCTGGGTTTTAACCCTCTTCAATGAAATCT
attB2R_37030_nostop	GGGGACCACTTTGTACAAGAAAGCTGGGTTACCCTCTTCAATGAAATCTC
attB1F_12680	GGGGACAAGTTTGTACAAAAAAGCAGGCTCAATGGAAGTTCCCAAAGGATT
attB2R_12680	GGGGACCACTTTGTACAAGAAAGCTGGGTTTTAGACAACATCCATGTCCG
attB2R_12680_nostop	GGGGACCACTTTGTACAAGAAAGCTGGGTTGACAACATCCATGTCCGG
AttB1F_MSBP2	GGGGACAAGTTTGTACAAAAAAGCAGGCTCAATGGTTCAGCAAATATGGGA
AttB2R_MSBP2	GGGGACCACTTTGTACAAGAAAGCTGGGTTTTACTCCTTTGCAGCATCAT
AttB2R_MSBP2_nostop	GGGGACCACTTTGTACAAGAAAGCTGGGTTCTCCTTTGCAGCATCATCAT
40640_L1rev	AGATCCGCCGCCTCCAGAACCTTTAATGACACCGAGAAGC
40640_L1fw	TCAGGCGGAGGAGGCTCAATCGTTTTATGCCCGCTTATATGC
40640_L2rev	AGATCCGCCGCCTCCAGAATATAGAGTCCAAATCGCGTGTAC
40640_L2fw	TCAGGCGGAGGAGGCTCATCGATAGCGAGTGCTAAACAGT
40640_L4fw	TCAGGCGGAGGAGGCTCAAAAGATGTTTGCTTTCACTCCTACT
40640_L4rev	AGATCCGCCGCCTCCAGAAAAATCACAAACAACGGTGAAACTG
27390_L1rev	AGATCCGCCGCCTCCAGATATAGTCACAACGAGGCATACG
27390_L1fw	TCAGGCGGAGGAGGCTCAGGCAACTCCGCGGTCATAC
27390_L2rev	AGATCCGCCGCCTCCAGACAAGATTGGTCCTACTTGTTTGG
27390_L2fw	TCAGGCGGAGGAGGCTCAAAGATCTTTCTATGCTTATGTCTTCC
27390_L3rev	AGATCCGCCGCCTCCAGAGGTGAAGCTGCGTTGCATG
27390_L3fw	TCAGGCGGAGGAGGCTCAGTTGTTCGGGATTTTAAAGATGTTT
eGFP_Lxrev	TGAGCCTCCTCCGCCTGACTTGTACAGCTCGTCCATGC
eGFP_Lxfw	TCTGGAGGCGGCGGATCTATGGTGAGCAAGGGCGAGG
Primers used for qPCR	
33	GGCGGTTCGAGATCAGTTC
34	CCCTCTGTTTGGTGAATCTTG
35	AAGACAACAATTCGGCTAAGG

36	GATCAGATCCATTGACACTTCC
51	GAGCCTCCAACGGGAATCTTG
52	TGACACCGAGAAGCAGTAAACC
53	TTTCACTGGTTTACTGCTTCTC
54	CAGAGTTTCCAATAGCCACAG
55	CTCGTATGCCTCGTTGTG
56	AGATTGGTCCTACTTGTTTGG
57	ACTTATGGATGAGCTGAAACAAAG
58	TCCCGAGAACTGAAACTACTAAAG
149	ATGGAAGTTCCCAAAGGATTCT
150	GCCAAGGAGCAGCAAGAG
151	TCTTCCTTACTTCTTCCT
152	TTATAGCAGATGATATTGGA
153	GTACATAGAAGCTCTTGAA
154	ATCCAGATTTCCTGTTTG
161	AATGTTGGAGTGATTCTT
162	TTGCTAGACTTAGACCTA
163	AAGGAATCAGCAGAAGGA
164	TAACCACTTGTCTGAACCT
Eef_Fw	ACGGAGACATGGACCAGAAC
Eef_rev	GCTGAGTTGGGAGATCGAAG

References

1. Ziegler, S., Pries, V., Hedberg, C. & Waldmann, H. Target identification for small bioactive molecules: finding the needle in the haystack. *Angew Chem Int Ed Engl* **52**, 2744–2792 (2013).
2. Tresch, S. Strategies and future trends to identify the mode of action of phytotoxic compounds. *Plant Sci*. **212**, 60–71 (2013).
3. Dejonghe, W. & Russinova, E. Target identification strategies in plant chemical biology. *Front Plant Sci* **5**, 352 (2014).
4. Cereto-Massagué, A. et al. Tools for in silico target fishing. *Methods* **71**, 98–103 (2015).
5. Hayashi, K.-I. et al. Rational design of an auxin antagonist of the SCF(TIR1) auxin receptor complex. *ACS Chem. Biol*. **7**, 590–598 (2012).
6. Park, S.-Y. et al. Agrochemical control of plant water use using engineered abscisic acid receptors. *Nature* **520**, 545–548 (2015).
7. Hicks, G. R. & Raikhel, N. V. Small Molecules Present Large Opportunities in Plant Biology. *Annu Rev Plant Biol* **63**, 13.1-13.22 (2012).
8. Bender, A. Databases: Compound bioactivities go public. *Nat Methods* **6**, 309–309 (2010).
9. Wang, Y. et al. PubChem: a public information system for analyzing bioactivities of small molecules. *Nucleic Acids Research* **37**, W623–33 (2009).
10. Koutsoukas, A. et al. From in silico target prediction to multi-target drug design: current databases, methods and applications. *J Proteomics* **74**, 2554–2574 (2011).
11. Ou-Yang, S.-S. et al. Computational drug discovery. *Acta Pharmacol. Sin.* **33**, 1131–1140 (2012).
12. Keiser, M. J. et al. Predicting new molecular targets for known drugs. *Nature* **462**, 175–181 (2009).
13. Fischer E. Einfluss der Configuration auf die Wirkung der Enzyme. *Ber Dtsch Chem Ges* **27**, 2985–93 (1894).
14. Mestres, J., Gregori-Puigjané, E., Valverde, S. & Solé, R. V. The topology of drug-target interaction networks: implicit dependence on drug properties and target families. *Mol Biosyst* **5**, 1051–1057 (2009).
15. Arooj, M. et al. Finding off-targets, biological pathways & target diseases for chymase inhibitors via structure-based systems biology approach. *Proteins* (2014).
16. Helms, J. B. & Rothman, J. E. Inhibition by brefeldin A of a Golgi membrane enzyme that catalyses exchange of guanine nucleotide bound to ARF. *Nature* **360**, 352–354 (1992).
17. Donaldson, J. G., Finazzi, D. & Klausner, R. D. Brefeldin A inhibits Golgi membrane-catalysed exchange of guanine nucleotide onto ARF protein. *Nature* **360**, 350–352 (1992).

18. Renault, L., Guibert, B. & Cherfils, J. Structural snapshots of the mechanism and inhibition of a guanine nucleotide exchange factor. *Nature* **426**, 525–530 (2003).

19. Jackson, C. L. & Casanova, J. E. Turning on ARF: the Sec7 family of guanine-nucleotide-exchange factors. *Trends Cell Biol* **10**, 60–67 (2000).

20. Anders, N. & Jürgens, G. Large ARF guanine nucleotide exchange factors in membrane trafficking. *Cell. Mol. Life Sci.* **65**, 3433–3445 (2008).

21. Nebenfuhr, A., Ritzenthaler C. & Robinson D. G. Brefeldin A: Deciphering an Enigmatic Inhibitor of Secretion. *Plant Physiol* **130**, 1102–1108 (2002).

22. Teh, O.-K. & Moore, I. An ARF-GEF acting at the Golgi and in selective endocytosis in polarized plant cells. *Nature* **448**, 493–496 (2007).

23. Ahmadian, M. et al. PPARγ signaling and metabolism: the good, the bad and the future. *Nat. Med.* **19**, 557–566 (2013).

24. Soccio, R. E., Chen, E. R. & Lazar, M. A. Thiazolidinediones and the promise of insulin sensitization in type 2 diabetes. *Cell Metab.* **20**, 573–591 (2014).

25. He, H. et al. Rosiglitazone causes cardiotoxicity via peroxisome proliferator-activated receptor γ-independent mitochondrial oxidative stress in mouse hearts. *Toxicol. Sci.* **138**, 468–481 (2014).

26. Lehmann, J. M. et al. An antidiabetic thiazolidinedione is a high affinity ligand for peroxisome proliferator-activated receptor gamma (PPAR gamma). *J Biol Chem* **270**, 12953–12956 (1995).

27. Nolte, R. T. et al. Ligand binding and co-activator assembly of the peroxisome proliferator-activated receptor-gamma. *Nature* **395**, 137–143 (1998).

28. Iwata, Y., Miyamoto, S., Takamura, M., Yanagisawa, H. & Kasuya, A. Interaction between peroxisome proliferator-activated receptor gamma and its agonists: docking study of oximes having 5-benzyl-2,4-thiazolidinedione. *J. Mol. Graph. Model*. **19**, 536–42, 598–600 (2001).

29. Kelley, L. A. & Sternberg, M. J. E. Protein structure prediction on the Web: a case study using the Phyre server. *Nature Protoc* **4**, 363–371 (2009).

30. Yin, Y. et al. BES1 accumulates in the nucleus in response to brassinosteroids to regulate gene expression and promote stem elongation. *Cell* **109**, 181–191 (2002).

31. Zhu, J.-Y., Sae-Seaw, J. & Wang, Z.-Y. Brassinosteroid signalling. *Development* **140**, 1615–1620 (2013).

32. Rigal, A., Doyle, S. M. & Robert, S. Live cell imaging of FM4-64, a tool for tracing the endocytic pathways in Arabidopsis root cells. *Methods Mol Biol* **1242**, 93–103 (2015).

33. Marc, J. et al. A GFP-MAP4 reporter gene for visualizing cortical microtubule rearrangements in living epidermal cells. *Plant Cell* **10**, 1927–1940 (1998).
34. The PyMOL Molecular Graphics System, Version 0.99rc6 Schrödinger, LLC.
35. Proost, S. et al. PLAZA 3.0: an access point for plant comparative genomics. *Nucleic Acids Research* **43**, D974–81 (2015).
36. Drakakaki, G. et al. Clusters of bioactive compounds target dynamic endomembrane networks in vivo. *Proc Natl Acad Sci USA* **108**, 17850–17855 (2011).
37. Benschop, J. J. et al. Quantitative phosphoproteomics of early elicitor signaling in Arabidopsis. *Mol Cell Proteomics* **6**, 1198–1214 (2007).
38. Schwacke, R. et al. ARAMEMNON, a novel database for Arabidopsis integral membrane proteins. *Plant Physiol* **131**, 16–26 (2003).
39. Luschnig, C., Luschnig, C., Vert, G. & Vert, G. The dynamics of plant plasma membrane proteins: PINs and beyond. *Development* **141**, 2924–2938 (2014).
40. Vandenbrink, J. P., Kiss, J. Z., Herranz, R. & Medina, F. J. Light and gravity signals synergize in modulating plant development. *Front Plant Sci* **5**, 563 (2014).
41. Jones, A. M. et al. Border control--a membrane-linked interactome of Arabidopsis. *Science* **344**, 711–716 (2014).
42. Petrey, D. et al. Template-based prediction of protein function. *Curr Opin Struct Biol* **32C**, 33–38 (2015).
43. Ou-Yang, S.-S. et al. Computational drug discovery. *Acta Pharmacol. Sin.* **33**, 1131–1140 (2012).
44. Hirst, J. et al. Characterization of TSET, an ancient and widespread membrane trafficking complex. *eLife Sciences* **3**, e02866 (2014).
45. Söding, J., Biegert, A. & Lupas, A. N. The HHpred interactive server for protein homology detection and structure prediction. *Nucleic Acids Research* **33**, W244–8 (2005).
46. Curran, A. et al. Calcium-dependent protein kinases from Arabidopsis show substrate specificity differences in an analysis of 103 substrates. *Front Plant Sci* **2**, 36 (2011).
47. Marc, J. et al. A GFP-MAP4 reporter gene for visualizing cortical microtubule rearrangements in living epidermal cells. *Plant Cell* **10**, 1927–1940 (1998).
48. Chan, K. F., Zhang, P. & Song, Z. Identification of essential amino acid residues in the hydrophilic loop regions of the CMP-sialic acid transporter and UDP-galactose transporter. *Glycobiology* **20**, 689–701 (2010).
49. Boruc, J. et al. Functional modules in the Arabidopsis core cell cycle binary protein-protein interaction network. Plant Cell 22, 1264–1280 (2010).
50. Di Rubbo, S. et al. The clathrin adaptor complex AP-2 mediates endocytosis of brassinosteroid insensitive1 in Arabidopsis. *Plant Cell* **25**, 2986–2997 (2013).

51. Van Leene, J. et al. A tandem affinity purification-based technology platform to study the cell cycle interactome in Arabidopsis thaliana. *Mol Cell Proteomics* **6**, 1226–1238 (2007).
52. Thompson, J. D., Gibson, T. J. & Higgins, D. G. Multiple sequence alignment using ClustalW and ClustalX. *Curr Protoc Bioinformatics* Chapter 2, Unit 2.3 (2002).
53. Tamura, K., Stecher, G., Peterson, D., Filipski, A. & Kumar, S. MEGA6: Molecular Evolutionary Genetics Analysis version 6.0. *Mol. Biol. Evol*. **30**, 2725–2729 (2013).

Chapter VI: Discussion

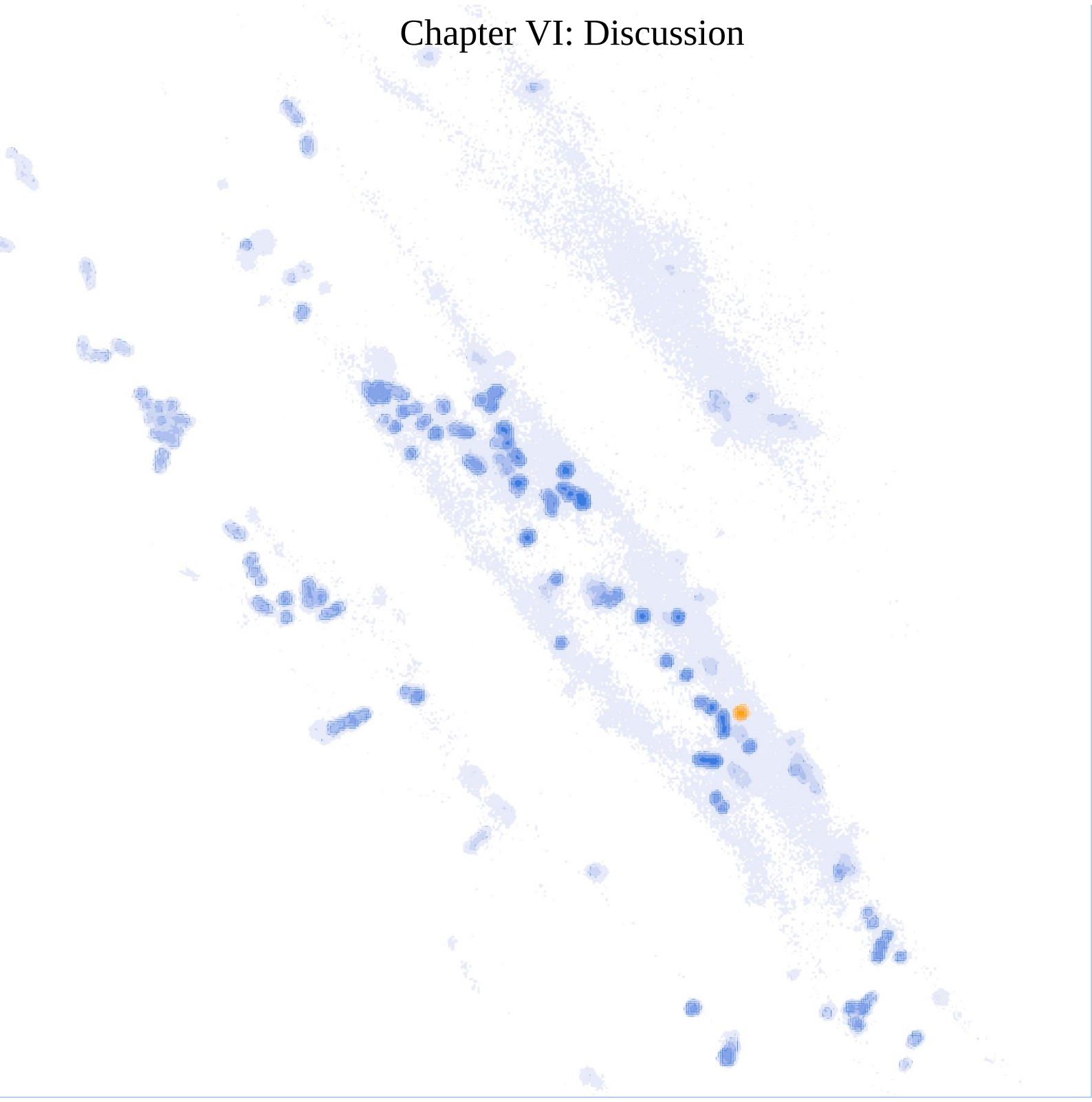

Conclusions and future challenges

Small molecule effectors of endomembrane trafficking have the potential to become valuable tools in cell biology, signaling pathways and other biological processes dependent on the endomembrane continuum. With a well-defined interactome they can provide novel insights in what is by nature a highly dynamic and often essential process. In this thesis we identified, characterized, and explored target identification and validation strategies for small molecule hits derived from a library of potential effectors of endomembrane trafficking[1]. We take a step back and discuss some general principles which emerged with our obtained results, while reflecting on the future direction of plant chemical biology.

Small molecules and cytotoxicity

An important consideration when identifying and working with small molecule hits is their ability to affect general metabolism or any other process affecting general cellular functions, which will reflect on overall cell viability and behavior. In this thesis we provided evidence that one of the commonly used endocytic inhibitors in plants, Tyrphostin A23 (TyrA23), is a potent inhibitor of mitochondrial function and uncouples proton gradients throughout the cell, similar to the mode of action of Carbonyl cyanide m-chlorophenyl hydrazine (CCCP)[2,3]. This has come as a surprise, but fits with a currently increasing awareness in mammalian drug discovery concerning undesirable side effects of small molecules on mitochondrial function[4,5]. Mammalian drug discovery suffers from low success rates, mostly due to undesirable side effects of lead molecules. Often these are only found in later stages of hit optimization, or when the drug is already released, leading to market withdrawal[6,7]. One of the major responsible complications concerns the ability of the small molecule hit to affect mitochondrial functions[4-7]. This notion is fairly recent, which can be partially attributed to a process whereby ATP is generated through glycolysis rather than mitochondrial oxidative phosphorylation, also referred to as the Crabtree effect[8]. Since mammalian cell cultures tested for small molecule induced mitochondrial side effects are often tumor-derived, and culture conditions include much higher concentrations of glucose compared to physiological conditions, mitochondrial side-effects often go unnoticed[5,8]. Although PSB-D wild type cell cultures used for ATP measurements in this study were not evaluated for the presence of functional glycolysis, it is reasonable to assume that most ATP in the cell was produced by the mitochondria, as they are dark grown, and given the strong effect of CCCP, TyrA23 and ES9. In addition, another major difference with mammalian cell cultures is the pH of the medium. For plant cell cultures medium has a pH in the range of 5.5 to 6, while for mammalian cell cultures pH is much closer to cytosolic values. Since CCCP has been described to affect proton gradients over the plasma membrane[5,9], it is reasonable to assume that protonophores will have a more pronounced effect in plant cell cultures opposed to mammalian cell cultures, as they

will induce a proton flux over the plasma membrane into the cytosol. The notion that a considerable amount of small molecule hits affect mitochondrial function was also reflected in preliminary experiments of our own. Aside ES9, a number of other small molecules inhibiting FM4-64 uptake were tested for ATP depletion, though were not further considered. From a total of 12, only 2 were found not to deplete ATP. In addition, small molecule 39 (Chapter 5, this thesis), which belonged to the same group of ES9 (Chapter 2, this thesis) also induced ATP depletion, though not as strong as ES9 (Chapter 5, this thesis). It is preliminary to conclude these small molecules would affect ATP depletion through a similar mechanism as ES9, though it illustrates the commonality of affecting mitochondrial functions. Taken together, above examples indicate that affecting mitochondrial functions is of frequent occurrence for small molecule hits, and this can be more pronounced depending on the biological material used.

Generally speaking, in mammalian drug discovery two approaches can be distinguished: target-based and phenotype-based[6]. While target-based approaches start from a particular protein, which serves as a template for small molecule fitting and later phenotypic validation, phenotype-based approaches start from the induced phenotype and subsequently try to identify the target. It is the latter strategy which frequently employs screening readouts related to cytotoxicity. Often the incentive is to arrest growth and kill tumor cells, thus cytotoxic effects are a desired feature, yet need to be specific as non-tumor cells should not be affected. Many assay types exist, among which ATP measurements[6,7]. In plants however, small molecule tools, not considering herbicides, are preferably perturbing the process of interest without affecting cell viability. They need to affect as specific as possible the process of interest, preferably in a direct manner. It would therefore be of use if new small molecules, and especially libraries designed and screened for the plant community, were evaluated for general cytotoxicity. One way could be through ATP measurements, which can be easily done in a high throughput fashion. Alternatively, cell cultures or other biologically relevant material could harbor a fluorescent marker induced upon cell death. Such readouts, when adopted for high throughput screening, could be used as one of the early screenings to eliminate small molecules which affect cell viability. Small molecules should be screened for such effects prior to any major commitments in the context of target identification or thorough description of target-linked effects.

The primary mode of action of ES9, as described in Chapter 3 of this thesis (**Figure1**), which is shared with TyrA23 and CCCP, is an illustration of how non-specific metabolic effects might complicate interpretation of results, especially when small molecules are transferred to other systems without a thorough assessment of small molecule implications on general metabolism, cell survival, and of-target effects. As different systems might present a different environment to the small molecule compared to the original system in which the small molecule was described, certain characteristics of the small molecule might be enhanced.

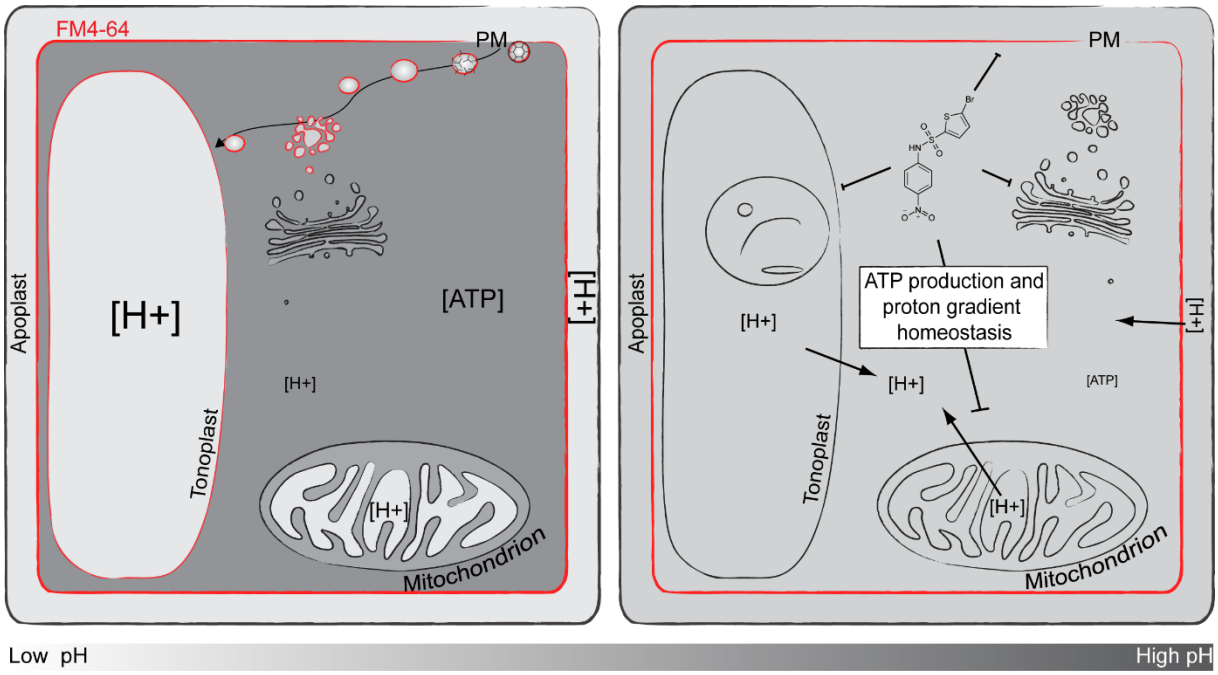

Figure 1 Schematic representation of ES9 mode of action

ES9 induced a dissipation of proton gradients throughout the cell, affecting processes such as ATP production, vacuolar morphology and clathrin mediated endocytosis.

Small molecules and target deconvolution.

Once established the small molecule of interest induces no undesirable side effects related to cell viability and overall function, the process of target identification can start. As outlined in the introduction, several small molecules identified through screening are known which affect endomembrane traffic in plants. Yet few have a well-defined target, and are considered as specific, thus are affecting only the target and process described. For a small molecule to become a useful tool in cell biology, the targets which have direct or indirect roles in endomembrane traffic should be known. As such the small molecule-induced perturbations of the endomembrane system can be interpreted correctly. In case targets remain obscure or not well defined, an element of uncertainty will remain in any conclusions drawn based on the small molecule induced perturbations. An example concerns the small molecule gravacin. Initially identified in a screen for small molecules able to inhibit vacuolar trafficking and gravitropic responses[10], gravacin was later identified as an interactor of the ATP-binding cassette (ABC) transporter P-glycoprotein 19 (PGP19)[11]. Yet the induced phenotype could not be explained entirely by inhibition of PGP19 alone, as the perturbed vacuolar trafficking appeared unaffected, while *pgp* mutants were only partially resistant to gravitropic bending.

A textbook example of a small molecule for which the target is known, and appears to be largely responsible for the observed phenotypes, is Brefeldin A (BFA). BFA was identified in the early 90ies as an inhibitor of the GTP conversion on ADP-ribosylation factor (ARF) proteins by guanine exchange factors (GEFs)[12,13]. Subsequent studies revealed that BFA acts as an uncompetitive

stabilizer of an otherwise transient ARF-GDP-GEF complex through binding the Sec7 domain of GEF proteins[14-16], which dictates BFA sensitivity of GEFs in different systems. The consequence is a failed recruitment of coat proteins which results in a fusion of mostly cis-Golgi compartments with the endoplasmic reticulum (ER), while more trans Golgi cisternae fuse with endosomal compartments to form the BFA body[17].

In plants, BFA has been shown to target the ARF-GEF interface through genetic means[18], while the current knowledge on BFA mode of action has allowed in recent years for a detailed dissection of endomembrane processes involving ARF-GEFs in plants[19-21]. BFA is therefore one of the few small molecules for which it is generally accepted that it targets mainly one protein family, while other probable targets have minor contributions to endomembrane disruptions mediated by BFA. Nonetheless, it would be interesting to gain insight on BFA target proteins proteome wide by biochemical means. As BFA related research has been going on for decades, while gravacin only emerged about 10 years ago, it could seem unfair to criticize specificity of gravacin. However, both examples are an illustration of the requirement for a thorough understanding of small molecule mode of action before it can become a useful tool in cell biology.

Although knowledge on target proteins is in any case useful, some small molecules can be used without detailed specification of their interactome. For example, inhibitors of enzymatic steps in metabolism or biosynthesis, such as Brassinazole (Brz)[22] are mostly evaluated for their effect on the pathway in question, for Brz the biosynthesis of brassinosteroids. They are often used to deplete the cell of a pathway intermediate or final product, which can be used as a discovery tool for signaling pathway components initiated by the final product[23]. Usually additional target proteins have little effect on the pathway in question, hence are not considered to interfere with the experimental outcome.

Clearly a high degree of specificity is favorable, but off-target proteins seem to be a necessary evil for most small molecules. The question arises if this high degree of specificity is really required. As is known in the mammalian drug discovery field, small molecules appear to have on average six target proteins[24,25], which all contribute to the overall observed phenotype, depending on the point of view. The crucial point here is the purpose and mode of action of the small molecule in question. As outlined above, enzyme inhibitors might be less prone to interference from off-target proteins as the phenotypic readout is usually very specific. In contrast, trafficking modulators are more sensitive as the endomembrane compartment is a complex and dynamic continuum, where additional targets affecting endomembrane traffic might complicate interpretation of results. It is therefore essential for endomembrane modulators, and preferable for other small molecules, to have knowledge on the entire interactome if possible, in order for the small molecule to become a valuable tool for biology.

Target identification and validation: the importance of biochemical approaches

Knowledge of the small molecule interactome is essential for modulators of trafficking, and as discussed in the introduction, classical genetics approaches are less suited, as they will fail to identify the entire interactome. Only few approaches allow interactome identification, including affinity purification and label free approaches. Yet all of them have pitfalls, most commonly related to modification of the small molecule and membrane proteins[26]. As we explored in this thesis, a combination of biochemical assays to identify and validate target binding holds the promise to reveal the most important contributors to the phenotype of interest. If the small molecule allows modification without losing activity, affinity purification can reveal candidate interactors based on the abundance and reproducibility in affinity purification. Subsequent selection of promising candidate target proteins for further validation can confirm the relevance of their presence in pull-down experiments. Depending on the resources available, several experimental approaches can be adopted, with some of the most accessible being cellular thermal shift assay (CETSA)[27] and drug affinity responsive target stability (DARTS)[28]. If possible target proteins score positive with CETSA and DARTS for binding, chances are high the small molecule of interest is a true interactor. This can be confirmed by further in-depth analysis of the small molecule-target protein complex using crystallographic studies or techniques such as isothermal titration calorimetry (ITC) and surface plasmon resonance (SPR). Finally, as the list of potential target proteins is reduced to few candidates, mutant analysis can provide further genetic proof of small molecule binding. Alternatively, depending on resources available, one could opt to start from a genetics perspective, screening mutant libraries for resistant individuals, which then serve to identify genomic mutations leading to the resistant phenotype. Subsequently targeted biochemical approaches are used to validate small molecule binding. Although successful examples exist[11,29-31], the chances are relatively high the target protein will not be directly involved in the phenotype of interest[32,33]. In addition, genetic strategies have an inherent pitfall when targets are of essential nature, certainly when the mutation renders the protein inactive. Redundancy can pose a significant problem as well, as only higher order mutants might reveal a phenotype on small molecule.

It is therefore more suited to approach target identification from a biochemical perspective rather than a genetic perspective, certainly when working with small molecule modulators of endomembrane traffic. Naturally not all small molecule hits are suited for affinity purification based approaches, as modification might interfere with small molecule activity, or when affinity for its target is not high enough for successful purification. To solve those issues, label free approaches have gained more attention over the recent years. Although most of them are relatively recent, technological advances in the coming years might propel label free target identification to the forefront of target identification. Especially proteome wide target identification holds big promises, as they allow an almost total view on the small molecule interactome. Examples are target identification by

chromatographic co-elution[34], and the recently described proteome-wide CETSA approach[35]. Although currently a major investment in terms of time and effort, future technological advances will increase accessibility of such approaches, and might provide solutions to current pitfalls such as membrane proteins, low abundant targets, and low affinity.

In conclusion, chemical biology approaches for cell biology hold great promises if certain criteria are met. First, the small molecule should not affect cell viability through interference with a variety of essential cellular processes, unless meant to. Second, small molecule interactomes are essential to fully explore and use the small molecule potential. This is best achieved through biochemical means, as genetic strategies fall short. Last, but certainly not least, is the role of chemists in projects as described in this thesis. It is one thing to work on a chemical biology project from a biologists point of view, yet completely different when viewed from a chemists point of view. Cross pollination of both disciplines can only propel a chemical biology project further, as both help each other in a better understanding of the biological problem in question, which alone they would not achieve.

Small molecules and CME

Small molecule inhibition of CME is currently a very active field of research, as few specific inhibitors have been identified, both in plant and mammalian systems. The best known examples are Pitstops[36] and Dynasore[37], but both have yet to find their way to the plant field. Specific inhibitors of clathrin have the potential to facilitate a better understanding of the different roles clathrin has in several aspects of plant biology in a conditional, reversible and dynamic fashion. They are therefore of great value, as genetic means cannot provide a similar versatile and quick inhibition of clathrin mediated processes. Though small molecule inhibitors of endocytosis are valuable tools in deciphering the molecular machinery driving CME, their use extends fundamental cell biology, and finds application in healthcare. As clathrin is essential for cell survival, major defects in CME are not expected in human disease[38]. However, subtle changes in functionality of CME machinery can have several implications for human health[38]. More importantly, engineering of CME machinery, which could involve clathrin, can be a tool to inhibit pathogen uptake into the cell[38].

Although the substantial investment in time and money will remain a major hurdle, it would be extremely interesting to inhibit CME at different points with small molecules. One group could comprise small molecule inhibitors of structural aspects, such as clathrin and vesicle formation, while another group could include inhibitors which interfere with cargo recognition and recruitment. The latter group might contain inhibitors which specifically inhibit cargo recognition at the level of cargo rather than adaptor complexes such as AP2, since highly specific inhibition of CME might be

achieved for a particular group of receptors. As such implications for cell biology could be evaluated without the risk that CME inhibition of other cargo would complicate interpretation of results.

On a final note this thought. Supposedly the ultimate goal for small molecule interference of endomembrane traffic can be illustrated by the following analogy: imagine a complex system like an ant colony, with its many supply routes, nurseries, soldiers and central command, all dependent on each other. One could imagine ants as individual proteins, while routes, nurseries or other chambers in the colony represent different endomembrane compartments and their complex connections. Our current efforts to understand its intricate behavior equals hitting the colony as hard as we can in a variety of ways, admittedly with a little thought, only to observe how it reassembles itself, if it survives the sudden disturbance. We ought to be able to disturb the colony in such a way, by subtly rerouting certain supply routes to the colony for example, that the system hardly notices the changes, and quietly readjusts to run as smooth as possible again. Only then we can start to appreciate the delicate hierarchical relations required to run a highly complex and dynamic system like an ant colony.

References

1. Drakakaki, G. et al. Clusters of bioactive compounds target dynamic endomembrane networks in vivo. *Proc Natl Acad Sci USA* 108, 17850–17855 (2011)

2. Heytler, P. G. Uncoupling of oxidative phosphorylation by carbonyl cyanide phenylhydrazones. I. Some characteristics of m-Cl-CCP action on mitochondria and chloroplasts. *Biochemistry* **2**, 357–361 (1963).

3. Kasianowicz, J., Benz, R. & McLaughlin, S. The kinetic mechanism by which CCCP (carbonyl cyanide m-chlorophenylhydrazone) transports protons across membranes. *J. Membr. Biol*. **82**, 179–190 (1984).

4. Chan, K., Truong, D., Shangari, N. & O'Brien, P. J. Drug-induced mitochondrial toxicity. *Expert Opin. Drug Metab. Toxicol.* **1**, 655–669 (2005).

5. Swiss, R., Niles, A., Cali, J. J., Nadanaciva, S. & Will, Y. Validation of a HTS-amenable assay to detect drug-induced mitochondrial toxicity in the absence and presence of cell death. *Toxicol In Vitro* **27**, 1789–1797 (2013).

6. Moffat, J. G., Rudolph, J. & Bailey, D. Phenotypic screening in cancer drug discovery - past, present and future. *Nat Rev Drug Discov* **13**, 588–602 (2014).

7. O'Brien, P. J. High-content analysis in toxicology: screening substances for human toxicity potential, elucidating subcellular mechanisms and in vivo use as translational safety biomarkers. *Basic Clin. Pharmacol. Toxicol*. **115**, 4–17 (2014).

8. Marroquin, L. D., Hynes, J., Dykens, J. A., Jamieson, J. D. & Will, Y. Circumventing the Crabtree effect: replacing media glucose with galactose increases susceptibility of HepG2 cells to mitochondrial toxicants. *Toxicol. Sci.* **97**, 539–547 (2007).

9. Kenwood, B. M. et al. Identification of a novel mitochondrial uncoupler that does not depolarize the plasma membrane. *Mol Metab* **3**, 114–123 (2014).

10. Surpin, M. et al. The power of chemical genomics to study the link between endomembrane system components and the gravitropic response. *Proc Natl Acad Sci USA* **102**, 4902–4907 (2005).

11. Rojas-Pierce, M. et al. Arabidopsis P-glycoprotein19 participates in the inhibition of gravitropism by gravacin. *Chem. Biol.* **14**, 1366–1376 (2007).

12. Helms, J. B. & Rothman, J. E. Inhibition by brefeldin A of a Golgi membrane enzyme that catalyses exchange of guanine nucleotide bound to ARF. *Nature* **360**, 352–354 (1992).

13. Donaldson, J. G., Finazzi, D. & Klausner, R. D. Brefeldin A inhibits Golgi membrane-catalysed exchange of guanine nucleotide onto ARF protein. *Nature* **360**, 350–352 (1992).

14. Renault, L., Guibert, B. & Cherfils, J. Structural snapshots of the mechanism and inhibition of a guanine nucleotide exchange factor. *Nature* **426**, 525–530 (2003).

15. Jackson, C. L. & Casanova, J. E. Turning on ARF: the Sec7 family of guanine-nucleotide-exchange factors. *Trends Cell Biol* **10**, 60–67 (2000).

16. Anders, N. & Jürgens, G. Large ARF guanine nucleotide exchange factors in membrane trafficking. *Cell. Mol. Life Sci.* **65**, 3433–3445 (2008).

17. Nebenfuhr, A., Ritzenthaler C. & Robinson D. G. Brefeldin A: Deciphering an Enigmatic Inhibitor of Secretion. *Plant Physiol* **130**, 1102–1108 (2002).

18. Teh, O.-K. & Moore, I. An ARF-GEF acting at the Golgi and in selective endocytosis in polarized plant cells. *Nature* **448**, 493–496 (2007).

19. Naramoto, S. et al. ADP-ribosylation factor machinery mediates endocytosis in plant cells. *Proc Natl Acad Sci USA* **107**, 21890–21895 (2010).

20. Naramoto, S. et al. Insights into the localization and function of the membrane trafficking regulator GNOM ARF-GEF at the Golgi apparatus in Arabidopsis. *Plant Cell* **26**, 3062–3076 (2014).

21. Richter, S. et al. Delivery of endocytosed proteins to the cell–division plane requires change of pathway from recycling to secretion. *eLife Sciences* **3**, e02131 (2014).

22. Asami, T. et al. Characterization of brassinazole, a triazole-type brassinosteroid biosynthesis inhibitor. *Plant Physiol* **123**, 93–100 (2000).

23. Wang, Z.-Y. et al. Nuclear-localized BZR1 mediates brassinosteroid-induced growth and feedback suppression of brassinosteroid biosynthesis. *Dev Cell* **2**, 505–513 (2002).

24. Mestres, J., Gregori-Puigjané, E., Valverde, S. & Solé, R. V. The topology of drug-target interaction networks: implicit dependence on drug properties and target families. *Mol Biosyst* **5**, 1051–1057 (2009).

25. Arooj, M. et al. Finding off-targets, biological pathways & target diseases for chymase inhibitors via structure-based systems biology approach. *Proteins* (2014).

26. Ziegler, S., Pries, V., Hedberg, C. & Waldmann, H. Target identification for small bioactive molecules: finding the needle in the haystack. *Angew Chem Int Ed Engl* **52**, 2744–2792 (2013).

27. Martinez Molina, D. et al. Monitoring drug target engagement in cells and tissues using the cellular thermal shift assay. *Science* **341**, 84–87 (2013).

28. Lomenick, B. et al. Target identification using drug affinity responsive target stability (DARTS). *Proc Natl Acad Sci USA* **106**, 21984–21989 (2009).

29. Park, S.-Y. et al. Abscisic acid inhibits type 2C protein phosphatases via the PYR/PYL family of START proteins. *Science* **324**, 1068–1071 (2009).

30. Santiago, J. et al. The abscisic acid receptor PYR1 in complex with abscisic acid. *Nature* **462**, 665–668 (2009).

31. Walsh, T. A. et al. Chemical genetic identification of glutamine phosphoribosylpyrophosphate amidotransferase as the target for a novel bleaching herbicide in Arabidopsis. *Plant Physiol* **144**, 1292–1304 (2007).

32. Zhao, Y. SIR1, an Upstream Component in Auxin Signaling Identified by Chemical Genetics. *Science* **301**, 1107–1110 (2003).

33. Dai, X. et al. Genetic and chemical analyses of the action mechanisms of sirtinol in Arabidopsis. *Proc Natl Acad Sci USA* **102**, 3129–3134 (2005).

34. Chan, J. N. Y. et al. Target identification by chromatographic co-elution: monitoring of drug-protein interactions without immobilization or chemical derivatization. *Mol Cell Proteomics* **11**, M111.016642 (2012).

35. Savitski, M. M. et al. Proteomics. Tracking cancer drugs in living cells by thermal profiling of the proteome. *Science* **346**, 1255784 (2014).

36. Kleist, von, L. et al. Role of the clathrin terminal domain in regulating coated pit dynamics revealed by small molecule inhibition. *Cell* **146**, 471–484 (2011).

37. Macia, E. et al. Dynasore, a cell-permeable inhibitor of dynamin. *Dev Cell* **10**, 839–850 (2006).

38. McMahon, H. T., McMahon, H. T., Boucrot, E. & Boucrot, E. Molecular mechanism and physiological functions of clathrin-mediated endocytosis. *Nat Rev Mol Cell Biol* **12**, 517–533 (2011).

Acknowledgements

Right, where do I start? I suppose at the beginning, now about 5 years ago when I finished a very nice and interesting period at the John Innes Centre in Norwich, U.K. Back then I had decided for myself that I would pursue a PhD in Biochemistry and Biotechnology, the question was where these four years would unfold. After a few considerations I decided to give it a go in Gent, at the Plant Systems Biology department of VIB and the University of Gent. After evaluation of most groups and their available projects I decided to contact Jenny regarding the chemical biology project she had on offer, as I found the interdisciplinary approach highly interesting. We agreed to apply for an IWT grant, for which a project proposal was quite advanced already. The following months were of intense preparation, followed by an oral defense in Brussels. The rest is history. In the following 4.5 years Jenny has always been very supporting, while encouraging the exploration of relatively new and uncharted experimental territories throughout. She has given me lots of opportunities from the beginning, and has been a guide for the rollercoaster of unexpected events that has been the ES9 project. For all this I owe her a big thank you.

Naturally it doesn't stop here. Many people have had a contribution in this work, and have given support, guidance and friendship along the way. A PhD is formed by interactions with people, either on a long-term basis or short, but a complete acknowledgement is nearly impossible. But I'll try my best anyway.

Past and present members of the brassin lab contributed in various ways of course. Niloufer, for her enthusiasm, thorough knowledge on elephants, and the lively discussions on all kind of crazy things during coffee breaks with Simone and Kiril. Simone, of course, for my proper introduction in the world of real coffee, but also for the games and occasional (spicy) drinks. Kiril, well, Kiril. A great many thanks for embarking with me on this affinity thingy, the guidance and advice, but also for letting me know where real yoghurt came from (Turkey, right?), and the countless, priceless bicycle, food and hunting related anecdotes. Camilla, for being often the support, and (one could say) the mommy of the lab. Evelien and Isabelle for helping tremendously with all kinds of practical things. Without you this would have been a completely different story. Of course the newcomers in the lab, Anaxi, Andres and Rahul. With their presence in the lab, topics have quite often taken a more male oriented direction, sometimes much to the despair of our female companions, but of course with much approvement from Kiril. Also for the fun moments outside the lab, and for providing often great opportunities for taking pictures a bit later at night. And Balkan, it was a short but very pleasant stay in the lab, and thank you for all the cookies that accompanied the coffee once in a while. To all of you, and all other past and present members, a big thank you.

The brassin lab has a good relation with the Alice lab, not only because we share the lab, but also because quite some of its members have had an episode in the brassin lab. Daniël for the very helpful discussions and critical comments, you have teached me a lot. Joanna for being there, always with a smile, and sometimes, a little on the crazy side as well. Annika for enthusiastically joining the occasional sangria sessions, though I had to miss them sometimes. Marjan and Sam for joining the coffee breaks, and for being very nice lab mates. And Ken, well I think I'm slowly starting to convert you into a coffee addict as well. Last but not least, to a lot of you, thank you for the countless times homemade cookies and sweets found safely their way to the lab.

I would also like to thank all our collaborators for the very useful discussions and additions to the ES9 story, especially Johan, Bram and Annemieke. The very convenient and quick supply line of small molecules, but equally the sometimes essential insights into the chemistry and biology have propelled this work further. Also Kris and An, for helping us out with the search for, and optimization of an affinity purification protocol.

PSB is home to some great support teams involved in preparing medium, sterilizing stuff, growing plants and much more. A big thank you therefore to all people who made everyday life in the lab that little bit easier. I would like to thank one of them especially though. His name is 'my friend', and he has been sharing his joy in life with me and the rest of the brassin lab almost since the very beginning. Lab life without him would have been much different. Thank you Wilson, I will for sure visit you one day in remote Chile.

At some point I became crazy enough to take up the challenge of organizing the 5th European Plant Science Retreat (EPSR), here in Gent. A big thank you to all people who helped and made this possible, also to our sponsors, but especially to Marieke, Pieter, Alan and Helga for the great work and enormous amount of energy and time that you guys have spent in the EPSR.

Not everything is related to work though. I'm very thankful for all the great moments that I had with so many colleagues, be-it a trip to Italy or Spain for meetings, coffee breaks after lunch or awesome parties till late at night, they made lab life much more fun.

Of course I would like to take the opportunity to thank friends and family for all the friendship and support throughout the years. As this PhD required quite some time and dedication, certainly towards the end, it was always a great way of taking my mind of things by joining my Mom, Dad, Els and Brecht on Fridays or Sundays for dinner or lunch, enjoy delicious food and fine wines, and feel at home. Naturally this is just a tiny fraction of what they mean to me, since they have directly or indirectly always been there for me, and there are simply no words to thank them enough. They have been, and still are the warmest nest you can think of.

Some would argue that I like to drink from a glass depicting a little goblin, and I can't deny such assertions. In fact, as the little goblin witnessed some truly nice occasions and events, I would like to take the opportunity to thank all my friends for those great moments I had with them, be-it a trip to Iceland, (cycling) weekends, kleurenwiezen, or (occasional) long nights in some pub.

And last but not least, Judith. We've met in quite a hectic period for both of us, but despite that found each other, and have been together since. And though we're two very different persons, we've grown towards each other. She has supported me throughout, and stuck with me during intense periods of working. I'm incredibly grateful for that, and can't thank her enough. She's stolen a little piece of me, and I believe there is a bright and exiting future ahead of us.

Curriculum Vitae

Personal Details

First Name:	Wim
Last Name:	Dejonghe
Address:	Lostraat 70
	9000, Gent
	Belgium
Mobile:	+32 (0)474 48 28 50
Email:	wim.dejonghe@psb.vib-ugent.be
Date of birth:	06.11.1984
Place of birth:	Deinze, Belgium

Research interests

Early on during my studies, I got interested in the cell biological and biochemical aspects of plant biology. I decided to focus on these aspects during my master studies, and after my experience at the John Innes Centre to pursue a PhD on plant chemical biology in the lab of Dr. E. Russinova. This highly multi-disciplinary project allowed me to explore further into areas of my interest, such as the cell biology of endomembrane traffic and in depth characterization of small molecules and affinity purification of their target proteins. I would like to continue in that direction, looking at complex dynamic endomembrane traffic responses to different environmental cues and conditions.

Education

2010-present

Doctoral studies in biochemistry and biotechnology

Title: Endomembrane trafficking and brassinosteroid signaling from a small molecule perspective. Characterization of small molecules which affect early endomembrane traffic such as endocytosis, thereby influencing brassinosteroid signaling. Strong emphasis on protein target identification through affinity purification and subsequent biochemical validation.

Promoter: Dr. Eugenia Russinova

Department of Plant Systems Biology, VIB, Ghent, Belgium

Department of Plant Biotechnology and Bioinformatics, Ghent University, Ghent, Belgium.

2007-2009

Master in biochemistry and biotechnology, distinction

Major focus on plant systems biology and minor focus on biochemistry and structural biology
Ghent University
Thesis: A functional investigation of NSP1 and NSP2, two transcriptional regulators involved in *Medicago truncatula* nodulation signaling
Department of Cell and Developmental Biology, John Innes Centre, Norwich NR4 7UH, United Kingdom.

2004-2007
Bachelor in biochemistry and biotechnology, distinction
Ghent University

Obtained fellowships

01/10/2010 - 30/09/2014
IWT (agency for Innovation through Science and Technology) fellowship
Highly competitive 4-year personal research fellowship from the government, with a focus on applicability of research.
Department of Plant Systems Biology, VIB, Ghent, Belgium
Department of Plant Biotechnology and Bioinformatics, Ghent University, Ghent, Belgium.

11/01/2010 - 09/07/2010
Leonardo da Vinci fellowship
European fellowship which allows you to gain working experience abroad.
Department of Cell and Developmental Biology, John Innes Centre, Norwich NR4 7UH, United Kingdom.

Teaching experience

Supervision of Cedric Pirlot, including design of the project 'Target identification strategies for novel endocytic inhibitors in Arabidopsis', design of experiments, technical assistance, proof reading and correction of the thesis.
Master in Plant Biotechnology
Academic year 2013-2014
Department of Plant Systems Biology, VIB, Ghent, Belgium
Department of Plant Biotechnology and Bioinformatics, Ghent University, Ghent, Belgium.

Supervision of Sara Vleminckx, Thomas Naert and Ali Isbilir, including design of the project 'Characterization of small molecules affecting endomembrane trafficking and brassinosteroid signaling', design of experiments, technical assistance, proof reading and correction of the thesis.

1st Master in Biochemistry and Biotechnology

Academic year 2012-2013

Department of Plant Systems Biology, VIB, Ghent, Belgium

Department of Plant Biotechnology and Bioinformatics, Ghent University, Ghent, Belgium.

Supervision of Tom De Saedeleer, Jan Hullaert and Bart Vanderstraten, including designing experiments and technical assistance for experiments conducted in the department of Plant Systems Biology for the project 'Synthesis and evaluation of analogues of molecules that show an in-vivo response related to the brassinosteroid regulated signaling pathway in Arabidopsis'

3rd Bachelor in Chemistry

Academic year 2011-2012

Laboratory for Organic Synthesis, Organic and Biomimetic Chemistry research group, Ghent University, Department of Organic Chemistry, Ghent, Belgium

Department of Plant Systems Biology, VIB, Ghent, Belgium

Department of Plant Biotechnology and Bioinformatics, Ghent University, Ghent, Belgium.

Administrative experiences

August 27th - 30th, 2013

Member of the organizing committee of the 16th European Network of Plant Endomembrane Research (ENPER) meeting.

Several supporting responsibilities such as organization of transport, poster session, lunch sessions and reception.

Ghent, Belgium

July 23rd - 26th, 2013

Chairman of the organizing committee of the 5th European Plant Science Retreat (EPSR) for PhD students

Taking the initiative of organizing and end responsibility of the event, coordination with the University of Ghent for housing, venue, financial administration and with the doctoral schools unit of the university. Contact person for European doctoral schools and participants, attracting funding and several other aspects such as transport and catering.

Ghent, Belgium

Conference participation and contributions

Participation was aimed at getting feedback on our work and to increase on international visibility and collaborations.

2014

25th International Conference on Arabidopsis Research (ICAR), Poster Presentation
Vancouver, Canada

BASF Research Forum Europe, Poster presentation
Antwerp, Belgium

2013

16th European Network of Plant Endomembrane Research (ENPER) meeting, Oral Presentation
Gent, Belgium

5th European Plant Science Retreat (EPSR) for PhD students
Gent, Belgium

2012

15th ENPER meeting, Poster Presentation
Madrid, Spain

4th EPSR for PhD students, Poster presentation
Norwich, UK

1st International Brassinosteroid Conference, Poster presentation
Barcelona, Spain

2011

14th ENPER meeting, Poster presentation
Assisi, Italy

Skills and attended courses

Languages:
Dutch: mother tongue. English: fluent. French: basic.

Selection of scientific techniques:
Confocal laser scanning microscopy, spinning disc microscopy, affinity purification of (small molecule) target proteins, Drug Affinity Responsive Target Stability, protein thermal shift assays, standard molecular biology techniques, qPCR, western blotting.

December 16th 2011
Mass spectrometry data analysis
Bioinformatics Training and Service Facility (BITS) of VIB
VIB, Ghent, Belgium

May 16th - 20th 2011
Summer school on advanced light microscopy
VIB research training course
VIB, Ghent, Belgium

Manuscripts in preparation

Wim Dejonghe, Sabine Kuenen, Evelien Mylle, Olivier Keech, Corrado Viotti, Fausto Andres Ortiz-Morea, Kiril Mishev, Simon Delang, Jiorgos Kourelis, Jaroslaw Kasprowicz, Le Son Long Nguyen, Andrzej Drozdzecki, Isabelle Van Houtte, Carlos Reis, Sandra Schmid, Gary Baisa, Sebastian Bednarek, Christa Testerink, Stephanie Robert, Dominique Audenaert, Annemieke Madder, Daniël Van Damme, Karin Schumacher, Johan Winne, Patrik Verstreken and Eugenia Russinova. Protonophore uncouplers are potent inhibitors of clathrin-mediated endocytosis in plants
Target journal: Nature Communications. In preparation.

Wim Dejonghe, Kiril Mishev, Bram Denoo, Evelien Mylle, Isabelle Van Houtte, Sabine Kuenen, Corrado Viotti, An Staes, Long Nguyen, Andrzej Drozdzecki, Wim Nerinckx, Dominique Audenaert, Daniël Van Damme, Annemieke Madder, Patrik Verstreken, Kris Gevaert, Johan Winne and Eugenia Russinova. Disruption of clathrin-mediated endocytosis in *Arabidopsis* through small molecule inhibition of clathrin heavy chain function

Target journal: Nature Chemical Biology. In preparation.

Dejonghe, W., Van Houtte, I., Russinova, E. Identification of a plant specific membrane-bound protein family involved in steroid homeostasis. In preparation

Publications

Dejonghe, W., Mishev, K. & Russinova, E. The brassinosteroid chemical toolbox. *Curr Opin Plant Biol*, **22**, 48-55 (2014).
Writing of the manuscript and parts of figure design

Dejonghe, W. & Russinova, E. Target identification strategies in plant chemical biology. *Front Plant Sci* **5**, 352 (2014).
Writing the manuscript and figure design

Kerchev, P. I., De Clercq, I., Denecker, J., Mühlenbock, P., Kumpf, R., Nguyen, L., Audenaert, D., Dejonghe, W. & Van Breusegem, F. Mitochondrial perturbation negatively affects auxin signaling. *Mol Plant* **7**, 1138–1150 (2014).
Confocal laser scanning microscopy analysis of mitochondrial membrane potential.

Di Rubbo, S., Irani, N. G., Kim, S. Y., Xu, Z. Y., Gadeyne, A., Dejonghe, W., Vanhoutte, I., Persiau, G., Eeckhout, D., Simon, S., Song, K., Kleine-Vehn, J., Friml, J., De Jaeger, G., Van Damme, D., Hwang, I. & Russinova, E. The clathrin adaptor complex AP-2 mediates endocytosis of brassinosteroid insensitive1 in Arabidopsis. *Plant Cell* **25**, 2986–2997 (2013).
Parts of qPCR analysis

Mishev, K., Dejonghe, W. & Russinova, E. Small molecules for dissecting endomembrane trafficking: a cross-systems view. *Chem Biol* **20**, 475–486 (2013).
Figure design and parts of manuscript writing

References

Dr. Eugenia Russinova
Department of Plant Systems Biology, VIB, Ghent, Belgium
Department of Plant Biotechnology and Bioinformatics, Ghent University, Ghent, Belgium.

Prof. Dr. Natasha Raikhel

Department of Botany and Plant Sciences, Center for Plant Cell Biology, Institute for Integrative Genome Biology, University of California, Riverside, CA 92521, USA

Dr. Daniël Van Damme

Department of Plant Systems Biology, VIB, Ghent, Belgium

Department of Plant Biotechnology and Bioinformatics, Ghent University, Ghent, Belgium.

Dr. Johan Winne

Department of Organic Chemistry, Polymer Research Group and Laboratory for Organic Synthesis, Ghent University, Krijgslaan 281 S4-bis, Ghent, Belgium

Cover: artistic representation of FM4-64 uptake in *Arabidopsis* root cells under control conditions.

Back: artistic representation of FM4-64 uptake in *Arabidopsis* root cells treated with ES9.

Chapter pages: artistic representation of stained mitochondria in *Arabidopsis* root cells